Oxidative processes - Insights in reaction mechanisms gained by high resolution and isotope ratio mass spectrometry

Dissertation

zur Erlangung des akademischen Grades eines
Doktors der Naturwissenschaften
– Dr. rer. nat. –

vorgelegt von

Sarah Willach

geboren in Oberhausen

Institut für Instrumentelle Analytische Chemie
der
Universität Duisburg-Essen

2020

DOI: 10.17185/duepublico/71987
URN: urn:nbn:de:hbz:464-20200708-112337-1

Die vorliegende Arbeit wurde im Zeitraum von Januar 2013 bis Juni 2017 im Arbeitskreis von Prof. Dr. Torsten C. Schmidt am Institut für Instrumentelle Analytische Chemie der Universität Duisburg-Essen durchgeführt.

Tag der Disputation: 26.06.2020

Gutachter: Prof. Dr. Torsten C. Schmidt

PD Dr. Thomas B. Hofstetter

Vorsitzender: Prof. Dr. Malte Behrens

Danksagung

Mein besonderer Dank gilt Prof. Dr. Torsten C. Schmidt, der mir die Möglichkeit gab diese Arbeit in seiner Arbeitsgruppe durchzuführen. Während der gesamten Zeit habe ich einen großen Freiraum genossen, um meine eigenen Ideen einzubringen und durch ihn die Rahmenbedingungen erhalten, diese auch umzusetzen zu können. Gleichermaßen stand er mir als verlässlicher Ansprechpartner zur Seite, um bei Problemen gemeinsam eine zielorientierte Lösungen zu finden. Darüber hinaus danke ich ihm für die einmalige Möglichkeit mit meiner Arbeit gleichzeitig in die Welt der oxidativen Prozesse und der Isotopenchemie einzutauchen, sowie an verschiedensten Konferenzen beider Fachgebiete teilnehmen zu können. PD Dr. Thomas B. Hofstetter danke ich für die Übernahme des Zweitgutachtens sowie die anregenden Diskussionen auf Konferenzen oder im Schriftverkehr.

Ausdrücklich bedanke ich mich bei Prof. Dr. Holger V. Lutze für die unzähligen und sehr hilfreichen Diskussion, Anregungen und die stets konstruktive Kritik. Ohne die gemeinsame Erörterung von Alternativen beim Auftreten diverser Sackgassen und sein unerschütterliches, hoffnungsvolles Gemüt, wäre ich sicherlich das ein oder andere Mal verzweifelt. Dank gebührt Jens Terhalle, der im Rahmen seines Research Praktikums wertvolle Vorarbeiten für ein Kapitel dieser Arbeit geleistet hat. Außerdem gilt mein Dank Katja Löppenberg und Michelle Lüling für ihre ausdauernde Unterstützung der Laborarbeiten.

Den aktuellen und ehemaligen Mitarbeitern des Lehrstuhls für Instrumentelle Analytische Chemie an der Universität Duisburg-Essen danke ich für die große Hilfsbereitschaft untereinander, die angenehme Arbeitsatmosphäre und die guten Gespräche beim Essen oder beim Kaffee. Insbesondere gebührt ein großes Dankeschön meiner AOP^{+}-Gruppe (Alexandra Beermann, Dr. Alexandra Fischbacher, Katharina Hupperich, Prof. Dr. Holger V. Lutze, Dr. Florian Metzelder, PD Dr. Uschi Telgheder, Jens Terhalle, Dr. Laura Wiegand und Vanessa Wirzberger) für alle hilfreichen, fachlichen Gespräche, die angenehme Atmosphäre im Büro und alle gemeinsamen Ausflüge miteinander.

Ich danke meiner Familie und ganz besonders meinen Eltern, die immer hinter mir stehen, für ihre stete Unterstützung und Ermutigung - und besonders dafür, dass sie mir diese großartige Ausbildung ermöglicht haben. Ein großer Dank richtet sich nicht zuletzt an meine Freunde: insbesondere an meinen unerschütterlichen und immer verlässlichen Weggefährten André sowie Nils, Miriam und Farina, die die Höhen und Tiefen dieser Arbeit mit mir mitgegangen sind, die immer an mich geglaubt und mich motiviert aber mich auch ab und an abgelenkt haben, wenn es nötig war.

Summary

Oxidative and phototransformation processes frequently contribute to micropollutant degradation in natural or engineered systems. For the remediation of contaminated sites or water treatment processes these may be, e.g., ozone (O_3), hydroxyl radicals ($^{\bullet}OH$), chlorine dioxide (ClO_2) or UV/vis light if the micropollutants contain one or more chromophores. However, the corresponding reaction mechanisms which are important to assess the formation of undesired transformation products (TPs) are mostly unknown. Currently, TP studies are regularly performed with the analysis by high-resolution mass spectrometry (HRMS) which enables the derivation of the TP sum formulas based on the exact masses. However, the reactive site and point of attack, respectively, remain mostly unknown. Here, compound-specific stable isotope analysis (CSIA) may be a useful tool to enlighten and further investigate reactions of micropollutants since degradation processes may reveal specific isotopic fractionation, which are related to the site of primary attack. Therefore, this study investigates the use of CSIA and HRMS as complementary tools to characterize various oxidative and phototransformation processes in order to elucidate the underlying reaction mechanisms. The sulfonamide antibiotic sulfamethoxazole (SMX) is chosen as a model compound in order to systematically investigate the pH dependent transformation caused by the oxidative and phototransformation processes listed above. SMX is a widely detected micropollutant in surface, ground- and wastewaters which may occur as neutral or anionic specie at typical pH values of water treatment or in natural waters.

In case of the oxidative processes, O_3 in presence and absence of $^{\bullet}OH$ and ClO_2, the reaction stoichiometry, product formation and reaction mechanisms were systematically investigated for reactions with SMX. Two moles of ClO_2 and approximately three moles of O_3 were consumed per mole SMX degraded. As revealed by HRMS, the oxidation of SMX with O_3 and ClO_2 leads to six major TPs in both cases. Tentatively formulated TP structures from other studies could partly be confirmed by CSIA. However, for one TP, a hydroxylated SMX, by HRMS alone it could not be decided whether hydroxylation occurred at the aromatic ring, as suggested in literature before, or at the anilinic nitrogen. By additional means of CSIA and an analytical standard it was possible to identify sulfamethoxazole hydroxylamine unequivocally as one of the TPs of the reaction of SMX with O_3 as well as with ClO_2. H-abstraction and electron transfer at the anilinic nitrogen are suggested as likely initial reactions of O_3 and ClO_2, respectively, leading to its formation. The oxidation of anionic SMX with O_3 did not show any significant isotopic fractionation whereas the other reactions studied resulted in a significant carbon isotope fractionation (e.g., $\varepsilon_C(O_3) = -2.2 \pm 0.1$ ‰ and $\varepsilon_C(O_3 + {}^{\bullet}OH) = -1.2 \pm 0.1$ ‰).

For the investigation of the phototransformation reactions of the two relevant SMX species, four different irradiation scenarios were employed, i.e., a low, medium, and high pressure Hg lamp as well as simulated sunlight. The observed phototransformation kinetics were faster for the neutral than for the anionic SMX species (from 3.4 (LP lamp) up to 6.6 (HP lamp) times). Furthermore, four phototransformation products (with m/z 189, 202, 242, and 260) were detected by HRMS that have not yet been described for direct photolysis of SMX. Isotopic fractionation occurred only if UV-B and UV-A wavelengths prevailed in the emitted irradiation and was most pronounced for the neutral species with simulated sunlight (ε_C = −4.8 ± 0.1 ‰). The phototransformation of SMX with UV-C light did not cause significant isotopic fractionation. Consequently, it was possible to differentiate sunlight and UV-C light induced phototransformation of SMX. Thus, CSIA might be implemented to trace back wastewater point sources or to assess natural attenuation of SMX by sunlight photolysis. In contrast to the wavelength range, pH-dependent speciation of SMX hardly impacted isotopic fractionation. However, regarding phototransformation no further comprehensive insights in the underlying reaction mechanisms could be gained by CSIA. This is attributed inter alia to the presence of sulfur and nitrogen as reactive sites in SMX and the current inability to determine any other but *C*-isotope values by liquid chromatography isotope-ratio mass spectrometry (LC-IRMS).

Consequently, much simpler model compounds without nitrogen or sulfur-containing moieties, i.e. benzene and its methylated and methoxylated analogs, were used in order to further systematically characterize the abiotic oxidative processes using O_3, $^{\bullet}OH$ or ClO_2 with CSIA. Carbon isotope enrichments factors (ε_C) were determined for reactions with O_3 (ε_C = −3.6 ‰ to −4.6 ‰) and $^{\bullet}OH$ (ε_C = < −1 ‰). The differences in isotope fractionation may be used to elucidate the contribution of the reactions with O_3 or $^{\bullet}OH$ to the overall transformation. Subsequently, apparent kinetic isotope effects (AKIEs) were derived for the reaction with O_3. This was nontrivial due to challenges in assigning reactive positions in the probe compounds for the monodentate attack leading to an O_3 adduct. Several options for this step are presented and the outcome is compared to quantum chemical characterizations of O_3 adducts. The data show that a general assignment of reactive positions for reactions of O_3 with aromatic carbon in *ortho*, *meta* or *para* positions is not feasible and that AKIEs of this reaction should be derived on a compound-by-compound basis.

In conclusion, this work has illustrated the potential added value of CSIA to characterize oxidative and phototransformation processes. Simultaneously, it became obvious that the chemistry of allegedly simple reactions is not yet fully understood and that further research is required to enable us to understand reaction mechanisms and isotopic fractionation on a more holistic level.

Zusammenfassung

Oxidative Prozesse - Einblicke in Reaktionsmechanismen durch hochauflösende und Isotopenverhältnis-Massenspektrometrie

Oxidative und Phototransformationsprozesse tragen häufig zum Abbau von Mikroverunreinigungen in natürlichen oder technischen Systemen bei. Zur Sanierung kontaminierter Stellen oder in Wasseraufbereitungsverfahren werden beispielsweise Ozon (O_3), Hydroxylradikale ($^{\bullet}OH$), Chlordioxid (ClO_2) oder UV/VIS-Licht eingesetzt. Die zugrunde liegenden Reaktionsmechanismen, die für die Beurteilung der Bildung unerwünschter Transformationsprodukte (TPs) wichtig sind, sind jedoch größtenteils ungeklärt. Derzeit werden TP-Untersuchungen oft mit hochauflösender Massenspektrometrie (HRMS) durchgeführt, die die Bestimmung der TP-Summenformeln anhand der exakten Massen ermöglicht. Die reaktive Stelle bzw. der Angriffspunkt im Zielmolekül bleiben hierbei jedoch größtenteils unbekannt. Hier kann die verbindungsspezifische Isotopenanalytik (engl. compound-specific stable isotope analysis, CSIA) ein nützliches Instrument zur Aufklärung und weiteren Untersuchung von Reaktionen von Mikroverunreinigungen sein, da Abbauprozesse zu spezifischen Isotopenfraktionierungen führen können, die Rückschlüsse auf den Ort des Primärangriffs liefern. Daher untersucht diese Studie die Verwendung von CSIA und HRMS als komplementäre Instrumente zur Charakterisierung verschiedener Transformationsprozesse, um die zugrunde liegenden Reaktionsmechanismen aufzuklären.

Im ersten Schritt dient das Sulfonamidantibiotikum Sulfamethoxazol (SMX) als Modellverbindung, um die pH-abhängige Umwandlung durch die oben aufgeführten Transformationsprozesse systematisch zu untersuchen. SMX ist ein weit verbreiteter Mikroschadstoff in Oberflächen-, Grund- und Abwässern, der bei typischen pH-Werten der Wasseraufbereitung oder in natürlichen Gewässern als neutrale oder anionische Spezies auftritt.

Für die oxidativen Prozesse – O_3 in An- und Abwesenheit von $^{\bullet}OH$ sowie ClO_2 – mit SMX wurden systematisch die Reaktionsstöchiometrie, Produktbildung und Reaktionsmechanismen untersucht. Pro Mol abgebautem SMX wurden zwei Mol ClO_2 und ungefähr drei Mol O_3 verbraucht. HRMS Messungen zeigten, dass bei Oxidation von SMX mit O_3 und ClO_2 jeweils sechs Haupt-TPs gebildet werden. Vorläufig formulierte TP-Strukturen aus anderen Studien konnten teilweise durch CSIA bestätigt werden. Für ein TP, ein hydroxyliertes SMX, konnte jedoch durch HRMS allein nicht geklärt werden, ob eine Hydroxylierung am aromatischen Ring, wie in der Literatur zuvor vorgeschlagen, oder am anilinischen Stickstoff vorlag. Mit Hilfe von CSIA und einem analytischen Standard konnte

Sulfamethoxazolhydroxylamin eindeutig als eines der TPs der Reaktion von SMX mit O_3 sowie mit ClO_2 identifiziert werden. Für die Bildung werden die H-Abstraktion und der Elektronentransfer am anilinischen Stickstoff als wahrscheinliche Primärreaktionen von O_3 bzw. ClO_2 vorgeschlagen. Die Oxidation von anionischem SMX durch O_3 zeigte keine signifikante Isotopenfraktionierung, während die anderen untersuchten Reaktionen zu einer signifikanten Kohlenstoffisotopenfraktionierung (ε_C) führten (z. B. ε_C (O_3) = –2,2 ± 0,1 ‰ und ε_C (O_3 + $^{\bullet}OH$) = –1,2 ± 0,1 ‰).

Zur Untersuchung der Phototransformationsreaktionen der beiden relevanten SMX-Spezies wurden vier verschiedene Bestrahlungsszenarien verwendet: ein Nieder-, Mittel- und Hochdruck-Hg-Strahler sowie simuliertes Sonnenlicht. Die beobachtete Phototransformationskinetik war für die neutrale SMX-Spezies schneller als für die anionische (Faktor 3,4 (LP-Lampe) bis 6,6 (HP-Lampe)). Darüber hinaus wurden vier, für die direkte Photolyse von SMX bisher unbeschriebene, Phototransformationsprodukte (mit *m*/*z* 189, 202, 242 und 260) durch HRMS nachgewiesen. Eine Isotopenfraktionierung trat nur auf, wenn bei der emittierten Strahlung UV-B- und UV-A-Wellenlängen überwogen und war für die neutrale Spezies mit simuliertem Sonnenlicht am ausgeprägtesten (ε_C = –4,8 ± 0,1 ‰). Die Phototransformation von SMX mit UV-C-Licht verursachte keine signifikante Isotopenfraktionierung. Folglich lässt sich unterscheiden, ob Phototransformation von SMX durch Sonnenlicht oder UV-C-Licht induziert wurde. Somit könnte CSIA eingesetzt werden, um Abwasserpunktquellen zurückzuverfolgen oder die natürliche Verringerung von SMX durch Sonnenlichtphotolyse zu bewerten. Im Gegensatz zum Wellenlängenbereich beeinflusste die pH-abhängige Speziation von SMX die Isotopenfraktionierung kaum. In Bezug auf die Phototransformation konnte CSIA jedoch keine weiteren umfassenden Einblicke in die zugrunde liegenden Reaktionsmechanismen liefern. Dies begründet sich unter anderem durch die vorhandenen reaktiven Stellen an Schwefel und Stickstoff in SMX und die derzeitige Einschränkung mit der Flüssigchromatographie-Isotopenverhältnis-Massenspektrometrie nur C-Isotopenwerte bestimmen zu können.

Um die abiotischen Oxidationsprozesse O_3, $^{\bullet}OH$ oder ClO_2 mit CSIA weiter systematisch zu charakterisieren, wurden deshalb viel einfachere, stickstoff- und schwefelfreie Modellverbindungen gewählt: Benzol und seine methylierten und methoxylierten Derivate. ε_C-Werte wurden für Reaktionen mit O_3 (ε_C = –3,6 ‰ bis –4,6 ‰) und $^{\bullet}OH$ (ε_C = <–1 ‰) bestimmt. Die Unterschiede in der Isotopenfraktionierung können verwendet werden, um den Beitrag der Reaktionen mit O_3 oder $^{\bullet}OH$ zum Gesamtabbau aufzuklären. Anschließend wurden abgeleitete kinetische Isotopeneffekte (engl. apparent kinetic isotope effects, AKIEs) für die Reaktion mit O_3 abgeleitet. Dies war nicht trivial, da die reaktiven Positionen der Modellverbindung für den einzähnigen Angriff identifiziert werden mussten, an der das

O_3-Addukt gebildet wird. Es werden verschiedene Varianten für diesen Schritt vorgestellt und die Ergebnisse mit quantenchemischen Rechnungen von O_3-Addukten verglichen. Die Daten zeigen, dass eine allgemeine Zuordnung der reaktiven Positionen für Reaktionen von O_3 mit aromatischem Kohlenstoff in *ortho*-, *meta*- oder *para*-Positionen nicht möglich ist und dass AKIEs dieser Reaktion verbindungsspezifisch abgeleitet werden sollten.

Zusammenfassend hat diese Arbeit den potenziellen Mehrwert von CSIA zur Charakterisierung oxidativer und Phototransformationsprozesse veranschaulicht. Gleichzeitig wurde deutlich, dass selbst vermeintlich einfache Reaktionen mechanistisch noch nicht vollständig verstanden sind und dass weitere Untersuchungen erforderlich sind, um die Reaktionsmechanismen und die Isotopenfraktionierung umfassender zu verstehen.

Table of contents

Chapter 1 -

Introduction

1.1 Oxidative processes in water treatment

Oxidative processes have become an elementary corner stone of water treatment in the 21st century. Originally, oxidative processes were implemented in drinking water treatment chains for disinfection in order to supply customers with microbiologically safe drinking water, e.g. to decrease the threat of lethal diseases like typhus or cholera. In the further development, oxidants such as ozone or chlorine dioxide were also used for oxidation of iron (II), manganese (II) or arsenic[1-3]. Additional important fields of application are color removal and taste and odor control[4]. Nowadays, oxidative processes are also implemented in water treatment chains of drinking and wastewater treatment facilities for micropollutant control such as pesticides or pharmaceuticals. Common representatives are ozone, chlorine, chloramine, chlorine dioxide or UV-treatment. The striking advantages of oxidative processes are the combination of disinfection and micropollutant control as well as avoidance of treating concentrates or solids as it is the case for membrane filtration or sorption processes using activated carbon, respectively. Nevertheless, formation of undesired byproducts, i.e. disinfection byproducts (DBPs) or transformation products (TPs), as well as handling of partially toxic chemicals are remaining drawbacks of these sophisticated processes[2].

1.1.1 Ozone as oxidative agent

The generation of ozone for drinking water or wastewater treatment purposes is rather simple compared to e.g. chlorine or chlorine dioxide applications because no hazardous or toxic chemicals need to be stored on site. Ozone may be generated by electrolysis[5] or in the plasma of microdischarge columns in a silent discharge process[6,7] using dry oxygen (O_2) or air as feed gas. The latter generation process is most common for commercial ozone generators[2,8].

The initial reason for implementation of an ozonation treatment step in drinking water treatment processes was disinfection in the beginning of the 20th century. In 1906, the first ozonation plant was built at the municipal water works in Nice, France[9]. At the same time, several water treatment plants with ozonation unit were opened in Germany (e.g. Hermannstadt, Paderborn or Wiesbaden) which were closed after a couple of years due to lower costs of disinfection by chlorination[10]. Today, the dissemination of ozonation as a drinking water treatment step in industrialized countries varies widely. In countries such as France and Switzerland ozonation is one of the major steps in drinking water treatment whereas in, e.g., the USA or Japan this plays only a minor role[2].

Every ozonation process in drinking or wastewater treatment will lead to formation of hydroxyl radicals $\left(^{\bullet}OH\right)$ at the same time. However, the resulting $^{\bullet}OH$ quantity depends on the given conditions of the water such as the pH or content of dissolved organic matter (DOM)[11]. One possibility for $^{\bullet}OH$ formation is the reaction of ozone with hydroxide ions $\left(OH^{-}\right)$ (see Scheme 1.1 & 1.2). According to thermokinetic and quantum chemical calculations, it is most likely that O_3 and OH^{-} form an adduct (Reaction 1.1) prior the decay to a perhydroxyl radical $\left(HO_2^{\bullet}\right)$ and a superoxide anion $\left(O_2^{\bullet-}\right)$ (Equilibrium 1.2)[12]. The $HO_2^{\bullet}$ ($pK_a(HO_2^{\bullet})$ = 4.8) is in equilibrium with $O_2^{\bullet-}$ (Equilibrium 1.3)[13]. In reaction of $O_2^{\bullet-}$ with ozone, an ozonide radical anion $\left(O_3^{\bullet-}\right)$ is formed (Reaction 1.4)[14] which is the $^{\bullet}OH$ precursor (Scheme 1.2).

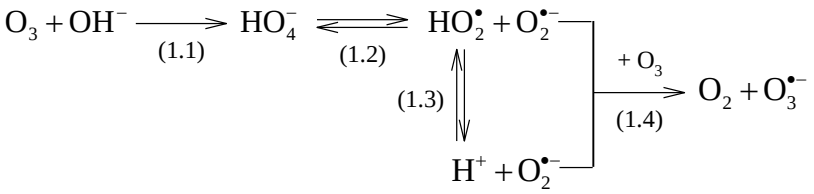

Scheme 1.1: Reaction of a hydroxide anion with ozone leading to formation of an ozonide radical anion[12-14].

The $O_3^{\bullet-}$ is in equilibrium with O_2 and $O^{\bullet-}$ in which the forward reaction rate constant is significantly slower than the backward reaction (Scheme 1.2, Equilibrium 1.5, k_5 = 1.9 x 10^3 s^{-1}, k_{-5} = 3.5 x 10^9 M^{-1} s^{-1})[15]. The resulting $O^{\bullet-}$ is in equilibrium with its conjugated acid, the $^{\bullet}OH$ (Equilibrium 1.6, $pK_a\left(^{\bullet}OH\right)$ = 11.8[2,16]). In contrast to $^{\bullet}OH$, only $O^{\bullet-}$ will react with O_2 so that the ultimate products of $O_3^{\bullet-}$ are O_2 and $^{\bullet}OH$ [2].

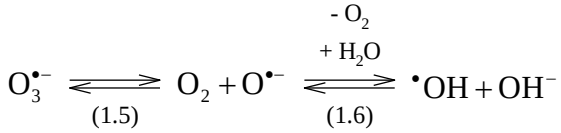

Scheme 1.2: Formation of a hydroxyl radical and hydroxide anion from an ozonide radical anion[2,15,16].

The hydroxide ion concentrations under environmental conditions, regularly found at pH 7-8, is low and the reaction rate constant of $k_{O_3+OH^-}$ = 70 M^{-1} s^{-1} [17] is comparably slow. Thus, the reactions depicted in Schemes 1.1 and 1.2 do not lead to significant generation of $^{\bullet}OH$ fed by OH^{-} found at typical water treatment conditions and may be neglected.

The kind and content of DOM of treated raw waters for drinking water or wastewaters plays a major role for $^{\bullet}OH$ formation during ozonation[18]. The electrophile O_3 will react with the electron-rich aromatic moieties contained in DOM (Scheme 1.3, Reaction 1.7)[2,11,19]. Several possible reaction pathways may lead to formation of an $O_3^{\bullet-}$ and a radical cation in the DOM fraction $\left([DOM]^{\bullet+}\right)$[2]. The $O_3^{\bullet-}$ will cause $^{\bullet}OH$ formation (Reactions 1.5 & 1.6). The radical cation reacts with water (cf. Norman et al.[20]) so that the $[DOM]^{\bullet+}$ is hydroxylated (Reaction 1.8). The remaining carbon centered radical $\left([DOM-OH]^{\bullet}\right)$ easily reacts with O_2 so that an additional superoxide is formed (Reaction 1.9). By consumption of one more O_3 molecule (Reactions 1.4-6) another $^{\bullet}OH$ will be formed. This particular pathway is called propagation[11]. The $^{\bullet}OH$ production will not cease when all electron-rich aromatic moieties in the DOM are hydroxylated[21]. The resulting phenols and phenolates will be involved in electron transfer to ozone so that further ozonide radical anions and thus significant quantities of $^{\bullet}OH$ are formed[22].

$$[DOM] \xrightarrow[(1.7)]{+\,O_3} [DOM]^{\bullet+} + O_3^{\bullet-} \xrightarrow[+\,H_2O\,(OH^-)]{-\,O_3^{\bullet-}} \xrightarrow[(1.8)]{-\,H^+} [DOM-OH]^{\bullet} \xrightarrow[(1.9)]{+O_2} [DOM-OH]^{+} + O_2^{\bullet-}$$

Scheme 1.3: Reaction of DOM with ozone and the initiation of the propagation reaction sequence[2,11,20,21].

In order to increase the $^{\bullet}OH$ yield in an ozone based oxidative process, hydrogen peroxide (H_2O_2) may be added (Scheme 1.4). This is termed peroxone process - one of the "advanced oxidation processes" (AOPs)[2,23]. The reaction of O_3 with H_2O_2 itself is very slow ($k_{O_3+H_2O_2}$ < 0.01 M^{-1} s^{-1}) contrary to the fast reaction with its anion, HO_2^- ($k_{O_3+HO_2^-}$ = 5.5 x 10^6 M^{-1} s^{-1})[17]. Thus, for generation of $^{\bullet}OH$ in the peroxone process, only the dissociated species is of relevance (Equilibrium 1.10, p$K_a(H_2O_2)$ = 11.8[24]). Lately, it has been shown that the formation of the adduct HO_5^- is very likely (Reaction 1.11). Hereafter, HO_5^- decomposes either into O_2 and OH^- (Reaction 1.13), so that no $^{\bullet}OH$ are formed, or to $HO_2^{\bullet}$ and $O_3^{\bullet-}$ (Reaction 1.12)[16,23] which will lead to $^{\bullet}OH$ formation (Reactions 1.5-6).

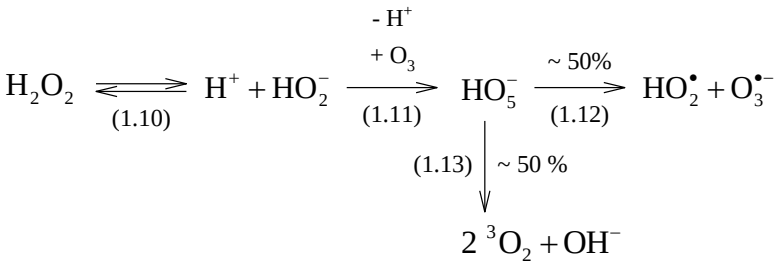

Scheme 1.4: Relevant reactions in the peroxone process[16,17,23]

Ozone is a highly selective oxidative agent. Preferred reactive sites of organic compounds are double bonds of olefins, activated aromatic systems, reduced sulfur moieties and deprotonated amines[2,11]. There are several possible primary reactions of ozone with such compounds. Regularly observed pathways are shown in Schemes 1.5-8. However, a much more detailed and comprehensive description can be found in von Sonntag and von Gunten[2]. The most prominent reaction pathway is the Criegee reaction which is usually found for olefins (Scheme 1.5) and is also observed for aromatic compounds (Scheme 1.6, Reactions 1.17 & 1.21). The reaction pathway may proceed via a zwitterion as intermediate (Reactions 1.14 & 1.15 or 1.17 & 1.21) or as concerted attack (Reaction 1.16). The result of any of the aforementioned cases will be an instable ozonide and its stepwise breakdown[2,11].

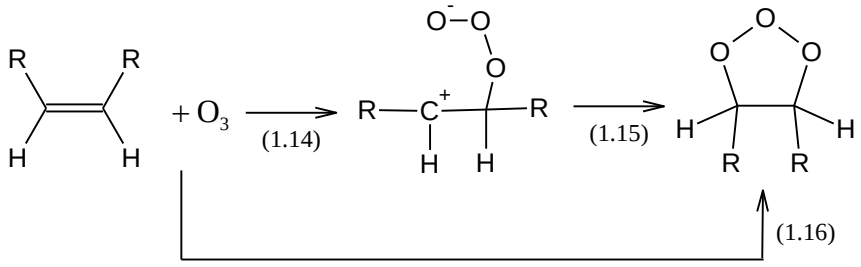

Scheme 1.5: Primary reactions of ozone with olefins[2,11]; "R" may be a placeholder for an H-atom or an organic moiety.

Further common reaction pathways after an adduct formation through electrophilic addition (Reaction 1.17) are either its dissociation into a radical cation and $O_3^{\bullet-}$ (Reaction 1.18) or the formation of an oxyl radical and $O_2^{\bullet-}$ (Reaction 1.19). Moreover, an oxygen transfer, leading to hydroxylation of the compound, and singlet O_2 as product is regularly found as well (Reaction 1.20). Additionally, the formation of a radical cation and $O_3^{\bullet-}$ is also feasible via a direct outer sphere electron transfer (Reaction 1.22)[2,11].

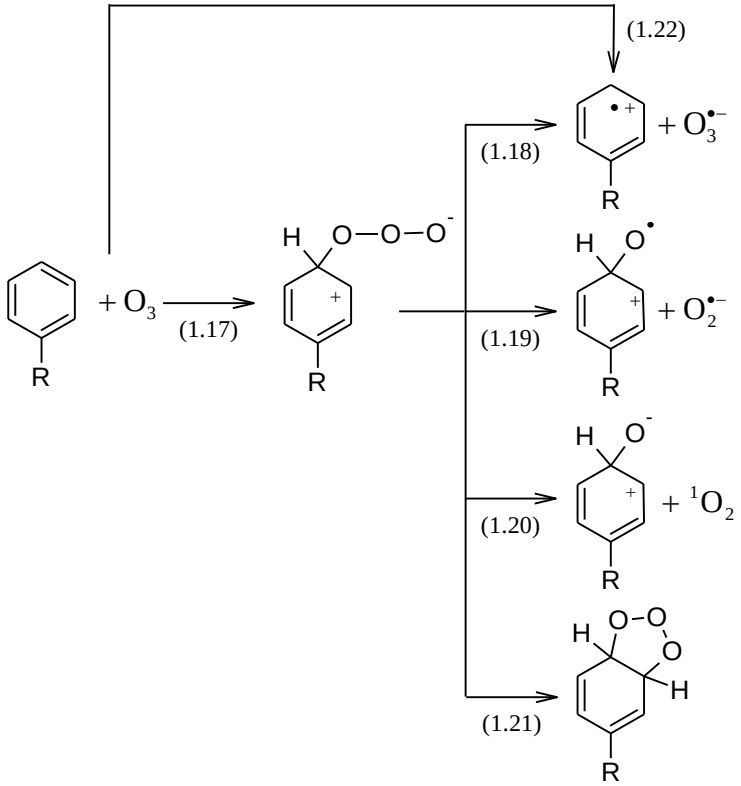

Scheme 1.6: Primary reactions of ozone with aromatic compounds[2,11]; "R" may be a placeholder for an H-atom, other organic or inorganic substituents or another aromatic moiety. Please note that "R" could also be placed in *ortho* or *meta* position and it is also possible that there are further substituents located at the aromatic ring instead of solely H-atoms.

Aliphatic and aromatic amines show a high reactivity towards ozone. However, in any case it is important that the lone ion pair is readily accessible for the oxidant. In the first step an adduct is formed which is exemplarily shown in Reaction 1.23 (Scheme 1.7). This adduct shares some of the decomposition pathways similarly to the ozone adducts of the aromatic compounds (cf. Scheme 1.6). This includes hydroxylation of the amine and loss of O_2 (cf. Reaction 1.20) or formation of an amine radical cation and $O_3^{\bullet-}$ (cf. Reaction 1.18). The latter reaction might also proceed directly via electron transfer (cf. Reaction 1.22). If aromatic amines i.e. anilines react with ozone an insertion reaction is also likely (Scheme 1.7), either after adduct formation (Reaction 1.23 & 1.24) or directly (Reaction 1.25)[2,25]. However, besides attack of ozone at the anilinic moiety a reaction at the aromatic ring is also highly likely due to the strong activation of the aromatic system by its substituent. A detailed description of the above mentioned and further reaction pathways of anilines with ozone can be found in Tekle-Röttering et al.[25].

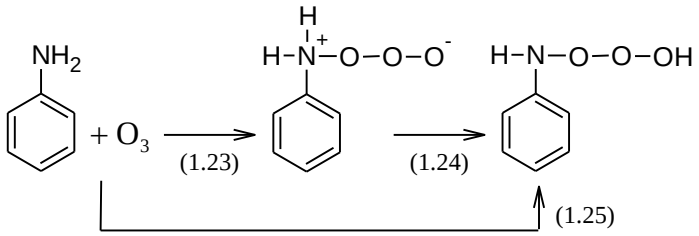

Scheme 1.7: One of the common primary reactions of ozone with the anilinic moiety of aromatic amines termed as insertion[2,25].

In case of sulfur, only reduced sulfur species show significant reaction rates with ozone. For sulfides, disulfides and sulfinic acids the depicted reaction mechanism in Scheme 1.8 (Reactions 1.26 & 1.27) is the only possible pathway since a 100 % yield of singlet oxygen is obtained (Reaction 1.27)[26]. For thiols the singlet oxygen yield is found around 50 % so that it was speculated that additionally to the mechanism shown in Scheme 1.8 another competing reaction occurs including an oxygen transfer, as it was suggested for ozonation of bisulfide[27]. However, this needs to be proven in future studies[2]. Lastly, the reactivity of sulfoxides with ozone is slow to insignificant so that such compounds appear to be ozone refractory in water treatment[2].

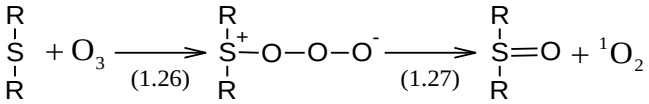

Scheme 1.8: Primary reactions of ozone with sulfides, disulfides and sulfinic acids[2]; "R" may be a placeholder for an H-atom or an organic or aromatic moiety.

Reaction rate constants range between very low to insignificant for compounds without a moiety of the abovementioned kind[28] so that such compounds are often termed ozone refractory[2,11]. As it has been shown above, the highly reactive and unselective $^{\bullet}OH$ is formed in many ozone related reactions and processes (e.g., Scheme 1.3). The main reaction pathway is addition[29] - preferably to C—C, C—N or S—O double bonds (e.g. Scheme 1.9, Equilibrium 1.28 & Reaction 1.29)[2,30,31] except for C—O double bonds which are unreactive towards an $^{\bullet}OH$ attack[2]. Moreover, electron-rich heteroatoms with lone ion pairs such as in amines or sulfides are also highly susceptible to addition reactions. Reaction rate constants of $^{\bullet}OH$ addition reactions are usually found at close to diffusion-controlled rates[2,32]. If an addition reaction is kinetically not feasible, a usually slower H-abstraction (e.g. Reaction 1.30) or a rather barely found electron transfer reaction may take place instead[2].

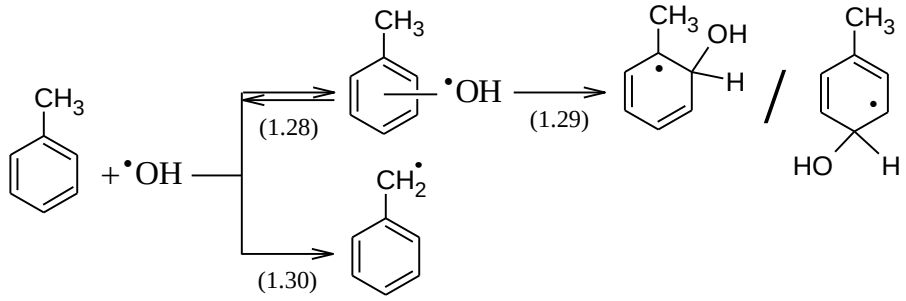

Scheme 1.9: Addition and H-abstraction reaction of an $^{\bullet}OH$ attack at toluene[33].

The presence of two different oxidative agents, i.e. ozone and $^{\bullet}OH$, in the ozonation process allows oxidation of a high variety of different compounds. However, if oxidation reactions of ozone alone are to be studied it is necessary to scavenge the formed $^{\bullet}OH$ adequately. Therefore, scavengers are necessary which show a high reactivity towards $^{\bullet}OH$ and are unreactive with ozone. Suitable candidates are *tertiary* butanol (*tert*-BuOH) or dimethyl sulfoxide (DMSO)[2]. Methanol fulfills these two requirements as well but leads to generation of $O_2^{\bullet-}$ which will additionally consume ozone (Reaction 1.4) and lead to formation of further $^{\bullet}OH$ [34], thus should not be used as scavenger in ozone-based systems. Nevertheless, methanol may be found as $^{\bullet}OH$ scavenger even in recent literature[35] so that $^{\bullet}OH$ yields were consequently overestimated.

Currently, ozone is the best chemical disinfectant in drinking water treatment[2,36]. Contrary to chlorine or chlorine dioxide, ozone is capable of inactivating pathogenic microorganisms such as protozoa, e.g. *Cryptosporidium parvum oocysts* or *Giardia spp*. under certain water treatment conditions[36]. Exemplarily, to obtain a 3-log reduction of *Giardia cysts* at 10 °C a CT value, i.e. residual concentration of oxidant [mg L^{-1}] multiplied by contact time [min], of 1.43 mg min L^{-1} ozone, 23 mg min L^{-1} chlorine dioxide and even 104 mg min L^{-1} chlorine have to be reached[37]. Ozone is a highly selective oxidant which is capable of entering the microbial cells. Here, it reacts with the nucleic acids of the DNA and RNA. The highest reaction rate has been determined for the neutral species of thymine ($k_{O3+thymine}$= 4.2 x 10^4 M^{-1} s^{-1}) and the overall reaction rate of ozone with DNA was found at k_{O3+DNA}= 4.1 x 10^2 M^{-1} s^{-1} [2,38]. Contrary to ozone, $^{\bullet}OH$ are not suitable as disinfection agents since their steady state concentration and their selectivity are too low. Consequently, $^{\bullet}OH$ have already reacted with outer cell compartments which are easily restored by the pathogens before $^{\bullet}OH$ would be able to find their way to the DNA or RNA to cause significant harm to the microorganism.

1.1.2 Chlorine dioxide as oxidative agent

The generation of chlorine dioxide (ClO_2) requires somewhat more effort than the generation of ozone. Due to the explosive nature of ClO_2, long term storage is undesirable. The critical aqueous concentration is > 10 g L^{-1} and 10 % in the gas phase[1]. For large-scale applications in water treatment ClO_2 is mostly produced by mechanical generators. Here, mostly sodium chlorite $(NaClO_2)$ is mixed with either gaseous chlorine $(Cl_{2(g)})$ (Reaction 1.31), hypochlorous acid $(HOCl)$ (Reaction 1.32) or hydrochloric acid (HCl) (Reaction 1.33). ClO_2 will be formed in the course of Reactions 1.31-33[1,37,39].

$$2NaClO_2 + Cl_{2(g)} \rightarrow 2ClO_{2(g)} + 2NaCl \quad (1.31)$$

$$2NaClO_2 + HOCl \rightarrow 2ClO_{2(g)} + NaCl + NaOH \quad (1.32)$$

$$5NaClO_2 + 4HCl \rightarrow 4ClO_{2(g)} + 5NaCl + 2H_2O \quad (1.33)$$

The Reactions 1.31-33 represent ideal conditions without any byproduct formation. Depending on the efficiency of the generator it may also be possible that unreacted chlorite (ClO_2^-) remains in the solution or that chlorate (ClO_3^-) or $HOCl$ are formed in side reactions[1,37]. Formation of $HOCl$, free chlorine, may lead to enhanced formation of chlorinated DBPs[4,40]. The elevated presence of chlorite and chlorate may result in exceedance of threshold limit values of given regulations, e.g. 0.2 mg L^{-1} ClO_2^- for German[41] or 1 mg L^{-1} ClO_2^- for US drinking water[42]. Mechanical generators are capable of reaching ClO_2 production efficiencies of > 90 % with these chlorine based methods described above[39]. However, also a generation method which produces chlorine-free ClO_2 solutions is known in which $NaClO_2$ is oxidized by persulfate. The produced ClO_2 is purged into chilled ultrapure water and remains stable if the solution is maintained cool and in the dark[1]. This method is mostly known for bench- or pilot-scale applications. Recently, also a patented variation of this bench method has become available on the market. Herewith, elevated levels of ClO_2^-, ClO_3^- or $HOCl$ are not introduced into the treated water due to the ClO_2 generation method[43].

Since its first discovery in 1811 it took more than one century until it was possible to implement ClO_2 in a drinking water treatment process. The reason for this was the lack of commercially available $NaClO_2$[1,39]. In the beginning, ClO_2 was used as substitute for

chlorine for disinfection of phenol containing waters. Large excess of chlorine would be necessary in order to avoid the undesired chlorophenol formation[44]. In case of ClO_2 much lower doses could be applied and olfactory or gustatory flaws of the treated water were avoided[45,46]. Additionally, it was believed that chlorinated DBPs will not form at all if ClO_2 is applied. . However, more recent studies have shown that this assumption cannot be fully verified[40,45,47].

Nowadays in Europe, ClO_2 is regularly used for secondary disinfection of finished drinking water, i.e., prior to water distribution to the drinking water network to maintain a residual disinfection. This is done in order to maintain the water quality and prevent microbial recontamination from deficient pipe systems[48]. In case of a fully functional distribution network, it may be even possible to renounce secondary disinfection with chlorine based disinfectants and solely keep these options available in case of emergency as, e.g., in the Mülheim process[2]. Contrary to Europe, in the United States of America and Canada ClO_2 is often used for preoxidation of raw waters for drinking water treatment[1,37,49].

As it has been shown for ozone above, ClO_2 is a highly selective oxidative and electrophilic agent, too. As a peculiarity, solely single electron transfer reactions have been proposed in literature of ClO_2 with its reactants which is described in the following. High reaction rates are observed for phenolates and many of its derivatives[48,50], anilines[51], neutral tertiary amines[52,53], reduced sulfur species such as thiolates[54] or some polycyclic aromatic compounds[55]. In general, as it is also observed for the electrophile ozone[2], reaction rate constants of ClO_2 with weak acids, e.g. phenols or thiols, and weak bases are strongly dependent on speciation (e.g. Scheme 1.10, Equilibrium 1.34) and thus on surrounding pH conditions[48,54]. Depending on the substituents of the phenolates, the reaction rate constants with ClO_2 are between five (4-acetylphenol) and up to nine orders of magnitude (2-hydroxyphenol) higher than for the neutral species[50]. It has been proposed that the oxidation of phenolates is initiated by a single electron transfer from the deprotonated oxygen of phenolate to ClO_2 so that ClO_2^- and a phenoxy radical are formed (Scheme 1.10, Reaction 1.35). The phenoxy radicals may either react with a second ClO_2 thus leading to formation of $HOCl$ and *p*-benzoquinone or more rarely to *o*-benzoquinone (Reaction 1.36) or the phenoxyl radicals are subjected to irreversible coupling reactions with each other or the surrounding substrate (Reaction 1.37)[4,40,50].

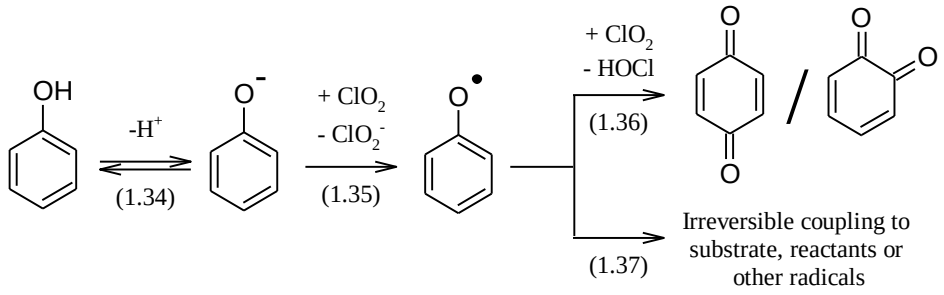

Scheme 1.10: Oxidation of phenolate by chlorine dioxide through electron transfer and further oxidation to *o*- or *p*-quinones or terminating coupling reaction[4,40,48].

Regarding possible reaction pathways of thiolates, Ison et al.[54] proposed that the initial oxidation reaction of ClO_2 with cysteine and glutathione is a single electron transfer at the deprotonated sulfur group. The resulting thiyl radical will react with another ClO_2 to form an adduct. However, depending on the pH different decay reactions of the adduct have been proposed. At acidic pH in case of cysteine, sulfinic acid and $HOCl$ are formed as intermediates leading to cysteic acid and Cl^- as detectable products. At basic pH, the thiyl radical reacts with the anionic cysteine species to form cystine and ClO_2^-[54]. This case illustrates the additional gain in information for mechanistic studies of ClO_2 reactions if additionally to organic product analyses inorganic chlorine species are identified and quantified as well.

In case of amines, the reaction rate constants with ClO_2 decrease from tertiary over secondary to very slow and thus mostly negligible reaction rate constants of primary amines[51,52]. In the reaction of one tertiary amine usually 2 moles of ClO_2 are consumed. Hull et al.[53] proposed that after a reversible single electron transfer from the lone ion pair of the nitrogen, ClO_2^- and an aminium radical cation are formed (Scheme 1.11, Equilibrium 1.38). By consumption of a second ClO_2, the aminium radical cation is converted to an imine (Reaction 1.39)[53].

This reaction pathway may also be applicable for secondary aliphatic amines[45]. A comparable reaction pathway has been proposed by Rosenblatt et al.[52] for arylic tertiary amines. In this case the moiety R^3 (Scheme 1.11) would represent an arylic substituent. However, the reaction mechanisms in Scheme 1.11 have not been proven yet, and are based on suppositions.

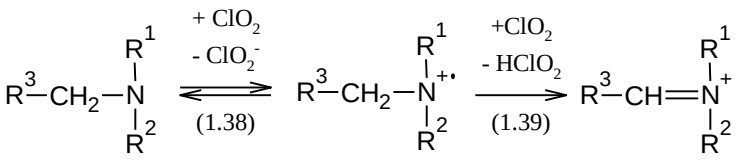

Scheme 1.11: Proposed oxidation reaction of chlorine dioxide with aliphatic tertiary amines (Reaction 1.35 & 1.36) which may also apply for aliphatic secondary amines[45,53].

Rav-Acha and Blits[55] have found strong evidence that oxidation of aromatic hydrocarbons by ClO_2 is solely possible by single electron transfer and thus only compounds which are prone to facile oxidation such as anthracene in contrast to the unreactive fluoranthene may act as reaction partners[55]. This is opposite to oxidation of the same compound class with Cl_2 which may react via various mechanisms such as single electron transfer, addition or electrophilic substitution[55,56].

The benefits of disinfection with ClO_2 are often compared to those of chlorine. First, ClO_2 does not show such a strong pH dependency for the disinfection efficacy such as chlorine (pK_a ($HOCl$) = 7.54[57]) does. In case of chlorine only the non-dissociated species, $HOCl$, is effective. Second, ClO_2 is equally or more efficient against *Giardia cysts*, as illustrated above, and significantly more efficient against *Cryptosporidium oocysts* than chlorine which has only little impact on reduction of protozoa at all[37]. Another often mentioned point is lowered formation of chlorinated DBPs. This is especially true for trihalomethanes[1,37]. It has been shown that treatment of the same drinking water matrix with ClO_2 yielded much less total organic halides (TOX) than in case of Cl_2[58,59]. The formation of TOX at all, was attributed to formation of $HOCl$ in the reaction of ClO_2 and its reaction with organic material later on[58].

On the other hand, some possible disadvantages have to be dealt with, e.g. that production costs for chlorine are lower than for ClO_2. For conventional ClO_2 production storage of two to three chemicals is necessary in comparison to only one for chlorination. The operator needs to be trained more intensely and required mechanical equipment is more sophisticated[1,37].

1.1.3 Photooxidation by various light sources

Besides chemical disinfection and oxidation processes such as ozonation, chlorination or chlorine dioxide use described before, photooxidation may be used as a physical treatment step, especially in drinking water treatment[41,60]. For treatment of drinking water low pressure

(LP) and medium pressure (MP) Hg lamps are permissible in Germany within a wavelength range of 240-290 nm[41]. LP Hg lamps emit virtually monochromatic light at 253.7 nm. Without usage of any filters, MP Hg lamps emit a polychromatic spectrum over the whole UV range (200-400 nm) with a generally higher intensity of the broad spectrum compared to LP lamp emission and with several intensive peaks within the overall spectrum[61]. In the USA these are also the lamp types typically used in water treatment[60].

The first reported large scale application implementing a photoreactor was opened in Marseille (France) in 1910. However, subordinating to technical shortcomings and improper UV lamps, the photoreactor had to be closed shortly after its launch. Due to the low costs of chlorination and the aforementioned problems, it lasted until 1955 until the first modern photoreactors using low-pressure UV lamps were installed in Switzerland and Austria[60,62].

The primary aim of photoreactors in drinking water treatment plants is disinfection of the pretreated drinking water. Moreover, UV disinfection is highly effective in inactivation of the drinking water critical protozoa *Giardia lamblia* cysts or *Cryptosporidium parvum* oocysts[60,63]. Inactivation of microorganisms and thus disinfection is achieved by ultraviolet (UV) radiation between 200 and 400 nm[62], i.e. UV-A (315-400 nm), UV-B (280-315 nm) and UV-C (200-280 nm) radiation[60,62]. Nucleosides and nucleotides, the basic building blocks of RNA and DNA absorb UV radiation very well[62,64], and the light absorption maximum of DNA was found slightly below 260 nm[62]. Consequently, the virtually monochromatic LP Hg lamp (λ = 253.7 nm) as well as the polychromatic MP Hg lamp are highly efficient for inactivation of microorganisms[60]. The absorption of UV light causes structural changes in the genetic material and e.g. leads to dimerization of adjacent thymine bases in case of DNA or cross links between the DNA strand and a protein. As a result, the microorganisms are incapable of replicating[60,62].

As a potential drawback, most microorganisms and viruses are capable of repairing or bypassing damages induced by UV-light — termed as dark and photoreactivation. In photoreactivation, the most common mechanism, UV-A light triggers the production of the enzyme photolase which splits the thymine dimers again. For dark reactivation no light absorption is required. Here, damaged DNA nucleotides (e.g. nucleotide dimers) are removed and replaced or a damaged DNA strand is partially resynthesized and replaced[62]. However, dark and photoreactivation may be substantially reduced if MP (Hg) lamps are employed rather than LP (Hg) lamps[65]. This discrepancy may be explained by several possible reasons. The polychromatic light of the MP (Hg) lamp may result in increased DNA and, maybe even more important, significant protein damage compared to the effect of a LP (Hg) lamp[66,67]. The latter also includes the required repair enzymes for photoreactivation.

In order to enable photochemical reactions through direct photolysis by (UV) light it is inevitable that the respective molecule absorbs light within this wavelength range. This necessity is termed the Grotthus-Draper law or the first law of photochemistry. If no (UV) light absorption occurs, no direct photochemical reaction is initiated if this component is exposed to the light source[62,68]. If (UV) light has been absorbed by a molecule, the molecule will change from its singlet ground state to an excited singlet state. Thereafter, the molecule may return to its ground state either by photon emission (fluorescence) or release of heat (internal conversion) followed by further energy release through vibronic relaxation. As a further possibility, the excited state may convert by intersystem crossing to another excited triplet state and is either followed by vibronic relaxation or emits photons (phosphorescence) in order to return to the ground state again. Last but not least, the energy of the molecule in the excited state, i.e. excited singlet or triplet state, may also lead to its transformation by monomolecular or bimolecular reactions, i.e., a photochemical reaction or phototransformation occurs[69]. The relation of moles of molecule that undergo a phototransformation and moles of photons, i.e., einstein, absorbed is termed quantum yield (Equation 1.40)[62,68].

$$\Phi = \frac{\text{moles of molecule transformed [mol]}}{\text{moles of photons absorbed [einstein]}} \tag{1.40}$$

Under environmental conditions phototransformation is induced by sunlight. The available wavelengths (λ) range from 800 nm in the near infrared to 290 nm of UV-B radiation. The lower limit of 290 nm is given by the UV absorption of the ozone layer in the earth's atmosphere which mostly absorbs radiation of $\lambda < 290$ nm. The available energy of one mole photons depends on the (UV) light's wavelength, the shorter the wavelength the higher is the energy, e.g. 150 kJ mol^{-1} ($\lambda = 800$ nm) and 414 kJ mol^{-1} ($\lambda = 290$ nm)[68].

To be able to quantitatively compare phototransformation rate constants or judge the efficiency of a photoreactor in a water treatment plant it is necessary to determine the fluence rate, i.e. how many photons are available per area and time in a given irradiation system (Equation 1.41)[70,71]. For determination of the fluence rate physical or chemical actinometers may be employed. Physical actinometers require regular checks and recalibration whereas chemical actinometers are highly reproducible but require experience at chemical techniques[72]. Usually, chemical actinometers are used at low optical density for characterization of photoreactors in water treatment[70] or environmental processes[72]. Depending on the wavelength or wavelength range different well characterized chemical actinometers are available. For example, for characterization of LP (Hg) lamps uridine[70,72,73] and for sunlight in aquatic systems either *p*-nitroacetophenon-pyridine (PNAP/pyr) or

p-nitroanisole-pyridine (PNA/pyr)[68,74,75] are well-known choices. For determination of fluence rates at low optical density of polychromatic irradiation sources such as MP (Hg) lamps covering the visible as well as the whole UV-range currently no suitable chemical actinometers are available. Here determination could only be obtained by polychromatic quantum counters. However, also these do not cover such large wavelength ranges so that this approach is in principle possible if several ones are available but the determination is laborious and not suitable for daily laboratory use[72].

$$E^0_{p,\lambda} = \frac{-k_{p,\lambda}(\text{chemical actinometer})}{2.303 \cdot \varepsilon_\lambda(\text{chemical actinometer}) \cdot \phi_\lambda(\text{chemical actinometer})} \tag{1.41}$$

$$E^0_{p,\lambda} = \text{fluence rate}\left[\text{einstein m}^{-2}\ \text{s}^{-1}\right]$$

$$-k_{p,\lambda}(\text{chemical actinometer}) = \text{first order deg radation rate}\left[\text{s}^{-1}\right]$$

$$\varepsilon_\lambda(\text{chemical actinometer}) = \text{molar absorptioncoefficient}\left[\text{m}^2\ \text{mol}^{-1}\right]$$

$$\phi_\lambda(\text{chemical actinometer}) = \text{quantum yield}\left[\text{mol einstein}^{-1}\right]$$

Additionally to disinfection, UV irradiation in water treatment plants or incident sunlight on surface waters may cause phototransformation of potentially present micropollutants such as pesticides or pharmaceuticals[76,77]. In order to facilitate phototransformation of micropollutants the absorbed light has to be of sufficient energy to promote an excited singlet state or triplet state after intersystem crossing. Besides the decay processes above, homolysis, heterolysis or photoionization are possible ways for transformation[78]. Further possible phototransformation mechanisms are photoinduced hydrolysis, isomerization, cyclization or rearrangement by e.g. photo-Fries, photo-Claisen or Beckmann rearrangement[79].

In general, phototransformation and the underlying mechanisms may differ strongly depending on the available (UV) radiation due to the reasons described above[79]. Nevertheless, even if preferable sites for cleavage have been identified for a compound class there are still many variations observed in the preferred phototransformation pathways of the single compounds if these have individual substituents or additional acidic, zwitterionic or basic moieties[78,79].

A further possibility for oxidation in direct photolysis processes is formation of reactive oxygen species such as singlet oxygen $\left({}^1O_2\right)$ or $O_2^{\bullet-}$. ${}^1O_2$ is formed if energy is transferred from a compound in an excited triplet state to a triplet oxygen $\left({}^3O_2\right)$ whereas $O_2^{\bullet-}$ is received if ${}^3O_2$ is subjected to photoelectrontransfer[69]. Both oxygen species can be converted into each other by transfer or abstraction of an electron, respectively[69]. Since

water treatment plants and phototransformation by sunlight will always happen under oxic conditions, $^1O_2$ and $O_2^{\bullet-}$ need to be considered as additionally available powerful oxidants. In indirect photolysis, further reactive oxygen species such as $^{\bullet}OH$ may be formed if DOM or nitrate are present[78,80]. However, indirect photolysis is not part of the presented work so that it will not further be tackled in the following.

1.1.4 Oxidative processes with regard to disinfection by-product formation and degradation of micropollutants

Today, a high number of different oxidative processes for water treatment are known, e.g. chlorine, chloramine[56], chlorine dioxide[1], permanganate[81], O_3 alone or as AOP in combination with H_2O_2 or UV radiation to increase the formation of $^{\bullet}OH$ [2,11] or UV radiation alone or in combination with H_2O_2 or $S_2O_8^{2-}$ to produce $^{\bullet}OH$ [82,83] or sulfate radicals[84], respectively.

Under certain conditions the chemical oxidation processes have all known DBP formation issues. In case of chlorine, trihalomethanes (THMs) or haloacetic acids (HAAs) may be formed in reactions with DOM[56,85]. These DBPs have been potentially linked to, e.g., bladder cancer[86] asthma, or miscarriages among many other health impacts[87]. Ozone is capable of reducing the DBP quantities such as chlorophenols or bromophenols, THMs or HAAs if it is used prior to post-chlorination. Nevertheless, ozone may also increase the formation of certain DBPs. The two most prominent ones are bromate and *N*-nitrosodimethylamine (NDMA)[2,36]. Both have been recognized as potential and suspected human carcinogens, respectively. Bromate has been regulated to a provisional guideline drinking water standard of 10 µg L^{-1} [88] which is also included in the German drinking water regulation as maximum permissible value[89]. Moreover, in case of NDMA a guideline value was set to 0.1 µg L^{-1} [88] and additionally a notification level of 10 ng L^{-1} was assigned by the California Department of Public Health[90]. If chlorine dioxide is used as substitute for chlorine in order to reduce THM formation chlorite and chlorate may be formed in exchange[1,37]. However, it is possible to control the DBP formation if the source water has been properly characterized prior to chemical oxidation and if the generation process of the chemical oxidant is properly adjusted.

With regard to micropollutant control, the usually applied oxidant doses in water treatment are insufficient to cause full mineralization of the majority of the relevant micropollutants but may lead to transformation products instead[40,91,92]. In general, von Gunten has elaborated that there may be three possible outcomes if TPs are formed from micropollutants giving illustrative examples[93]. First and most desirable, the TP loses the biological activity of the

parent compound as it was observed for ozonation of antibiotics[94,95] or estrogenic compounds such as 17α-Ethinylestradiol[96]. Second, the resulting TP is another (potentially) regulated, more toxic compound. A case in point is the chlorination of the antimicrobial triclosan which leads to formation of chloroform among other chlorinated TPs[97,98]. For instance, the German drinking water regulation limits the sum of chlorine and bromine containing trihalomethanes to 50 µg L^{-1} [89]. Third, a toxic or bioactive TP is formed from a low biologically active parent compound. Such a case is observed for ozonation of the nontoxic metabolite *N,N*-dimethylsulfamide originating from the fungicide tolylfluanide which leads to formation of the genotoxic NDMA[99]. Consequently, not all micropollutant borne problems in drinking and wastewater treatment may be overcome by oxidative processes or are even caused by them.

1.1.5 High-resolution mass spectrometry for identification of transformation products

Today, high-resolution mass spectrometry (HRMS) is a well-established tool in environmental analyses for screening and identification of unknown micropollutants[100,101] as well as their TPs[102-105] and rarely, albeit with increasing tendency, for quantification of known target analytes[105-107].

High resolving power (*R*) (20.000 up to 2.000.000 *R* at full width at half maximum), mass resolution accuracy (3-1 ppm) and sensitivity (pico- to femtogram range) are key features of HRMS in a typical mass-to-charge-ratio range of 300-400[108,109]. The most recognized three HRMS instrument options differ mainly in regard to the resolving power. These are quadrupole time of flight mass spectrometer (qToF; 10.000-60.000 *R*; 1-5 ppm)[102,110,111], linear ion trap/orbitrap (LTQ Orbitrap; >450.000 *R*; < 2 ppm)[109,111,112] and Fourier transform ion cyclotron resonance mass analyzers (FT-ICR; 2.000.000 *R*; < 1 ppm)[109]. Even though FT-ICR mass analyzers offer currently the highest available resolving power and mass resolution accuracy, they represent also the most cost-intensive option which is the reason for the increased application of the less expensive LTQ Orbitrap[108,109]. Gas or liquid chromatography (GC, LC) may be coupled to all HRMS options listed above in order to separate analytes from each other prior to mass spectrometric analysis[106,107]. However, coupling of fast chromatographic separation is not possible for FT-ICR mass analyzers due to the elongated scan times which are required to obtain the extraordinary high resolving power[113]. Generally, LC separation dominates the field of water analysis by HRMS at the moment[106,107].

Generally, by means of HRMS, the exact mass of a TP may be determined so that it is possible to derive the most probable sum formulas and, eventually, to formulate tentative TP

molecule structures[114,115]. These structures remain tentative until the probable molecule structures have been verified by an analytical standard with regard to retention time and fragmentation spectra or other analytical techniques such as nuclear magnetic resonance or infrared spectroscopy[107,108].

Despite the remarkable advantages of HRMS, there are also some shortcomings and limitations to be faced[108]. Exemplarily, the occurrence of false negatives, i.e. a compound present in the sample is not identified, cannot be excluded easily[101,108]. Such a case may occur if isobaric substances, i.e. substances with the same exact mass, are present in an analytical run. These isobaric substances have the same molecular formula and may even share a highly similar structure. In the latter case chromatographic separation is hardly possible and differentiation of isobaric substances becomes challenging as illustrated by Schymanski et al. for triazine-derivative herbicides and their TPs[101]. Fragmentation experiments, i.e. MS^n-experiments, represent a possible solution to distinguish some isobaric substances[100,102,104]. Nevertheless, if different collision energies do not lead to specific fragmentation products but, e.g., only to CO_2 or H_2O or highly similar analytes result in similar fragmentation spectra, this approach is not expedient[108]. These circumstances may pose a problem in identification of transformation pathways of oxidative processes. Due to the potential formation of isobaric TPs, the initial point of attack of the oxidant at the reactive site(s) of the detected TPs may often remain ambiguous. The oxidation of the antibiotic sulfamethoxazole by various oxidants illustrates this case[116]. Additionally, several oxidative processes may lead to formation of similar TPs which do not necessarily need to be formed by the same reaction pathways. In order to investigate the underlying mechanisms or to distinguish between several degradation processes compound-specific stable isotope analysis (CSIA) has been shown to be a useful proxy[117-119] (compare also chapter 2.4 below “CSIA: Current fields of application - use and limits”).

1.2 Stable Isotope Analysis

1.2.1 Delta notation and normalization

Stable isotope ratio measurements are obtained by determining the ratio of the light and the heavy isotope of an element. In order to express the stable isotope ratio measurement values according to internationally used scales, i.e. the delta scale (δ-scale), it is inevitable to use reference materials (Equation 1.42). The δ-scale is usually expressed in per mil [‰], i.e. parts per thousands[120].

$$\delta^{\text{heavy}}\text{E}_{\text{c,ref}} = \frac{\text{R}_\text{c}\left({}^{\text{heavy}}\text{E} / {}^{\text{light}}\text{E}\right) - \text{R}_{\text{ref}}\left({}^{\text{heavy}}\text{E} / {}^{\text{light}}\text{E}\right)}{\text{R}_{\text{ref}}\left({}^{\text{heavy}}\text{E} / {}^{\text{light}}\text{E}\right)} = \frac{\text{R}_\text{c}\left({}^{\text{heavy}}\text{E} / {}^{\text{light}}\text{E}\right)}{\text{R}_{\text{ref}}\left({}^{\text{heavy}}\text{E} / {}^{\text{light}}\text{E}\right)} - 1 \qquad (1.42)$$

Where $\delta^{\text{heavy}}\text{E}_{\text{c,ref}}$ is the δ-value of a compound *c* related to the reference *ref*, R_c and R_{ref} are the ratios of the heavy to light isotope *E*.

In case of carbon, the ratios of ^{13}C to ^{12}C are determined. Carbon stable isotope ratio measurements are commonly related to the primary reference material, i.e. the international standard, Vienna Pee Dee Belemnite (VPDB)[120]. The δ-value of this marine carbonate is zero per definition and its $R(^{13}C/^{12}C)$ is 0.0111802[121]. To decrease the overall consumption of the international standard VPDB, several calibration materials, i.e. primary standards, are normalized against the primary reference material[120]. In order to enable normalization of stable isotope values on a wide range several different reference materials have been evaluated, normalized against the available calibration materials and are listed by the Commission on isotopic abundances and atomic weights (CIAAW)[122] or the Joint Research Centre of the European Union in Geel, Belgium (JRC)[123]. A comprehensive list for various reference materials for e.g. hydrogen, oxygen, carbon or nitrogen, can also be found in Jochmann and Schmidt[120].

In this work three different approaches have been used to normalize the measured stable isotope values to the international δ-scale and are listed below. Since these are also the most widely applied options in the field of stable isotope analysis (SIA)[120] they will be described in more detail in the following. There are further possibilities for normalization strategies explained by Paul et al.[124].

1. Two-point normalization for the in-house reference material
2. Normalization versus an in-house reference material during sample analysis
3. Normalization of the stable isotope value of the analyte vs. a referenced working gas

In the first case, two internationally accepted reference materials are required which span over a wide range of the δ-scale. Ideally, the two standards are bracketing the investigated range of the δ-scale, thus, serving as two anchor points for the linear regression of measured versus true, i.e. internationally accepted, δ-values. The true δ-value of the compound ($\delta^{heavy}E_{c,true}$), e.g. an in-house reference material, is calculated with Equation 1.43.

$$\delta^{heavy}E_{c,true} = \frac{\delta^{heavy}E_{true-ref\,1} - \delta^{heavy}E_{true-ref\,2}}{\delta^{heavy}E_{m-ref\,1} - \delta^{heavy}E_{m-ref\,2}} \times \left(\delta^{heavy}E_{c,m} - \delta^{heavy}E_{m-ref\,2}\right) + \delta^{heavy}E_{true-ref\,2} \qquad (1.43)$$

Where $\delta^{heavy}E_{true-ref\,1}$ and $\delta^{heavy}E_{true-ref\,2}$ are the internationally accepted and $\delta^{heavy}E_{m-ref\,1}$ and $\delta^{heavy}E_{m-ref\,2}$ are the measured δ-values of the two reference materials, respectively, and $\delta^{heavy}E_{c,m}$ is the measured δ-values of the compound[120,124].

In the second case, $\delta^{heavy}E_{c,true}$ is normalized by a reference material, e.g. an internationally accepted reference material or a normalized in-house reference material. The reference material should be included in the same analytical run according to the “principle of identical treatment”[121]. The molecular structure and its δ-value should be as close as possible to the δ-value of the compound in order to increase accuracy of the normalization. $\delta^{heavy}E_{c,true}$ is calculated according to Equation 1.44[120].

$$\delta^{heavy}E_{c,true} = \frac{\left(\delta^{heavy}E_{c,m} + 1\right) \times \left(\delta^{heavy}E_{true-ref} + 1\right)}{\delta^{heavy}E_{m-ref} + 1} - 1 \qquad (1.44)$$

Where $\delta^{heavy}E_{c,m}$ and $\delta^{heavy}E_{m-ref}$ are the measured δ-values of the compound and the reference material, respectively, $\delta^{heavy}E_{c,true}$ and $\delta^{heavy}E_{true-ref}$ are the internationally accepted δ-values of the compound and the reference material, respectively.

In the third case, a working or reference gas is used for normalization. In this case pulses of the working or reference gas are injected in the beginning and/or in the end of each analytical run. The calculation of the δ-value of the compound is usually done automatically by the IRMS software (Equation 1.45). The working or reference gas has to be normalized beforehand with an international reference material[120,124].

$$\delta^{heavy}E_{c,true} = \delta^{heavy}E_{c,m} + \delta^{heavy}E_{true-refgas} + \delta^{heavy}E_{c,m} \times \delta^{heavy}E_{true-refgas} \quad (1.45)$$

Where $\delta^{heavy}E_{c,m}$ is the δ-value of the compound and $\delta^{heavy}E_{c,true}$ and $\delta^{heavy}E_{true-refgas}$ are the internationally accepted δ-values of the compound and the normalized working or reference gas, respectively.

1.2.2 Isotopic fractionation

In the course of chemical reactions isotopic fractionation may be observed and is mainly attributed to two kinds of effects — first, the mass-dependent isotope effect (MDE) and second, the mass-independent isotope effect (MIE)[118,125].

In MDEs the additional neutrons of the heavier isotope influence the atomic motions of the involved mass so that this effect originates mostly from different vibrational behavior of light and heavy isotopes[118,125]. Up to now, the kinetic isotope effect (KIE), a MDE, has been described very well[126]. The KIE occurs if a specific bond is broken and the activation energy required to reach the rate limiting transition state differs between light and heavy isotopes located at the reacting position. In the usual case the light isotope reacts faster than the heavier one(s) so that KIE > 1 (Equation 1.46)[118].

$$KIE_{element} = \frac{^{light}k}{^{heavy}k} \quad (1.46)$$

where $KIE_{element}$ is the kinetic isotope effect of the element under investigation, e.g. carbon, oxygen or nitrogen, $^{light}k$ and $^{heavy}k$ are the reaction rate constants of the compound containing the light and heavy isotope under investigation, respectively.

As a consequence the reactant is enriched with compounds carrying heavy isotopes at the reacting position. This is also termed *normal* isotope effect. The opposite is called *inverse* isotope effect, i.e. if the heavier isotope reacts faster than the light one so that the reactants are enriched in light isotopes[118,120]. As it has been illustrated by Elsner[118], the KIE may be differentiated as primary or secondary isotope effect. Primary isotope effects are observed if the element under investigation is present in the reacting bond, secondary ones occur if the respective element is located next to the reacting bond[118,127].

In case of the MIE, the magnetic MIE, i.e. dependence on nuclear spin selectivity, is recognized as one of the most important representatives so far. The magnetic MIE originates from different reaction rates of nuclear spins and nuclear magnetic moments and is found during reactions of radicals which have been generated during e.g. photolysis or radiolysis[125,128].

To quantify the isotopic fractionation occurring during a transformation reaction, the bulk isotopic enrichment factor ε_E^{bulk} of element *E* is often determined. ε_E^{bulk} is given in per mil [‰] and may be obtained by the logarithmic form of the Rayleigh equation (Equation 1.47)[120,127].

$$\frac{R_{t,c}\left({}^{heavy}E / {}^{light}E\right)}{R_{0,c}\left({}^{heavy}E / {}^{light}E\right)} = \ln\left(\frac{\delta^{heavy}E_{t,c}+1}{\delta^{heavy}E_{0,c}+1}\right) = \varepsilon_E^{bulk} \times \ln\left(\frac{c_{t,c}}{c_{0,c}}\right) \qquad (1.47)$$

Where $R_{0,c}$ and $R_{t,c}$ are the ${}^{heavy}E / {}^{light}E$ ratios and $c_{t,c}$ and $c_{0,c}$ are the concentrations of the compound *c* at time *0* and time *t*, respectively, and ε_E^{bulk} is the bulk isotope enrichment factor of element *E*.

ε_E^{bulk} represents the isotopic fractionation of all isotopes of element *E* contained in the compound. Thus, if several atoms of element *E* are contained in the compound but not all are located in reactive positions this leads to a “dilution” effect and ε_E^{bulk} becomes smaller overall[127]. For instance, ε_C^{bulk} for carbon cannot be determined if the compound contains more than C_{10}-C_{14} since dilution by the unreactive carbon atoms will prevail and fractionation will not be detectable anymore[129].
In order to determine the apparent kinetic isotope effect (AKIE) for the isotope E in the reactive position(s) of a compound without dilution effects of heavy isotopes in unreactive positions or intramolecular competition caused by the presence of several heavy and light isotopes in not distinct reactive positions Equation 1.48 is to be used[127].

$$AKIE_E = \frac{1}{1+z\cdot\frac{n}{x}\cdot\varepsilon_E^{bulk}} \qquad (1.48)$$

Where *n* is the number of atoms of the same element, *x* is the number of atoms in a reactive position, *z* is the number of atoms which are in intramolecular competition with each other and ε_E^{bulk} is the bulk isotope enrichment factor of the respective element *E*.

This approach requires apriori knowledge, e.g. of the reactive positions or whether intramolecular competition occurs[118,130]. In general, the AKIE of an elementary reaction directly reflects the KIE of a reaction. Nevertheless, transformation reactions of abiotic or biotic nature are usually divided in several elementary reaction steps which may be rate-limiting to a certain extent. As a consequence masking effects may occur if further reactions are comprised by the overall AKIE which are less or not isotope sensitive[130]. Additional insights may be achieved by comparison of isotopic data received from experimental and computational studies[131,132].

1.2.3 Instrumentation (LC-, GC- & EA-IRMS)

Stable isotope analysis may be performed in three different approaches, i.e. bulk stable isotope ratio analysis (BSIA), compound-specific stable isotope analysis or position-specific stable isotope analysis[133]. Since the latter was not part of this work it will not further be discussed in the following.

With the BSIA, e.g. employing an elemental analyzer (EA) (compare Figure 1.1), a bulk sample is combusted and the contained compounds are converted to low molecular weight gases. Hereafter, these are separated by gas chromatography (GC) so that a consecutive determination of several elements is enabled using an isotope ratio mass spectrometer (IRMS). It has to be noted that the resulting BSIA values represent the whole sample[134]. With EA-IRMS it is for example possible to determine isotope ratios for hydrogen, carbon, oxygen, nitrogen and sulfur which are detected as H_2, CO_2, CO, N_2 or SO_2, respectively[120,134].

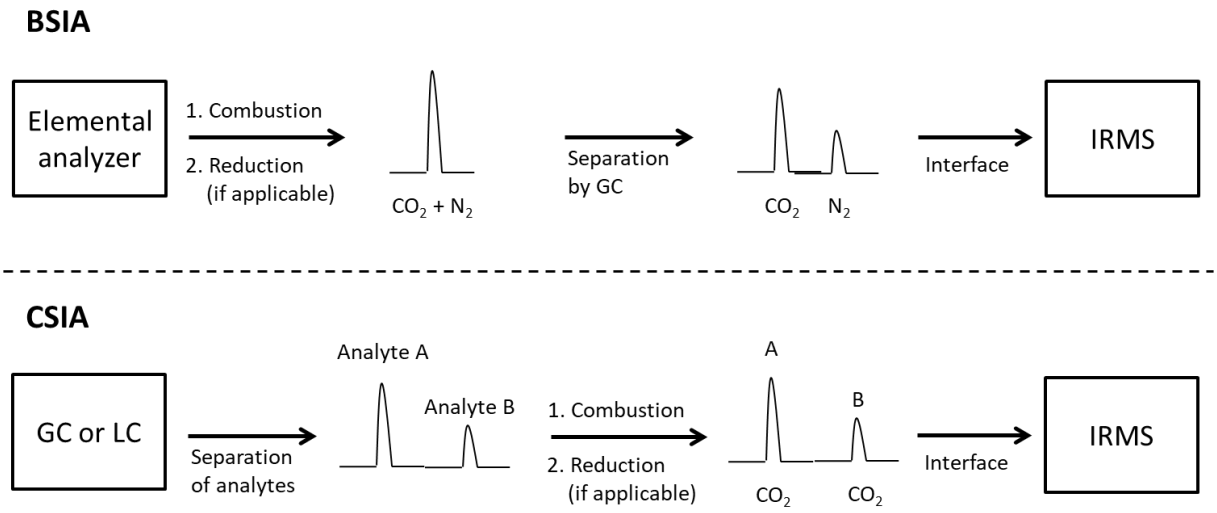

Figure 1.1: Schematic comparison of the setups for bulk stable isotope ratio analysis (upper panel) or compound-specific stable isotope analysis (lower panel) (cf. Jochmann and Schmidt[120] and Elsner et al.[135])

With CSIA, all compounds contained in a sample are first separated by either GC (compare Figure 1.1) or liquid chromatography (LC; compare Figures 1.1 and 1.2). Subsequently, the separated compounds are oxidized to low molecular weight gases in an interface and the different isotopes of one element may be detected with IRMS.

However, GC-IRMS is only applicable for compounds which may be properly transferred to the gas phase. Derivatization has been shown to enable GC-IRMS analysis for a certain range of non-volatile compounds[136]. In case of large molecules or if derivatization of the molecule is not possible LC-IRMS may be an alternative. Here, carbon stable isotope values are readily determined via CO_2. However, if stable isotope values for carbon ought to be

determined it is inevitable that no organic solvents are used for compound separation with LC since these would significantly interfere with the analyte stable isotope values. Consequently, LC-IRMS measurements are only possible for a limited number of compound classes for which a purely aqueous phase separation is applicable. If the compound is thermostable a high temperature gradient for improved separation may be used as well[137]. Oxidation of the analyte molecules to CO_2 in the interface shown in Figure 1.2 is achieved in a wet chemical oxidation process by sulfate radicals which are obtained by thermal activation, i.e. homolysis, of sodium persulfate at 99.9 °C at acidic pH. After the oxidation step, the generated CO_2 is separated from the aqueous phase via a gas-permeable membrane to the gas phase so that it can be analyzed in the IRMS. Consequently, using such an interface, the analytes have to be amenable for oxidation by sulfate radicals additionally to the requirements listed above. Recently, a different interface has been presented by Federherr et al. which converts the analyte molecules to CO_2 by thermal combustion[138]. Moreover, in this setup it was possible to determine nitrogen stable isotope values in the same run via N_2 for the first time. In order to avoid isobaric interferences of the N_2 relevant mass-to-charge ratios 28, 29 and 30 with, e.g. intermediary formed carbon monoxide, it is necessary to obtain a complete mineralization of the analyte and a complete separation of carbon and nitrogen oxidation products[138].

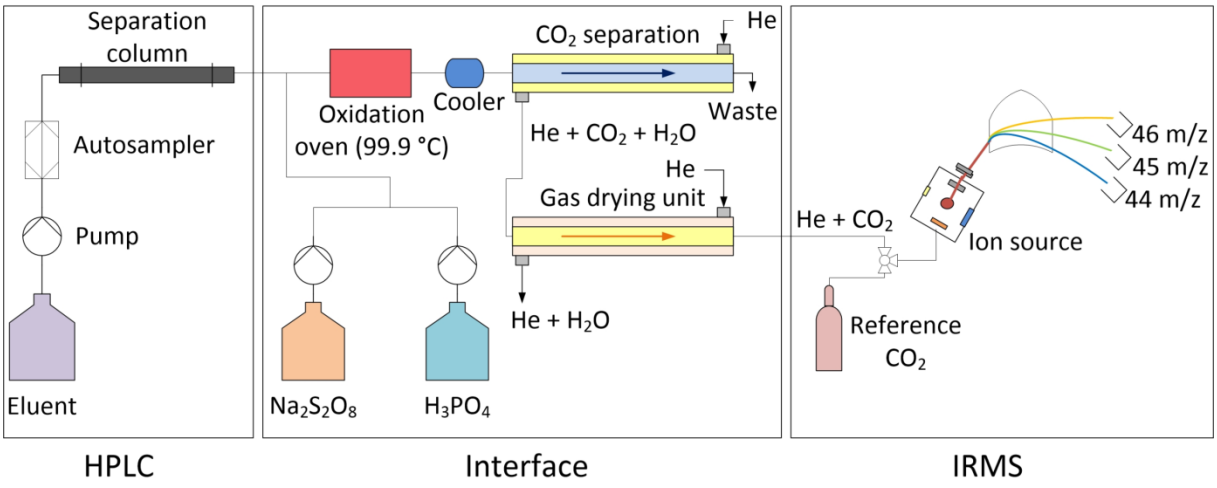

Figure 1.2: Schematic setup of a HPLC-IRMS system for detection of carbon stable isotope values equipped with a wet chemical oxidation interface (compare LC IsoLink from Thermo Scientific, Bremen, Germany).

The IRMS in the illustrated EA-IRMS, GC-IRMS and LC-IRMS systems in Figures 1.1 and 1.2 are usually magnetic sector field mass spectrometers equipped with a triple Faraday cup detector. Each Faraday cup is set to a fixed mass-to-charge ratio in order to obtain a maximum stability for detection. Consequently, in these setups a detection of three different mass-to-charge ratios is possible simultaneously, e.g. 44, 45, 46 for CO_2 or 28, 29, 30 for

N_2[139]. In order to be able to detect the small variations in isotopic abundances these kinds of mass-spectrometers with a precision of usually four to six significant decimals are required[133]. For instance, carbon or nitrogen isotopes, i.e. $^{13}C/^{12}C$ and $^{15}N/^{14}N$, respectively, show a relative mass difference of 1.08 (12 u (exactly)/13.003354838(5) u) and 1.07 (14.0030740074(18) u/15.000108973(12) u), respectively[140]. Moreover, bearing in mind that the natural abundance of the lighter isotope is much higher than the heavier one, i.e. 98.89 % for ^{12}C and 99.63 % for ^{14}N, respectively[140], it becomes obvious why such a high instrumental precision is inevitable in order to detect changes in isotope ratios during transformation reactions.

The IRMS are used in SIA due to the high required precision as described above. Nevertheless, the available SIA high precision IRMS devices have a lack in sensitivity compared to the standard HRMS so that low environmental concentration ranges which are generally detectable with HRMS are hardly amenable for IRMS measurements[119]. For this reason, enrichment techniques have to be employed in many cases if environmental samples are to be analyzed. For these cases, solid-phase extraction[141,142], purge and trap[143,144] or solid-phase microextraction[145,146] represent feasible solutions. Remaining matrix interferences after solid-phase microextraction may substantially be reduced in combination with subsequent preparative HPLC[141,147]. Moreover, the successful use of custom-made molecularly imprinted polymers for selective enrichment of the target analyte, e.g. 1*H*-benzotriazole, has been presented lately[148]. These enrichment techniques are either not applicable or have not yet been modified and validated for LC-IRMS so that this remains a future goal in order to enable analysis of non-GC compatible compounds.

1.2.4 CSIA: Current fields of application - use and limits

In many environmental chemistry studies HRMS is the analytical method of choice since it enables determination of concentration changes of a target compound or detection of potential transformation products. Complementary to these key features, CSIA is a powerful tool to close further analytical gaps which cannot be answered by HRMS alone. With CSIA transformation processes in the environment or in batch experiments in the laboratory may be tracked[118,119,130]. Additionally, it may be possible to distinguish dilution, sorption or volatilization from transformation effects in the environment. In this case two requirements need to be fulfilled: the potentially observed transformation needs to be accompanied by isotopic fractionation whereas transport or dilution processes are generally assumed to cause minor or even negligible isotope effects[119,149]. However, one exception has been described so far for the transport of petroleum hydrocarbons within a sandy unsaturated zone in the ground[150]. Consequently, the given field prerequisites and their resulting effects

for transport on isotopic fractionation have to be known beforehand in order to draw the appropriate conclusions. Additionally, the origin of contaminants in the environment may be traced and identified by CSIA since industrial synthesis or biogenic processes cause different isotopic fractionation processes during their generation in combination with the isotopic composition of the precursor material(s) and thus leaving a typical “isotopic fingerprint”[119,149].

Besides the plain distinction between dilution and transformation effects, CSIA may also provide valuable hints for identification of certain transformation mechanisms or enable distinction between several mechanisms or different oxidation processes. This is possible in certain cases because isotope fractionation is specific for each mechanism[118]. For the herbicide isoproturon it was shown that isotopic fractionation differed not only between abiotic and biotic hydrolysis but also depending on the respective bacterial or fungal strain responsible for biotransformation[151]. Furthermore, CSIA has allowed valuable insights in the formation pathways of N-nitrosodimethylamine[152,153], degradation mechanisms of diclofenac in the environment and water treatment processes[154], oxidation of atrazine induced by the abiotic factors $^{\bullet}OH$, excited triplet states or direct photolysis[155]. Moreover, several studies have illustrated that the pH is a master variable which significantly influences isotopic fractionation if the reactant may exist as protonated and deprotonated specie etc., e.g. during permanganate or electrochemical oxidation of *p*-methylaniline and further substituted anilines[156] or photolysis of chloroanilines[157,158].

Recently, it was stated that the variety of micropollutants in the environment has reached such a high level that it is rather impossible to investigate TP formation for every single compound and identify each TP potentially formed. Instead, future research should focus on functional group behavior and oxidants which may be applied to whole micropollutant classes in the next step[93]. Consequently, this claim does not only apply to HRMS but also to CSIA analyses. Permanganate as oxidant has already been systematically studied in detail for oxidation of substituted anilines[156] or several nitrotoluenes[132] whereas CSIA regarding other chemical oxidants such as ozone[154] have only slightly been tackled or not at all in case of chlorine dioxide. To fill this gap with systematic planned studies considering influences of pH or different functional groups of a compound class remains a challenging task for the future.

Chapter 2 -

Aims & Scope

In the introduction, compound-specific stable isotope analysis (CSIA) was identified as suitable tool for investigation of transformation processes and, eventually, as additional proxy for elucidation of underlying reaction mechanisms. The major aim of this work is to explore the applicability of CSIA for such purposes in abiotic oxidative processes which have been barely investigated in the current literature so far. Figure 2.1 represents a graphical overview that illustrates the content of the three major chapters of the presented work.

In the first approach to this objective, CSIA is complementary used to high-resolution mass spectrometry (HRMS). The latter is frequently implemented in investigations of transformation products (TPs). To this end, **Chapters 3** and **4** deal with the pH dependent transformation of the model compound sulfamethoxazole (SMX), a widely detected micropollutant in surface, ground- and wastewaters.

In **Chapter 3** typical oxidative water treatment processes are considered using the oxidative agents ozone (O_3) in absence and presence of hydroxyl radicals ($^{\bullet}OH$) or chlorine dioxide (ClO_2). The reaction stoichiometry of the oxidative agents with the neutral and anionic species of SMX is systematically investigated. In combination with results from TP analysis and CSIA, tentatively formulated TP structures from other studies are evaluated and respective reaction mechanisms are successfully derived.

Complementary, in **Chapter 4**, four irradiation sources, i.e. a low, medium and high pressure Hg lamp and simulated sunlight are applied for transformation of SMX. These irradiation sources emit wavelengths present in natural or engineered systems. Observed phototransformation kinetics are determined and complemented by HRMS and CSIA measurements.

The results of **Chapter 4** have pointed out that SMX itself is too complex as a model compound. Consequently, much simpler model compounds without nitrogen or sulfur-containing moieties, i.e. benzene and its methylated and methoxylated derivatives, are used in **Chapter 5**. Here, the abiotic oxidative processes using O_3, $^{\bullet}OH$ or ClO_2 are further systematically characterized with CSIA. Exemplarily, the apparent kinetic isotope effect (AKIE) for oxidation of the model compounds with O_3 ought to be determined which turned out to be nontrivial. As a consequence, different approaches for AKIE determination are presented and discussed. Additionally, quantum chemical calculations are implemented to address this problem more deeply and assess the different approaches.

Last but not least, an overall conclusion of the obtained results of this work is summarized in **Chapter 6** and an outlook describing required future studies resulting from the presented thesis is given.

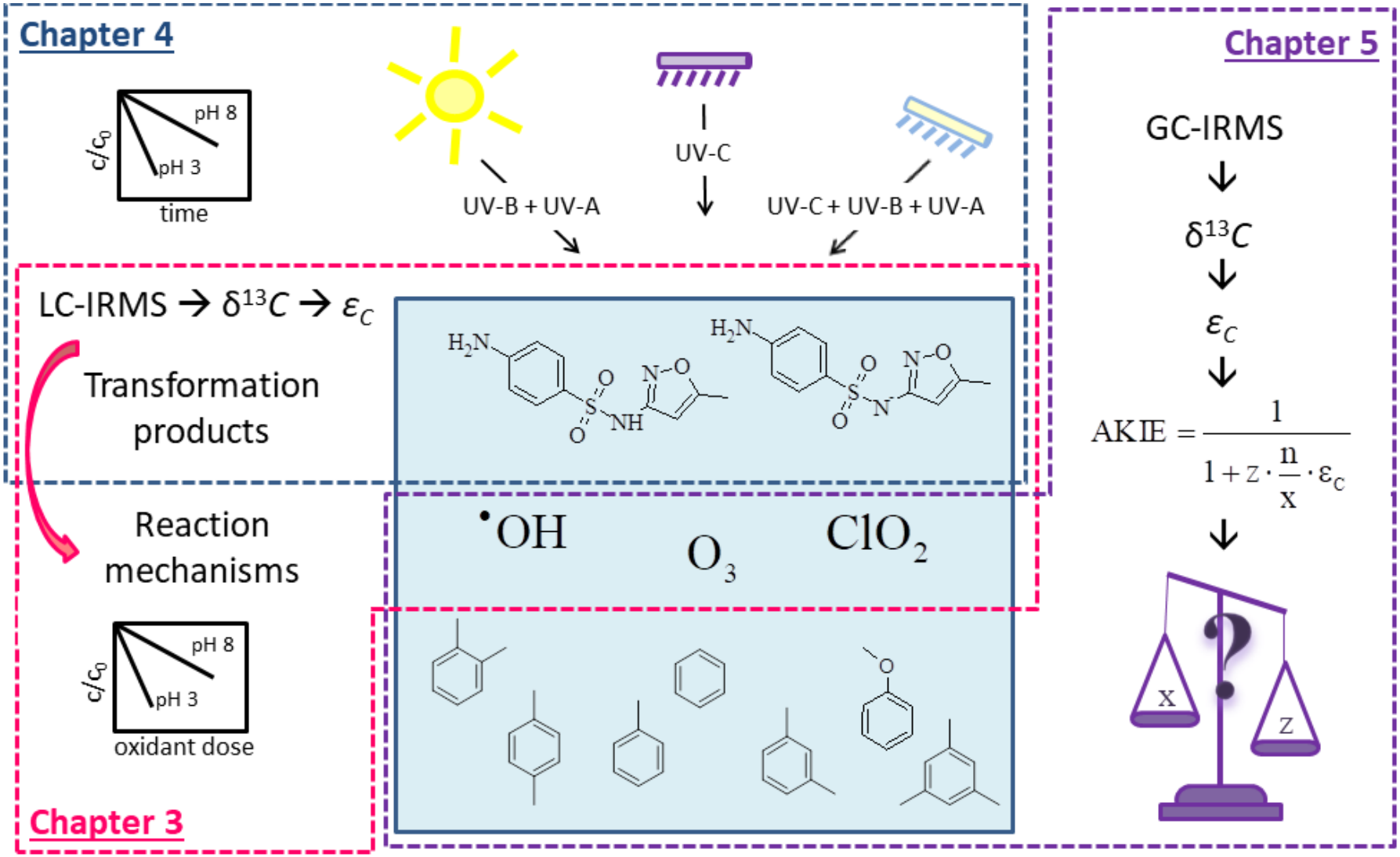

Figure 2.1: Graphical overview of the major content of this work. The geometric shapes indicate the subject matter, connection and intersections of the single chapters.

Chapter 3 -
Reactions of O_3, $O_3/^{\bullet}OH$ and ClO_2 with SMX

Adapted from: Willach, S., Lutze, H.V., Eckey, K., Löppenberg, K., Lüling, M., Terhalle, J., Wolbert, J.-B., Jochmann, M.A., Karst, U., Schmidt, T.C., Degradation of sulfamethoxazole using ozone and chlorine dioxide - Compound-specific stable isotope analysis, transformation product analysis and mechanistic aspects. *Water Research*, **2017**, 122, 280-289; DOI: 10.1016/j.watres.2017.06.001

3.1 Abstract

The sulfonamide antibiotic sulfamethoxazole (SMX) is a widely detected micropollutant in surface and groundwaters. Oxidative treatment with e.g. ozone or chlorine dioxide is regularly applied for disinfection purposes at the same time exhibiting a high potential for removal of micropollutants. Especially for nitrogen containing compounds such as SMX, the related reaction mechanisms are largely unknown. In this study, we systematically investigated reaction stoichiometry, product formation and reaction mechanisms in reactions of SMX with ozone and chlorine dioxide. To this end, the neutral and anionic SMX species, which may occur at typical pH-values of water treatment were studied. Two moles of chlorine dioxide and approximately three moles of ozone were consumed per mole SMX degraded. Oxidation of SMX with ozone and chlorine dioxide leads in both cases to six major transformation products (TPs) as revealed by high-resolution mass spectrometry (HRMS). Tentatively formulated TP structures from other studies could partly be confirmed by compound-specific stable isotope analysis (CSIA). However, for one TP, a hydroxylated SMX, it was not possible by HRMS alone to identify whether hydroxylation occurred at the aromatic ring, as suggested in literature before, or at the anilinic nitrogen. By means of CSIA and an analytical standard it was possible to identify sulfamethoxazole hydroxylamine unequivocally as one of the TPs of the reaction of SMX with ozone as well as with chlorine dioxide. H-abstraction and electron transfer at the anilinic nitrogen are suggested as likely initial reactions of ozone and chlorine dioxide, respectively, leading to its formation. Oxidation of anionic SMX with ozone did not show any significant isotopic fractionation whereas the other reactions studied resulted in a significant carbon isotope fractionation.

3.2 Introduction

In recent years, organic micropollutants have been increasingly detected in aquatic environments worldwide[76,159]. In this context the sulfonamide antibiotic sulfamethoxazole (SMX) is one important representative. Originally designed for human medicine, today SMX is also widely used in veterinary medicine as preventive measure. Common fields of application are poultry farming[76] or aquacultures[160]. As a consequence, SMX is frequently detected in related surface or groundwaters[159,161]. Moreover, the elimination of SMX in wastewater treatment plants is poor, hence wastewater poses another source of contamination of receiving water bodies[162-164].

Surface or groundwaters are common resources for drinking water. One option for removing SMX in drinking water treatment is oxidation, which can be achieved e.g. by ozone[2,165] or chlorine dioxide[51,166]. Corresponding reaction mechanisms are largely unknown but are important to assess formation of undesired products.

Due to its two pK_a-values (1.7 and 5.6) SMX has a cationic, neutral or anionic form (Figure 3.1)[167]. However, under environmental conditions only the latter two species are of relevance. The speciation of SMX strongly influences the kinetics of degradation which demonstrates the necessity of separate investigation of both relevant species. This is also evident from the second-order rate constants of neutral and anionic SMX with ozone are $4.7 \pm 0.9 \times 10^4$ $M^{-1} s^{-1}$ and $5.7 \pm 1.0 \times 10^5$ $M^{-1} s^{-1}$, respectively[165], and with chlorine dioxide <100 $M^{-1} s^{-1}$ and $7.9 \pm 0.9 \times 10^3$ $M^{-1} s^{-1}$, respectively[166]. Previous studies have identified the aniline moiety of SMX as the main reactive side during oxidation with ozone either experimentally[165] or computationally[168]. Additionally, Yu et al.[168] computed that a hydrogen transfer at the anilinic nitrogen of the neutral SMX is most favorable. However, it remained open to which degree the negative charge of the anionic SMX influences the preferences of the ozone attack.

Figure 3.1: Speciation of SMX according to the respective pK_a-values. SMX^+, SMX and SMX^- denote the cationic, neutral and anionic species, respectively (data adapted from Boreen et al.[167]).

High-resolution mass spectrometry (HRMS) analysis is often used in product studies[169,170]. However, with exact masses, only according sum formulas may be derived. The reactive site

and point of attack, respectively, remains mostly unknown. Here, compound-specific stable isotope analysis (CSIA) may be a useful tool to enlighten and further investigate reactions of micropollutants. The according degradation processes may reveal specific isotopic fractionation, which is related to the site of primary attack[120,127]. In most cases, the lighter isotopes (e.g. ^{12}C) at the specific position of attack of a molecule react faster than the heavier isotope (e.g. ^{13}C). Consequently, the ratio of ^{13}C to ^{12}C in the remaining reactant fraction increases as the reaction proceeds (*normal* isotope effect). An *inverse* isotope effect would be observed if the heavier isotopes reacted faster. The observed isotope effect varies depending on how pronounced the difference between the two reaction rates of the according isotopes is[120,127]. Using CSIA, it is possible to differentiate degradation pathways and to identify potential reaction sites as shown for atrazine[155] or diclofenac[154]. Exemplarily, in the latter study the authors found evidence that diclofenac is attacked by ozone in *para*-position to the nitrogen at the nonchlorinated aromatic ring which was indicated by *inverse* nitrogen isotope fractionation.

CSIA is regularly applied for isotopes of hydrogen, carbon, nitrogen or chlorine. Most commonly gas chromatography-isotope ratio mass spectrometry (GC-IRMS) is used which is, however, limited to volatile or semi-volatile compounds or requires derivatization of the analyte[120,135]. Liquid chromatography coupled to isotope-ratio mass spectrometry (LC-IRMS) represents an alternative for polar and non-volatile compounds[120,171], which is currently under further development[138]. Few studies have been published up to now dealing with LC-IRMS method development for analysis of sulfonamide drugs, inter alia SMX[171], or investigation of biotic and photolytic degradation of SMX[172].

This study investigates the carbon stable isotope fractionation of SMX to elucidate the oxidation of the neutral and the anionic SMX species in reactions with ozone or chlorine dioxide at two different pH values (3 and 8). Besides consumption evaluation for SMX degradation by ozone (in absence and presence of hydroxyl radical (•OH) scavengers) and chlorine dioxide, •OH yields are determined for the reaction of SMX and O_3. To our knowledge, this is the first time that transformation products (TPs) and carbon stable isotope values are determined for the oxidation of SMX with chlorine dioxide. Reaction mechanisms were proposed using both, CSIA data and HRMS data for product identification.

3.3 Materials and methods

3.3.1 Chemicals

All chemicals and solvents were used as received from the according supplier. A complete list of all chemicals used can be found in the supporting information in Text S3.1.

3.3.1.1 Generation of ozone and chlorine dioxide stock solutions

For preparation of ozone stock solutions, oxygen was used as feed-gas for the ozone generator BMT 802X (BMT Messtechnik, Berlin, Germany). The generated ozone gas was led into an impinger filled with ultrapure water. The bottle was ice-cooled to enhance the ozone solubility. The ozone concentration was determined by spectrophotometrical absorption measurements (see subchapter 3.3.3.1 below) of a 1:3-diluted ozone stock solution at 258 nm, ε_{O3} = 3200 M^{-1} cm^{-1} [2]. The concentrations of ozone stock solutions were in the range of 1.2-1.6 mM O_3 (note that during use of the ozone stock solution continuous purging with gaseous ozone was assured).

Chlorine dioxide stock solutions were prepared by mixing of 50 mL of a 0.885 M $NaClO_2$ solution with 50 mL of a 0.164 M $Na_2S_2O_8$ solution. Further purification steps were performed in reference to a method described by Gates[1]. The setup is shown and explained in Figure S3.1. The resulting concentrations were determined by spectrophotometrical absorption measurements of a 1:30-diluted chlorine dioxide stock solution at 359 nm, ε_{ClO2} = 1200 M^{-1} cm^{-1} [48]. The concentrations of the two chlorine dioxide stock solutions used during this study were 14.0 and 18.4 mM ClO_2, respectively.

3.3.2 Sample preparation

High (790 µM) and low (79 µM) concentrated SMX solutions were directly prepared in 10 mM phosphate buffered water either at pH 3 (neutral species prevails) or pH 8 (anionic species prevails). This was necessary due to the limited solubility of SMX in water (ca. 2 mM)[173]. Samples were prepared as batch samples each in 20-mL headspace screw cap vials. For a detailed overview on sample composition see SI (Table S3.1 and S3.2). Ozone experiments were carried out in presence and absence of 150 mM *tert*-butanol (*tert*-BuOH) or 183 mM dimethyl sulfoxide (DMSO) for scavenging of hydroxyl radicals (•OHs), which can be formed in the reaction of ozone[2]. In case of ozone experiments in presence of an •OH scavenger, the final sample solutions were composed of SMX solutions, varying volumes of ozone stock solution and constant concentrations of scavenger stock solution (for a detailed overview see Table S3.3 and S3.4). For ozone experiments in absence of an •OH scavenger, the

composition was similar to the one described above with the exception that an equivalent substitute of ultrapure water was dosed instead of the scavenger stock solution (Table S3.3 and S3.4). All oxidant dosages were determined in pre-experiments to guarantee that a full oxidant consumption was possible while a detectable concentration of SMX remained.

In ˙OH scavenging experiments, the concentration of *tert*-BuOH was adjusted to scavenge at least 95 % of ˙OH and at most 5 % of ozone (see Table S3.5 and explanation Text S3.3). In case of DMSO the concentration was sufficient to scavenge a minimum of 99.5 % of the formed ˙OH. DMSO itself also resulted in a consumption of ozone. At the highest ozone dosages at pH 3 (neutral species of SMX) 16.6 % and at pH 8 (anionic species) 1.7 % of ozone reacted with DMSO. This difference in consumption of ozone by DMSO is due to the ten times slower reaction rate constant of ozone with the neutral SMX species compared to the anionic SMX species (Table S3.5). The scavenging of ozone by DMSO has to be taken into account, when comparing ozone consumption in absence and presence of DMSO. For quantification of ˙OH the DMSO assay is a suitable tool[2]. In the reaction of DMSO with ˙OH methanesulfinic and methanesulfonic acid are formed[174] which can be quantified by ion chromatography. The sum of methanesulfinic and methanesulfonic acid reflects 92 % of the overall ˙OH yield[31]. This condition was considered when calculating the ˙OH yields. Ozone consumption by DMSO in SMX samples prepared from the 790 µM solution at pH 3 was not negligible (> 5 %). In order to give a uniform and consistent result, it was decided to correct all ozone concentration values, i.e. of high and low initial SMX concentration samples of pH 3 and pH 8. (Text S3.4).

3.3.3 Analytical methods

3.3.3.1 UV/vis-spectrometry

For absorption measurements, a UV-1650PC spectrophotometer (Shimadzu, Duisburg, Germany) equipped with a quartz cuvette with an optical path length of 1 cm was used.

3.3.3.2 Quantification of anions by ion chromatography

The quantification of anions (methanesulfonic acid (MSUS), methanesulfinic acid (MSIS), chloride, chlorite and chlorate) was performed with an ion chromatograph 881 Compact IC pro – Anion – MCS (Metrohm, Herisau, Switzerland). Calibration standards were freshly prepared with equidistant concentrations for every run. The calibration range was chosen covering the ion concentrations in the sample. Further details can be found in Text S3.5. For identification of chlorate in chlorine dioxide treated samples, the pH 3 SMX sample with the

highest applied chlorine dioxide dosage was spiked with 91 µM ClO_3^-, resulting in an increase of the corresponding peak in the chromatogram.

3.3.3.3 Quantification of SMX by HPLC-DAD

The concentration of SMX was determined by a HPLC-DAD system of the vp series (LC-10AT coupled to the DAD (SPD-M10A) (Shimadzu)). Calibration standards were prepared from 99-790 µM SMX or 9.9-79 µM SMX depending on the initial SMX concentration of the samples. Further details can be found in Text S3.6.

3.3.3.4 Isotope-ratio measurements

Isotope-ratio measurements by high-temperature-liquid chromatography isotope-ratio mass spectrometry (HT-LC-IRMS) of SMX were performed according to Kujawinski et al.[171] with modifications as described in Text S3.7. Briefly, the HTLC system was composed of a binary piston pump (Rheos Allegro, Flux Instruments/Thermo Scientific, Bremen, Germany), a HTC PAL autosampler (CTC Analytics, Zwingen, Switzerland; supplied by Axel Semrau, Sprockhövel, Germany), a HT HPLC 200 column oven (SIM, Oberhausen, Germany), a LC IsoLink interface connected to a DeltaV Advantage isotope-ratio mass spectrometer (both: Thermo Scientific). Separation was performed on an X-Bridge C_{18} column (100 x 2.1 mm, particle size 3.5 µm) (Waters, Eschborn, Germany) by a temperature gradient. Regularly, reference gas pulses of varying amplitudes were used to control linearity and precision performance of the IRMS. All samples were measured as triplicates and every third measurement was followed by a single measurement of a 390 µM SMX standard.

Aliquots of the analytical standards of SMX were weighed in tin cups (4 x 6 mm, IVA, Analysentechnik, Meerbusch, Germany) and analyzed with an elemental analyzer (vario PYRO Cube, Elementar Analysensysteme GmbH, Langenselbold, Germany) coupled to an IRMS (IsoPrime100, Isoprime Ltd., Stockport, UK). The reference materials USGS40 (International atomic energy agency (IAEA), Vienna, Austria; L-glutamic acid, $\delta^{13}C$: -26.389 ‰) and USGS41 (IAEA; L-glutamic acid $\delta^{13}C$: +37.626 ‰) were used to normalize the working standard acetanilide to the international Vienna Pee Dee Belemnite (VPDB) scale[120].

3.3.3.5 Data handling and calculations

Data from HT-LC-IRMS measurements were processed using by Isodat 2.5 (Thermo Scientific). Data from EA-IRMS were treated with IonVantage (Isoprime Ltd.). The carbon

isotope enrichment factor ε_C was calculated using the logarithmic form of the Rayleigh equation 3.1[120]:

$$\ln\left(\frac{R_{t,SMX}(^{13}C/^{12}C)}{R_{0,SMX}(^{13}C/^{12}C)}\right) = \ln\left(\frac{\delta^{13}C_{t,SMX}+1}{\delta^{13}C_{0,SMX}+1}\right) = \varepsilon_C \cdot \ln\left(\frac{c_{t,SMX}}{c_{0,SMX}}\right) \quad (3.1)$$

where $R_{0,SMX}$ and $R_{t,SMX}$ are the $^{13}C/^{12}C$ ratios and c_0 and c_t are the concentrations of SMX at time 0 and time t, respectively, ε_C is the carbon isotope enrichment factor and $\delta^{13}C$ values of SMX , are calculated according to equation 3.2:

$$\delta^{13}C_{SMX,VPDB} = \left(\frac{R_{SMX}\left(^{13}C/^{12}C\right) - R_{VPDB}\left(^{13}C/^{12}C\right)}{R_{VPDB}\left(^{13}C/^{12}C\right)}\right) \quad (3.2)$$

Kujawinski et al.[171] have shown that $\delta^{13}C$ values of SMX obtained by HT-LC-IRMS are concentration independent in the investigated concentration range. The reported $\delta^{13}C$ values were normalized to the VPDB scale and all standard deviations refer to a minimum of triplicate measurements. Additionally, the $\delta^{13}C$ values of the SMX samples obtained by the HT-LC-IRMS were corrected according to the principle of identical treatment as it was proposed by Werner and Brand[121]. Therefore, the EA-IRMS normalized SMX standard was measured every third HT-LC-IRMS measurement for correction and normalization of the degradation experiment samples.

3.3.3.6 Transformation product identification

For the detection of TPs, a high performance liquid chromatograph (Shimadzu) coupled to a time-of-flight mass spectrometer (Bruker micrOTOF, Bruker Daltonics, Bremen, Germany) with electrospray ionization in negative mode (HPLC-ESI(-)-ToF-MS) was used. In addition, fragmentation experiments were carried out employing an esquire6000 ion trap mass spectrometer (Bruker Daltonics) coupled to an HPLC system (Shimadzu) for using tandem mass spectrometry. Further details can be found in Text S3.8.

3.4 Results and Discussion

3.4.1 Ozone reaction stoichiometry and hydroxyl radical yield

The reaction stoichiometry is an important means to characterize an oxidation reaction. The stoichiometry of the oxidation reaction with ozone (Figure 3.2a and Table 3.1) is mostly independent of the SMX species, i.e. neutral or anionic species.

In the reaction of SMX with ozone, at least three possible reaction pathways may lead to the formation of ˙OH, i.e. via electron transfer at the aromatic ring or at its anilinic nitrogen, respectively, inter alia leading to formation of an ozonide radical anion ($O_3^{\bullet-}$) or via H-abstraction at the anilinic nitrogen inter alia forming a hydrotrioxyl radical ($HO_3^{\bullet}$). The reaction of $O_3^{\bullet-}$ with water or the decay of $HO_3^{\bullet}$ will give rise to ˙OH (Scheme S3.1, pathways S3.1-3; mechanisms are adapted from the reaction of aniline with ozone, which have been described by Tekle-Röttering et al.[25]. Indeed, 40.2 ± 6.7 % and 36.9 ± 0.7 % ˙OH per mol ozone consumed are formed in the reaction of ozone with the neutral and anionic species of SMX, respectively (Table 3.1). Similar ˙OH yields have been reported for the reaction of ozone with aniline (34 ± 3.1 %)[25].

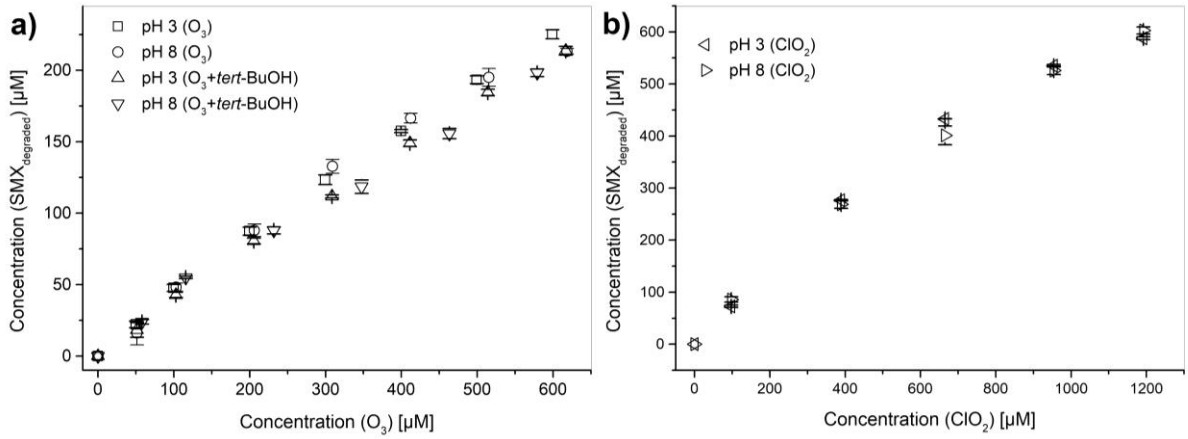

Figure 3.2: Degraded SMX per oxidant consumed (solely high initial SMX concentrations): a) with ozone (pH 3: squares; pH 8: circles) or with ozone in presence of 150 mM *tert*-BuOH as ˙OH scavenger (pH 3: triangle upward; pH 8: triangle downward) and b) chlorine dioxide (pH 3: triangle rightward; pH 8: triangle leftward). Concentration ($SMX_{degraded}$) denotes the SMX concentration of a reference sample minus the residual SMX concentration of the oxidized sample. Error bars represent standard deviation of triplicates. All samples were buffered with 10 mM phosphate buffer.

In order to investigate the influence of these intrinsically formed ˙OH on the overall ozone consumption, SMX was additionally oxidized with ozone in presence of the ˙OH scavenger *tert*-BuOH. However, the consumption of ozone per SMX degraded in absence and presence

of *tert*-BuOH is found in a comparable range (Figure 3.2a, Table 3.1). This is surprising, since one would expect a lower consumption of ozone in presence of such high ˙OH concentrations because these react rapidly with SMX (Table S3.5) and, thus, also contribute to the oxidation of SMX. However, one explanation is that the ˙OH initiate the additional formation of (*N*-centered) aminyl radicals (Scheme 3.1) as suggested by Sein et al.[175] and Tekle-Röttering et al.[25]. It is assumed that aminyl radicals react with ozone to form nitroxyl radicals that themselves consume ozone. The latter reaction may reform the aminyl radical resulting in an ozone consuming chain reaction. This extra consumption of ozone compensates the additional fraction of SMX, which is degraded by ˙OH. In comparison, the additional ozone consuming effect is even more pronounced in oxidation of diclofenac[175] or anilines[25]. Here, the ozone consumption is significantly higher in presence of ˙OH than in their absence.

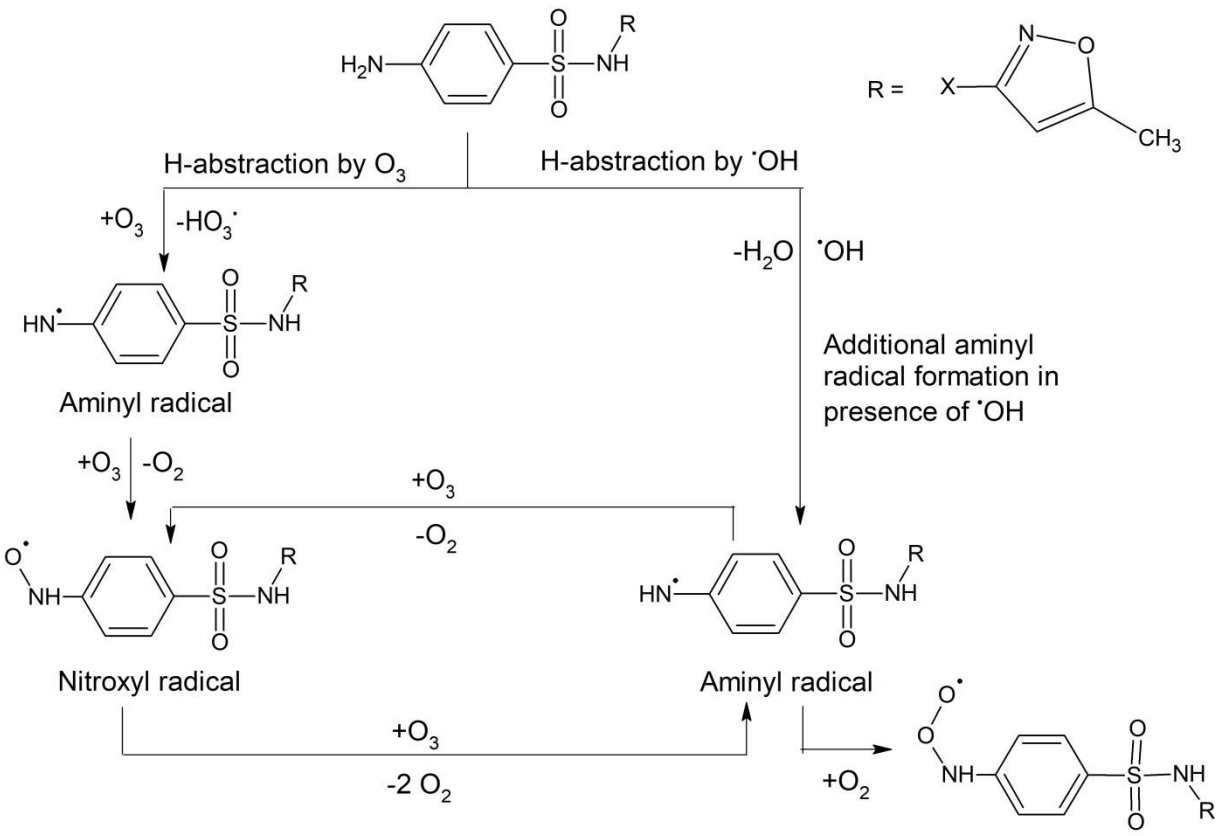

Scheme 3.1: Proposed reaction scheme of the nitroxyl-aminyl radical chain reaction following the postulates of Tekle-Röttering et al.[25] and Sein et al.[175]

Due to the carbon stable isotope measurements (discussed below) it was necessary to use high initial SMX concentrations. Nevertheless, SMX concentrations in the aquatic environment are usually much smaller[159]. In order to check applicability of the above listed concept for lower SMX concentrations, oxidation experiments with ozone and chlorine dioxide were carried out using ten times lower initial concentrations of SMX (Table 3.1). The

comparison of the ozone consumption obtained with *tert*-BuOH at high SMX concentration and with DMSO at low SMX concentration is possible in this case without restrictions (cf. Text S3.3 and S3.4). The results (Table 3.1) show that $^{\bullet}OH$ yields for the oxidation of the neutral SMX species are in a comparable range for both starting conditions, whereas the $^{\bullet}OH$ yield observed for the anionic SMX species at low initial SMX concentration is somewhat higher compared to the high initial SMX concentration. Nevertheless, consumption data support the above discussion on aminyl-nitroxyl radical chain reaction. The less SMX is available in solution the more ozone is consumed in the aminyl-nitroxyl radical chain reaction in the first place until an interrupting reaction occurs. The lower ozone consumption per mole SMX at high initial SMX concentrations can be explained by scavenging of aminyl- or nitroxyl radicals by SMX itself so that the ozone consuming radical chain reaction is less pronounced. Moreover, higher $^{\bullet}OH$ yields were observed at low initial SMX concentration at pH 8, further feeding aminyl radicals into the ozone consuming chain reaction. This leads to an increased ozone consumption so that even more ozone is necessary to oxidize one SMX (3.3 O_3/SMX at high and 4.9 O_3/SMX at low initial SMX concentrations, respectively) (Table 3.1 and Figure S3.2).

Table 3.1: Degradation of SMX per consumed oxidant, i.e. ozone in absence or presence of the $^{\bullet}$OH scavenger *tert*-BuOH (150 mM) or DMSO (10 mM) or chlorine dioxide (left section). $^{\bullet}$OH yields formed in the reaction of SMX and ozone (right section). Each section shows data for the neutral and anionic SMX species at high and low initial SMX concentrations.

	SMX degraded [%] per oxidant consumed[a, b]					$^{\bullet}$OH yield per O_3 consumed [%][a, c]	
	O_3 (w/o)	O_3 + *tert*-BuOH	O_3 + DMSO	ClO_2			
c_i (SMX)	high	high	low	high	low	high	low
Neutral SMX (pH 3)	36.6 ± 1.1	34.3 ± 1.0	26.0 ± 1.1	50.5 ± 5.0	n.d.[f]	40.2 ± 1.3[d] (6.7)[e]	43.8 ± 2.7[d]
Anionic SMX (pH 8)	35.0 ± 2.7	30.1 ± 1.5	20.7 ± 0.6	50.3 ± 3.6	49.8 ± 2.4	36.9 ± 0.7[d]	43.9 ± 1.7[d]

[a]In all cases pH was kept constant with phosphate buffer (10 mM).
[b]Values are derived from the resulting slopes of oxidant consumed [µM] versus degraded SMX [µM] (see Figure 3.2 for high concentration; data for low concentration are not shown). Uncertainties represent the standard deviations of the according slope.
[c]$^{\bullet}$OH yields were determined by the DMSO assay applying 183 mM and 10 mM DMSO, respectively. Values are derived from the resulting slopes of ozone consumed [µM] versus $^{\bullet}$OH yield [µM]. Ozone concentrations were corrected in all cases for consumption by DMSO.
[d]Uncertainty represents the 95 % confidence limit of the standard deviations of the according slope.
[e]Uncertainty represents 95 % confidence limit of the standard deviations of the according slope plus an expanded uncertainty (see Text S3.4 for further explanation).
[f]n.d. = not determined

3.4.2 Chlorine dioxide reaction stoichiometry and chlorite and chloride yields

The stoichiometry of the oxidation reaction with chlorine dioxide (Figure 3.2b and Table 3.1) is mostly independent of the SMX species, i.e. neutral or anionic species, as it was observed for ozone as well. In the oxidation of both SMX species with chlorine dioxide, 50 % SMX are degraded per chlorine dioxide consumed, i.e. two moles of ClO_2 are necessary to oxidize one mole of SMX. This is in accordance with results for phenols[40] and different amines[53]. Hull et al.[53] and Rav-Acha and Choshen[176] proposed that chlorine dioxide tends to react via an electron transfer in a first step. During this reaction, the organic molecule is transformed into a reactive intermediate, which may rapidly consume another chlorine dioxide molecule (cf. Hull et al.[53] and Rav-Acha and Choshen[176]). However, in this latter reaction, hypochlorous acid may be formed as a product[40,177] which may also react with the substrate (i.e. SMX).

Comparing the consumption of ozone and chlorine dioxide described above, it can be concluded that chlorine dioxide is more selective and thus more efficient in oxidizing SMX, regardless of reaction kinetics.

In the reaction of chlorine dioxide with organic compounds chlorite and chloride are regularly formed. At pH 8, 55.5 ± 1.2 % chlorite and 45.3 ± 0.5 % chloride were detected per mole chlorine dioxide consumed (Figure S3.3) so that the mass balance of chlorine dioxide is readily achieved by these two products. The observed stoichiometry is in accordance to chlorite formation during oxidation of phenols by chlorine dioxide where 0.5 moles of chlorite are formed per mole chlorine dioxide consumed[40]. The mechanism how chloride is formed is yet unkown. Under acidic conditions at pH 3, 64.1 ± 3.0 % chloride is formed per mole chlorine dioxide. However, at this pH, no linear relationship of chlorite formation vs. chlorine dioxide consumption was found (Figure S3.4). Moreover, approximately one third of chlorine is missing in the chlorine mass balance. Since no major peaks of chlorinated TPs have been found (see section 3.4.4) another chlorine species is likely to be formed. Jia et al.[178] suggested that under acidic conditions in presence of phosphate buffers, an acid-catalyzed reaction of hypochlorous acid and chlorite is likely to occur (compare reaction 13 in Jia et al.[178]). This reaction leads to the formation of chlorate and additionally to chloride[178]. Thus, the increased chloride yield of SMX samples oxidized at pH 3 could be explained. Indeed, it was possible to identify a chlorate signal in the ion chromatograms by retention time comparison and standard addition experiments. However, in total, the detected concentration could only account for 5.3 % of the overall chlorine mass balance and such low yields of ClO_3^- may partly originate from the ClO_2 stock solution. Hence, other chlorine species are likely to be formed under acidic conditions, too.

3.4.3 Compound-specific stable isotope analysis

Carbon stable isotope values were determined for SMX samples treated with ozone in absence and presence of DMSO as •OH scavenger as well as with chlorine dioxide at both pH values each. The results are shown in Figure 3.3 and summarized in Table 3.2. All observed isotopic fractionations occurred as *normal* isotope effects.

Table 3.2: Stable carbon isotope enrichment factors (ε_C) and peak area ratios (PAR) of the products after oxidation with ozone in absence or presence of the •OH scavenger dimethyl sulfoxide (DMSO; 183 mM) or with chlorine dioxide. In all cases, pH was kept constant with a phosphate buffer (10 mM).

	O_3 (pH 8)	O_3 (pH 3)	O_3+DMSO (pH 8)	O_3+DMSO (pH 3)	ClO_2 (pH 8)	ClO_2 (pH 3)
ε_C[a] [‰]	n.s.[a]	-1.2 ± 0.1	n.s.[a]	-2.2 ± 0.1	-1.3 ± 0.1	-0.8 ± 0.1
$SMX_{remaining}$[b]	0.44	0.33	0.40	0.42	0.12	0.12
TP177[b]	0.02	0.01	0.01	0.01	0.05	0.06
TP226a[b]	0.08	0.01	n.s.	n.s.	n.s.	n.s.
TP226b[b]	n.s.	n.s.	n.s.	n.s.	n.s.	0.07[d]
TP268[b]	0.06	0.01	0.12	0.01	0.13	0.02
TP269[b]	0.01	0.11	0.03	0.11	0.09	0.03
TP282[b]	0.14[c]	0.09	0.08[e]	0.04[c]	0.23[e]	0.13[e]

[a]Any ε_C below 0.5 ‰ was excluded due to measurement uncertainties (compare Jochmann et al.[143] and Sherwood Lollar et al.[179]) and is thus denoted as not significant (n.s.).
[b]The semiquantitative peak area ratio of each product is the ratio of product peak area and the peak area of initial SMX in the sample (results originate from the highest applied oxidant dosage after complete oxidant consumption). In case two or more isomers were detected for the same *m/z*, these were summed up. Exact *m/z* can be found in Table S3.9.
[c]2 isomers detected; [d]3 isomers detected; [e]4 isomers detected

The most pronounced ε_C was found for the oxidation of the neutral SMX species by ozone in presence of DMSO (ε_C = -2.2 ± 0.1 ‰) (Figure 3.3b) followed by the same oxidation conditions in absence of DMSO (ε_C = -1.2 ± 0.1 ‰) (Figure 3.3a). In contrast to that, no significant carbon isotope fractionation could be observed for the oxidation of the anionic SMX species with ozone at pH 8 in absence and presence of DMSO (Figure 3.3a & b). This is in agreement with results described by Maier et al.[154] who did also not observe any shift for carbon stable isotope values after oxidation of the anionic species of diclofenac with ozone in presence and absence of an •OH scavenger. These results show, that isotopic fractionation of SMX during oxidation with ozone depends on the prevailing SMX species (neutral or anionic) so that the pH acts as the master variable determining the potentially observable isotopic fractionation of SMX in environmental samples later on.

Dodd et al.[165] performed additional experiments in which SMX and *N*(4)-acetyl-sulfamethoxazole were oxidized by ozone. The authors could show that the sulfonamide

nitrogen is not the ozone reactive site and that the primary site of attack is the aromatic ring and/or its anilinic nitrogen. Complementary to the study of Dodd et al.[165], the above results suggest that in case of neutral SMX ozone may attack a carbon containing moiety (presumably the aromatic ring) while the anionic species may be attacked at a hetero atom (possibly the anilinic nitrogen). As it was not possible for Dodd et al.[165] to indicate the definite site of attack by kinetic studies, stable isotope analysis appears to be a useful tool to assist mechanistic considerations.

In case of oxidation of SMX with chlorine dioxide, a slight carbon isotope fraction was detected for both species, i.e. $\varepsilon_c = -0.8 \pm 0.1$ ‰ and $\varepsilon_c = -1.3 \pm 0.1$ ‰ for pH 3 and pH 8, respectively (Figure 3.3c). The observed isotopic fractionation indicates that carbon bonds were involved in the reactions of both species with chlorine dioxide. Contrary to SMX samples oxidized with ozone, the ε_c is more pronounced for the anionic than for the neutral species. Additionally, as prospect for a future research it would be possible to distinguish SMX oxidation by ozone and chlorine dioxide, respectively, in environmental samples exhibiting a slightly alkaline pH (only anionic SMX present) by use of CSIA.

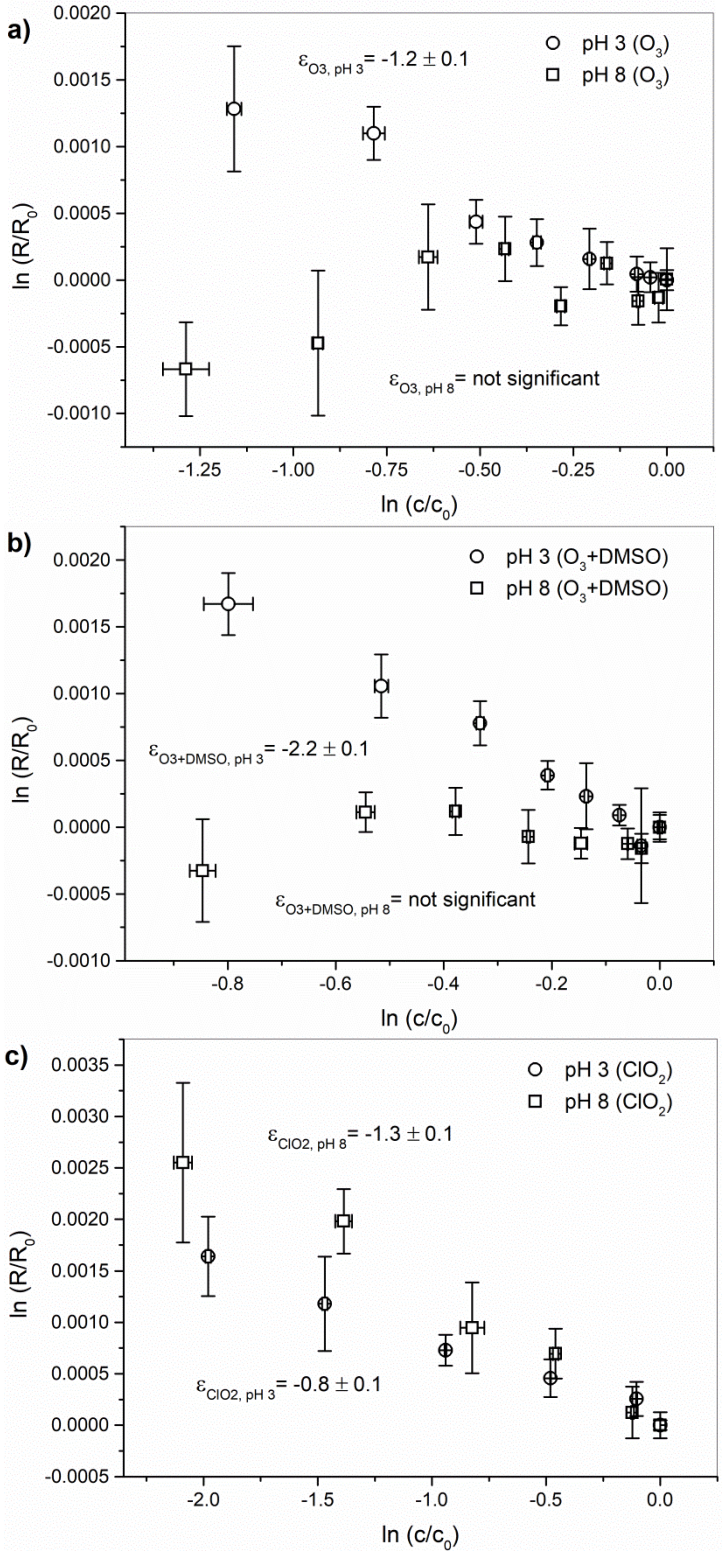

Figure 3.3: Rayleigh-plots of SMX oxidation with a) ozone in absence of any scavenger b) ozone in presence of dimethyl sulfoxide (183 mM) as $^{\bullet}$OH scavenger and c) chlorine dioxide ((pH 3: diamonds (neutral SMX species); pH 8: squares (anionic SMX species)); ln(c/c_0) error bars represent standard deviations of experimental triplicates and ln(R/R_0) error bars represent triplicate measurements with LC-IRMS of experimental triplicates

3.4.4 Transformation products and possible reaction mechanisms

In LC-ESI(-)-ToF-MS measurements, six major TPs with *m/z*-ratios of TP177, TP226a/b, TP268, TP269 and TP282 were detected in varying intensities among other minor products (see Table 3.2, Table S3.9 and Figure S3.5-7). For most of the detected TPs, analytical standards were not commercially available. In order to allow a comparison between the different oxidation setups the TP peak areas are given as peak area ratios (PAR), i.e. as ratio of product peak area to the peak area of initial SMX in the sample. The initial SMX peak area was determined from reference samples which were treated identically to the oxidation samples except that the amount of oxidant added was replaced by ultrapure water (Table S3.1 & S3.3). In several cases, two or more isomers were found for the transformation products TP226b and TP282 as indicated in Table 3.2. In this study, it was not possible to identify the different isomers. In order to present a virtually complete picture of PAR, these were summed up to a concerted value each (Table 3.2).

If one compares the product distribution with the according ε_C values (Table 3.2), it appears that the PARs are related to the ε_C values. This is most distinct for TP268 and TP269 in case of oxidation with ozone, i.e. the less TP268 and the more TP269, respectively, is formed the stronger pronounced is the isotopic fractionation (Table 3.2). The same trend can be observed for TP269 in reactions of ClO_2 with SMX. These results indicate that formation of TP269 might be linked to isotopic fractionation. The overall PARs of TP177 are more pronounced for samples treated with chlorine dioxide than for samples treated with ozone. Nevertheless, TP177 is detected in equal measures in each oxidation setup independently of the pH. Thus its formation does not seem to be influenced by speciation of SMX. TP226a could only be detected in SMX samples oxidized with ozone in absence of an $^{\bullet}OH$ scavenger. Hence, it is likely that TP226a is an $^{\bullet}OH$ borne reaction product. The PAR was higher for oxidation of SMX at pH 8. One possible reason could be that the $^{\bullet}OH$ react rather unselectively with the neutral SMX species leading to various products among TP226a, whereas the point of attack at the anionic SMX species could be directed to the oxazole ring due to the increase of electron density by the deprotonated sulfonamide nitrogen.

Additionally to the listed TPs (Table 3.2), one chlorinated TP was found for SMX degradation with chlorine dioxide at pH 8 with *m/z* of 272 as $[M\text{-}H]^-$. The evidence for a chlorinated TP given by the most suitable sum formula for TP272 (i.e. $C_9H_7ClN_3O_3S^-$) was confirmed by the chlorine isotope distribution found in the product spectrum (Figure S3.8). The relative abundance in relation to the intensity of the SMX peak at the highest chlorine dioxide dosage was 0.01 and thus the sixth most intense peak. Despite that, the absolute product amount of TP272 is expected to be rather small since the chlorine mass balance of chlorine dioxide and

its inorganic reaction products, respectively, was well closed. However, the corresponding chlorine dioxide sample at pH 3 did not show any signal for TP272. One likely explanation is that TP272 is a hypochlorous acid reaction product. As explained above, hypochlorous acid has been postulated as one possible product in chlorine dioxide reactions with anilines[177] or other hydrocarbons[40,176].

In case of TP268, which represents the formal addition of one oxygen atom, several references suggest its addition to the aromatic ring of the aniline moiety[116,170,180]. The described fragmentation patterns herein do not distinguish whether oxygen was added to the aromatic ring (TP268a, Figure 3.4) or whether a hydroxylamine (TP268b, Figure 3.4) was formed. In principle, it is possible to formulate reasonable formation mechanisms for both TPs, i.e. TP268a and TP268b, respectively (cf. Scheme S3.2), which cannot be distinguished by HRMS. Attempts in this study to clarify which of the two TPs was actually formed by MS^n-experiments were fruitless. Since no carbon isotope fractionation was observed for ozonation at pH 8 in presence of DMSO where TP268 was most intense it is likely that TP 268b was formed (reaction at the anilinic nitrogen). This assumption could be verified by comparison of retention times with a commercially available standard of sulfamethoxazole hydroxylamine and the agreement of the related fragmentation patterns in MS^2-experiments of the standard and the sample peak (cf. Figure S3.9 & S3.10). Sulfamethoxazole hydroxylamine may be formed upon H-abstraction by ozone from the anilinic nitrogen leading to formation of an aminyl radical[168] which easily reacts with oxygen to form a peroxyl radical[2]. Finally, two peroxyl radicals may form a tetroxide in order to decay via the Russell mechanism[2] and form a sulfamethoxazole hydroxylamine.(Scheme 3.1a). Another possibility for sulfamethoxazole hydroxylamine formation may be initiated by electron transfer at the anilinic nitrogen either by ozone or chlorine dioxide leading to formation of an aminyl radical cation which is in equilibrium with the aminyl radical (Scheme 3.1a). Overall, this example demonstrates how it was possible to specify the actually formed TP and the according mechanisms by the aid of CSIA.

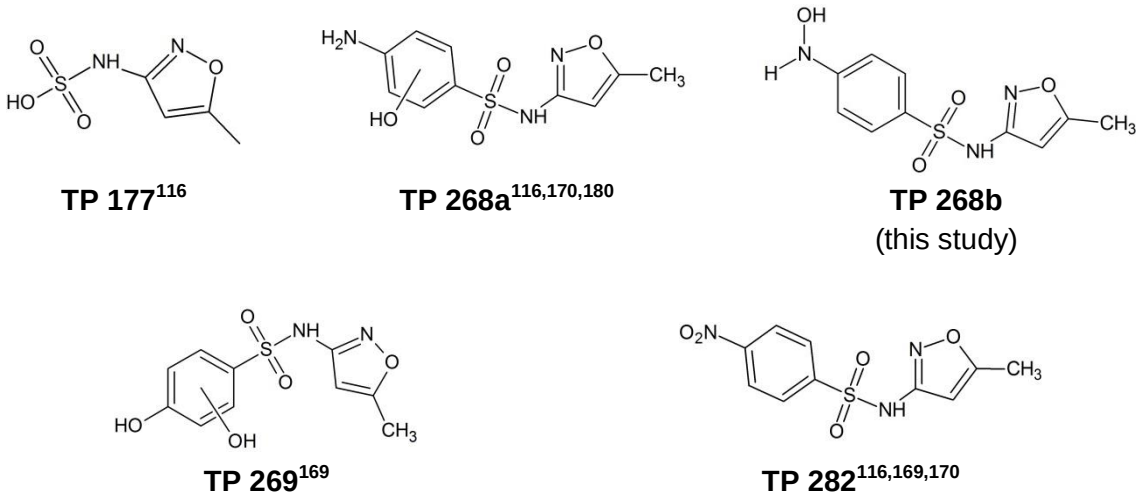

TP 177[116] **TP 268a**[116,170,180] **TP 268b** (this study)

TP 269[169] **TP 282**[116,169,170]

Figure 3.4: Probable structures for determined *m/z*-ratios. TP268a has been suggested in other references but was not found in this study, TP268b represents the structure, which has been verified by an analytical standard in this study. TP177, TP269 and TP282 have been proposed by other authors and are consistent with the findings of this study.

For TP177, TP269 and TP282 according structures have been suggested in literature (Figure 3.4). These agree with the determined ε_c values of this study (Table 3.2). The formation of TP177 and TP269 may be preceded by an attack at aromatic carbon bonds which involves carbon isotope fractionation (Scheme S3.3 and Scheme 3.2b) and TP282 may be formed after an attack at the anilinic nitrogen. The latter mechanism is strongly supported by computational studies of Yu et al.[168]. The substantial formation of TP177 explains why a significant ε_C value is found for oxidation of SMX with chlorine dioxide at pH 3 even though very low amounts of TP269 have been detected.

During the formation of TP269, the anilinic nitrogen is cleaved from the aromatic ring and replaced by a quinone group. The mechanism has been postulated in accordance to Aguilar et al.[177] (Scheme 3.2b). For the formation of TP282 during ozonation, at least two pathways are possible, which have been postulated in conformity to the reaction of ozone with anilines (see Scheme S3.4)[2,25]. Regarding TP226a and TP226b, it was not possible to propose a reasonable structure in the current study. In case of ozone, TP226a is possibly an $^{\bullet}$OH borne TP since it does only occur in absence of an $^{\bullet}$OH scavenger. Martín de Vidales et al.[181] have postulated a possible structure for a similar *m/z* (Table S3.9). However, the according TP was obtained after conductive-diamond electrochemical oxidation so that in their study, significantly different oxidation conditions prevailed. It is very likely that the structure postulated by Martín de Vidales et al.[181] requires several oxidative attacks, which can easily happen at the electrode surface, but is unlikely to appear in reactions with ozone or chlorine dioxide.

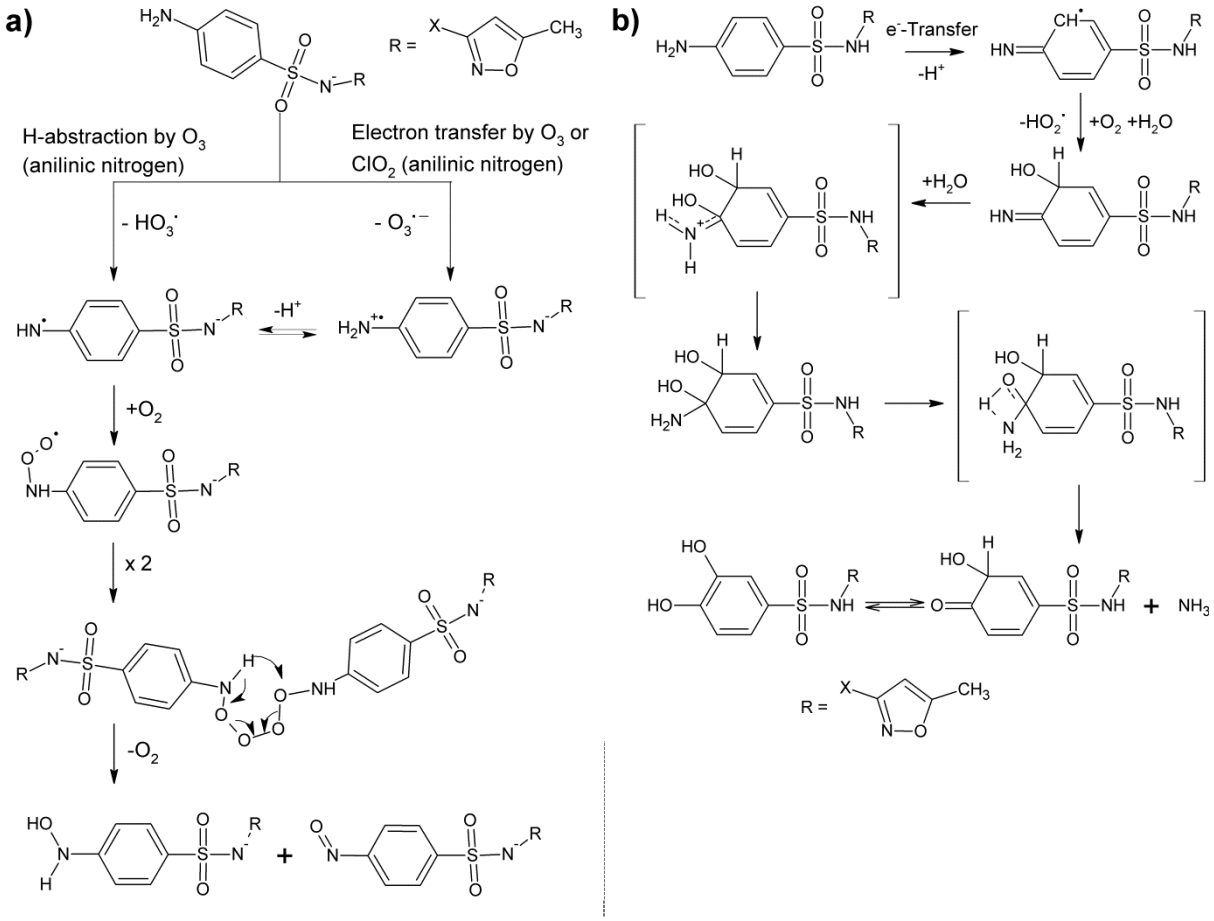

Scheme 3.2: Proposed reaction mechanism for the formation of a) TP268b in the reaction of ozone with SMX and b) TP269 in the reaction of either ozone or chlorine dioxide with SMX

3.5 Conclusion

The presented study shows that CSIA is a useful tool for the elucidation of TPs if standard fragmentation experiments in e.g. MS/MS-mode reach their limits. Moreover, in the demonstrated case, it was possible to prove the formation of sulfamethoxazole hydroxylamine, first, by evidence of observed ε_C values and, second, by comparison of retention times in HPLC with a commercially available analytical standard and to postulate the according reaction mechanism. Additionally, ε_C values may even serve as indicators for variations of transformation product patterns. In the presented case, it could be shown that oxidation of SMX with ozone or chlorine dioxide leads to a number of common main TPs. However, the observed PARs of the reaction of the neutral and the anionic SMX species with the two oxidants followed opposite trends. This highlights the impact of the reaction pH on the resulting product patterns and PARs for micropollutants such as SMX with a pK_a close to environmental pH conditions.

3.6 Supplementary Information

Text S3.1: Chemicals

All solutions were prepared in ultrapure water (18.1 MΩ·cm, TOC < 10 ppb; ELGA LabWater, Veolia Water Technologies Deutschland GmbH, Celle, Germany).

The following chemicals were used for preparation of the samples: acetanilide (99.9 %, Merck KGaA, Darmstadt, Germany), acetonitrile (HPLC-grade, VWR Chemicals, Leuven, Belgium), dimethyl sulfoxide (p.a., ACS C, AppliChem, Darmstadt, Germany), dipotassium hydrogen phosphate (≥ 99 %, p.a., AppliChem), formic acid (99-100 %, Sigma-Aldrich, Steinheim, Germany), helium (5.0; Air Liquide, Düsseldorf, Germany), methanesulfinic acid sodium salt (95 %, Alfa Aesar GmbH & Co KG, Karlsruhe, Germany), methanesulfonic acid ((≥ 99 %, Merck KGaA), methanol (99,99 % HPLC grade, Fisher Scientific, Loughborough, United Kingdom), nitrogen (5.0; Air Liquide), *ortho*-phosphoric acid (85 %, p.a., AppliChem), oxygen (4.8; Air Liquide), potassium dihydrogen phosphate (≥ 98 %, AppliChem), sodium carbonate (ACS reagent, ≥ 99.5 %; Sigma-Aldrich), sodium chlorate (puriss. p.a., ≥ 99 %, Sigma-Aldrich), sodium chloride (≥ 99.5 %; Bernd Kraft, Duisburg, Germany), sodium chlorite (puriss. p.a. 80 %, Sigma-Aldrich), sodium hydrogen carbonate (ACS reagent, ≥ 99.7 %; Sigma-Aldrich), sodium hydroxide (≥ 99 %, VWR Chemicals), sodium peroxodisulfate (99 %, Sigma-Aldrich), sulfamethoxazole (analytical standard, Sigma-Aldrich), sulfuric acid (> 95 %, Fisher Scientific), *tert*-butanol (99 %, p.a., AppliChem).

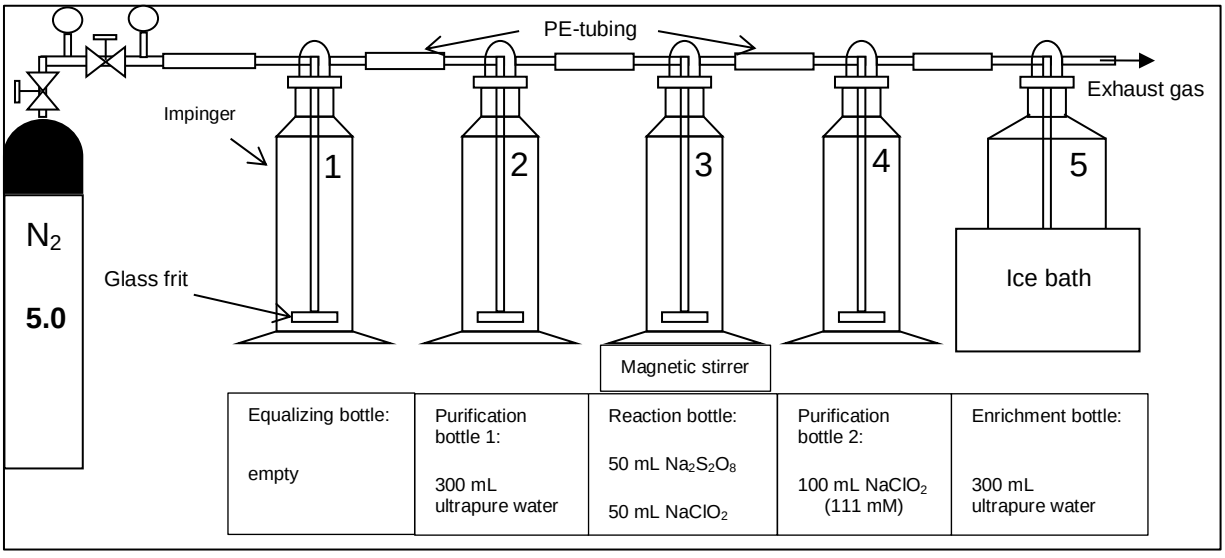

Figure S3.1: Experimental setup for the generation of chlorine dioxide. Impingers are connected with PE tubes (1-5). The nitrogen is led through the glass frits into each bottle. The magnetic stirrer below the third bottle ensures the mixing of the reaction solution. The whole reaction time is one hour. Hereafter, the solution in bottle 5 shows a dark yellow colour and chlorine dioxide can be quantified by spectrophotometrical absorption measurements.

Text S3.2: Sample compositions in Tables S3.1-4

Note that accuracies of added oxidant dosages vary due to the accuracies of the syringes applied for small (< 1 mL) and larger volumes (> 1 mL). In all cases of oxidant dosage glass syringes were employed.

Table S3.1: Volumes used for the preparation of high initial SMX concentration samples treated with chlorine dioxide. Concentrations of stock solutions were: c (ClO_2) = 14 mM; c (SMX) = 790 µM. For evaluation of results, each dosage was corrected for the volume difference (volume deviation from the reference to the highest dosage (1400 µL ClO_2) < 10 %).

	V (ClO_2) [µL]	V (SMX) [mL]	V (total) [mL]
Reference	0	15	15.000
ClO_2 sample	105	15	15.105
ClO_2 sample	430	15	15.430
ClO_2 sample	750	15	15.750
ClO_2 sample	1100	15	16.100
ClO_2 sample	1400	15	16.400

Table S3.2: Volumes used for the preparation of low initial SMX concentration samples treated with chlorine dioxide. Concentrations of stock solutions were: c (ClO_2) = 18.4 mM; c (SMX) = 79 µM. Chlorine dioxide was dosed from a working solution (c (ClO_2) = 6.13 mM). For evaluation of results each dosage was corrected for the volume difference (volume deviation from the reference to the highest dosage (1400 µL ClO_2) < 10 %).

	V (ClO_2) [µL]	V (SMX) [mL]	V (total) [mL]
Reference	0	15	15.000
ClO_2 sample	24	15	15.024
ClO_2 sample	122	15	15.122
ClO_2 sample	196	15	15.196
ClO_2 sample	294	15	15.294
ClO_2 sample	367	15	15.367

Table S3.3: Volumes used for the preparation of high initial SMX concentration samples treated with ozone in presence and absence of an OH radical scavenger. Concentrations of stock solutions were: c (O_3) = 1.2-1.6 mM; c (SMX) = 790 µM; c (scavenger = *tert*-BuOH) = 2 M or c (scavenger = DMSO) = 2.44 M. In case that no scavenger was added, the volume of 1.125 mL was replaced by an aliquot of water. For all dosages, two reference samples and three ozone treated samples were prepared each.

	V (O_3) [mL]	V (H_2O) [mL]	V (SMX) [mL]	V (scavenger) [mL]	V (total) [mL]
O_3 sample	0.6	-	13.275	1.125	15
Reference	-	0.6	13.275	1.125	15
O_3 sample	1.2	-	12.675	1.125	15
Reference	-	1.2	12.675	1.125	15
O_3 sample	2.4	-	11.475	1.125	15
Reference	-	2.4	11.475	1.125	15
O_3 sample	3.6	-	10.275	1.125	15
Reference	-	3.6	10.275	1.125	15
O_3 sample	4.8	-	9.075	1.125	15
Reference	-	4.8	9.075	1.125	15
O_3 sample	6.0	-	7.875	1.125	15
Reference	-	6.0	7.875	1.125	15
O_3 sample	7.2	-	6.675	1.125	15
Reference	-	7.2	6.675	1.125	15

Table S3.4: Volumes used for preparation of low initial SMX concentration samples treated with ozone in presence and absence of an OH radical scavenger. Concentrations of stock solutions were: c (O_3) = 1.2-1.6 mM; c (SMX) = 79 µM; c (scavenger = DMSO) = 1.5 M. In case no scavenger was added, the volume of 0.1 mL was replaced by an aliquot of water. For all dosages, two reference samples and three ozone treated samples were prepared each.

	V (O_3) [mL]	V (H_2O) [mL]	V (SMX) [mL]	V (scavenger) [mL]	V (total) [mL]
O_3 sample	0.2	-	14.7	0.1	15
Reference	-	0.2	14.7	0.1	15
O_3 sample	0.4	-	14.5	0.1	15
Reference	-	0.4	14.5	0.1	15
O_3 sample	0.6	-	14.3	0.1	15
Reference	-	0.6	14.3	0.1	15
O_3 sample	0.8	-	14.1	0.1	15
Reference	-	0.8	14.1	0.1	15
O_3 sample	1.0	-	13.9	0.1	15
Reference	-	1.0	13.9	0.1	15
O_3 sample	1.2	-	13.7	0.1	15
Reference	-	1.2	13.7	0.1	15
O_3 sample	1.4	-	13.5	0.1	15
Reference	-	1.4	13.5	0.1	15
O_3 sample	1.6	-	13.3	0.1	15
Reference	-	1.6	13.3	0.1	15

Table S3.5: Reaction rate constants of all relevant reactions in ozonation of the anionic (SMX^-) and the neutral (SMX) species of sulfamethoxazole in absence and presence of the OH radical scavengers *tert*-butanol and DMSO

Reaction	Second order rate constant k [M^{-1} s^{-1}]	Reference
SMX + O_3	$4.7\pm0.9 \times 10^4$	Dodd et al.[165]
SMX^- + O_3	$5.7\pm1.0 \times 10^5$	Dodd et al.[165]
SMX + $^\bullet OH$	-	-
SMX^- + $^\bullet OH$	$5.5\pm0.7 \times 10^9$	Huber et al.[182]
$^\bullet OH$ + O_3	$1.1\pm0.2 \times 10^8$	Sehested et al.[183]
$H_2PO_4^-$ + O_3	4×10^{-4}	Hoigné et al.[184]
H_3PO_4 + O_3	2×10^{-2}	Hoigné et al.[184]
tert-butanol+ O_3	3×10^{-3}	Hoigné and Bader[185]
tert-butanol+ $^\bullet OH$	6×10^8	Buxton et al.[32]
DMSO + O_3	8×10^0	Pryor et al.[186]
DMSO + $^\bullet OH$	7×10^9	Buxton et al.[32]
$^\bullet NH_2$ + O_2	$3.0\pm0.2 \times 10^8$	Laszlo et al.[187]

Text S3.3: Determination of the minimal necessary and maximal possible scavenger concentrations

The minimal concentrations of the OH radical scavenger *tert*-butanol and DMSO necessary to scavenge a minimum of 95 % of OH radicals generated were calculated according to equation S3.1 using the rate constants given in Table S3.5 (exemplarily shown for *tert*-butanol):

$$c_{\text{tert-butanol(min)}} = \frac{f_{\bullet\text{OH+tert-butanol}} \cdot c_{\text{SMX}\cdot} \cdot k_{\bullet\text{OH+SMX}} + f_{\bullet\text{OH+tert-butanol}} \cdot c_{O_3} \cdot k_{\bullet\text{OH+O}_3}}{k_{\bullet\text{OH+tert-butanol}} \cdot \left(1 - f_{\bullet\text{OH+tert-butanol}}\right)} \quad \text{(S3.1)}$$

The maximal concentrations of the OH radical scavenger *tert*-butanol and DMSO possible at which less than 5 % of ozone react with the scavenger were calculated according to equation S3.2 using the rate constants given in Table S3.5 (exemplarily shown for *tert*-butanol):

$$c_{\text{tert-butanol(max)}} = \frac{f_{\text{O}_3\text{+tert-butanol}} \cdot c_{\text{SMX}} \cdot k_{\text{O}_3\text{+SMX}}}{k_{\text{O}_3\text{+tert-butanol}} \cdot \left(1 - f_{\text{O}_3\text{+tert-butanol}}\right)} \quad \text{(S3.2)}$$

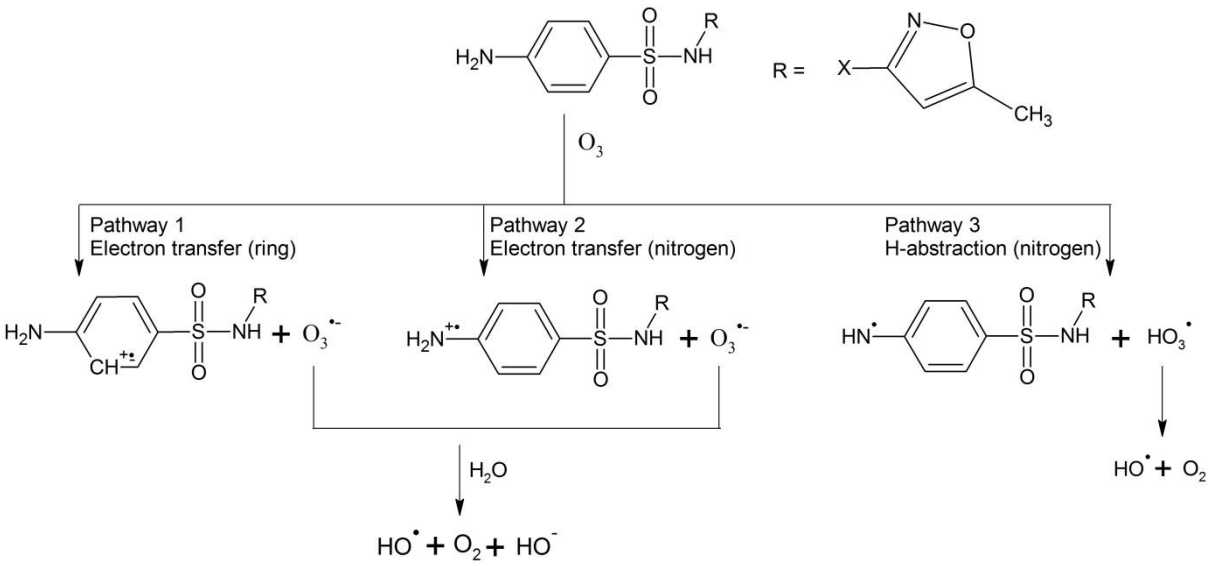

Scheme S3.1: Proposed reaction scheme of OH radical formation following the postulates of Tekle-Röttering et al.[25] for the reactions of aniline with ozone

Text S3.4: Derivation of the uncertainties of OH radical yields and consumption data for SMX degradation by ozone in presence of DMSO at initial stock solution concentration of 78.9 µM

For all given OH radical yields, the plotted ozone concentrations have been corrected by consumption of ozone by DMSO itself. In case of pH 8 samples this correction is only marginal since the ozone consumption was 0.4 % and 1.7 % (183 mM DMSO, 789 µM c_i(SMX)) and 0.2 % and 0.5 % (10 mM DMSO, 78.9 µM c_i(SMX)) each for the lowest and highest dosage, respectively. However, at pH 3, the second order reaction rate constant of SMX and ozone is ten times lower than for the anionic species at pH 8 so that ozone consumption by DMSO could not be neglected here. DMSO consumption was 4.5 % and 16.6 % (183 mM DMSO, 789 µM c_i(SMX)) and 2.6 % and 6.2 % (10 mM DMSO, 78.9 µM c_i(SMX)) each for the lowest and highest dosage, respectively. In order to give a uniform and consistent result, it was decided to correct all values, i.e. pH 3 and pH 8. The fraction of ozone consumed by DMSO was determined as shown below (Equation S3.3):

$$f_{DMSO+O_3} = \frac{c_{DMSO} \cdot k_{DMSO+O_3}}{c_{DMSO} \cdot k_{DMSO+O_3} + c_{SMX(reacted)} \cdot k_{SMX+O_3} + c_{H_3PO_4} \cdot k_{H_3PO_4+O_3}} \quad \text{(S3.3)}$$

This fraction was subtracted from the determined ozone concentrations in each batch sample thus resulting in the residual ozone concentration available for SMX oxidation.

Each uncertainty given is the 95 % confidence limit derived from the standard deviation of the slope multiplied by the quantile of student t-distribution (α = 0.05, n-2) for a two sided

statistical test (according to DIN 32 645). In case of ozonation of SMX at pH 3 (c_i = 789 µM) the ozone consumption by DMSO was particularly pronounced. In literature, to the authors' knowledge, there has been only one indication found that the reaction of ozone and DMSO can also lead to methanesulfinic and methanesulfonic acid as potential products among others[188] without any indication of the underlying stoichiometry. However, in the given experimental set-up described by Wu et al.[188] it cannot be fully excluded that the reaction of ozone and DMSO investigated is not interfered by OH radicals. Wu et al.[188] used *tert*-butanol as additional OH radical scavenger. DMSO was provided at an initial concentration of 13 mM and *tert*-butanol at 50 mM. Since *tert*-butanol reacts 10 times slower with OH radicals than DMSO does (compare Table S3.5, reaction rate constants) the minimum concentration of *tert*-butanol would have needed to be >130 mM to scavenge the majority OH radicals.
However, methanesulfinic and methanesulfonic acid are used for the quantification of OH radicals by ion chromatography in this study and as described above it could not be fully excluded that the reaction of DMSO and ozone does not contribute to OH radical formation. However, in order to display the worst case scenario, i.e. to include the possibility that 100 % of the DMSO reacted with ozone lead to formation of OH radicals (lowered OH radical yield) or that 100 % of the DMSO reacted with ozone could lead to formation of OH radicals (increased OH radical yield), both options were calculated. For the lowest four dosages, these "worst-case scenario" data could be fitted by a linear regression each, bracketing the measurement data. Furthermore, only measurement values for correlation of ozone vs. OH radicals were included for which the "worst-case scenario" data were situated within a 95 % confidence limit. Finally, it was decided to give an expanded uncertainty for this experimental data set, i.e. the relative standard deviation was derived from the square root of the sum of the squared 95 % confidence limit of the standard deviation of the slope (1.3 %) and the difference of the two slopes determined in the "worst-case scenario" (6.6 %). In case of ozonation of SMX at pH 3 (c_i = 78.9 µM) values resulting from a fraction of > 5 % ozone consumption by DMSO were excluded so that the given value complies with the 95 % confidence limit perfectly.

Text S3.5: Quantification of anions by ion chromatography

The quantification of anions was performed with the ion chromatograph 881 Compact IC pro – Anion – MCS (Metrohm, Herisau, Switzerland) connected to an autosampler (814 USB Sample Processor, Metrohm). The injection volume was 20 µL. Separation of methanesulfonic acid (MSUS) and methanesulfinic acid (MSIS) was performed isocratically using the anion exchange column Metrosep A Supp 4 (250 x 4.0 mm with 9 µm particles) at

a flow rate of 1 mL min^{-1}. The eluent contained 0.36 mM Na_2CO_3 and 0.34 mM $NaHCO_3$. For isocratic separation of chloride, chlorite and chlorate the anion exchange column Metrosep A Supp 5 (250 x 4.0 mm with 5 µm particles) was run at a flow rate of 0.7 mL min^{-1}. The eluent composition was 3.2 mM Na_2CO_3 and 1.0 mM $NaHCO_3$. Calibration standards were freshly prepared with equidistant concentrations for every run, bracketing the sample concentrations. Limits of quantification (LOQ) were 2.0 µM (MSIS), 11 .8 µM (MSUS), 0.3 µM (chloride), 1.2 µM (chlorite) and 5.2 µM (chlorate). The LOQs were determined according to the calibration method described in DIN 32645 (2008).

Text S3.6: Quantification of SMX by HPLC-DAD

The concentration of SMX was determined by a HPLC-DAD system of the vp-series consisting of LC-10AT, FCV-10AL, SCL-10A, SPD-M10A, SIL-10AD, CTO-10AS (Shimadzu, Duisburg, Germany). The injection volume was 10 µL. The analytical column was a ProntoSIL C-18 (250 x 4 mm, particle size 5 µm) (Bischoff Analysentechnik und -geräte GmbH, Leonberg, Germany) using an isocratic eluent (35:65 Methanol:Water (pH 2); flow: 0.5 mL/min). Absorption at 270 nm was used for quantification. Calibration standards were prepared from 99 - 790 µM SMX or 9.9-79 µM SMX depending on the initial SMX concentration of the samples. LOQ was 2.3 µM SMX (determination according to DIN 32645:2008-11[189]. Data processing was performed by LC solutions, version 1.25, SP4 (Shimadzu).

Text S3.7: Isotope-ratio measurements by high-temperature-liquid chromatography-isotope-ratio mass spectrometry

Isotope ratio measurements by HT-LC-IRMS of SMX were performed according to Kujawinski et al.[171] with modifications as described below. The HT-LC system was composed of a binary piston pump (Rheos Allegro, Flux Instruments/Thermo Scientific, Bremen, Germany), a HTC PAL autosampler (CTC Analytics, Zwingen, Switzerland; supplied by Axel Semrau, Sprockhövel, Germany), a HT HPLC 200 column oven (SIM, Oberhausen, Germany), a LC IsoLink interface connected to a DeltaV Advantage isotope ratio mass spectrometer (both: Thermo Scientific). Separation was performed on an X-Bridge C_{18} column (100 x 2.1 mm, particle size 3.5 µm) (Waters, Eschborn, Germany) with an acidic eluent (pH 3 buffered with 2.5 mM sodium phosphate) at a flow rate of 300 µL min^{-1}. The temperature gradient was started at 30 °C, increased after sample injection instantaneously

by 5 °C min^{-1} until the maximum of 85 °C and then held for 9 min. For an improved temperature transfer the eluent was pre-heated by the oven. Additionally, the entire column was embedded between two custom made aluminum blocks. After separation, the column effluent was mixed with 30 µL min^{-1} of 1.5 M *ortho*-phosphoric acid and 70 µL min^{-1} 0.84 M sodium peroxodisulfate in the interface. Afterwards, the mixture was led into the oxidation oven which was set to 99.9 °C. After passing the gas separation unit the generated CO_2 was transferred by a helium stream at a flow rate of 1.2 mL min^{-1} to the open split of the IRMS. The IRMS was tuned to maximum linearity. Regularly, reference gas pulses of varying amplitudes were used to control linearity and precision performance of the IRMS. All samples were measured as triplicates and every third measurement was followed by a single measurement of a 390 µM SMX standard.

Text S3.8: Transformation product identification

For the detection of transformation products, a high performance liquid chromatographic separation coupled to a time-of-flight mass spectrometer (HPLC-ESI(-)-ToF-MS) was used. In addition an ion trap mass spectrometer was employed for fragmentation experiments. For the chromatographic separation 5 µL of sample solution were injected onto a reversed-phase C18 column (Hypersil Gold, 150 x 2.1 mm, 3 µm particle size, 175 Å, Thermo Scientific, Bremen, Germany). A solution of 0.1% formic acid in bidistilled water (eluent A) and acetonitrile (eluent B) were used as eluents in a binary gradient which is shown in Table S3.6. Separation was carried out at 40°C and the total flow rate was set to 0.3 mL/min.

Determination of accurate masses was achieved with a Bruker micrOTOF (Bruker Daltonics, Bremen, Germany) with an electrospray ionization interface operated in negative mode. This mass spectrometer was coupled to an LC system by Shimadzu (Shimadzu Germany, Duisburg, Germany) consisting of two LC-10ADVP pumps, a SIL-HTA autosampler, a DGU-14A degasser, and a CTO-10ADVP column oven containing a 0.5 mL mixing chamber. Detailed mass spectrometric parameters are given in Table S3.7. The mass spectrometer was controlled by micrOTOFControl 1.1 software, the LC system by LC Solution 1.25. For high mass accuracy, each analysis was calibrated internally using the SMX signal and its accurate theoretical mass.

Additionally, fragmentation experiments have been carried out by coupling an esquire6000 ion trap mass spectrometer (Bruker Daltonics, Bremen, Germany) to a Shimadzu LC system (Shimadzu Germany, Duisburg, Germany) consisting of two LC-20AD pumps, a SIL-20ACHT autosampler, a CBM-20A controller, a DGU-20A3 degasser, and a CTO-20AC column oven.

This separation was performed on the same column, using the same binary gradient as described in Table S3.6. Detailed mass spectrometric parameters are given in Table S3.8. Data acquisition was performed using HyStar 3.2 software from Bruker Daltonics (Bremen, Germany). The fragmentation experiments of the transformation product with *m*/*z* 268.0 were carried out using an isolation width of 0.7 u and fragmentation amplitude of 0.7.

For data evaluation DataAnalysis 4.0 software from Bruker Daltonics (Bremen, Germany) and OriginPro 9.3 by OriginLab Corporation (Northampton, MA, USA) were used.

Table S3.6: Gradient profile for the LC separation of transformation products of SMX.

***t* [min]**	0	3	14	15	16	17	25
%B (Acetonitrile)	5	5	30	90	90	5	5

Table S3.7: Mass spectrometric parameters for the determination of exact masses of transformation products of SMX analyzed by liquid chromatography coupled to time-of-flight mass spectrometry.

Ionization mode	negative	Hexapole 1 voltage	-26.7 V
Mass range	*m*/*z* 50 – 550	Hexapole 2 voltage	-22.1 V
Spectra rate	1.0 Hz	Hexapole RF voltage	90 Vpp
Nebulizer gas pressure	1.5 bar	Lens transfer time	49.0 µs
Dry gas flow rate	8.6 L/min	Pre pulse storage time	9.0 µs
Dry heater temperature	200 °C	Lens 1 storage voltage	-30.0 V
Capillary voltage	4000 V	Lens 1 extraction voltage	-20.5 V
Endplate offset voltage	-500 V	Lens 2 voltage	-12.0 V
Capillary exit voltage	-90.0 V	Lens 3 voltage	16.0 V
Skimmer 1 voltage	-30.0 V	Lens 4 voltage	-0.3 V
Skimmer 2 voltage	-22.1 V	Lens 5 voltage	30.0 V

Table S3.8: Mass spectrometric parameters for the determination of transformation products of sulfamethoxazole analyzed by liquid chromatography coupled to ion trap mass spectrometry.

Ionization mode	negative	Capillary exit voltage	-100.4 V
Mass range	*m/z* 50 – 550	Skimmer voltage	-40.0 V
Nebulizer gas pressure	35 psi	Octapole 1 voltage	-12.0 V
Dry gas flow rate	8.5 L/min	Octapole 2 voltage	-1.7 V
Dry gas temperature	320 °C	Octapole RF	137.5 Vpp
Capillary voltage	4000 V	Lens 1 voltage	5.0 V
Endplate offset voltage	-500 V	Lens 2 voltage	60.0 V
ICC target	7000	Trap Drive	46.3
Max. accu. time	100 ms		

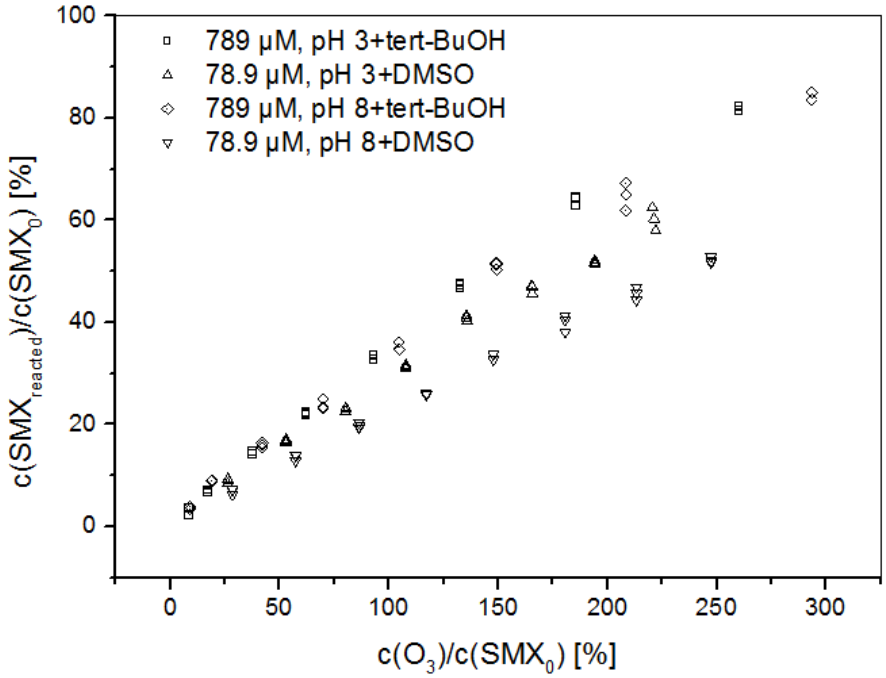

Figure S3.2: Comparison of ozone consumption during oxidation of SMX with initial concentrations of the stock solutions of 789 µM (ozone in presence of 150 mM *tert*-butanol: pH 3: square; pH 8: diamond) and 78.9 µM (ozone in presence of 10 mM DMSO: pH 3: triangle up; pH 8: triangle down). Each ozone dosage is represented by experimental triplicates. Concentration ($SMX_{reacted}$) denotes the actual reacted concentration, i.e. concentration of blank sample minus extant concentration of oxidized sample. All solutions were buffered with a 10 mM phosphate buffer.

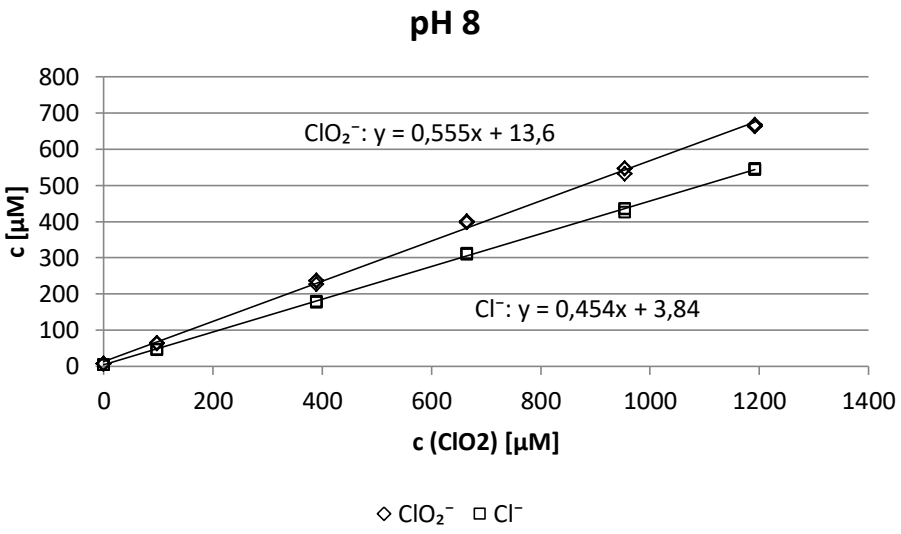

Figure S3.3: Quantification of chloride (squares) and chlorite (diamonds) after oxidation of SMX samples (c_i(SMX) = 789 µM) with chlorine dioxide at pH 8. Each chlorine dioxide dosage is represented by experimental triplicates. All solutions were buffered with 10 mM phosphate buffer.

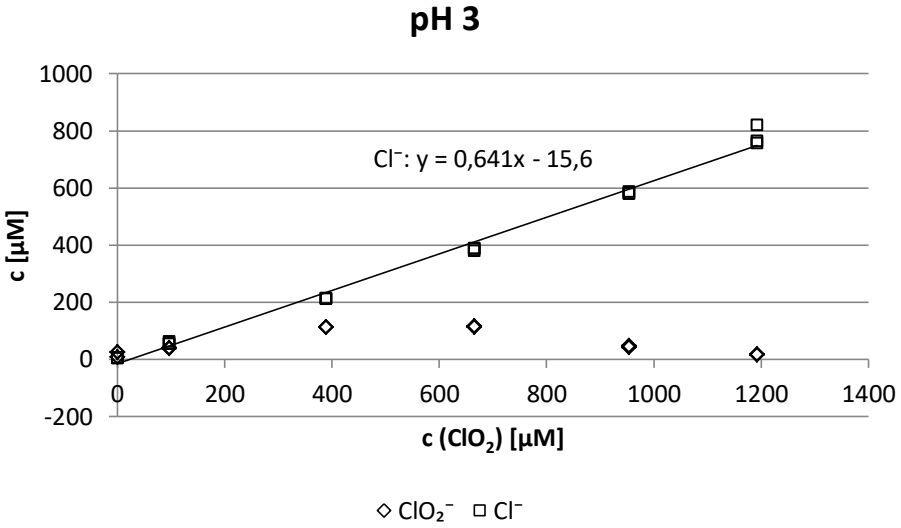

Figure S3.4: Quantification of chloride (squares) and chlorite (diamonds) after oxidation of SMX samples (c_i(SMX) = 789 µM) with chlorine dioxide at pH 3. Each chlorine dioxide dosage is represented by experimental triplicates. All solutions were buffered with 10 mM phosphate buffer.

Table S3.9: Main transformation products found for the oxidation of SMX at pH 3 and pH 8 with ozone in absence and presence of DMSO and with chlorine dioxide. For each transformation product, the according retention time (t_R), the measured mass-to-charge-ratio (m/z) as $[M-H]^-$, the derived elemental composition and the according calculated mass-to-charge-ratio (m/z) as $[M-H]^-$, the deviation from measured to calculated m/z and its double bond equivalent (DBE).

	Name	t_R [min]	Measured *m/z* $[M-H]^-$	Elemental composition [M-H]	Calculated *m/z* $[M-H]^-$	Error [ppm]	DBE
O_3, pH 3	TP177	2.6	176.9983	$C_4H_6N_2O_4S$	176.9976	-4.24	3
	TP226a	13.6	225.9922	$C_7H_5N_3O_4S$	225.9928	2.65	7
	TP268	13.4	268.0386	$C_{10}H_{11}N_3O_4S$	268.0398	4.29	7
	TP269	13.9	269.0243	$C_{10}H_{10}N_2O_5S$	269.0238	-1.97	7
	TP282	17.9	282.0179	$C_{10}H_9N_3O_5S$	282.0190	3.94	8
	SMX	14.4					
O_3, pH 8	TP177	2.7	176.9983	$C_4H_6N_2O_4S$	176.9976	-4.24	3
	TP226a	13.7	225.9922	$C_7H_5N_3O_4S$	225.9928	2.65	7
	TP268	13.5	268.0386	$C_{10}H_{11}N_3O_4S$	268.0398	4.29	7
	TP269	14.0	269.0243	$C_{10}H_{10}N_2O_5S$	269.0238	-1.97	7
	TP282	13.0	282.0152	$C_{10}H_9N_3O_5S$	282.0190	13.51*	8
	TP282	17.9	282.0179	$C_{10}H_9N_3O_5S$	282.0190	3.94	8
	SMX	14.4					
O_3+DMSO, pH 3	TP177	2.8	176.9980	$C_4H_6N_2O_4S$	176.9976	-2.54	3
	TP268	13.5	268.0408	$C_{10}H_{11}N_3O_4S$	268.0398	-3.92	7
	TP269	14.0	269.0243	$C_{10}H_{10}N_2O_5S$	269.0238	-0.45	7
	TP282	13.0	282.0164	$C_{10}H_9N_3O_5S$	282.0190	9.25*	8
	TP282	17.9	282.0195	$C_{10}H_9N_3O_5S$	282.0190	-1.74	8
	SMX	14.5					
O_3+DMSO, pH 8	TP177	2.8	176.9985	$C_4H_6N_2O_4S$	176.9976	-5.37	3
	TP268	13.5	268.0400	$C_{10}H_{11}N_3O_4S$	268.0398	-0.56	7
	TP269	14.0	269.0250	$C_{10}H_{10}N_2O_5S$	269.0238	-4.57	7
	TP282	4.5	282.0205	$C_{10}H_9N_3O_5S$	282.0190	-5.28*	8
	TP282	11.3	282.0205	$C_{10}H_9N_3O_5S$	282.0190	-5.39*	8
	TP282	13.0	282.0196	$C_{10}H_9N_3O_5S$	282.0190	-2.09	8
	TP282	17.9	282.0198	$C_{10}H_9N_3O_5S$	282.0190	-2.80	8
	SMX	14.5					
ClO_2, pH 3	TP177	3.0	176.9977	$C_4H_6N_2O_4S$	176.9976	-0.85	3
	TP226b	9.6	226.0299	$C_8H_9N_3O_3S$	226.0292	-3.14	6
	TP226b	10.0	226.0301	$C_8H_9N_3O_3S$	226.0292	-4.03	6
	TP226b	11.0	226.0299	$C_8H_9N_3O_3S$	226.0292	-3.14	6
	TP268	13.9	268.0394	$C_{10}H_{11}N_3O_4S$	268.0398	1.31	7
	TP269	14.5	269.0237	$C_{10}H_{10}N_2O_5S$	269.0238	0.26	7
	TP282	9.6	282.0190	$C_{10}H_9N_3O_5S$	282.0190	-0.07	8
	TP282	11.0	282.0164	$C_{10}H_9N_3O_5S$	282.0190	9.25*	8
	TP282	13.9	282.0165	$C_{10}H_9N_3O_5S$	282.0190	8.90*	8
	TP282	18.0	282.0180	$C_{10}H_9N_3O_5S$	282.0190	3.58	8
	SMX	15.0					

	Name	t_R [min]	Measured *m/z* $[M-H]^-$	Elemental composition [M-H]	Calculated *m/z* $[M-H]^-$	Error [ppm]	DBE
ClO_2, pH 8	TP177	3.0	176.9967	$C_4H_6N_2O_4S$	176.9976	4.80	3
	TP226b	10.3	226.0311	$C_8H_9N_3O_3S$	226.0292	-8.45*	6
	TP226b	11.2	226.0311	$C_8H_9N_3O_3S$	226.0292	-8.45*	6
	TP268	14.2	268.0387	$C_{10}H_{11}N_3O_4S$	268.0398	3.92	7
	TP269	14.6	269.0242	$C_{10}H_{10}N_2O_5S$	269.0238	-1.60	7
	TP272	14.1	271.9905	$C_9H_8ClN_3O_3S$	271.9902	-1.07*	7
	TP272	14.1	271.9894	$C_9H_8ClN_3O_3S$	271.9902	2.98	7
	TP282	5.8	282.0191	$C_{10}H_9N_3O_5S$	282.0190	-0.32	8
	TP282	12.2	282.0191	$C_{10}H_9N_3O_5S$	282.0190	-0.32	8
	TP282	14.1	282.0185	$C_{10}H_9N_3O_5S$	282.0190	1.81	8
	TP282	18.0	282.0192	$C_{10}H_9N_3O_5S$	282.0190	-0.67	8
	SMX	15.1					

*Peaks showed intensities below 150 cps thus often resulting in increased errors (ppm)

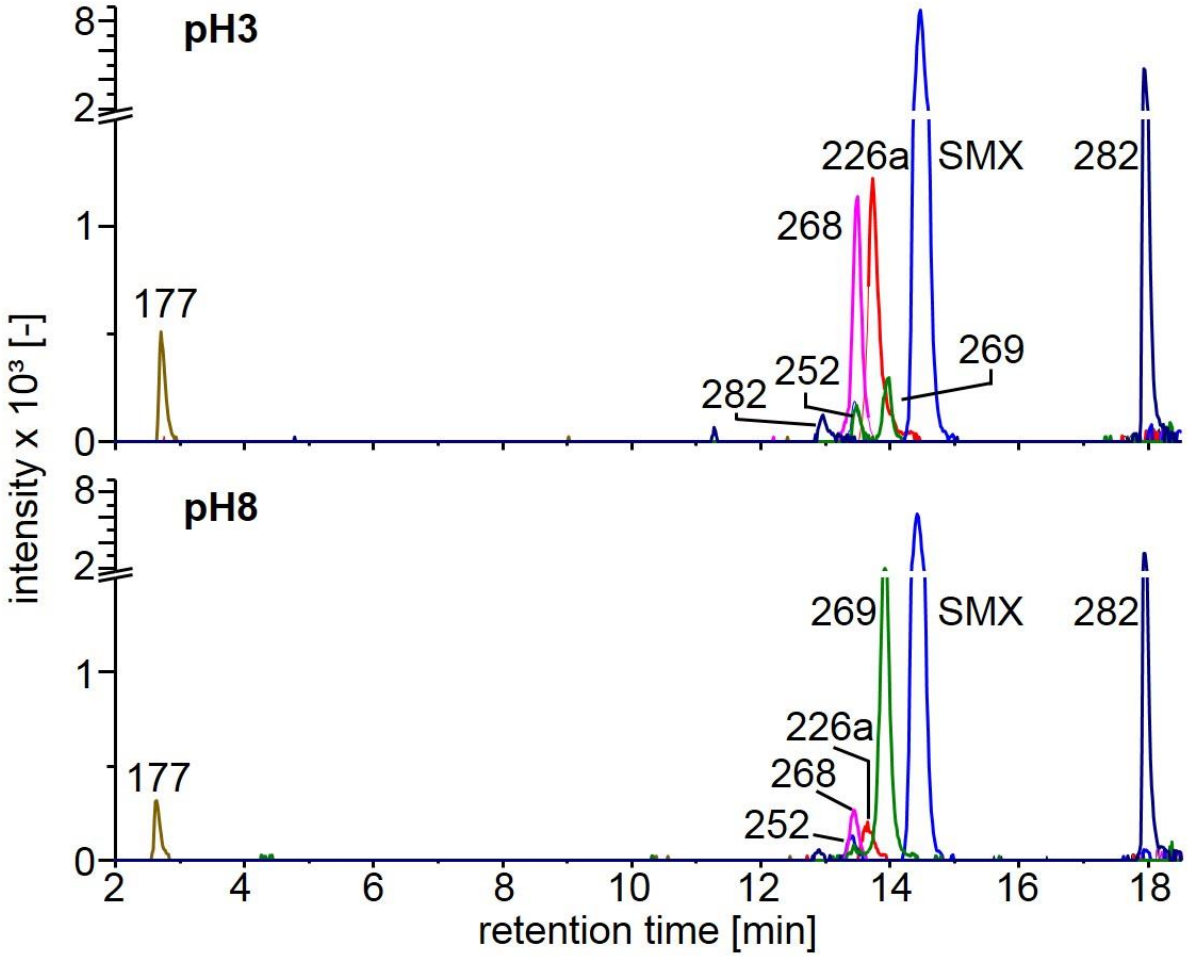

Figure S3.5: Main degradation products of the oxidation of SMX with ozone in absence of an OH radical scavenger. Exact *m/z* and further product information can be found in Table S3.9.

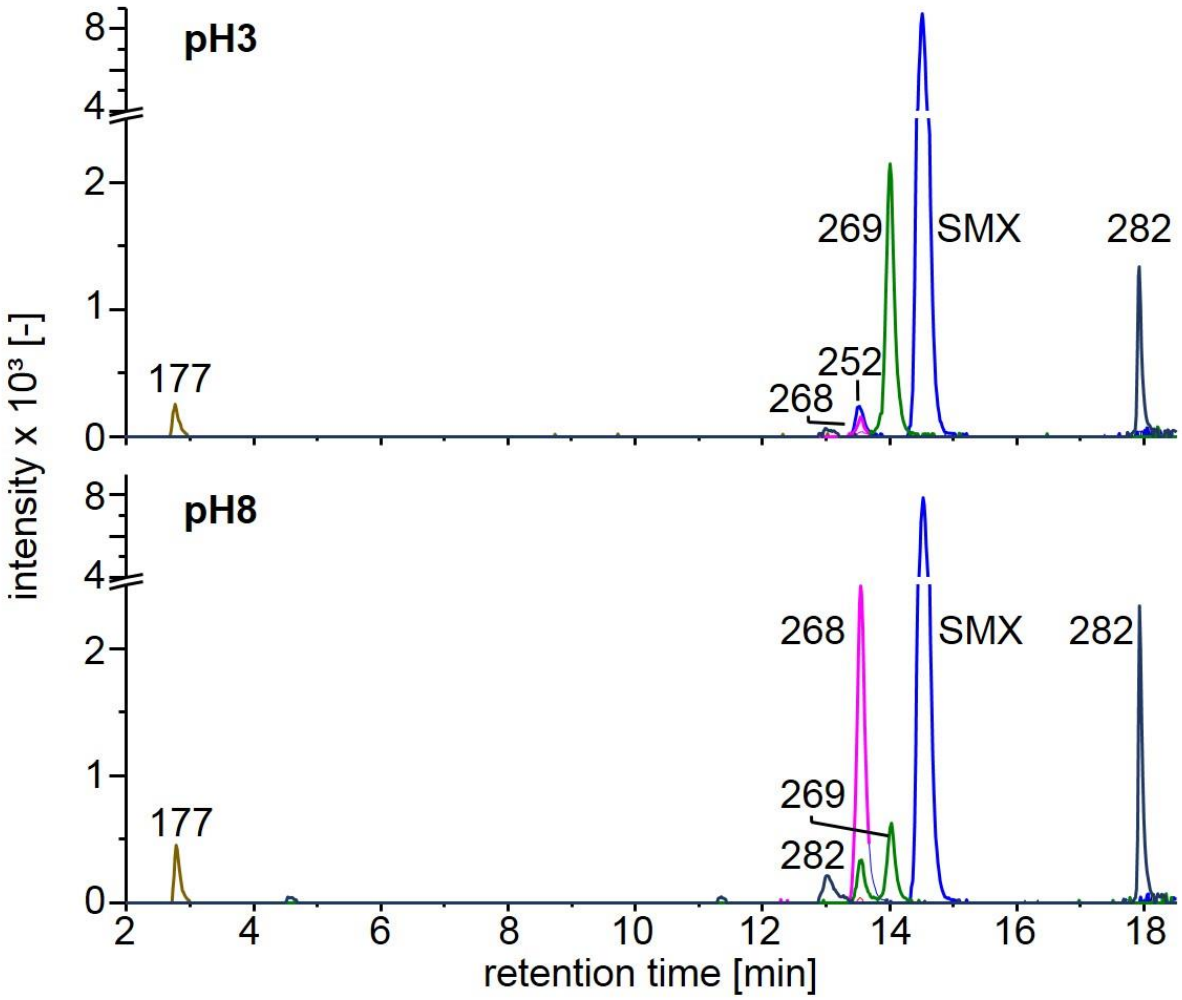

Figure S3.6: Main degradation products of the oxidation of SMX with ozone in presence of the OH radical scavenger DMSO. Exact *m/z* and further product information can be found in Table S3.9.

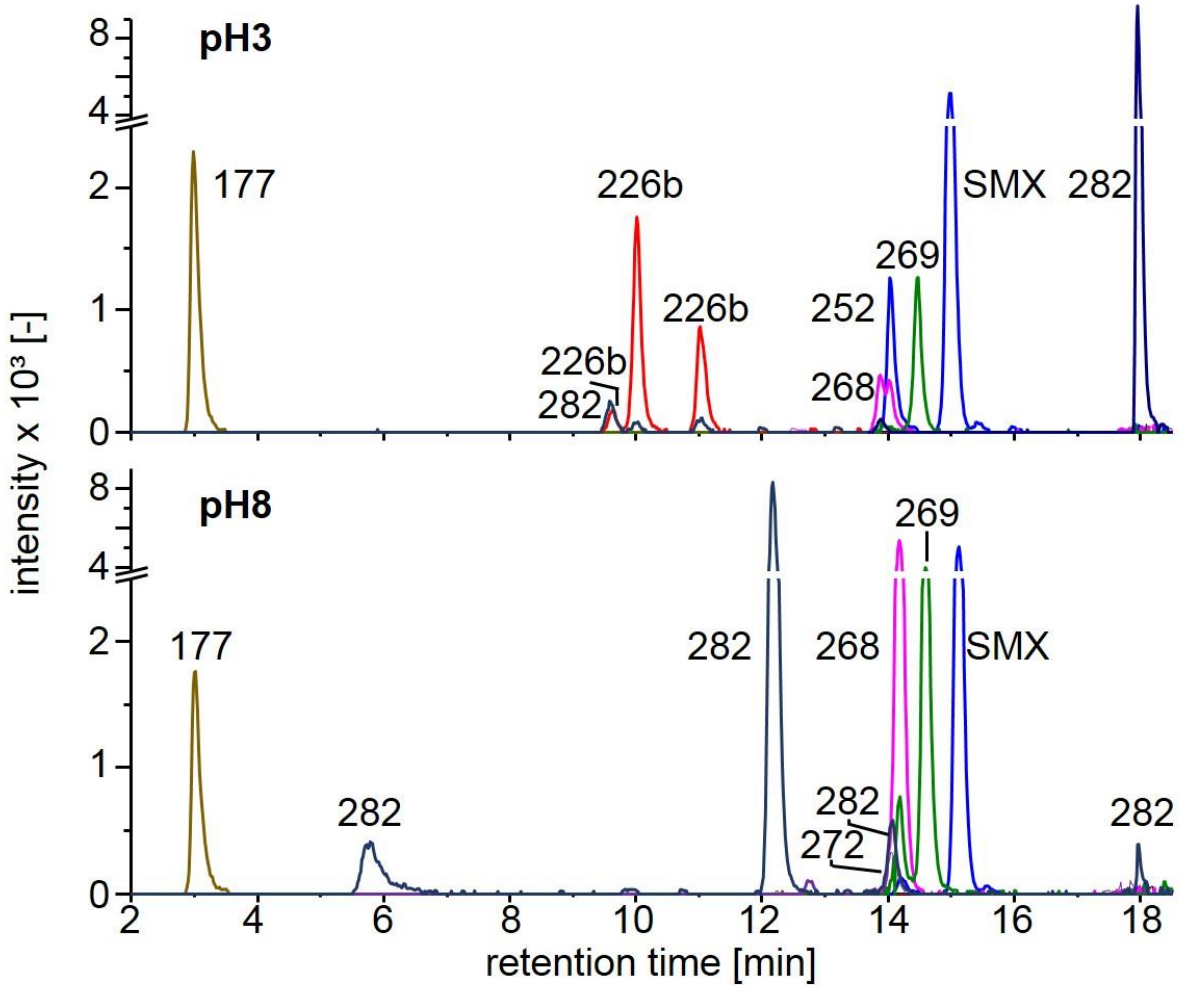

Figure S3.7: Main degradation products of the oxidation of SMX with chlorine dioxide. Exact *m/z* and further product information can be found in Table S3.9.

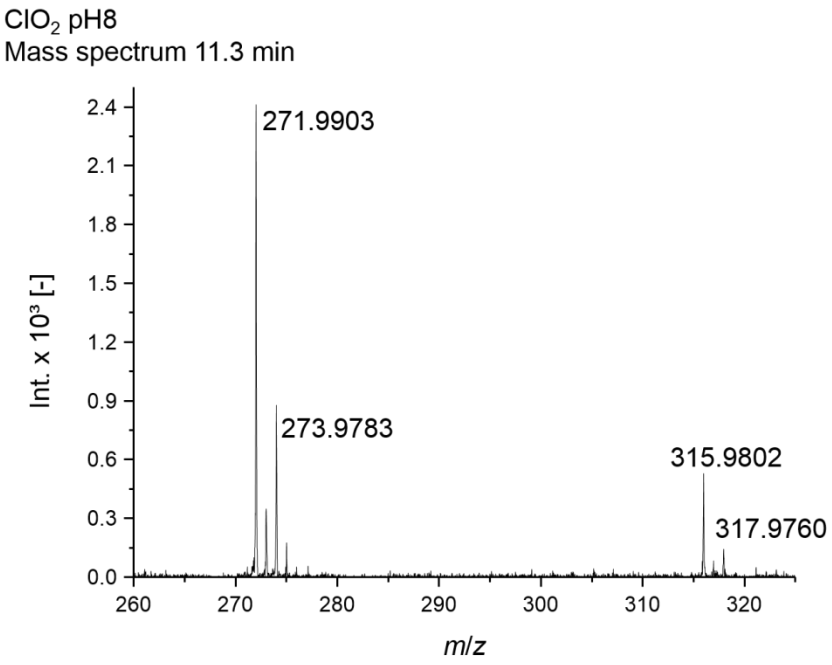

Figure S3.8: Product spectrum of TP272 found for SMX samples treated with chlorine dioxide at pH 8. Typical 3:1-distribution of the two masses 271.9903 and 273.9783, respectively, indicating the presence of one chlorine atom in the product.

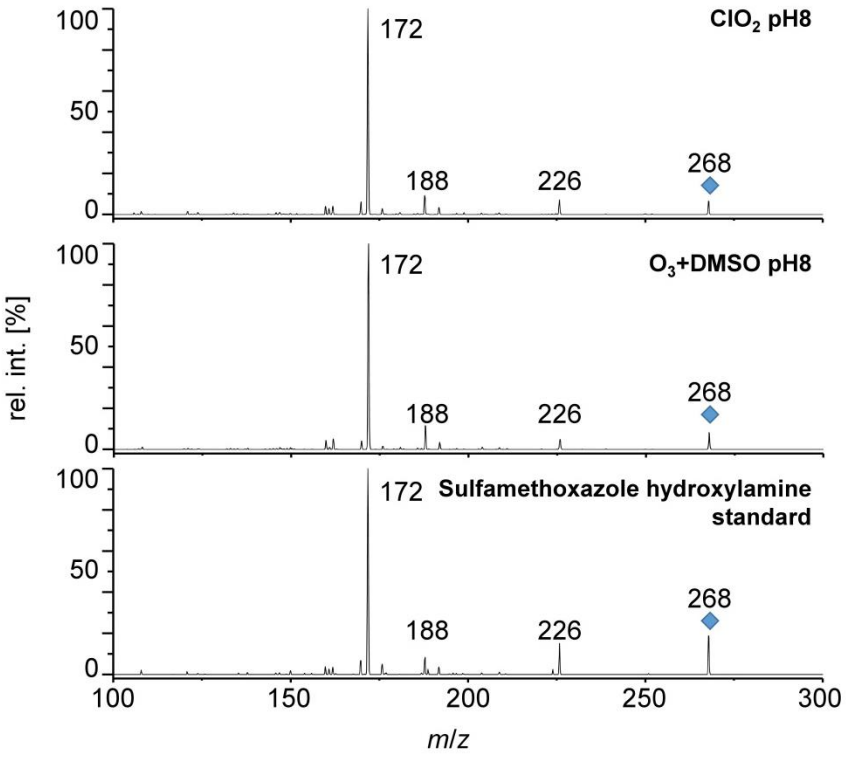

Figure S3.9: Comparison of TP268 detected in SMX samples oxidized with ozone in the presence of DMSO and chlorine dioxide at pH 8 each (exemplarily shown) to the commercially available analytical standard of sulfamethoxazole hydroxylamine.

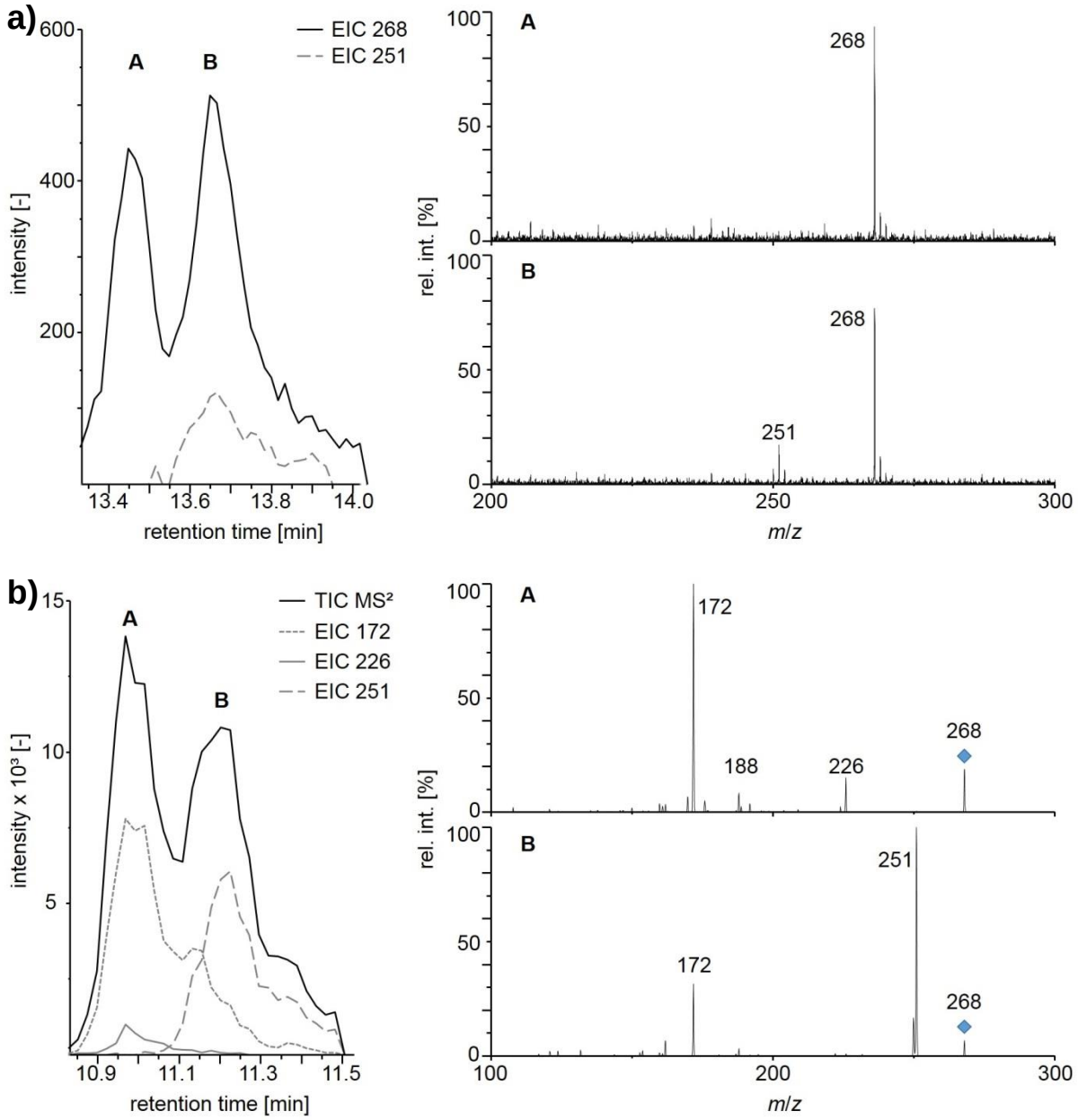

Figure S3.10: Mass spectra of the analytical standard of sulfamethoxazole hydroxylamine obtained with a) LC-ESI(-)-ToF-MS and b) with the LC-ion trap-MS after MS^2-fragmentation. The analyte peak consisted of two conformers "A" and "B" which could not be fully baseline separated. Peak "B" showed the additional characteristic *m/z* 251 as indicated by the dotted lines in the chromatograms. Peak "A" corresponded to the retention times of TP268 detected in the oxidized SMX samples whereas "B" was not detected in the oxidized SMX samples (see Figure S3.9). It has to be noted that retention times of LC-ESI(-)-ToF-MS and LC-ion trap-MS differ because two different LC-systems were employed (cf. Materials and methods section)

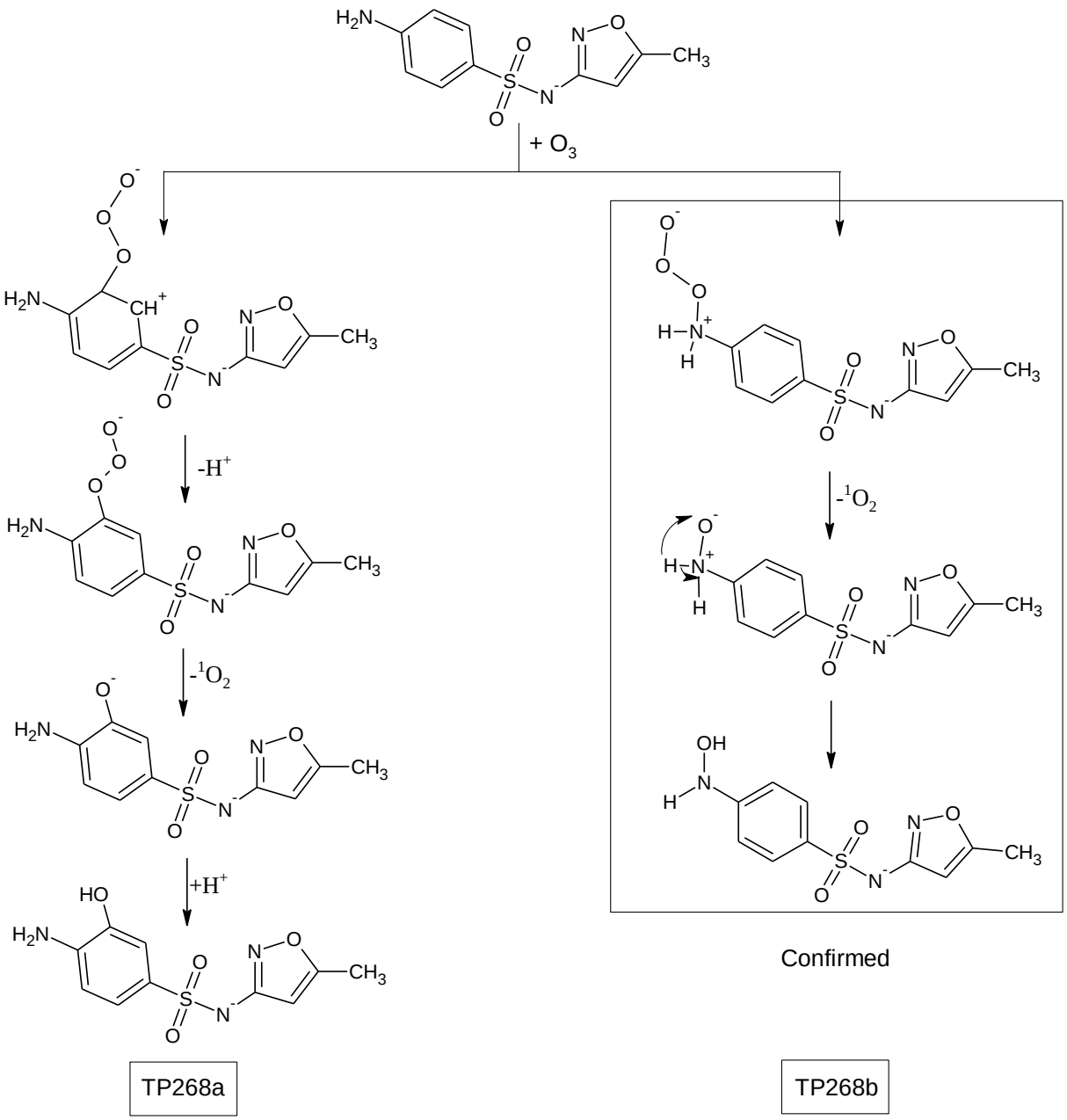

Scheme S3.2: Possible reaction mechanisms for formation of TP268a and TP268b. TP268b could be confirmed by comparison of retention times with analytical standard of sulfamethoxazole hydroxylamine and related fragmentation patterns in MS^n-experiments

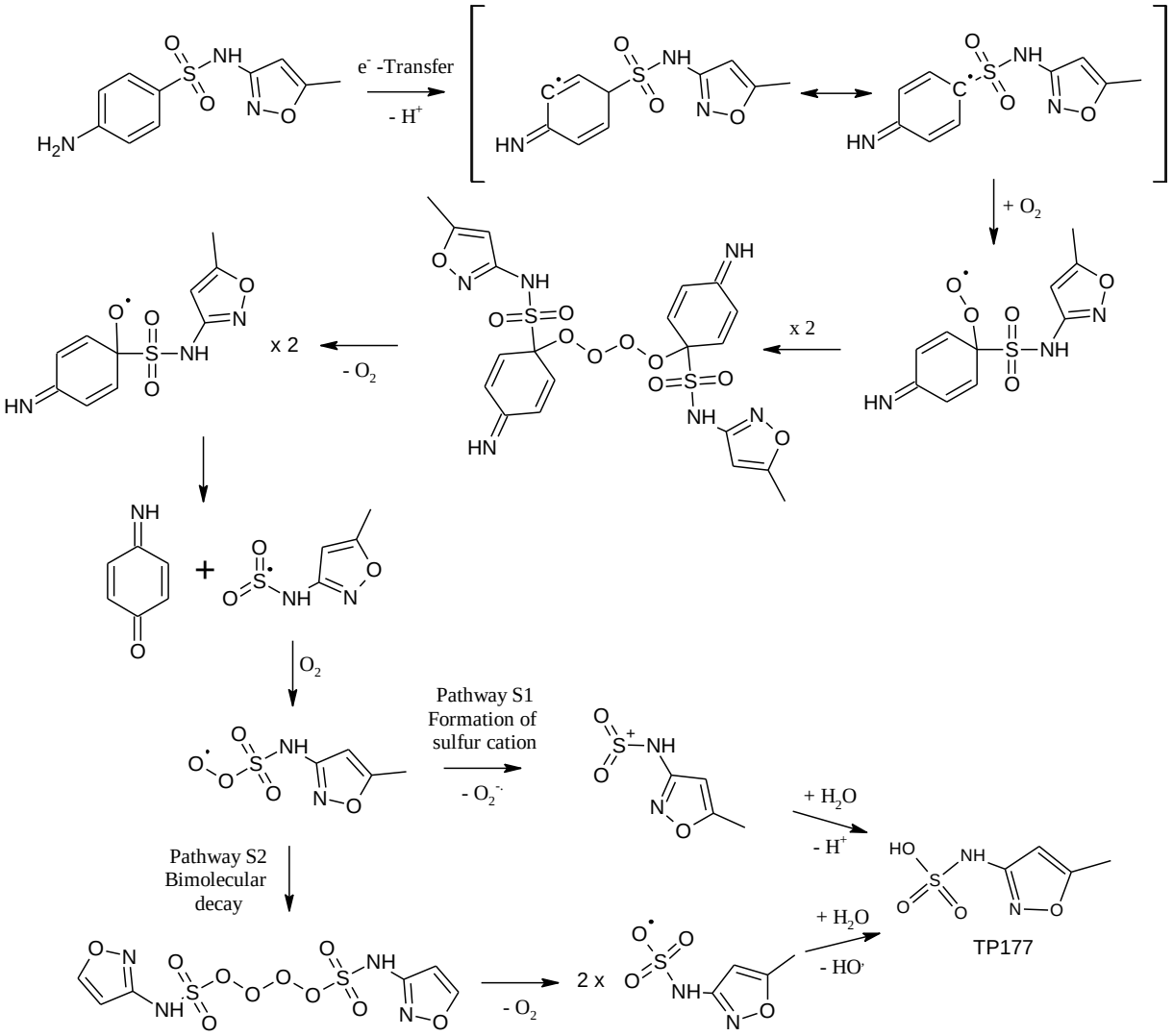

Scheme S3.3: Proposed reaction mechanisms for the formation of TP177 in the reaction of ozone with SMX. Although the postulated formation of the sulfur-centered radical could not be found in the available literature, the authors believe that the mechanism shown is a possible way of formation of TP177. Additionally, Pathway S2, which includes the bimolecular decay of the peroxyl radical appears to be more likely than Pathway S1. The other presented radical reaction pathways have been described in detail by von von Sonntag and Schuchmann[190].

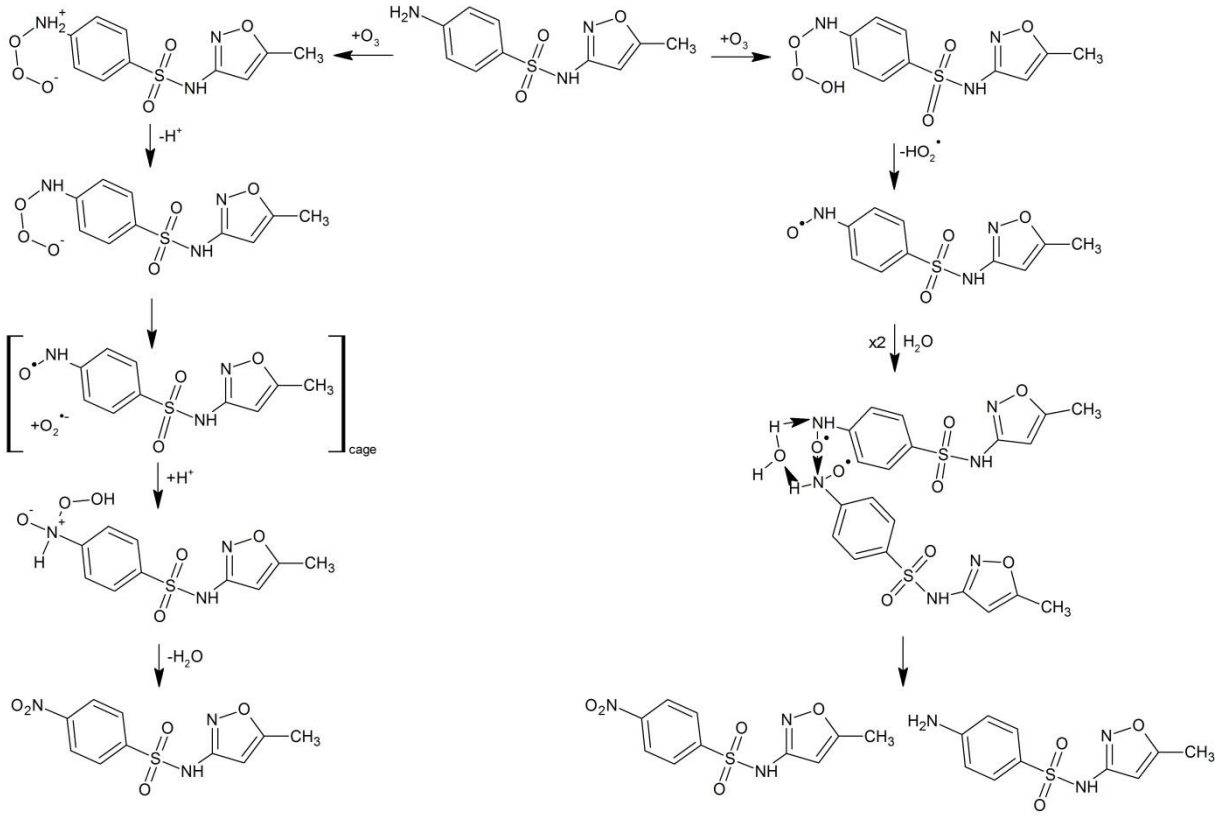

Scheme S3.4: Proposed reaction mechanisms for formation of TP282 in the reaction of ozone with SMX following postulates of Tekle-Röttering et al.[25] and von Sonntag and von Gunten[2].

Chapter 4 -
Direct photolysis of SMX with UV/vis-light

Reproduced with permission from: Willach, S., Lutze, H. V., Eckey, K., Löppenberg, K., Lüling, M., Wolbert, J.-B., Kujawinski, D. M., Jochmann, M. A., Karst, U., Schmidt, T. C., Direct photolysis of sulfamethoxazole using various irradiation sources and wavelength ranges - Insights from degradation product analysis and compound-specific stable isotope analysis. *Environmental Science and Technology*, **2018**, 52 (3), 1225-1233; DOI: 10.1021/acs.est.7b04744

4.1 Abstract

The environmental micropollutant sulfamethoxazole (SMX) is susceptible to phototransformation by sunlight and UV-C light which is used for water disinfection. Depending on the environmental pH conditions SMX may be present as neutral or anionic species. This study systematically investigates the phototransformation of these two relevant SMX species using four different irradiation scenarios, i.e. a low, medium and high pressure Hg lamp and simulated sunlight. The observed phototransformation kinetics are complemented by data from compound-specific stable isotope and transformation product analysis using isotope-ratio and high-resolution mass spectrometry (HRMS). Observed phototransformation kinetics were faster for the neutral than for the anionic SMX species (from 3.4 (LP lamp) up to 6.6 (HP lamp) times). Furthermore, four phototransformation products (with m/z 189, 202, 242, and 260) were detected by HRMS that have not yet been described for direct photolysis of SMX. Isotopic fractionation occurred only if UV-B and UV-A wavelengths prevailed in the emitted irradiation and was most pronounced for the neutral species with simulated sunlight (ε_C = -4.8 ± 0.1 ‰). Phototransformation of SMX with UV-C light did not cause significant isotopic fractionation. Consequently, it was possible to differentiate sunlight and UV-C light induced phototransformation of SMX. Thus CSIA might be implemented to trace back waste water point sources or to assess natural attenuation of SMX by sunlight photolysis. In contrast to the wavelength range, pH-dependent speciation of SMX did hardly impact isotopic fractionation.

4.2 Introduction

In recent years, the number of micropollutants detected in the aqueous environment has steadily increased.[77,161,191] One important representative is sulfamethoxazole (SMX), a sulfonamide antibiotic. There are numerous sources for its release into the aquatic environment. Besides the original use in human medicine for treatment of respiratory[192] or urinary tract infections[193], SMX is extensively used as preventive measure in veterinary medicine such as aquacultures or livestock farming.[77,160,194] Consequently, SMX is regularly detected in surface- or groundwaters.[76,161] Additionally, the metabolism of SMX in the human body and the removal of SMX during treatment in wastewater treatment plants (WWTPs) are incomplete.[77,195-197] The presence of elevated concentrations of antibiotics may lead to the development of microbial resistance genes,[198,199] thus, their control and reduction are of major public concern. Loos et al. have found SMX at average concentrations of 76 ng L^{-1} in 75 % of the investigated European rivers.[191] Among 112 evaluated micropollutants, SMX was classified as one out of six priority pharmaceuticals and personal care products with the greatest potential risk in the Chinese aquatic environment.[161] Under environmental conditions the neutral and the anionic species of SMX are of relevance due to its p$K_{a,2}$ of 5.7 ± 0.2 (Figure 4.1).[167]

Figure 4.1: The three possible species of SMX as cationic, neutral or anionic form (adapted from Boreen et al.[167]).

Possible degradation pathways of SMX in the aquatic environment are microbial degradation[172,200] as well as direct[167,172] and indirect photolysis.[197,201] Besides natural sunlight, SMX is also readily photolysed by UV light implemented in drinking-water disinfection[70] or wastewater treatment.[202-205] Several studies have investigated the transformation products (TPs) resulting from the numerous ways of (environmental) degradation of SMX.[167,206-209] Typically, high-resolution mass spectrometry (HRMS) is used for TP identification.[103,114,206,207] Moreover, identification of certain or unique TPs may permit conclusions about the underlying degradation process. However, current literature shows that identical TPs may be formed in different degradation processes. Two illustrative examples are (5-methylisoxazol-3-yl)sulfamate or the hydroxylated isomers of SMX which are regularly detected after ozonation[116,170,180,210], direct photolysis[91,206] or oxidation with chlorine dioxide[210]. Thus, TP analysis alone may not be capable of tracking the underlying degradation processes in case

of SMX degradation. However, it might be of interest to be able to distinguish natural degradation processes in the environment and transformation processes in engineered systems, i.e. water treatment and disinfection, e.g., with the oxidative processes listed above.

Compound-specific stable isotope analysis (CSIA) has recently been shown to be useful as an additional proxy in the characterization of transformation reactions[132,154,155,172] as well as in identification of contaminant sources[118,130]. The measurement of the isotopic ratio of the parent compound allows to detect isotopic fractionation if, e.g., kinetic isotope effects (*KIE*) occur. A *normal* isotope effect is observed if the reaction rates of the lighter isotopes (e.g. ^{12}C) involved in the chemical bond broken react faster than the heavier ones (e.g. ^{13}C). As a result, the ratio of ^{13}C to ^{12}C of the remaining parent compound is increased.[120,127] The opposite case (ratio of ^{13}C to ^{12}C decreases) can also occur and is termed *inverse* isotope effect.[127] If isotopic effects occur, it may be possible to distinguish different degradation processes such as biodegradation or photolysis[172] by CSIA of the parent compound without identification or quantification of resulting TPs or a detailed knowledge of the underlying degradation mechanisms.[118,211] Moreover, it has recently been shown that it is possible with CSIA to differentiate micropollutant degradation caused by biotransformation and abiotic processes such as photolysis by sunlight, respectively.[154,172] Birkigt et al. investigated isotopic fractionation during photolysis of SMX by sunlight and found evidence that isotopic fractionation might be pH-dependent, i.e., linked to the prevailing species of SMX.[172] However, other constituents present in the irradiated samples may also have affected the isotopic fractionation of SMX such as the nutrient medium used. This may contain photosensitizers, which may result in indirect phototransformation of SMX.

The aim of this study was to investigate the direct photolysis of SMX caused by different wavelengths and wavelength ranges which may be relevant in engineered systems and under natural conditions. For characterization of the different scenarios degradation kinetics, transformation products and data from CSIA are combined. To that end, the two environmentally relevant species of SMX, i.e. the neutral and anionic species, are subjected to direct photolysis. To cover the whole variety of UV light sources which may be used in water treatment plants, a low pressure (LP), a medium pressure (MP) and a high pressure (HP) Hg lamp were employed. For simulation of sunlight the MP lamp was used in combination with a cut-off filter that absorbed radiation below $\lambda = 310$ nm. For complementary purposes, SMX was subjected to photolysis by laser light ($\lambda = 266$ nm). The latter results are available in the supporting information in Text S4.10 and Figure S4.8.

4.3 Materials and Methods

4.3.1 Chemicals

All chemicals and solvents were used as received from the supplier. A detailed list of all chemicals used can be found in Text S4.1.

4.1.1 Preparation of samples

SMX solutions of 790 µM were directly prepared in 10 mM phosphate buffered water either at pH 3 (neutral species prevails) or pH 8 (anionic species prevails). The stability of pH was rechecked after every experiment and maintained constant for every setup.

4.1.2 Photolysis experiments

Three different irradiation setups were employed for direct photolysis experiments, which are described in detail in Text S4.2-5. Briefly, first, a merry-go-round photoreactor for irradiation with a low-pressure (LP) (λ = 254 nm; TNN 15/32, nominal power 15 W, Heraeus Noblelight, Hanau, Germany, 185 nm band suppressed) and a medium-pressure (MP) mercury lamp (λ = 200-600 nm; TQ 718, nominal power 700 W, Heraeus Noblelight; both lamps were supplied by Peschl Ultraviolet, Mainz, Germany) (Figure S4.1a)) was used. The merry-go-round photoreactor (Figure S4.3 & Text S4.3) has been described previously.[212,213] The LP and MP lamp were placed in a cooling jacket in the center of the photoreactor. A volume of 70 mL of the SMX solution was filled in quartz glass tubes positioned circularly around the lamp. The cooling jacket and the glass container were filled with ultrapure water to maintain a temperature of 25.0 ± 0.2 °C. The light absorption of the ultrapure water within the emitted wavelength range was negligible. The fluence rate of the LP lamp was determined by uridine actinometry and varied in a range of 54-63 µeinstein m^{-2} s^{-1} with an average of 60 ± 4 µeinstein m^{-2} s^{-1} (cf. Text S4.3) and controlled on a daily basis.[72]

In case of the MP Hg lamp, a second approach was used to simulate sunlight irradiation conditions. Therefore, the cooling water in the cooling jacket was replaced by a potassium hydrogen phthalate solution which caused total absorption for wavelengths below 310 nm. The efficacy of the cut-off filter was controlled by spectrophotometric absorption measurements of the potassium hydrogen phthalate solution (Figure S4.4) and atrazine control samples (Figure S4.5), which were run simultaneously with the SMX samples (cf. Text S4.3). In order to simulate SMX photolysis by sunlight irradiation, it is not necessary to provide the full sunlight spectrum with wavelengths up to 800 nm[68] since the neutral and anionic species of SMX do not significantly absorb irradiation above 320 nm

(cf. Figure S4.1). Hence, even if natural sunlight emission is typically more pronounced at longer wavelength, radiation of λ > 320 nm may not contribute to photolysis of SMX.

Second, a high-pressure (HP) Hg lamp (*λ* = 220-500 nm; SUV-DC-P Deep-UV, Lumatec, Deisenhofen, Germany) connected to a liquid lightguide (series 250, ø5 mm x 1000 mm; Lumatec) (Figure S4.1b), S4.2, S4.6 & Text S4.4) was used. Samples were irradiated from above in an open crystallizing dish while being stirred continuously.

Third, for complementary purposes, a wavelength-quadrupled neodymium-doped yttrium aluminum garnet ($Nd:Y_3Al_5O_{12}$) laser (Nd:YAG-laser) (*λ* = 266 nm; Polaris II, New Wave Research, St Neots, UK) was used, and was integrated in a flow-through setup with a 5 cm quartz laser cuvette connected to an HPLC pump (PLATINblue; Knauer, Berlin, Germany) to precisely control different flow rates (Figure S4.7, Text S4.5 & Table S4.1). All results are shown in Figure S4.8 and discussed in Text S4.10.

4.1.3 Analytical methods

A UV-1650PC spectrophotometer (Shimadzu, Duisburg, Germany) was used for absorption measurements with a quartz cuvette with an optical path-length of 1 cm. For pH measurements, a pH-meter (827 pH lab with aquatrode both from Metrohm, Herisau, Switzerland) was used, which was calibrated with standard buffers every working day.

SMX and atrazine were quantified by an HPLC-DAD system (LC-10AT pump coupled to a SPD-M10A detector; Shimadzu, Duisburg, Germany). Calibration standards were prepared from 99-790 µM SMX and 1-6 µM atrazine, respectively (cf. Text S4.6 & S4.7).

Compound-specific stable isotope values of SMX samples were determined by high-temperature-liquid chromatography isotope-ratio mass spectrometry (HT-LC-IRMS). The system consisted of a binary piston pump (Rheos Allegro, Flux Instruments/Thermo Fisher Scientific, Bremen, Germany), a HTC PAL autosampler (CTC Analytics, Zwingen, Switzerland; supplied by Axel Semrau, Sprockhövel, Germany), a HT HPLC 200 column oven (SIM, Oberhausen, Germany) and a LC IsoLink interface connected to a DeltaV Advantage isotope-ratio mass spectrometer (both: Thermo Fisher Scientific). For separation, a temperature gradient was run on an X-Bridge C_{18} column (100 x 2.1 mm, particle size 3.5 µm, 130 Å) (Waters, Eschborn, Germany). More details can be found in Kujawinski et al. with modifications described in Willach et al. and Text S4.8.[171,210] Linearity and precision test were run regularly. Each sample was measured in triplicate and was followed by a 390 µM SMX standard. SMX carbon isotope values are given in reference to the international Vienna Pee Dee Belemnite (VPDB) scale according to Equation 4.1 (cf. Text S4.8).[120]

$$\delta^{13}C_{SMX,VPDB} = \left(\frac{R_{SMX}\left({}^{13}\mathrm{C}/{}^{12}\mathrm{C}\right) - R_{VPDB}\left({}^{13}\mathrm{C}/{}^{12}\mathrm{C}\right)}{R_{VPDB}\left({}^{13}\mathrm{C}/{}^{12}\mathrm{C}\right)} \right) \quad (4.1)$$

where R_{SMX} and R_{VPDB} are the ratios of ${}^{13}\mathrm{C}/{}^{12}\mathrm{C}$ of SMX samples and VPDB. The given standard deviations refer to a minimum of three replicate measurements. The carbon isotope enrichment factor (ε_C) of each photolytic degradation of SMX could be determined by application of the Rayleigh-equation (Equation 4.2):[120]

$$\ln\left(\frac{R_{t,SMX}({}^{13}\mathrm{C}/{}^{12}\mathrm{C})}{R_{0,SMX}({}^{13}\mathrm{C}/{}^{12}\mathrm{C})} \right) = \ln\left(\frac{\delta^{13}\mathrm{C}_{t,SMX}+1}{\delta^{13}\mathrm{C}_{0,SMX}+1} \right) = \varepsilon_C \cdot \ln\left(\frac{c_{t,SMX}}{c_{0,SMX}} \right) \quad (4.2)$$

where $\delta^{13}\mathrm{C}_0$ and $\delta^{13}\mathrm{C}_t$ and the concentrations of SMX, i.e. c_0 and c_t, originate from sampling time 0 and time t, respectively.

Transformation product analysis was conducted with a high performance liquid chromatographic system (Shimadzu) coupled to a time-of-flight mass spectrometer (Bruker micrOTOF, Bruker Daltonics, Bremen, Germany) with electrospray ionization in negative ionization mode (HPLC/ESI(-)-ToF-MS). Further details are provided in Text S4.9 and Tables S4.2-4.

4.4 Results and Discussion

4.4.1 SMX transformation by direct photolysis

The reaction kinetics are an important cornerstone for characterization of transformation reactions. In general different irradiation setups, as they were used in this study, may only reasonably be compared on the basis of fluence rates.[70,71] However, fluence rates could not be determined for the polychromatic radiation sources since suitable actinometers were lacking. Hence, the fluence rate was only determined for the monochromatic LP lamp. In the following the results of pH 3 and 8 of each setup may be directly compared. Comparisons between the four setups though are only of a qualitative nature. In all four mercury lamp irradiation setups, the transformation of the neutral species is significantly faster than that of the anionic one (Figure 4.2), i.e. in a range of 3.41 ± 0.02 times faster in case of the LP lamp and even 6.58 ± 0.02 times faster in case of the HP lamp. These findings are in agreement with results from Boreen et al. and Zhou and Moore, who observed significantly higher phototransformation rates for the neutral species in comparison to the anionic one.[167,214] Moreover, the results for phototransformation with the LP lamp are in line with data of Canonica et al., who found that the neutral SMX species is transformed faster by a factor of 3.30 ± 0.46 over the anionic one (Table S4.5).[70] Additionally, the quantum yields for

λ = 254 nm were determined by Canonica et al. to be 0.212 ± 0.018 mol einstein^{-1} (neutral species) and 0.046 ± 0.021 mol einstein^{-1} (anionic species), which readily explains why phototransformation is more efficient for the neutral species than for the anionic one at λ = 254 nm even though the molar absorption coefficient is 1.4 times higher for the anionic SMX species (Table S4.5).[70]

Moreover, the monochromatic LP lamp (λ = 254 nm) and the polychromatic MP lamp (Figure 4.2a-d) revealed comparable ratios of first order apparent photolysis rate constants (k_p^{app}) of neutral to anionic SMX species each (further details Figure S4.1). For LP and MP lamp in absence of the cut-off filter, the ratios are (k_p^{app}(neutral SMX/anionic SMX)) 3.41 ± 0.02 and 3.64 ± 0.03, respectively. The comparable ratios are possibly due to the strong emission of the MP lamp at 254 nm which seems to predominate over the emission at UV-B and UV-A wavelengths.

In contrast to that, the ratio of k_p^{app} for neutral over anionic SMX species shifts to 5.63 ± 0.05 if only simulated sunlight, i.e. UV-B, UV-A plus visible light (MP lamp + cut-off filter), is used for irradiation and, overall, the apparent transformation for both SMX species is significantly slowed down (Figure 4.2e & f). This observation indicates that if UV-C light is available for SMX phototransformation, UV-B, UV-A and visible light wavelengths are not important anymore. The fraction of SMX degradation by UV-B, UV-A and visible light (in presence of the cut-off filter) compared to degradation with the full emission spectrum of the MP lamp (absence of the cut-off filter) is 11.5 ± 0.3 % (pH 3) and 7.41 ± 0.05 % (pH 8) (k_p^{app}(MP+cut-off filter)/k_p^{app}(MP)).

In case of phototransformation under HP lamp irradiation (Figure 4.2g & h), the highest ratio of k_p^{app} (neutral SMX)/k_p^{app} (anionic SMX) was observed, i.e. 6.58 ± 0.02. This result may be attributed to two reasons. First, the irradiation with the HP lamp was conducted using a liquid lightguide which has a lower transmission for UV-C (~70 %) than for UV-B and UV-A light (~80 %) (Figure S4.2) thus leading to a stronger reduction of the phototransformation rate of the anionic than of the neutral SMX species (cf. Figure S4.1b). Second, the slightly shifted absorption spectrum of the neutral SMX species to longer wavelengths in combination with the high intensity of UV-B and UV-A light of the HP lamp (Figure S4.1b) leads to an overall increased phototransformation rate of the neutral species.

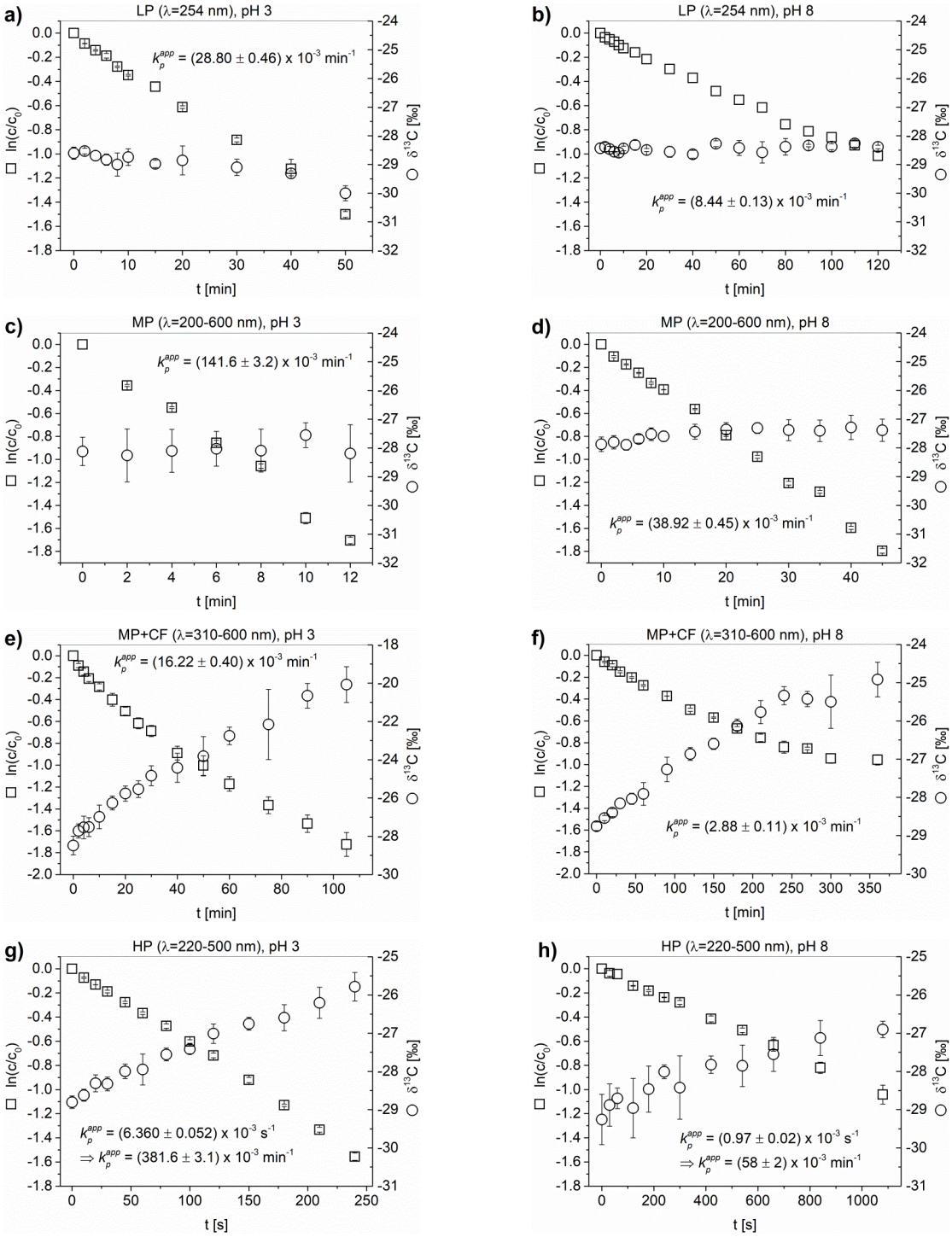

Figure 4.2: Photolysis of SMX with monochromatic (a & b) and non-monochromatic light sources (c-h). Data are shown for the LP lamp, MP lamp, MP lamp plus cut-off filter (CF) and HP lamp in dependence of the time *t* at pH 3 (a, c, e & g) and pH 8 (b, d, f & h), respectively. Concentration decrease is given as ln(c/c_0) (squares; error bars represent standard deviations of experimental replicates) and carbon isotope values as δ^{13}C (circles; error bars represent standard deviations of experimental replicates plus the triplicate measurement of each sample). First order apparent photolysis kinetic rate constants (k_p^{app}) shown in each according graph are derived from the slopes of *t* vs. ln(c/c_0). The given uncertainty originates from the standard deviation of the related slope.

An additional explanation for the differences between the irradiation setups in transformation kinetics could be that other chromophores are excited at 254 nm than at longer wavelengths. Therefore, the absorption spectra of SMX and three of its possible TPs (Figure S4.9) are compared with each other. It appears that the TPs carrying a sulfanilic moiety absorb UV light rather similarly to SMX whereas 3-amino-5-methylisoxazole does only significantly absorb light in the lower UV-C range (λ < 250 nm) at both pHs. In this view, it appears rather likely that the sulfanilic moiety is the relevant chromophore in all irradiation setups applied in this study. Consequently, the higher energy of UV-light is the decisive factor for the differing transformation kinetics.

Canonica et al. have determined photon fluence-based rate constants ($k_{E_p^0}$) for the direct phototransformation of neutral and anionic SMX at 254 nm[70], which were obtained from low optical density solutions. However, the LC-IRMS measurements required high initial SMX concentrations of 790 µM, which led to a significant absorption at 254 nm (Table S4.6). In order to calculate the apparent photon fluence-based rate constants ($k_{E_p^0}^{app}$) from the apparent pseudo-first-order rate constants for phototransformation (k_p^{app}) it is crucial to determine the average fluence rate ($E_{\lambda=254nm}^{avg}$) in the SMX containing sample. Since it is hardly possible to measure the fluence rates at such high optical densities, it was determined in pure water (Text S4.3) and corrected for the optical density in the SMX system using the Morowitz correction.[71] The according formulas and all intermediate results are shown in Text S4.11 and Table S4.6. The quotient of k_p^{app} and $E_{\lambda=254nm}^{avg}$ results in the photon fluence-based rate constant. The values for $k_{E_p^0}^{app}$ of our study are 240 m^2 $einstein^{-1}$ ± 4 m^2 $einstein^{-1}$ (neutral SMX) and 107 m^2 $einstein^{-1}$ ± 2 m^2 $einstein^{-1}$ (anionic SMX), respectively, and are comparable with the $k_{E_p^0}$ of Canonica et al. (580 ± 48 m^2 $einstein^{-1}$ (neutral species) and 176 ± 80 m^2 $einstein^{-1}$ (anionic species); Table S4.5).[70] Given the pH conditions of the experimental setup in this study, the $k_{E_p^0}^{app}$ are equivalent to species-related $k_{E_p^0}$ values without further correction since either the neutral or the anionic SMX species prevails without significant influences from the other SMX species. Even though Canonica et al., used much smaller initial concentrations of SMX their $k_{E_p^0}^{app}$ agreed well with our study, indicating that our results are also representative for smaller SMX concentrations.[70] In addition, the molar absorptivity of two out of three typically formed transformation products of SMX phototransformation, i.e. sulfanilic acid and sulfanilamide, absorb UV-C light at 254 nm to a

similar degree compared to SMX (Figure S4.9).[167,206,208,209] This implies that the optical density would not be changed if these transformation products are formed during the phototransformation of SMX. The observation that SMX photolysis follows the same first order rate constants during the whole experimental runs corroborates this, since a change in the absorptivity of the solution would result in different fluence rates and thus, different first-order reaction rates.

4.4.2 Transformation product analysis

Analysis with HPLC/-ESI(-)-ToF-MS revealed ten major transformation products (TPs) among other minor products (Figure 4.3 and Table S4.7). According to their *m/z*-ratios, these were termed as TP177, TP189, TP202, TP214, TP242, TP252, TP260, TP266, TP268 and TP270 (cf. Table S4.8 and Figures S4.10-13). It has to be noted that TP189 and TP260 were only observed after irradiation of SMX at pH 3, whereas TP242 was solely detected in significant amounts after phototransformation of SMX at pH 8. Several of these TPs and their exact masses have been reported by previous researchers, namely TP177 as (5-methylisoxazol-3-yl)-sulfamate[206,215,216], TP214[217] as sulfacarbamide, TP252, i.e. the photoisomer of SMX,[91,206,208,209,214,216-218], TP266 as SMX-NO[215], TP268 as various isomers of hydroxylated SMX (SMX-OH)[91,206,208,214-216] and TP270 that Zhou and Moore derived to be the hydrated product of 2H-azirine[214]. However, the double-bond equivalency of 6 (Table S4.7) would also support a hydroxylation of the methylisoxazole-moiety as it was proposed by Trovó et al. and Yang et al..[91,208] So far, TP242 has only been observed as a TP resulting from an OH radical attack in a photo-Fenton reaction.[219] Apart from this, TP189, TP202, TP242 and TP260 have not been reported as TPs after direct phototransformation of SMX. Tentatively formulated structures are shown in the Table S4.8 for TP189, TP202 and TP242. For TP260, no reasonable structure could be derived. Nevertheless, the most probable sum formula ($C_{13}H_{15}N_3O_3$) suggests the extrusion of SO_2 which has been described for SMX and other sulfonamide drugs in literature before.[206,217,220] Additionally, the isotopic pattern of TP260 supports the loss of SO_2 (Figure S4.14). Bonvin et al. identified TP202 as 4-(hydroxyamino)benzenesulfonic acid after phototransformation of SMX-NO.[206] Since SMX-NO (TP266) was also identified in this study (Tables S4.7 and S4.8) in all irradiation setups, it appears reasonable that TP202 could also have originated as a secondary TP from TP266. However, it has to be noted that TP202 was not detected after irradiation with the LP and MP lamp at pH 8 even though TP266 was detected. Thus, even the formation of secondary TPs appears to be dependent on the pH and irradiation range.

Analytical standards were not commercially available for most of the TPs. In order to enable a comparison of the TPs between the different irradiation setups, the according peak areas

are given as peak area ratios (PAR). The PAR is the ratio of each TP peak area to the initial SMX peak area of a sample withdrawn before the irradiation was started (Figure 4.3). For several TPs, two or more isomers were detected (cf. Table S4.7). It was not the aim of this study to identify the different isomers. However, in order to give the best possible overview, these were summed up to a combined PAR value.

In general, the formation patterns shown in Figure 4.3 appear to be species-dependent. In case of the anionic SMX species, small TPs such as TP177 and TP214 are more preferably formed than for the neutral species where the photoisomer of SMX, TP252, shows the highest PAR. Zhou and Moore as well as Periša et al. state that similar phototransformation products are formed regardless of the prevailing SMX species.[214,217] Our study has shown that this does apply for certain products (e.g., TP252 or TP270) but not for the whole variety and yields of TPs formed.

In conclusion this means that it is not possible in case of SMX to distinguish the different photolysis scenarios, e.g. monochromatic UV-C light from simulated sunlight, solely by TP analysis. A comparable situation was found for degradation of methyl *tert*-butyl ether (MTBE) by acid hydrolysis, aerobic or anaerobic transformation which uniformly result in the common TP *tert*-butyl alcohol. Nevertheless, Elsner et al. could differentiate the three degradation processes by CSIA.[221] In order to check for differences on the isotopic level of the SMX photolysis by the various photoirradiation setups, the samples were subjected to CSIA (see below).

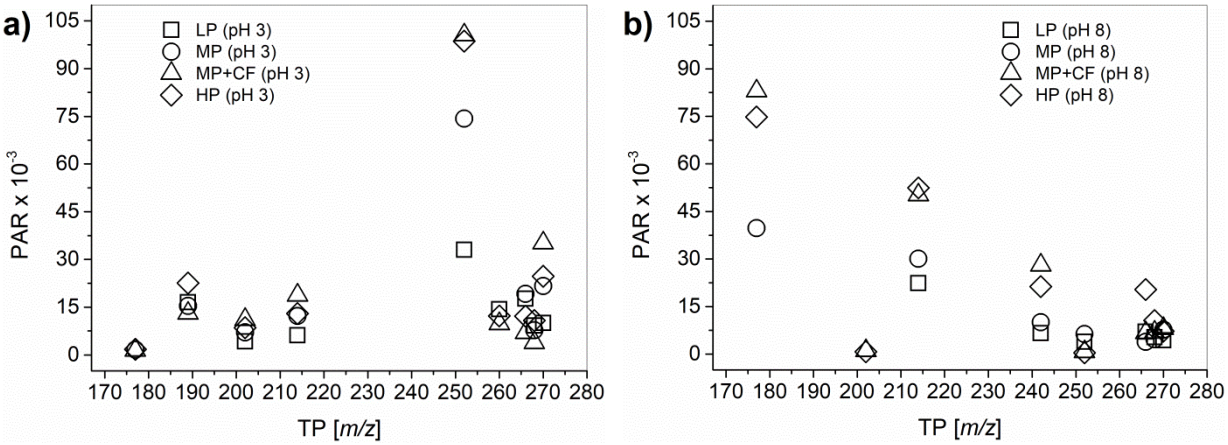

Figure 4.3: Formation patterns of the TPs after phototransformation with LP, MP, MP lamp with cut-off filter (MP+CF) and HP lamp at a) pH 3 and b) pH 8. TPs are represented as peak area ratios (PAR), i.e. the ratio of product peak area and of the peak area of initial SMX in each photolysis setup. Results originate from the longest irradiation times each (cf. Figure 4.2). Peak areas were summed up in case two or more TPs were found for the same *m/z*. The exact *m/z* can be found in Table S4.7.

4.4.3 Compound-specific stable isotope analysis

For all SMX samples generated in the investigated irradiation setups, carbon stable isotope values have been determined (Figure 4.2). The resulting ε_C values are summarized in Table 4.1. Isotopic fractionation occurred during phototransformation with the MP lamp in presence of the cut-off filter and with the HP lamp as *normal* isotope effect at both pH values. The most pronounced ε_C value was detected for the MP lamp with cut-off filter at pH 3. Solely, for phototransformation with the LP lamp at pH 3 a minor *inverse* isotope effect was observed, i.e. reaction rates of ^{13}C were faster so that the ratio of ^{13}C to ^{12}C of the remaining parent compound decreased. However, since the degree of isotope fractionation is very small, no further speculations will be added to that result. For the other remaining irradiation setups, no significant isotope fraction was observed.

It is remarkable that only irradiation of SMX samples with sunlight related wavelengths, i.e. MP lamp with cut-off filter and HP lamp, resulted in significant isotope fractionation. This is most obvious from the comparison of the MP lamp in absence and presence of the cut-off filter. If UV-C light is not cut off, no isotope fractionation is observed. It can therefore be concluded that phototransformation with UV-C light does not or only slightly (cf. LP lamp, pH 3) lead to isotope fractionation. The 254 nm emission line of the MP lamp is very strong, i.e. 3.2 times stronger than of the LP lamp (Figure S4.1a), so that the major phototransformation in absence of the cut-off filter proceeds via light absorption of SMX in the UV-C range (Figure S4.1a) and prevents any significant influences of UV-B and UV-A light. This concept is further supported by the significantly smaller apparent degradation rate of SMX using the MP lamp in presence of the cut-off filter, where only UV-B and UV-A light contribute to phototransformation in comparison with the MP lamp without filter solution.

In case of the HP lamp, UV-C light was not cut off so that the 254 nm mercury emission line partially contributes to the phototransformation. However, due to the reduced transmission in the UV-C range of the liquid lightguide of the HP lamp, the intensity is reduced by more than 30 % (Figure S4.2). This additional irradiation setup points out that carbon stable isotope fractionation is wavelength dependent. It illustrates that isotopic fractionation may occur even if UV-C irradiation is present on the premise that the sunlight related wavelengths are significantly more intense (cf. Figure S4.1b). This may also explain why a considerable ε_C was observed, albeit to a smaller extent than in case of a complete elimination of UV-C irradiation using the MP lamp with cut-off filter.

Previously, it was shown that equilibrium isotope fractionation for H^+-exchange at primary anilines such as 4-CH_3-aniline may result in significant nitrogen isotope fractionation with

deviations up to -20 ‰ and even minor carbon isotope fractionation of approximately -0.5 ‰.[222] Thus, it could have been expected to observe at least a small influence on isotopic fractionation due to H^+-exchange at the sulfonamide nitrogen of SMX for the neutral species. However, for irradiation with the HP lamp, no significant pH dependence and for the MP lamp with the cut-off filter only a slight pH dependence could be observed. These findings regarding the influence of the pH and the resulting dominant species are divergent and it appears questionable that the difference of approximately 1 ‰ in case of the MP lamp with cut-off filter has been caused by H^+-exchange at the sulfonamide nitrogen. Consequently, in our experiments ε_C-values of SMX are mainly influenced by the applied wavelength range and the effect of pH is rather small. However, the difference of approximately 1 ‰ of the two SMX species for phototransformation with sunlight related irradiation is in agreement with the results of Birkigt et al.[172].

At the moment it cannot be excluded that the observed ε_C-values are a product of primary and secondary isotope effects. TP analysis has shown that the other elements contained in SMX are located at relevant bond positions. During formation of TP177, TP189 and TP 202 sulfur is directly involved in the bond cleavage. A nitrogen bond is directly involved in formation of TP189, TP202, TP214, TP242, TP252, TP266 and TP268 (cf. Table S4.8) so that an additional influence on carbon isotopic fractionation seems possible due to secondary isotope effects. Secondary isotope effects have been reported for carbon[132,223] as well as nitrogen[154,155] atoms in various transformation processes. However, with the instrumentation available in the present study it was not possible to determine other isotopic values than for carbon. Nevertheless, the information supplied by nitrogen stable isotope analysis may additionally help to distinguish transformation reactions as it was possible for atrazine[155] or diclofenac[154] which will be addressed in future work. Furthermore determination of ε_N-values could also help to clarify the impact of H^+-exchange on isotopic fractionation values discussed above as in a previous study.[158] Ratti et al. have substantially investigated the direct photolysis of chloroanilines.[157,158] In these studies it was shown that ε_C- and ε_N-values are strongly dependent on the position of the chlorine substituent, the pH and the excited states, i.e. singlet or triplet states. Additionally, all three chloroanilines were affected differently by variations of the variables listed before so that it was impossible to deduce a unique trend for each variable.

The irradiation sources used in our study resulted in different isotopic fractionation and one might have expected different phototransformation products for each irradiation setup. For instance, the MP lamp with cut-off filter revealed the strongest effect on isotopic fractionation of SMX (Table 4.1). Hence, one would expect that products from reactions involving C—C

bond cleavage are most pronounced in this experimental setup. However, such products, e.g. TP214, TP252 or TP270, were observed in all experiments and, thus, no distinct TP could be identified as indicator for the isotopic fractionation. One possible explanation is that the detected TPs are a mixture of excited singlet and triplet state reactions. If photophysical processes governed TP formation it is also likely that magnetic mass-independent isotope effects (MIE) determined the observed ε_C-values as it was suggested in previous studies[155,157,158]. In magnetic MIE reaction rates of chemical reactions are dependent on nuclear spin selectivity in contrast to mass-dependent isotope effects where different energies of light and heavy nuclei govern the observed isotope effects.[125,224] As a consequence, the variations in ε_C-values observed in this study may not be explained by C-C bond cleavage alone. Moreover, one intriguing question remains to be addressed, i.e. why does photolysis by UV-B and UV-A light lead to isotopic fractionation whereas UV-C light does not? It is possible that UV-A, UV-B and UV-C light result in different populations of excited states (i.e. singlet or triplet), which might also explain different ε_C-values. It is known from previous studies that either singlet or triplet excited states may determine isotopic fractionation.[157,158] Thus to gain further insight in underlying reaction mechanisms one would need to quantify the influence of the different excited states and, if further instrumental developments allow, determine isotopic fractionation of the other elements, e.g. nitrogen or sulfur. However, these further investigations are out of scope of the present study.

Overall it could be shown that the investigated irradiation setups lead to formation of similar TPs. Depending on pH and irradiation source their relative quantities varied but a distinction of the irradiation source based on product formation studies alone was not feasible. Nevertheless, the distinct CSIA results have shown that there are differences in the underlying degradation processes which cannot be identified, yet, and deserve further research. Based on CSIA it might be possible to distinguish between different wavelength ranges causing a phototransformation of SMX, i.e., CSIA may enable to distinguish engineered (e.g., UV-disinfection with LP-lamps) from natural photodegradation processes of SMX. UV-disinfection has recently been implemented in regular WWTPs[202,205] to improve the overall water quality of receiving waters. As a consequence, wastewater point sources could be traced back especially if photolysis by natural sunlight occurred. In such a case stable carbon isotope signatures would become more negative the closer samples are taken at the source. Additionally, it would be possible to determine the influence of direct sunlight photolysis on natural attenuation of micropollutant contaminations such as SMX.

Table 4.1: Carbon stable isotope enrichment factors (ε_C) for direct photolysis of SMX in different irradiation setups

Irradiation source	ε_C[a] [‰]	
	pH 3	pH 8
LP (254 nm)	0.8 ± 0.1	n.s.
MP (200-600 nm)	n.s.	n.s.
MP + cut-off filter (310-600 nm)	-4.8 ± 0.1	-3.9 ± 0.1
HP (220-500 nm)	-1.9 ± 0.1	-2.2 ± 0.2

[a] ε_C-values below 0.5 ‰ were excluded due to measurement uncertainties (compare Jochmann et al. and Sherwood Lollar et al.)[143,179] and marked as not significant (n.s.); uncertainties represent the standard deviation of the slope

4.5 Supporting Information

Text S4.1: Chemicals

All solutions were prepared in ultrapure water (18.1 MΩ·cm, TOC < 10 ppb; ELGA LabWater, Veolia Water Technologies Deutschland GmbH, Celle, Germany).

Following chemicals were used for preparation of the samples: acetanilide (99.9 %, Merck KGaA, Darmstadt, Germany), acetonitrile (HPLC-grade, VWR Chemicals, Leuven, Belgium), 3-amino-5-methylisoxazole (≥ 97 %, Sigma-Aldrich, Steinheim, Germany), atrazine (97.4 %, pestanal, analytical standard, Sigma-Aldrich), carbon dioxide (4.5 %, Air Liquide, Düsseldorf, Germany), dipotassium hydrogen phosphate (≥ 99 %, p.a., AppliChem, Darmstadt, Germany), formic acid (99-100 %, Sigma-Aldrich), helium (5.0; Air Liquide), methanol (99,99 % HPLC-grade, Fisher Scientific, Loughborough, United Kingdom), *ortho*-phosphoric acid (85 %, p.a., AppliChem), pH-reference solutions pH 4 (citric acid, sodium hydroxide, sodium chloride) and pH 7 (phosphate mixture) (both Bernd Kraft, Duisburg, Germany), potassium dihydrogen phosphate (≥ 98 %, AppliChem), potassium hydrogen phthalate (Reag. Ph Eur., p.a., Merck KGaA), sodium hydroxide (≥ 99 %, VWR Chemicals), sulfamethoxazole (analytical standard, Sigma-Aldrich), sulfanilamide (≥ 99 %, puriss. p.a., Sigma-Aldrich), sulfanilic acid (99 %, Sigma-Aldrich), sulfuric acid (> 95 %, Fisher Scientific), uridine (≥ 99 %, Sigma-Aldrich).

Text S4.2: Photoirradiation setups - Sources of irradiation

Three different irradiation setups were employed for direct photolysis experiments: a merry-go-round photoreactor for irradiation with the low- (LP) (λ = 254 nm; TNN 15/32, nominal power 15 W, Heraeus Noblelight, Hanau, Germany) and the medium-pressure (MP) mercury lamp (λ = 200-600 nm; TQ 718, nominal power 700 W, Heraeus Noblelight; both lamps were supplied by Peschl Ultraviolet, Mainz, Germany), the latter in absence and presence of a cut-off filter solution, a high-pressure (HP) mercury lamp (λ = 220-500 nm; SUV DC DeepUV, Lumatec, Deisenhofen, Germany) connected to a liquid lightguide (series 250, ø5 mm x 1000 mm; Lumatec) and a neodymium-doped yttrium aluminum garnet (Nd:$Y_3Al_5O_{12}$) laser (Nd:YAG-laser) (λ = 266 nm; Polaris II, New Wave Research, St Neots, UK) integrated in a flow-through setup.

The emission spectra of the LP, MP and HP Hg lamps in comparison to the molar absorptivity of the neutral (pH 3) and the anionic (pH 8) species of SMX are shown in Figure S4.1. Additionally, the wavelength-dependent transmission of the liquid lightguide employed in combination with the HP lamp is shown in Figure S4.2.

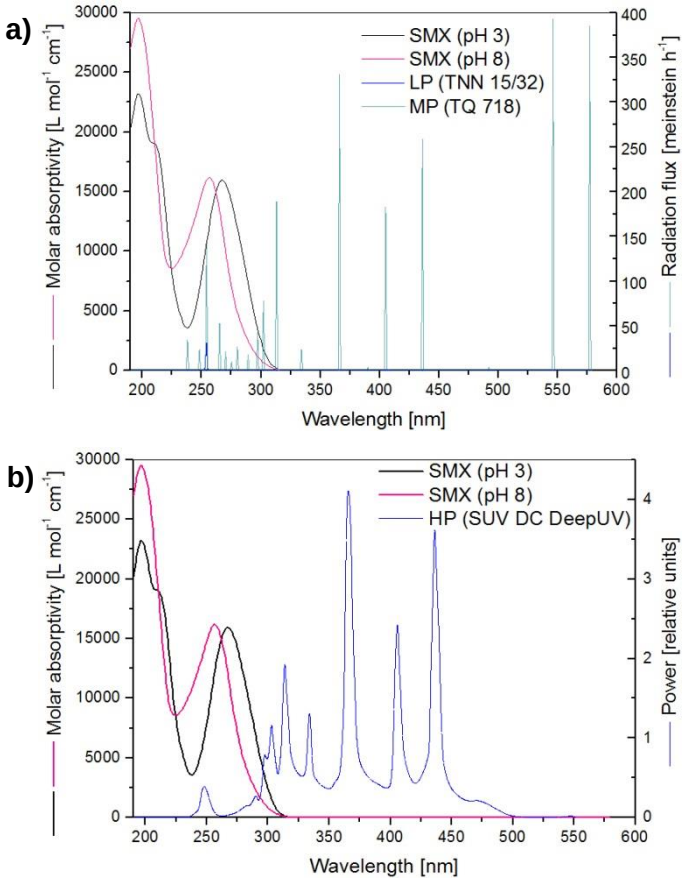

Figure S4.1: Molar absorptivity of the neutral (pH 3) (black line) and anionic (pH 8) (pink line) species of SMX are shown in comparison to the emission spectra of a) the LP lamp (TNN 15/32) (dark blue) and MP lamp (TQ 718) (light blue) and b) the HP lamp (SUV DC DeepUV) connected to the liquid lightguide (ø5 mm x 1000 mm) (dark blue).

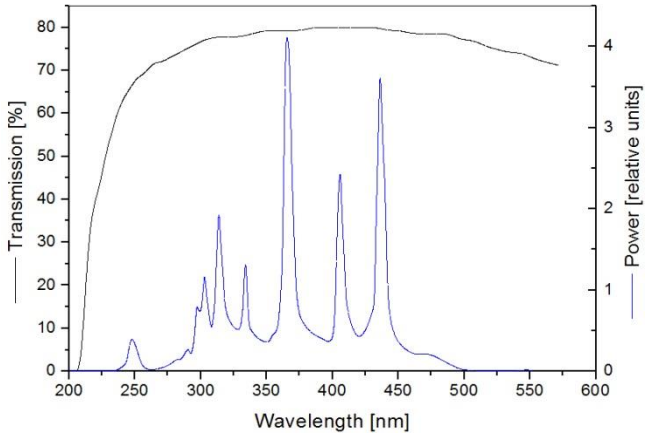

Figure S4.2: Transmission properties of the liquid lightguide (black line) in comparison to the emission spectrum of the HP Hg lamp. The HP Hg lamp data were recorded with the liquid lightguide already connected to it.

Text S4.3: Photoirradiation setups - Merry-go-round photoreactor

For irradiation with the LP and the MP lamp, the merry-go-round photoreactor shown in Figure S4.3 was used. The lamp was placed in the center of the photoreactor within a quartz glass cooling jacket. The cooling jacket and the glass container were filled with ultrapure water. In both cases the light absorption within the emitted wavelength range was negligible. The temperature of the feed water of the cooling jacket was controlled so that the temperature of the water surrounding the samples was kept constant at 25.0 ± 0.2 °C. 70 mL of aqueous SMX solution, either buffered at pH 3 or pH 8, were filled in quartz glass tubes which were then immersed in the glass container of the photoreactor. Aliquots were withdrawn in certain time intervals. Moreover, it was made sure that a minimum sample volume of 17.5 mL remained in the quartz glass tubes. This was necessary because irradiation was unevenly distributed at the bottom of the quartz glass tubes which led to significant lower degradation rates in preliminary tests (data not shown). In case of LP lamp phototransformation experiments were performed as duplicate for SMX at pH 3 and single experiments at pH 8. In case of MP lamp phototransformation experiments were performed as triplicate for SMX at pH 3 and duplicate at pH 8.

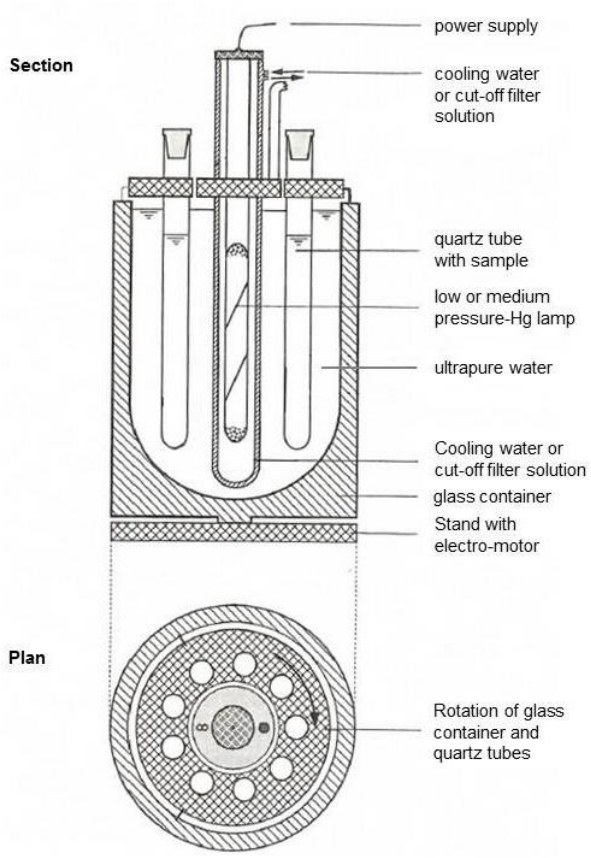

Figure S4.3: Merry-go-round photoreactor for irradiation with LP and MP lamp. In case of the MP lamp, the setup was either run with ultrapure water or 1.1 % w/v potassium hydrogen phthalate as cooling water. In the latter case all wavelengths below 310 nm were cut off. Figure was adapted from Wegelin et al.[212] and modified accordingly.

The fluence rate of the LP lamp was determined every working day by chemical actinometry using the uridine actinometer[72] at low optical density.[70] A 10 µM uridine solution buffered with 10 mM phosphate at pH 7 was irradiated for 10 min in total with molar absorption coefficient (ε_λ) of $\varepsilon_{\lambda=254nm}$ (uridine) = 841 $m^2\ mol^{-1}$ and a quantum yield (Φ_λ) of $\Phi_{\lambda=254nm}$ (uridine) = 0.019 mol $einstein^{-1}$.[72,73] Aliquots were withdrawn in between every 2 min. Absorption measurements of residual uridine were done spectrophotometrically at 262 nm with $\varepsilon_{\lambda=262nm}$ (uridine) = 1040 $m^2\ mol^{-1}$.[73] The pseudo-first order degradation rate constant (k_p) of uridine was obtained from the slope of the regression of time [s] vs. ln($c_{uridine}/c_{0,uridine}$). The fluence rate at vanishing absorbance ($E^0_{p,\lambda=254nm}$) was calculated with Equation S4.1.[70]

$$E^0_{p,\lambda=254nm} = \frac{-k_{p,\lambda=254nm}(uridine)}{2.303 \cdot \varepsilon_{\lambda=254nm}(uridine) \cdot \phi_{\lambda=254nm}(uridine)} \qquad \text{(S4.1)}$$

In a second approach, the cooling water in the cooling jacket was replaced by a cut-off filter solution for total absorption of wavelengths below 310 nm. According to Montalti et al., a 0.5 % w/v solution of potassium hydrogen phthalate solution will lead to total absorption over a path length of 1 cm for wavelengths below 310 nm.[225] In the given setup the cut-off filter solution was filled into the cooling jacket of the photoreactor and continuously exchanged by a thermostat, which was simultaneously used to maintain a temperature of 25.0 ± 0.2 °C within the glass container. The path-length of the cooling jacket was 0.45 cm, thus, to obtain a similar total absorption for λ < 310 nm, a 1.1 % w/v solution of potassium hydrogen phthalate solution was used. The total absorption was controlled via two ways. First, every 30 min, aliquots of the cut-off filter solution were taken and absorption was determined spectrophotometrically. An absorption spectrum of the potassium hydrogen phthalate solution after different irradiation times with the MP-lamp is shown in Figure S4.4. Second, additionally to the quartz-glass tubes filled with sample solution, one quartz-glass tube was filled with a 5 µM atrazine solution buffered at pH 7 with a 5 mM phosphate buffer. Due to the higher stability of atrazine in aqueous solution, this was used instead of the uridine actinometer. This setup has been described as a suitable chemical actinometer for characterization of LP lamps for wavelength in a range of 238-334 nm.[70] As atrazine does not absorb light at wavelengths above 310 nm, it was used to reassure the efficacy of the cut-off filter within the system. Figure S4.5 shows irradiation of the 5 µM atrazine solution in presence and absence of the cut-off filter solution. It is remarkable that atrazine is not detectable after more than five minutes of irradiation with the MP lamp in absence of the cut-off filter solution. Phototransformation experiments were performed as triplicates for SMX at pH 3 and duplicates at pH 8 with the MP lamp in presence of the cut-off filter.

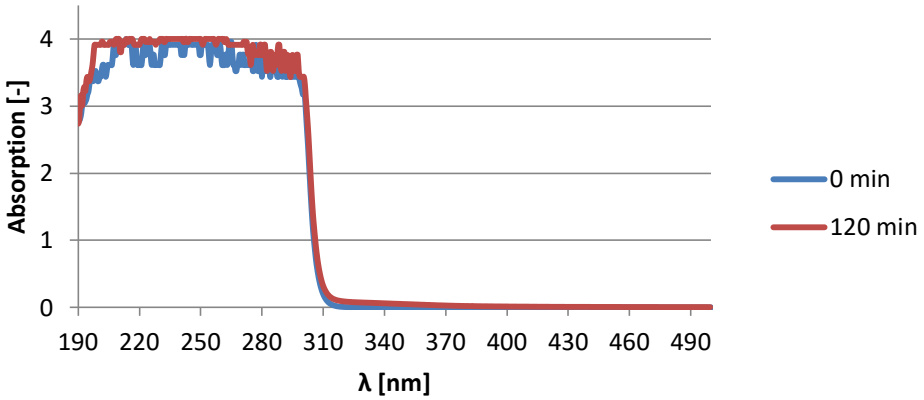

Figure S4.4: Example of absorption of the filter solution used for the MP lamp after 0 min and 120 min of irradiation. The concentration in the cooling jacket was 1.1 % w/v potassium hydrogen phthalate. Absorption was measured at a path length of 1 cm (cf. materials and methods section in the main paper). In order to depict absorption conditions within the cooling jacket of the irradiation setup (path length of 0.45 cm) with the MP lamp, the original solution was diluted using ultrapure water to a concentration of 0.5 % w/v potassium hydrogen phthalate. It becomes easily visible that wavelengths below 310 nm are completely absorbed.

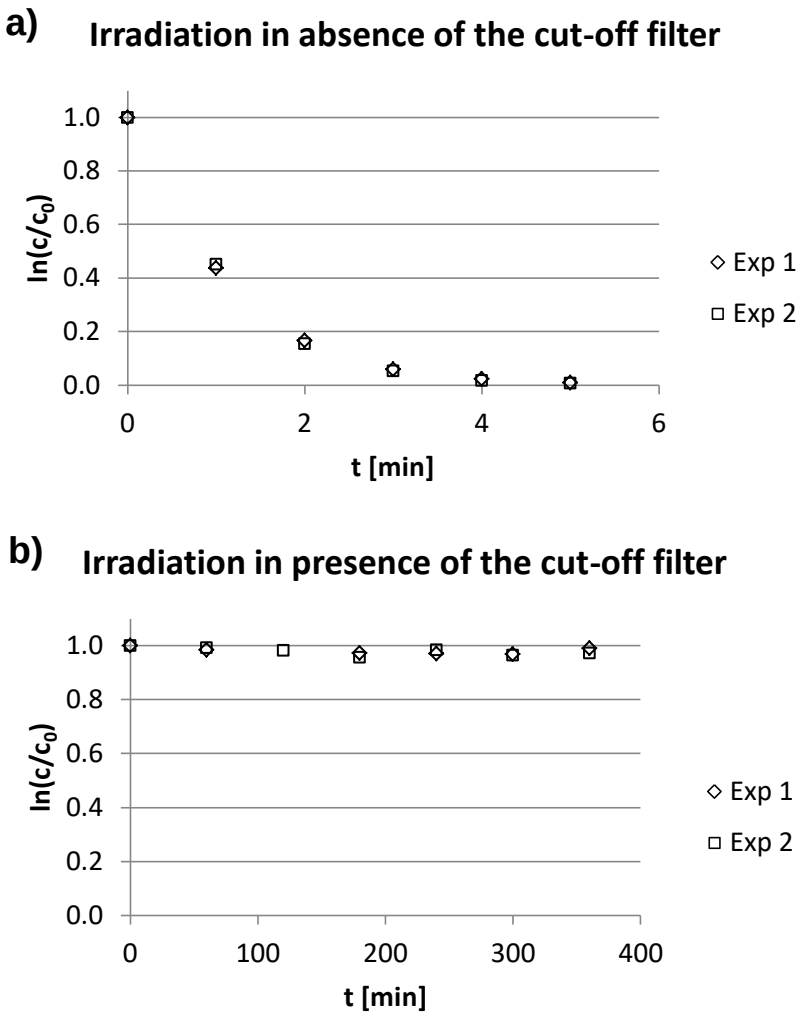

Figure S4.5: Comparison of two irradiation experiments of a 5 µM atrazine solution buffered at pH 7 with 5 mM phosphate in a) absence and b) presence of the 1.1 % w/v potassium hydrogen phthalate cut-off filter solution.

Text S4.4: Photoirradiation setups - HP lamp

The irradiation setup using the HP Hg lamp is shown in Figure S4.7. In each experiment, 50 mL of SMX solution were filled into the crystallizing dish (inner diameter 7.7 cm) and continuously stirred using a magnetic stirrer. The whole setup was encased during the irradiation to prevent interactions with other light sources. The distance between the crystallizing dish and the tip of the liquid lightguide was chosen so that the area of the SMX sample solution was completely irradiated by the light beam. Aliquots of 1.5 mL of sample solution were withdrawn at each time samples were taken. Phototransformation experiments were performed as triplicates for SMX at pH 3 and duplicates at pH 8.

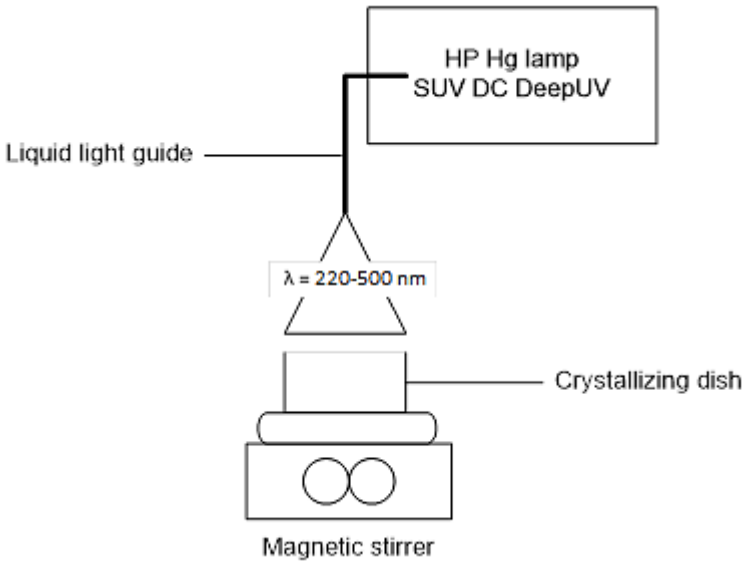

Figure S4.6: Irradiation setup employing a HP Hg lamp connected to a liquid lightguide. The liquid lightguide was permanently fixed directly above the crystallizing dish in order to apply same conditions to all samples.

Text S4.5: Photoirradiation setups - Nd:YAG laser

The Nd:YAG laser was integrated in a flow-through setup shown in Figure S4.6. The SMX solutions were pumped by an HPLC-pump (PLATINblue; Knauer, Berlin, Germany) through a laser quartz glass cuvette (path length = 5 cm) with an irradiated area of 3.98 mm², a repetition rate of 10 Hz and a pulse energy of 3.7 mJ. The flow rates of the pump were adjusted to obtain defined numbers of laser shots per volume as shown in Table S4.1. Phototransformation experiments were performed as triplicate for SMX at pH 3 and pH 8.

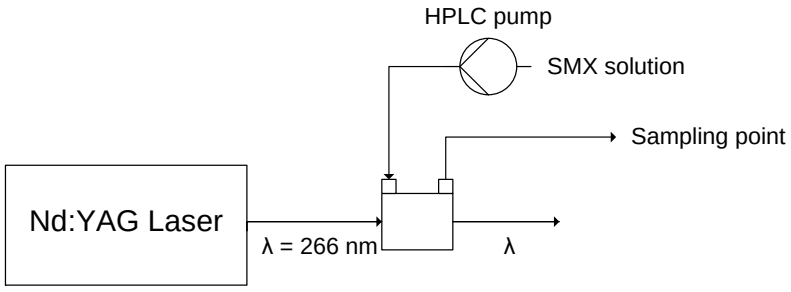

Figure S4.7: Flow-through setup with a Nd:YAG laser irradiating a laser cuvette with a path length of 5 cm and an irradiated area of 3.98 mm². Transport of SMX solution at defined flow rates was conducted with an HPLC pump.

Table S4.1: Various flow rates (Q) which were set by the HPLC pump in order to obtain the different numbers of shots applied to the SMX solution.

Number of shots	100	200	300	400	500	600	700	800	900	1000
Q [mL min^{-1}]	1.193	0.596	0.398	0.298	0.239	0.199	0.170	0.149	0.133	0.119

Text S4.6: Quantification of SMX by HPLC-DAD (fully adapted from Willach et al.[210])

The concentration of SMX was determined by an HPLC-DAD system consisting of LC-10AT (pump), FCV-10AL (degasser), SCL-10A (system controller), SPD-M10A (detector), SIL-10AD (autosampler) and CTO-10AS (column oven, isothermally run at 30 °C) (Shimadzu, Duisburg, Germany). The injection volume was 10 µL. The analytical column was a ProntoSIL C-18 (250 x 4 mm, particle size 5 µm; pore size 120 Å) (Bischoff Analysentechnik und -geräte GmbH, Leonberg, Germany) using an isocratic eluent (35:65 methanol:water (pH 2); flow: 0.5 mL/min). Absorption at 270 nm was used for quantification. Calibration standards were prepared from 99 - 790 µM SMX or 9.9-79 µM SMX depending on the initial SMX concentration of the samples. Limit of quantification (LOQ) was 2.3 µM SMX (determination according to DIN 32645)[189]. Data processing was performed by LC solutions, version 1.25, SP4 (Shimadzu).

Text S4.7: Quantification of atrazine by HPLC-DAD

The concentration of atrazine was determined using the same HPLC-DAD system, analytical column and data processing software already described in Text S4.6. The eluent was isocratic (70:30 methanol:water (pH 2); flow: 0.5 mL/min). Absorption at 220 nm was used for quantification. The calibration range was 1-6 µM atrazine. LOQ was 0.6 µM atrazine (determination according to DIN 32645, 2008)[189].

Text S4.8: Isotope-ratio measurements by high-temperature-liquid chromatography-isotope-ratio mass spectrometry (fully adapted from Willach et al.[210])

Isotope ratio measurements by HT-LC-IRMS of SMX were performed according to Kujawinski et al.[171] with modifications as described below. The HT-LC system was composed

of a binary piston pump (Rheos Allegro, Flux Instruments/Thermo Scientific, Bremen, Germany), a HTC PAL autosampler (CTC Analytics, Zwingen, Switzerland; supplied by Axel Semrau, Sprockhövel, Germany), an HT HPLC 200 column oven (SIM, Oberhausen, Germany) and a LC IsoLink interface connected to a DeltaV Advantage isotope ratio mass spectrometer (both: Thermo Scientific). Separation was performed on an X-Bridge C_{18} column (100 x 2.1 mm, particle size 3.5 µm; pore size 130 Å) (Waters, Eschborn, Germany) with an acidic eluent (pH 3 buffered with 2.5 mM sodium phosphate) at a flow rate of 300 µL min^{-1}. The temperature gradient was started at 30 °C, increased after sample injection instantaneously by 5 °C min^{-1} until the maximum of 85 °C and then held for 9 min. For an improved temperature transfer the eluent was pre-heated by the oven. Additionally, the entire column was embedded between two custom made aluminum blocks. After separation, the column effluent was mixed with 30 µL min^{-1} of 1.5 M *ortho*-phosphoric acid and 70 µL min^{-1} 0.84 M sodium peroxodisulfate in the interface. Afterwards, the mixture was led into the oxidation oven which was set to 99.9 °C. After passing the gas separation unit the generated CO_2 was transferred by a helium stream at a flow rate of 1.2 mL min^{-1} into the open split of the IRMS. The IRMS was tuned to maximum linearity. Regularly, reference gas pulses of varying amplitudes were used to control linearity and precision performance of the IRMS. All samples were measured as triplicates and every third measurement was followed by a single measurement of a 390 µM SMX standard. The method's detection limit of SMX was 0.3 µg C on column and was determined according to the moving mean procedure.[143]

The obtained data sets were tested for outliers by the three Grubbs-test explained in detail by Ellison et al..[226] Only if one measurement data point was clearly identified by these tests it was marked as an outlier and was not further considered.

Aliquots of the analytical standards of SMX were weighed in tin cups (4 x 6 mm, IVA, Analysentechnik, Meerbusch, Germany) and analyzed with an elemental analyzer (vario PYRO Cube, Elementar Analysensysteme GmbH, Langenselbold, Germany) coupled to an IRMS (IsoPrime100, Isoprime Ltd., Stockport, UK). The reference materials USGS40 (International atomic energy agency (IAEA), Vienna, Austria; L-glutamic acid, $\delta^{13}C$: -26.389 ‰) and USGS41 (IAEA; L-glutamic acid $\delta^{13}C$: +37.626 ‰) were used to normalize the working standard acetanilide to the international Vienna Pee Dee Belemnite (VPDB) scale.[120]

Kujawinski et al. have shown that $\delta^{13}C$ values of SMX obtained by HT-LC-IRMS are concentration independent in the investigated concentration range.[171] The reported $\delta^{13}C$ values were normalized to the VPDB scale and all standard deviations refer to a minimum of triplicate measurements. Additionally, the $\delta^{13}C$ values of the SMX samples obtained by the

HT-LC-IRMS were corrected according to the principle of identical treatment as it was proposed by Werner and Brand.[121] Therefore, the EA-IRMS normalized SMX standard was measured after every third HT-LC-IRMS measurement for correction and normalization of the degradation experiment samples. Data from HT-LC-IRMS measurements were recorded and processed by Isodat 2.5 (Thermo Scientific). Data from EA-IRMS were treated with IonVantage (Isoprime Ltd.).

Text S4.9: Transformation product identification (fully adapted from Willach et al.[210])

For the detection of transformation products, a high performance liquid chromatographic separation coupled to a time-of-flight mass spectrometer (HPLC/ESI(-)-ToF-MS) was used. In addition, an ion trap mass spectrometer was employed for fragmentation experiments. For the chromatographic separation, 5 µL of sample solution were injected onto a reversed-phase C18 column (Hypersil Gold, 150 x 2.1 mm, 3 µm particle size, 175 Å, Thermo Scientific, Bremen, Germany). A solution of 0.1% formic acid in bidistilled water (eluent A) and acetonitrile (eluent B) were used as eluents in a binary gradient which is shown in SI (Table S4.2). Separation was carried out at 40°C and the total flow rate was set to 0.3 mL/min.

Determination of accurate masses was achieved with a Bruker micrOTOF (Bruker Daltonics, Bremen, Germany) with an electrospray ionization interface operated in negative mode. This mass spectrometer was coupled to a LC system by Shimadzu (Shimadzu Germany, Duisburg, Germany) consisting of two LC-10ADVP pumps, a SIL-HTA autosampler, a DGU-14A degasser, and a CTO-10ADVP column oven. Detailed mass spectrometric parameters are given in Table S4.3). The mass spectrometer was controlled by micrOTOFControl 1.1 software (Bruker), the LC system by LC Solution 1.25 (Shimadzu). For high mass accuracy, each analysis was calibrated internally using the SMX signal and its accurate theoretical mass. For highly polar, low-mass transformation products sodium formate clusters were used as an internal mass calibration standard.

For data evaluation, DataAnalysis 4.0 software from Bruker Daltonics (Bremen, Germany) and OriginPro 9.3 by OriginLab Corporation (Northampton, MA, USA) were used.

Table S4.2: Gradient profile for the LC separation of transformation products of SMX.

***t* [min]**	0	3	14	15	16	17	25
%B (Acetonitrile)	5	5	30	90	90	5	5

Table S4.3: Mass spectrometric parameters for the determination of exact masses of transformation products of SMX analyzed by liquid chromatography coupled to time-of-flight mass spectrometry.

Ionization mode	negative	Hexapole 1 voltage	-26.7 V
Mass range	*m*/*z* 50 – 550	Hexapole 2 voltage	-22.1 V
Spectra rate	1.0 Hz	Hexapole RF voltage	90 Vpp
Nebulizer gas pressure	1.5 bar	Lens transfer time	49.0 µs
Dry gas flow rate	8.6 L/min	Pre pulse storage time	9.0 µs
Dry heater temperature	200 °C	Lens 1 storage voltage	-30.0 V
Capillary voltage	4000 V	Lens 1 extraction voltage	-20.5 V
Endplate offset voltage	-500 V	Lens 2 voltage	-12.0 V
Capillary exit voltage	-90.0 V	Lens 3 voltage	16.0 V
Skimmer 1 voltage	-30.0 V	Lens 4 voltage	-0.3 V
Skimmer 2 voltage	-22.1 V	Lens 5 voltage	30.0 V

Table S4.4: Mass spectrometric parameters for the determination of transformation products of sulfamethoxazole analyzed by liquid chromatography coupled to ion trap mass spectrometry.

Ionization mode	negative	Capillary exit voltage	-100.4 V
Mass range	*m*/*z* 50 – 550	Skimmer voltage	-40.0 V
Nebulizer gas pressure	35 psi	Octapole 1 voltage	-12.0 V
Dry gas flow rate	8.5 L/min	Octapole 2 voltage	-1.7 V
Dry gas temperature	320 °C	Octapole RF	137.5 Vpp
Capillary voltage	4000 V	Lens 1 voltage	5.0 V
Endplate offset voltage	-500 V	Lens 2 voltage	60.0 V
ICC target	7000	Trap Drive	46.3
Max. accu. time	100 ms		

Table S4.5: Kinetics parameters for the direct phototransformation of SMX under 254 nm irradiation fully adapted from Canonica et al.[70]

	ε^a [m^2 mol^{-1}]	Φ^b [einstein mol^{-1}]	$k_{E_p^0}{}^c$ [m^2 $einstein^{-1}$]
pH 3 (neutral species)	1189 ± 23	0.212 ± 0.018	580 ± 48
pH 8 (anionic species)	1676 ± 38	0.046 ± 0.021	176 ± 80

[a] Molar absorption coefficient; [b] Quantum yield; [c] photon fluence-based rate constant

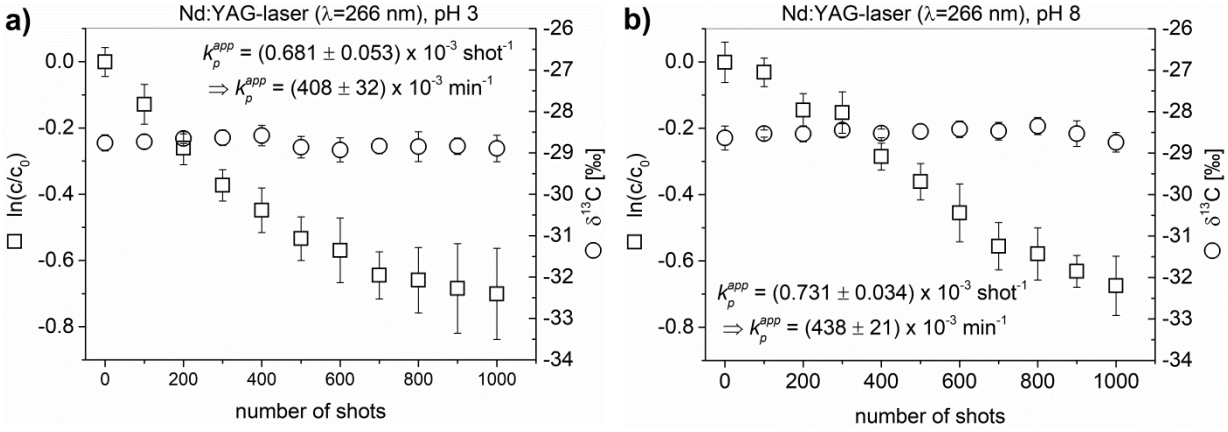

Figure S4.8: Photolysis of SMX with Nd:YAG-laser light at pH 3 (a) and pH 8 (b). Data are shown in dependence of the number of shots. Concentration decrease is given as ln(c/c_0) (squares; error bars represent standard deviations of experimental replicates) and carbon isotope values as $\delta^{13}C$ (circles; error bars represent standard deviations of experimental replicates (n = 3) plus the triplicate measurement of each sample). First order apparent photolysis kinetic rate constants (k_p^{app}) shown in each according graph are derived from the slopes of number of shots, respectively, vs. ln(c/c_0). Time based k_p^{app} were calculated with 600 laser shots min^{-1}. The given uncertainty originates from the standard deviation of the related slope.

Text S4.10: SMX degradation by laser light - kinetics and CSIA results

Please note that transformation products of the phototransformation of SMX by laser light were not determined. Thus, in the following only results from degradation kinetics and CSIA will be presented and discussed.

Phototransformation kinetics of SMX using virtually monochromatic laser light (λ = 266 nm) appears to be largely independent of the SMX species, i.e. neutral or anionic one (Figure S4.8). This different behavior compared to phototransformation with the various mercury lamps may originate from the unique character of laser light. In general, laser sources emit monochromatic coherent electromagnetic radiation.[227] Since the radiation of the Nd:YAG-laser is pulsed and focused on a small area, the resulting radiation intensity is very high including photon flux and photon density.[227] Additionally, the emitted monochromatic wavelength differs by 12 nm from the mercury arc lamp so that at this emitted wavelength the absorption coefficient of the neutral species is slightly higher than that of the anionic species. Consequently, photolysis of SMX caused by mercury arc lamps differs strongly from the one originating from laser light. However, it could not be clarified in the course of this study why no significant difference between the two SMX species (neutral and anionic) could be observed in contrast to all other photolysis setups regardless of the wavelengths. Nevertheless, to find the cause of these results should be the aim of future studies.

For photolysis of the neutral and the anionic SMX species with the Nd:YAG-laser no significant isotope fractionation was detected. For photolysis of SMX by the LP lamp a slight inverse isotope fractionation for the neutral species and no significant fractionation for the anionic species were determined. However, for both SMX species irradiated with laser light no significant carbon isotope fractionation was detected. Thus, it is currently not possible to make any further judgement on differences originating from the different irradiation sources. Solely considering the results from CSIA it might have been concluded that UV-C light does not or only slightly cause carbon isotope fractionation. However, taking the kinetic data into account it appears unlikely that both kinds of photolysis proceeded via the same mechanism. If it becomes possible to determine isotope values for nitrogen or sulfur, further insights will probably be possible. Unfortunately, at the moment further conclusions are not possible due to the limited amount of data.

Text S4.11: Morowitz correction factor adapted from Katsoyiannis et al.[71]

The average fluence rate ($E^{avg}_{\lambda=254nm}$) in the quartz glass tubes of the merry-go-round photoreactor was obtained by Equation S4.2:

$$E^{avg}_{\lambda=254nm} = S_{\lambda=254nm} \cdot E^{0}_{p,\lambda=254nm} = \frac{1-10^{-A_{\lambda=254\,nm}}}{2.303 \cdot A_{\lambda=254nm}} \cdot E^{0}_{p,\lambda=254nm} \qquad \text{(S4.2)}$$

where $S_{\lambda=254nm}$ is the Morowitz correction factor, $E^{0}_{p,\lambda=254nm}$ is the fluence rate at vanishing absorbance. The absorbance $A_{\lambda=254nm}$ is approximated by Equation S4.3:

$$A_{\lambda=254nm} = \alpha_{\lambda=254nm} \cdot l^{avg} \qquad \text{(S4.3)}$$

where $\alpha_{\lambda=254nm}$ is the absorption coefficient of the sample, i.e. 790 µM SMX solution plus 10 mM phosphate buffer, and the average optical path-length of the quartz glass tube l^{avg}.

The resulting values of the Morowitz correction for the LP lamp with the merry-go-round photoreactor are listed in Table S4.6.

Table S4.6: Correction of the apparent pseudo first order rate constant of SMX degradation under monochromatic 254 nm irradiation with the LP lamp in the merry-go-round photoreactor

		pH 3	**pH 8**
$\alpha_{\lambda=254nm}$	[cm^{-1}]	9.389	13.234
$A_{\lambda=254nm}$ [a]	[-]	14.83	20.91
$S_{\lambda=254nm}$ [a]	[-]	0.0293	0.0208
$E^{avg}_{\lambda=254nm}$ [b]	[µeinstein m^{-2} s^{-1}]	1.756	1.246
k_p^{app} [c]	[min^{-1}]	0.02880 ± 0.00046	0.00844 ± 0.00013
$k_{E_p^0}^{app}$ [d]	[m^2 $einstein^{-1}$]	240 ± 4	107 ± 2

[a] calculated with l^{avg} = 1.58 cm

[b] calculated with $E^0_{p,\lambda=254nm}$ = 60 µeinstein m^{-2} s^{-1}

[c] measured in this study

[d] calculated from $k^{app}_{E_p^0} = \frac{k_p^{app}}{E^{avg}_{\lambda=254nm}}$ [70]

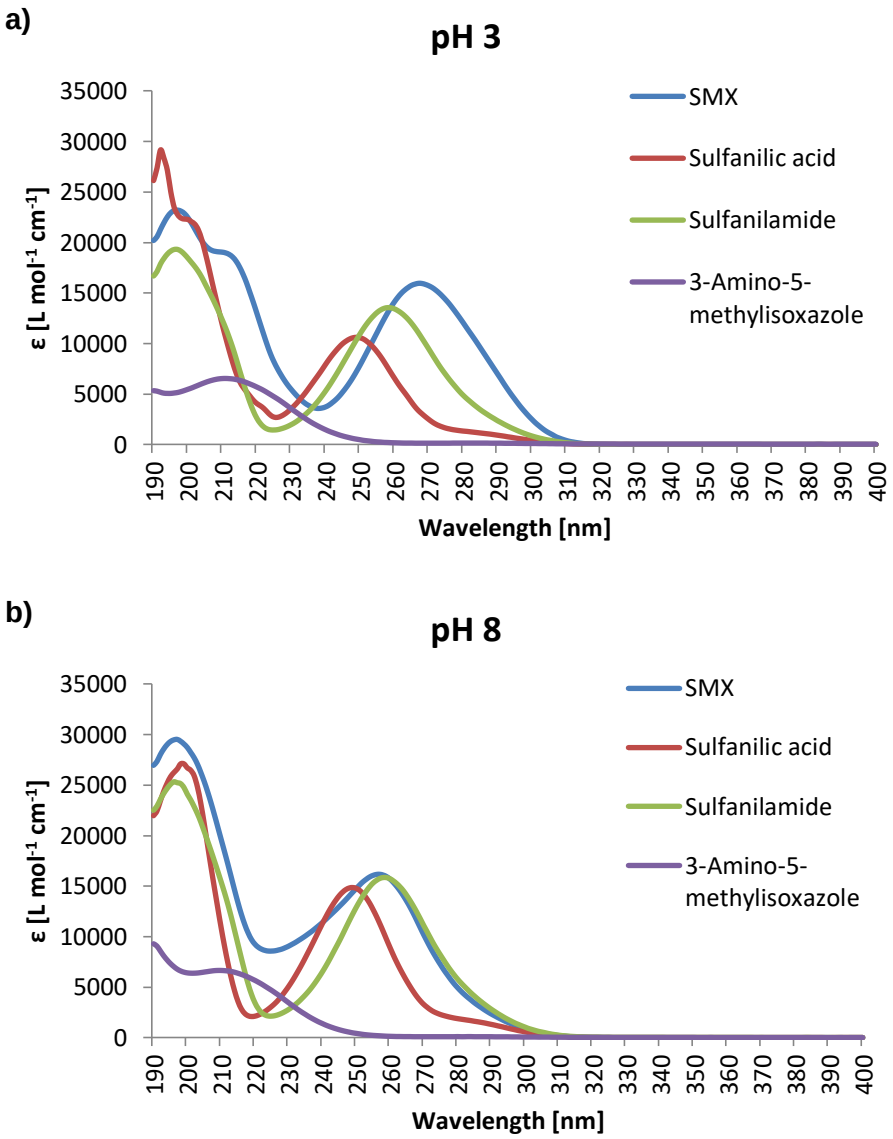

Figure S4.9: Comparison of the molar absorptivity of three typical transformation products of SMX at a) pH 3 (neutral SMX species prevails) and b) pH 8 (anionic SMX species prevails). A significant absorption between 400 nm and 800 nm was not detected.

Table S4.7: Main transformation products found for the phototransformation of SMX at pH 3 and pH 8 with the LP, MP, MP+CF and HP lamp. For each transformation product, the according retention time (t_R), the measured mass-to-charge-ratio (m/z) as $[M-H]^-$, the derived elemental composition and the according calculated mass-to-charge-ratio (m/z) as $[M-H]^-$, the deviation from measured to calculated m/z and its double bond equivalent (DBE) are given.

	Name	t_R [min]	Measured *m/z* $[M-H]^-$	Elemental composition [M-H]	Calculated *m/z* $[M-H]^-$	Error [ppm]	DBE
LP pH 3	189	1.64	188.9842	$C_6H_6O_5S$	188.9863	11.21	4
	214	2.09	214.0291	$C_7H_9N_3O_3S$	214.0292	0.40	5
	189	2.31	188.9866	$C_6H_6O_5S$	188.9863	-1.49	4
	214	3.11	214.0291	$C_7H_9N_3O_3S$	214.0292	0.40	5
	214	4.24	214.0290	$C_7H_9N_3O_3S$	214.0292	0.86	5
	260	4.40	260.1033	$C_{13}H_{15}N_3O_3$	260.1041	2.94	8
	260	4.80	260.1034	$C_{13}H_{15}N_3O_3$	260.1041	2.56	8
	270	5.62	270.0558	$C_{10}H_{13}N_3O_4S$	270.0554	-1.48	6
	202	5.71	201.9811	$C_6H_5NO_5S$	201.9816	2.31	5
	252	6.84	252.0444	$C_{10}H_{11}N_3O_3S$	252.0448	1.75	7
	268	6.86	268.0405	$C_{10}H_{11}N_3O_4S$	268.0398	-2.80	7
	266	8.42	266.0221	$C_{10}H_9N_3O_4S$	266.0241	7.52	8
	268	11.41	268.0400	$C_{10}H_{11}N_3O_4S$	268.0398	-0.93	7
	SMX	12.39					
	266	13.40	266.0238	$C_{10}H_9N_3O_4S$	266.0241	1.13	8
LP pH 8	268	2.97	268.0398	$C_{10}H_{11}N_3O_4S$	268.0398	-0.19	7
	214	3.07	214.0281	$C_7H_9N_3O_3S$	214.0292	5.07	5
	242	3.66	242.0240	$C_8H_9N_3O_4S$	242.0241	0.41	6
	270	5.59	270.0553	$C_{10}H_{13}N_3O_4S$	270.0554	0.37	6
	252	6.82	252.0451	$C_{10}H_{11}N_3O_3S$	252.0448	-1.03	7
	268	11.40	268.0395	$C_{10}H_{11}N_3O_4S$	268.0398	0.93	7
	SMX	12.38					
	266	13.39	266.0245	$C_{10}H_9N_3O_4S$	266.0241	-1.50	8
MP pH 3	189	1.63	188.9868	$C_6H_6O_5S$	188.9863	-2.55	4
	177	2.13	176.9959	$C_4H_6N_2O_4S$	176.9976	9.33	3
	189	2.29	188.9863	$C_6H_6O_5S$	188.9863	0.10	4
	214	3.06	214.0282	$C_7H_9N_3O_3S$	214.0292	4.60	5
	214	4.18	214.0288	$C_7H_9N_3O_3S$	214.0292	1.80	5
	270	5.55	270.0551	$C_{10}H_{13}N_3O_4S$	270.0554	1.11	6
	202	5.62	201.9808	$C_6H_5NO_5S$	201.9816	3.80	5
	252	6.79	252.0446	$C_{10}H_{11}N_3O_3S$	252.0448	0.95	7
	266	8.38	266.0239	$C_{10}H_9N_3O_4S$	266.0241	0.75	8
	268	11.38	268.0394	$C_{10}H_{11}N_3O_4S$	268.0398	1.31	7
	SMX	12.35					
	266	13.32	266.0234	$C_{10}H_9N_3O_4S$	266.0241	2.63	8

	Name	t_R [min]	Measured *m/z* $[M-H]^-$	Elemental composition [M-H]	Calculated *m/z* $[M-H]^-$	Error [ppm]	DBE
MP pH 8	214	2.08	214.0317	$C_7H_9N_3O_3S$	214.0292	-11.75	5
	177	2.14	176.9969	$C_4H_6N_2O_4S$	176.9976	3.68	3
	214	3.08	214.0290	$C_7H_9N_3O_3S$	214.0292	0.86	5
	242	3.66	242.0241	$C_8H_9N_3O_4S$	242.0241	0.00	6
	268	5.48	268.0399	$C_{10}H_{11}N_3O_4S$	268.0398	-0.56	7
	270	5.57	270.0555	$C_{10}H_{13}N_3O_4S$	270.0554	-0.37	6
	252	6.80	252.0448	$C_{10}H_{11}N_3O_3S$	252.0448	0.16	7
	268	11.38	268.0392	$C_{10}H_{11}N_3O_4S$	268.0398	2.05	7
	SMX	12.35					
	266	13.33	266.0238	$C_{10}H_9N_3O_4S$	266.0241	1.13	8
MP+CF pH 3	189	1.63	188.9864	$C_6H_6O_5S$	188.9863	-0.43	4
	177	2.13	176.9975	$C_4H_6N_2O_4S$	176.9976	0.29	3
	189	2.29	188.9862	$C_6H_6O_5S$	188.9863	0.62	4
	214	3.04	214.0289	$C_7H_9N_3O_3S$	214.0292	1.33	5
	214	4.16	214.0285	$C_7H_9N_3O_3S$	214.0292	3.20	5
	260	4.24	260.1032	$C_{13}H_{15}N_3O_3$	260.1041	3.33	8
	260	4.64	260.1039	$C_{13}H_{15}N_3O_3$	260.1041	0.63	8
	270	5.52	270.0547	$C_{10}H_{13}N_3O_4S$	270.0554	2.59	6
	202	5.59	201.9815	$C_6H_5NO_5S$	201.9816	0.33	5
	268	5.78	268.0390	$C_{10}H_{11}N_3O_4S$	268.0398	2.80	7
	252	6.76	252.0448	$C_{10}H_{11}N_3O_3S$	252.0448	0.16	7
	266	8.37	266.0241	$C_{10}H_9N_3O_4S$	266.0241	0.00	8
	266	9.52	266.0241	$C_{10}H_9N_3O_4S$	266.0241	0.00	8
	268	11.38	268.0402	$C_{10}H_{11}N_3O_4S$	268.0398	-1.68	7
	SMX	12.34					
	266	13.31	266.0236	$C_{10}H_9N_3O_4S$	266.0241	1.88	8
MP+CF pH 8	214	2.08	214.0290	$C_7H_9N_3O_3S$	214.0292	0.86	5
	177	2.13	176.9968	$C_4H_6N_2O_4S$	176.9976	4.24	3
	202	2.17	201.9831	$C_6H_5NO_5S$	201.9816	-7.59	5
	214	3.06	214.0283	$C_7H_9N_3O_3S$	214.0292	4.13	5
	242	3.63	242.0238	$C_8H_9N_3O_4S$	242.0241	1.24	6
	270	5.53	270.0546	$C_{10}H_{13}N_3O_4S$	270.0554	2.96	6
	202	5.61	201.9812	$C_6H_5NO_5S$	201.9816	1.82	5
	266	8.38	266.0240	$C_{10}H_9N_3O_4S$	266.0241	0.38	8
	266	10.50	266.0239	$C_{10}H_9N_3O_4S$	266.0241	0.75	8
	252	11.01	252.0441	$C_{10}H_{11}N_3O_3S$	252.0448	2.94	7
	268	11.39	268.0392	$C_{10}H_{11}N_3O_4S$	268.0398	2.05	7
	SMX	12.35					
	266	13.33	266.0242	$C_{10}H_9N_3O_4S$	266.0241	-0.38	8

	Name	t_R [min]	Measured *m/z* $[M-H]^-$	Elemental composition [M-H]	Calculated *m/z* $[M-H]^-$	Error [ppm]	DBE
HP pH 3	177	2.17	176.9972	$C_4H_6N_2O_4S$	176.9976	1.98	3
	189	2.33	188.9864	$C_6H_6O_5S$	188.9863	-0.43	4
	214	3.09	214.0287	$C_7H_9N_3O_3S$	214.0292	2.27	5
	214	4.30	214.0285	$C_7H_9N_3O_3S$	214.0292	3.20	5
	260	4.56	260.1041	$C_{13}H_{15}N_3O_3$	260.1041	-0.13	8
	260	5.01	260.1040	$C_{13}H_{15}N_3O_3$	260.1041	0.25	8
	270	5.63	270.0552	$C_{10}H_{13}N_3O_4S$	270.0554	0.74	6
	202	5.71	201.9810	$C_6H_5NO_5S$	201.9816	2.81	5
	268	5.90	268.0398	$C_{10}H_{11}N_3O_4S$	268.0398	-0.19	7
	252	6.74	252.0447	$C_{10}H_{11}N_3O_3S$	252.0448	0.56	7
	268	6.76	268.0404	$C_{10}H_{11}N_3O_4S$	268.0398	-2.43	7
	268	10.69	268.0398	$C_{10}H_{11}N_3O_4S$	268.0398	-0.19	7
	SMX	11.84					
	266	13.03	266.0235	$C_{10}H_9N_3O_4S$	266.0241	2.26	8
HP pH 8	242	2.00	242.0212	$C_8H_9N_3O_4S$	242.0241	11.98	6
	214	2.07	214.0290	$C_7H_9N_3O_3S$	214.0292	0.86	5
	177	2.14	176.9965	$C_4H_6N_2O_4S$	176.9976	5.94	3
	214	3.07	214.0287	$C_7H_9N_3O_3S$	214.0292	2.27	5
	242	3.65	242.0241	$C_8H_9N_3O_4S$	242.0241	0.00	6
	270	5.55	270.0554	$C_{10}H_{13}N_3O_4S$	270.0554	0.00	6
	202	5.65	201.9813	$C_6H_5NO_5S$	201.9816	1.32	5
	266	8.41	266.0242	$C_{10}H_9N_3O_4S$	266.0241	-0.38	8
	266	10.52	266.0243	$C_{10}H_9N_3O_4S$	266.0241	-0.75	8
	252	11.04	252.0446	$C_{10}H_{11}N_3O_3S$	252.0448	0.95	7
	268	11.38	268.0393	$C_{10}H_{11}N_3O_4S$	268.0398	1.68	7
	SMX	12.35					
	266	13.35	266.0238	$C_{10}H_9N_3O_4S$	266.0241	1.13	8

Table S4.8: The suggested structures of the ten most abundant phototransformation products of SMX photolysis with the LP, MP, MP+CF and HP lamp. Names are referring to the nomenclature from Table S4.7.

Name	Calculated molecular mass of neutral suggested structure [g mol^{-1}]	Suggested structure	Reference to Literature
TP177	178.1664	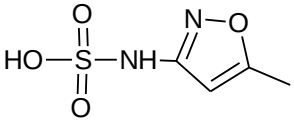	206,215,216
TP189	190.1738	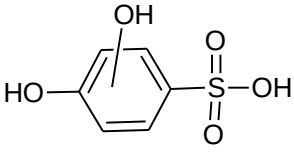	Newly identified *m/z*

Name	Calculated molecular mass of neutral suggested structure [g mol^{-1}]	Suggested structure	Reference to Literature
TP202	203.1736	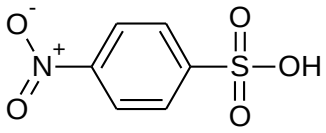	Newly identified *m/z*
TP214	215.2297	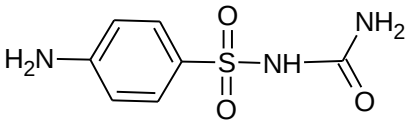	208
TP242	243.2398	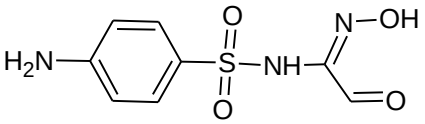	219 Found in photo-Fenton
TP252	253.2776	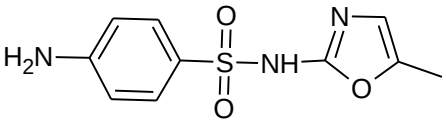	91,206,208,209,214,216-218
TP260	?	?	Newly identified *m/z*
TP266	267.2612	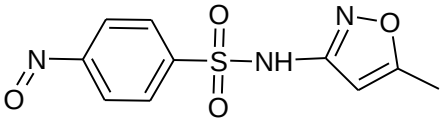	215
TP268	269.2770	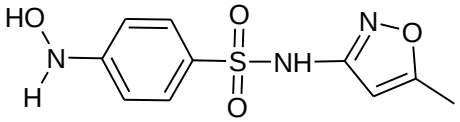	91,206,208,215,216
TP270	271.2929	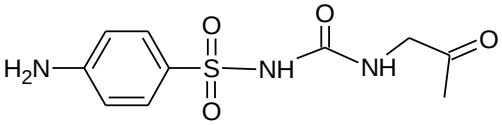 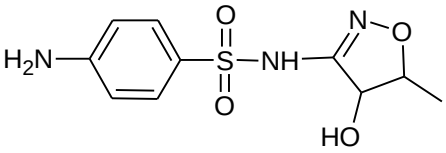	214,216 91,208

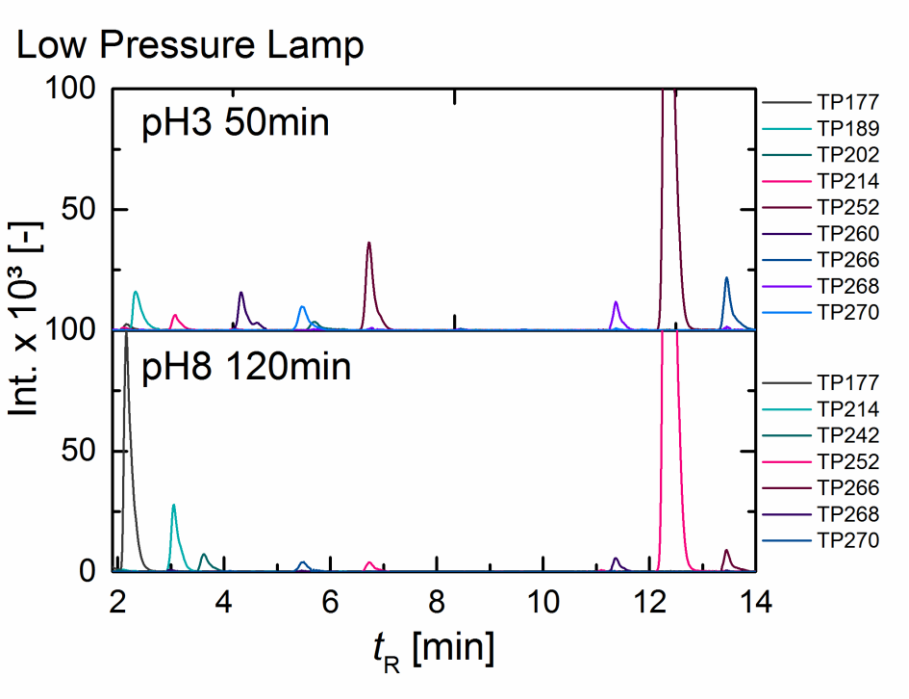

Figure S4.10: Main transformation products of the photodegradation of SMX with the LP lamp at pH 3 and pH 8. Exact *m/z* and further product information can be found in Table S4.7.

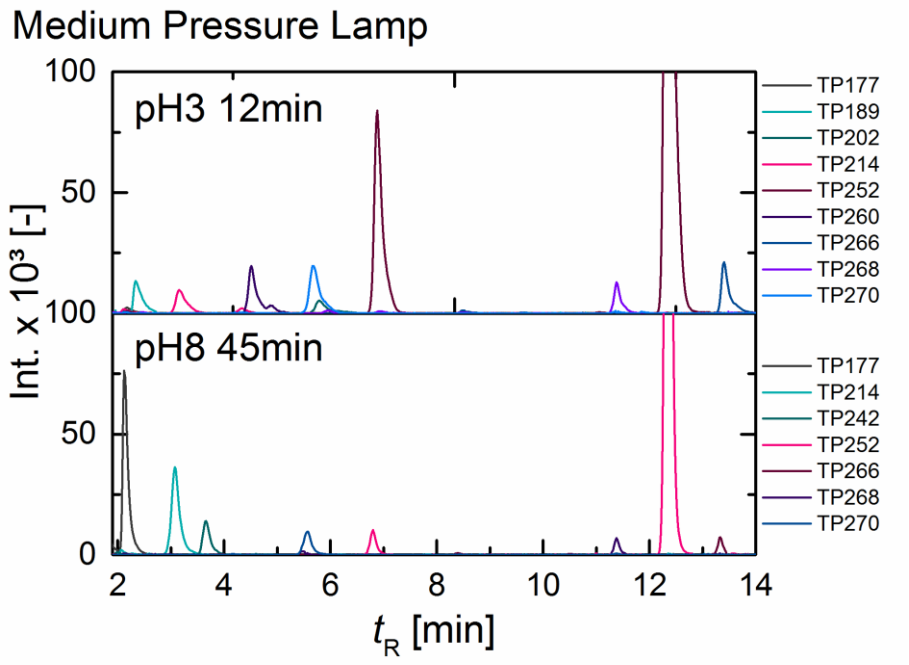

Figure S4.11: Main transformation products of the photodegradation of SMX with the MP lamp at pH 3 and pH 8. Exact *m/z* and further product information can be found in Table S4.7.

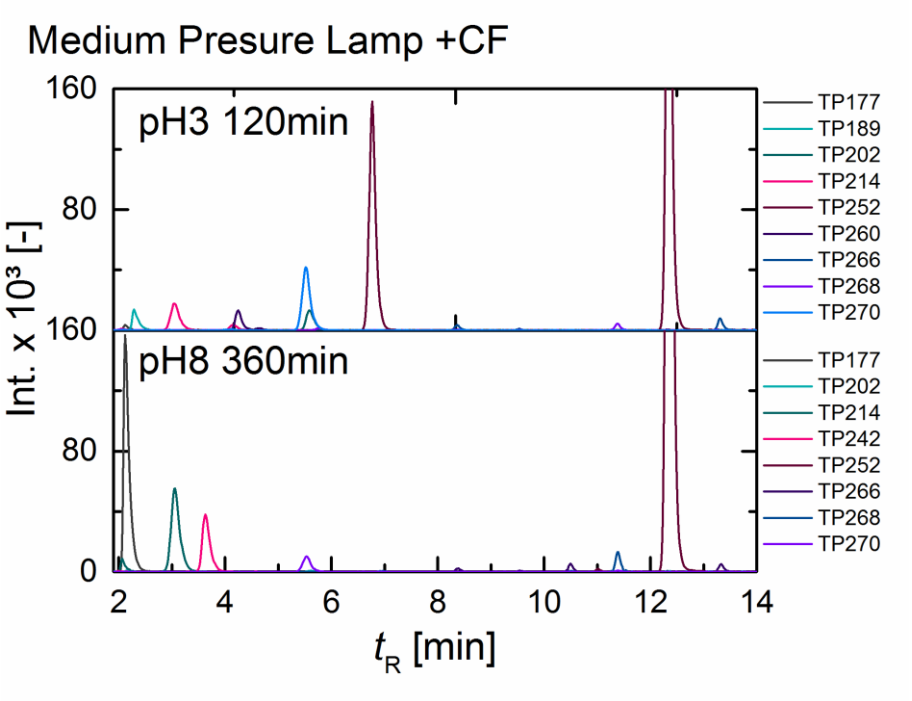

Figure S4.12: Main transformation products of the photodegradation of SMX with the MP lamp with cut-off filter at pH 3 and pH 8. Exact *m/z* and further product information can be found in Table S4.7.

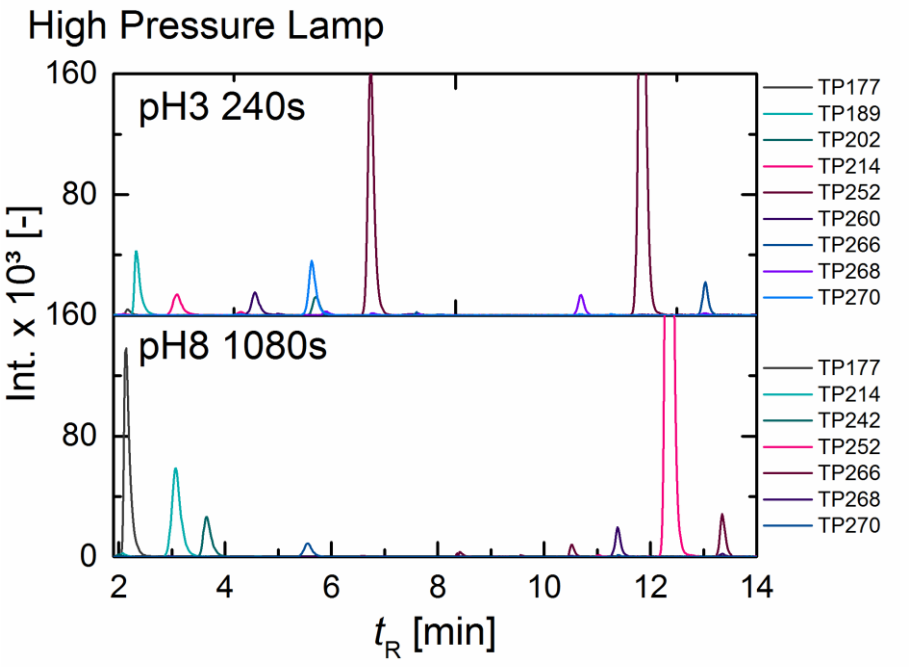

Figure S4.13: Main transformation products of the photodegradation of SMX with the HP lamp at pH 3 and pH 8. Exact *m/z* and further product information can be found in Table S4.7.

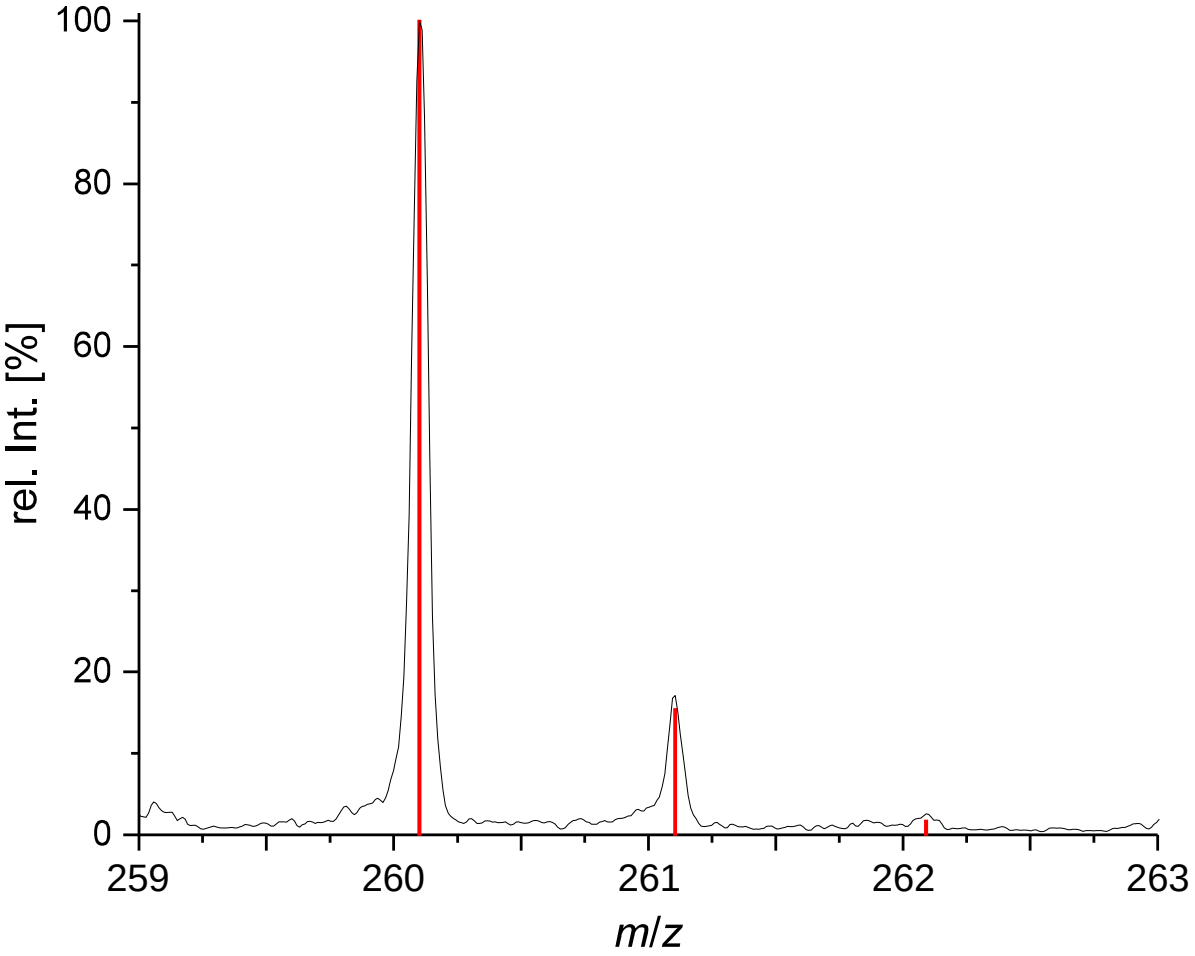

Figure S4.14: Isotopic pattern of TP260 exemplarily shown for HP pH 3, *t* = 240 s. The relative peak abundance of *m/z* (260.1033:261.1034:262.0981) is 100 %:15.95 %:2.23 % with a standard deviation of 1 %. Theoretically, the calculated relative peak abundance for the elemental composition "$C_{13}H_{15}N_3O_3$" of *m/z* (260.1041: 261.1074: 262.1107) is 100%:15.44%:1.73%. The relative peak abundance of a sulfur-containing TP with *m/z* (X:X+2) would have been 100 %:4.4 %.

Chapter 5 -
Reactions of O_3, $^{\bullet}OH$ and ClO_2 with benzene and its analogs

5.1 Abstract

Oxidative processes frequently contribute to organic pollutant degradation in natural and engineered systems such as during the remediation of contaminated sites and in water treatment processes. Because a systematic characterization of abiotic reactions of organic pollutants with oxidants such as ozonation or hydroxyl radicals by compound-specific stable isotope analysis (CSIA) is lacking, stable isotope-based approaches have rarely been applied for the elucidation of mechanisms of such transformations. Here, we investigated the carbon isotope fractionation associated with the oxidation of benzene and several methylated and methoxylated analogs, namely toluene, three xylene isomers, mesitylene and anisole, and determined their carbon isotope enrichments factors (ε_C) for reactions with ozone (ε_C = −3.6 ‰ to −4.6 ‰) and hydroxyl radicals (ε_C = < −1 ‰). The differences in isotope fractionation may be used to elucidate the contribution of the reactions with ozone or hydroxyl radicals to overall transformation. Subsequently, apparent kinetic isotope effects (AKIEs) were derived for the reaction with ozone. This was nontrivial due to challenges in assigning reactive positions in the probe compounds for the monodentate attack leading to an ozone adduct. We present several options for this step and compare the outcome to quantum chemical characterizations of ozone adducts. Our data show that a general assignment of reactive positions for reactions of ozone with aromatic carbon in *ortho*, *meta* or *para* positions is not feasible and that AKIEs of this reaction should be derived on a compound-by-compound basis.

5.2 Introduction

Oxidative processes play an important role in pollutant degradation in natural[156,228] and numerous engineered systems such as during the remediation of contaminated sites[229-231] and water treatment processes[2]. In water treatment processes a broad variety of oxidants are used and including chlorine dioxide (ClO_2)[49,166], ozone (O_3)[2,182] or hydroxyl radicals ($^{\bullet}OH$)[2]. Common processes to generate significant amounts of $^{\bullet}OH$ in water treatment, are, e.g., H_2O_2/UV or the peroxone process (O_3/H_2O_2).[2,232] Usually, oxidative processes cause chemical modifications, e.g. through electron transfer and oxygenation[2,166] of the otherwise persistent pollutants which enable their further degradation[228]. Detecting the resulting oxidation products to assess the utility of oxidative processes in removing pollutants is often challenging and may be hampered if their susceptibility for further oxidation is higher than that of the original contamination. One option to monitor such reactions is compound-specific stable isotope analysis (CSIA).[118,119]

CSIA is a widely used tool to track the origin and fate of environmental contaminants and to distinguish environmental degradation processes over much longer timescales of years to decades.[118-120] Examples include the monitoring and distinction of biotic and abiotic remediation activities if differences in isotope fractionation of the (bio)transformation processes occur.[118,119,129,130,229,233] Those distinctions are possible because the isotope effects determining the observable isotope fractionation in a pollutant are indicative of a reaction mechanism.[118] This feature enables one, for example, to differentiate aerobic and anaerobic biodegradation or acid hydrolysis of methyl *tert*-butyl ether (MTBE) from each other - three transformation pathways which otherwise could not be differentiated from the reaction product because those reactions all lead to *tert*-butyl alcohol (*tert*-BuOH).[118,221] However, up to now only a few studies applied CSIA for investigation of oxidation processes relevant in water treatment.[154,210,234]

Isotopic enrichment factors (ε_E) and apparent kinetic isotope effects ($AKIE_E$s) of an isotopic element E are the key parameters in CSIA for assessing how contaminants react. Whereas ε_E values enable one to apply and interpret CSIA to specific pollutants, $AKIE_E$s allow for general mechanistic insights into reaction mechanisms.[120,153,233,235] These two parameters are related as specified in eq. 5.1.[127]

$$AKIE_E = \frac{1}{1 + z \cdot \frac{n}{x} \cdot \varepsilon_E} \quad (5.1)$$

where *n* is the number of atoms of the considered element (i.e., in this study carbon atoms) of which the number of *x* atoms are located at a reactive position and *z* is the number of equivalent reactive positions in intramolecular competition.[127]

As a consequence, it is possible to assign certain ranges of AKIEs to specific reaction mechanisms under the assumption that they share one major rate-determining reaction step.[127,233] Such AKIE ranges may be helpful in future environmental or technical process oriented investigations to infer reaction mechanisms of pollutant degradation from ε_E value(s).[127,233] However, due to the lack of experimental data no appropriate ranges for AKIEs originating from oxidation reactions with O_3 or ClO_2 of benzene and its analogs have been defined, yet. In case of $^{\bullet}OH$, a first AKIE data set has been determined.[234]

In order to define the required variables *x* and *z* (eq. 5.1) it is necessary to have a well-understood hypothesis for the reaction mechanism.[127] Regarding ozonation of benzene and its analogs, it is a general obstacle that their primary ozonation products are muconic or phenolic compounds. These products show significantly higher reaction rate constants with O_3 (cf. von Sonntag & von Gunten[2]) than the respective reactants ($< 10^3\ M^{-1}\ s^{-1}$;[236] cf. Table S5.1). O_3 reacts with muconic products at approximately $10^4\ M^{-1}\ s^{-1}$.[2] In case of phenolic compounds (cf. Table S5.1) (pK_a(phenol) = 9.9)[236], the very fast reaction rate constant of the anion is the reason why traces of phenolate even at neutral pH are sufficient to cause observable reaction rate constants $> 10^6\ M^{-1}\ s^{-1}$.[2] The reactivity pK_a is found at pH ≈ 4[2], that is the pH where the reacting quantities of neutral and anionic species are equal. Consequently, it is hardly possible to quantify the primary ozonation reaction products of benzene and its analogs with a reasonable effort which would give insights on the initial point of attack. Hence, a complementary approach such as computational chemistry is required to derive appropriate values for the variables *x* and *z* (eq.5.1).

The aim of this study was to elucidate isotopic fractionation trends pertinent to the oxidation reaction of the well-established oxidative processes applied in water treatment (i.e., ozonation, $^{\bullet}OH$ treatment and chlorine dioxide) using benzene and its methylated or methoxylated analogs as model compounds for reactive aromatic moieties in organic pollutants. The second objective was to present ^{13}C-AKIE-values, which define characteristic ranges for the oxidation reactions of O_3 with the used model compounds. The determination of AKIEs turned out to be nontrivial and the assignment of reactive moieties for reactions of the probe compound with O_3 is elucidated here with quantum chemical calculations.

5.3 Material and Methods

5.3.1 Chemicals

Chemicals and solvents were used as received from the supplier. A complete list of all chemicals used is given in the supporting information (SI) in Text S5.1.

5.3.2 Generation of ozone stock solutions

O_3 was generated by an O_3 generator BMT 802X (BMT Messtechnik, Berlin, Germany) using oxygen as feed-gas. The O_3 gas was led into an ice cooled impinger filled with ultrapure water. The O_3 stock solution was continuously purged with O_3 gas throughout its utilization. The O_3 concentration of this stock solution was determined spectrophotometrically of a 1:3-diluted O_3 stock solution at 258 nm, ε_{O3} = 3200 M^{-1} cm^{-1}.[2] The resulting O_3 concentrations were in a range of 1.6-1.7 mM O_3.

5.3.3 Sample preparation

The stock solutions of each probe compound including benzene and its analogs for preparation of calibration standards were prepared in methanol. Stock solutions for oxidation experiments with O_3 or $^{\bullet}OH$ were prepared in ultrapure water because the presence of methanol may lead to formation of undesired reactive species such as superoxide radicals ($O_2^{\bullet-}$) which could accelerate O_3 decay due to $^{\bullet}OH$ formation.[34] The aqueous stock solutions were prepared in Erlenmeyer flasks by addition of an aliquot of one pure probe compound to ultrapure water and subsequent shaking for at least 48 h. Due to the limited solubility in water the remaining organic phase was removed thereafter. Final concentrations of the aqueous stock solutions were determined with HPLC-DAD. The aqueous stock solutions were used within a day of their preparation. Reactors were prepared as batch samples in 20-mL headspace screw cap vials. In case of oxidation with O_3 the pH was kept constant at pH 7 with 5 mM phosphate buffer. Additionally, *tert*-BuOH was added in order to scavenge $^{\bullet}OH$ which may be formed in the reaction with O_3.[2] The *tert*-BuOH concentrations were chosen individually for each compound so that ≥ 95 % of $^{\bullet}OH$ formed were scavenged (Text S5.2 and Table S5.1). A detailed overview on sample composition is shown in Tables S5.2-8. In case of oxidation with $^{\bullet}OH$ the peroxone process was utilized (i.e., $^{\bullet}OH$ are generated by the reaction of O_3 with hydrogen peroxide).[2,24] The amounts of hydrogen peroxide required to obtain ≥ 99 % reaction with O_3 were calculated using the corresponding reaction rate constants (Text S5.4 and Table S5.1). Due to the faster reaction rate constant of O_3 with the hydrogen peroxide anion ($k_{O_3+HO_2^-}$ = 9.6 x 10^6 M^{-1} s^{-1})[24] than with the neutral species

($k_{O_3+H_2O_2}$ < 10^2 M^{-1} s^{-1})[17], peroxone reaction experiments were carried out at pH 9 ($k_{obs(O_3+HO_2^-)}$ = 1.5 x 10^4 M^{-1} s^{-1}, cf. Table S5.1). The pH was controlled with a 5 mM borate buffer. The individual sample compositions depended on the reaction rate constants of each benzene analog with O_3 and $^{\bullet}OH$ and are given in SI in Tables S5.9-15.

A detailed description of oxidation experiments with ClO_2, the respective sample preparation and the generation of the required ClO_2 stock solutions can be found in the SI in Text S5.6, Tables S5.16-22 and Text S5.5, respectively.

5.3.4 Analytical methods

For determination of UV-vis absorption a UV-1650PC spectrophotometer (Shimadzu, Duisburg, Germany) was used with a quartz cuvette with an optical path length of 1 cm. For pH measurements, a pH-meter (827 pH lab with aquatrode both from Metrohm, Herisau, Switzerland) was used which was calibrated with standard buffers every working day.

Quantification of benzene and its analogs in the aqueous stock solutions was performed with an HPLC-UV/vis system (LC-20AT coupled to SPD-20A; Shimadzu, Duisburg, Germany). A detailed description can be found in Text S5.7.

Compound-specific stable carbon isotope values of benzene and its analogs were determined by gas chromatography isotope-ratio mass spectrometry (GC-IRMS) which is described in detail in Text S5.8. Briefly, a Trace GC Ultra coupled by the combustion interface Finnigan GC-C/TC III to a Finnigan MAT 253 isotope ratio mass spectrometer (all from Thermo Scientific, Bremen, Germany) was used. The GC system was additionally equipped with a HTX PAL autosampler (CTC Analytics, Zwingen, Switzerland; supplied by Axel Semrau, Sprockhövel, Germany) with an agitator and an Optic 3 injector (ATAS GL-Sciences, Eindhoven, Netherlands; supplied by Axel Semrau). After sample conditioning in the agitator 500 µL of the headspace were injected. Compounds were separated on a Rxi® 5Sil MS column (60m x 0.25 mm i.d., 0.25 µm film thickness; Restek, Bad Homburg, Germany) using different temperature gradients described in Table S5.23. After separation, the analytes were oxidized to CO_2 at 940 °C in the combustion interface equipped with Pt, CuO and NiO wires, which were reoxidized each time (i.e., after 40 to 60 injections) before a new sample set was run. At least every fourth sample run was a reference sample without oxidant addition for quality control. Linearity and precision tests were run regularly. The carbon isotope values are given in reference to the international Vienna Pee Dee Belemnite (VPDB) scale according to eq. 5.2 (cf. Text S5.8).[120]

$$\delta^{13}C_{sample,VPDB} = \left(\frac{R_{sample}(^{13}C/^{12}C) - R_{VPDB}(^{13}C/^{12}C)}{R_{VPDB}(^{13}C/^{12}C)} \right) \quad (5.2)$$

Where R_{sample} and R_{VPDB} are the ratios of $^{13}C/^{12}C$ of the samples and VPDB, respectively. At least two to three calibrated CO_2 reference gas pulses were included in each chromatographic run for referencing. The peak areas used for the ratio of concentration to initial concentration (c/c_0) originate from the $^{12}CO_2$ peak (*m/z* 44).

The carbon isotope enrichment factors (ε_C) of the different oxidation experiments of benzene and its analogs with O_3 or $^{\bullet}OH$ were determined by application of the Rayleigh equation (eq. 5.3):[120]

$$\ln\left(\frac{R_{i,sample}(^{13}C/^{12}C)}{R_{0,sample}(^{13}C/^{12}C)} \right) = \ln\left(\frac{\delta^{13}C_{i,sample}+1}{\delta^{13}C_{0,sample}+1} \right) = \varepsilon_C \cdot \ln\left(\frac{c_{i,sample}}{c_{0,sample}} \right) \quad (5.3)$$

Where $\delta^{13}C_0$ and $\delta^{13}C_i$ and the concentrations of each model compound, i.e. c_0 and c_i, relate to the sampling point *0* (no oxidant added) and sampling point *i* (transformation after full oxidant turnover at defined oxidant doses), respectively.

5.3.5 Quantum chemical calculations

Quantum chemical calculations have been performed to gain more insight into the reactions on a molecular scale.[237] Three scenarios (i.e., calculations type 1-3) have been conducted for further elucidation. All calculations were performed with the Gaussian09 and Gaussian16 program packages[238].

Calculations type 1 focused on the determination of optimized geometries of possible adduct compounds originating from a monodentate attack of ozone on the various substituted benzene derivatives. These calculations were performed at the unrestricted UMP2 level using a moderately sized segmented valence double zeta 6-31+G(2d,p) basis set with polarization functions on all atoms and a set of diffuse functions on non-hydrogens.[239-241] To account for liquid phase conditions all calculations were embedded in a self-consistent reaction field (SCRF) in form of the polarizable continuum model (PCM)[242] assuming water as solvent. In calculations type 1, it turned out that a full set of adduct compounds including a number of different conformers and isomers could only be derived if the electronic triplet state was assumed. In addition, transition states could be located and optimized for the corresponding reverse reactions of ozone cleavage. However, these transition states and adduct molecules correspond to a reactive electronic triplet surface, e.g. accessible by the singlet state benzene derivative plus an exited state triplet ozone molecule.

Calculations type 2 were started to reoptimize the various ozone adduct structures in an open shell singlet electronic state. Again, these calculations made use of the unrestricted UMP2/6-31+G(2d,p) method embedded in a PCM reaction field.[239-242] The unrestricted treatment for the singlet electronic state was forced by mixing alpha and beta molecular orbitals, thus destroying spatial symmetries in the initial guesses of the wave function in every step of the geometry optimization. Unfortunately, only few calculations converged and resulted in the desired singlet state adduct, despite the previously optimized (triplet) starting geometries. In summary, we were able to derive complete triplet state as well as singlet state reaction paths (including transition states) only for triplet/singlet ozone added to benzene and *p*-xylene, respectively. These results were later used to calculate the kinetic isotope effect via statistical reaction kinetics using ISOEFF[243].

In calculations type 3, the electronic properties of the various substituted benzene derivatives such as electrostatic potential mapped onto the electron density and regional Fukui functions (cf. SI Text S5.9) were derived. Fukui functions were derived with a calculation program,[244] publicly available under GPL 3.0 License in accordance to the work of Contreras et al.[245]. In addition to the already calculated geometries at the PCM/MP2-level (see above) also PCM/B3LYP/6-31++G(2df,p)[246] ones were utilized as base geometries. The corresponding structural optimizations with the B3LYP Hybrid-DFT method[247] along with a slightly larger basis set served as additional check for our previous calculations at the MP2 level.

5.4 Results and discussion

5.4.1 Isotope fractionation in transformation of benzene and its analogs

Carbon stable isotope values were determined for benzene, its methylated analogs and anisole (methoxybenzene) oxidized with $^{\bullet}OH$ and O_3. The according Rayleigh-plots (cf. eq. 5.3) are shown in Figure S5.1. The observed isotopic fractionations always occurred as *normal* isotope effect, that is molecules containing the heavier ^{13}C isotope reacted slower than molecules containing exclusively ^{12}C so that the residual substrate fraction is depleted in molecules with the lighter ^{12}C. As a consequence, the ratio of $^{13}C/^{12}C$ increased as the oxidation reactions proceeded further. The determined ε_C values (cf. eq. 5.3) for the investigated transformation reactions (i.e., ε_C(oxidation with $^{\bullet}OH$) ranging between −0.0 ± 0.2 ‰ and −1.2 ± 0.1 ‰ and ε_C(oxidation with O_3) ranging between −3.7 ± 0.1 ‰ and −5.4 ± 0.3 ‰) are shown in Figure 5.1 and are listed as numerical values in Table S5.24.

Additionally, transformation reactions of benzene and its analogs were conducted with chlorine dioxide (ClO_2) as oxidant (see Figures S5.2-8). However, except for mesitylene it

was not possible to cause a significant reactant transformation. Even with mesitylene it was not possible to obtain a trend of carbon isotope signatures so that no further conclusions will be drawn from the experimental setups with ClO_2. One reason for the negligible turnover of reactants could be the slow reaction rate constants of ClO_2 with the studied compounds. However, the reaction rate constants have not been determined, yet. Lee et al. have illustrated that reaction rate constants of ClO_2 are regularly found approximately 100 – 1000 times slower than for O_3 with the same reactant.[248] Based on the available reaction rate constants for O_3 with benzene and its analogs listed in Table S5.1, ranging between $k_{O_3+benzene}$ = 2 x 10^0 M^{-1} s^{-1} [185] and $k_{O_3+mesitylene}$ = 7 x 10^2 M^{-1} s^{-1} [185], it is highly probable that reaction rate constants for ClO_2 and the respective compounds are thus extremely slow.

5.4.1.1 Oxidation with hydroxyl radicals

Benzene and its analogs were oxidized with the peroxone process (i.e., with •OH). All resulting ε_C values for benzene and its methylated analogs (Figure 5.1) were found at similarly low values of < −1 ‰. Only, the ε_C value for anisole was somewhat higher (−1.2 ± 0.1 ‰). This overall low but still measurable isotope fractionation for oxidation of benzene and its analogs was also observed by Zhang et al. with H_2O_2/UV - another •OH generating water treatment process.[234] The related values are included in Figure 5.1 and Table S5.24 in order to facilitate direct comparison. The slight variations between the ε_C values for each single compound may be attributed to the different experimental setups applied for generation of •OH (i.e., O_3/H_2O_2 (this study) and H_2O_2/UV (Zhang et al.)[234]). For degradation of toluene with the Fenton-like reaction, another •OH based oxidation process, an ε_C value of −0.2 ‰ was determined.[249] Hence, based on these results it is possible to assign a distinct range for ε_C values to be expected for •OH based oxidation of benzene and its methylated analogs between 0 ‰ and −1 ‰.

5.4.1.2 Oxidation with ozone

The ε_C values for oxidation of benzene and its methylated analogs with O_3 are within a range of 1 ‰ (i.e., between −3.6 ‰ and −4.6 ‰) whereas the ε_C for the methoxy analog anisole is even more pronounced (i.e. −5.4 ± 0.3 ‰; cf. Figure 5.1 and Table S5.24). For the compounds under study, the ε_C values for the oxidation with O_3 (•OH excluded) are different from those obtained for oxidation with •OH (< −1 ‰). Hence, a second distinct range for ε_C values (i.e., from −3.6‰ to −4.6‰) may be ascribed for oxidation of benzene and its methylated analogs with O_3. Consequently, oxidation of benzene and its analogs with •OH or O_3 may be differentiated from each other by comparison of ε_C values determined by CSIA.

This result is in agreement with the kinetic rate constants (Table S5.1) which already indicated that •OH reactions are close to diffusion controlled rates[2], thus resulting in less pronounced ε_C values, whereas O_3 is a more selective oxidant[2] showing elevated ε_C values.

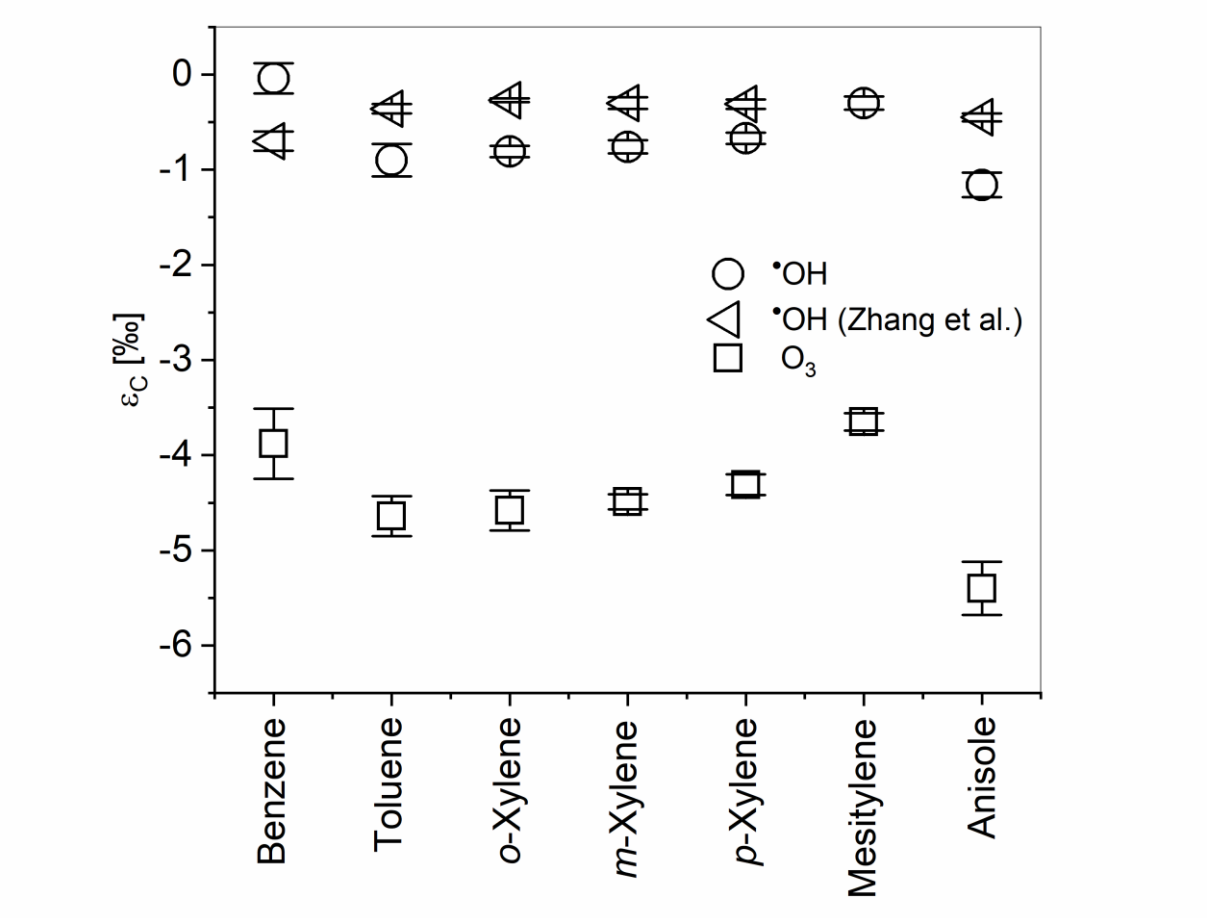

Figure 5.1: Stable isotope enrichment factors (ε_C) for oxidation of benzene and its analogs with either O_3 or •OH (generated by the peroxone process). pH was kept constant, i.e. at pH 9 with 5 mM borate buffer (•OH reactions, peroxone) and at pH 7 with 5 mM phosphate buffer (O_3 reactions). In oxidations with O_3, intrinsically formed •OH after reaction of O_3 with one of the compounds were scavenged with *tert*-BuOH (cf. sample preparation); error bars represent the standard deviation of the slope of each Rayleigh equation. For comparison, ε_C values of oxidation by •OH generated by UV/H_2O_2 (triangle leftward; Zhang et al.[234]) are included. Note: Mesitylene was not investigated by Zhang et al.[234].

These insights from CSIA could be incorporated in future applications of oxidative drinking water treatment to identify the primary oxidation conditions such as for estimating the R_{ct} which is an important parameter to describe ozonation of water and wastewater.[2,250,251] The parameter R_{ct} equals the ratio of •OH- and O_3-concentration and exposure, respectively, in an ozonation process (eq 4)[250] (note that •OH are formed in reactions of O_3 with water matrix constituents such as natural organic matter (NOM))[2]. The R_{ct} value mainly depends on the water matrix constituents and the oxidant dose and has to be determined for every individual

ozonation process, which requires regular sampling and performing according laboratory experiments.[250] Once the R_{ct} value is known, one can calculate $^{\bullet}OH$ exposures from O_3 exposures (eq. 5.4). Since O_3 exposures are easily determined online[251], the R_{ct} value allows to assess also $^{\bullet}OH$ exposures online. With these two exposures at hand, one can monitor disinfection and pollutant degradation during ozonation if according reaction rate constants are available in literature.

$$R_{ct} = \frac{\left[{}^{\bullet}OH\right]}{\left[O_3\right]} \tag{5.4}$$

where $[^{\bullet}OH]$ and $[O_3]$ are the concentrations or exposures of $^{\bullet}OH$ and O_3, respectively.

A complementary approach to determination of the R_{ct} value could be the determination of the ε_C value of e.g. a methylated benzene analog such as mesitylene. The obtained ε_C value would allow conclusions on the oxidative process conditions, that is $\varepsilon_C \geq -0.4$ ‰ is purely $^{\bullet}OH$ governed, -0.4 ‰ $> \varepsilon_C > -3.6$ ‰ mixed conditions with a contingent tendency and $\varepsilon_C \leq -3.6$ ‰ purely O_3 governed. By regular verification of the ε_C value either the validity of the R_{ct} value could be confirmed or the need for its reevaluation could be identified if, e.g., seasonal changes occur. A distinct influence on the R_{ct} value has been illustrated for changes in temperature, pH, alkalinity and concentration or constitution of NOM.[252]

Moreover, it could also be possible to assess the effectiveness of an O_3 based oxidative process in water or wastewater treatment with CSIA. If there is a minor pollution with benzene or its methylated analogs, CSIA could be used to determine the proportion of degradation initiated by ozone within the entire oxidation process of these potential tracer compounds. Thus, the plant operator would obtain a reliable measure for the evaluation of the overall treatment train.

5.4.2 Determination of the apparent kinetic isotope effect

In the oxidation reaction of O_3 with simple aromatic compounds such as benzene and its analogs, it was postulated that the initial reaction step is the adduct formation of O_3 with the aromatic ring through a monodentate attack of the electrophile O_3.[2,253] This initial reaction step is predicted to be rate determining.[2,253] Consequently, once the adduct formation has been successful, the subsequent reactions to products are assumed to proceed faster as described elsewhere.[2,254] For example, possible reactions of an ozone adduct could be the formation of a Criegee ozonide, which further decomposes in water, formation of an oxyl

radical and a superoxide anion $\left(O_2^{\bullet-}\right)$ or oxygen transfer resulting in hydroxylation of the aromatic compound and singlet oxygen.[2,254] However, since these subsequent reactions are predicted to be fast[2,253], the back reaction from products to adduct is negligible[2,253] and thus not contributing to the isotopic fractionation of the reaction of the probe compound with O_3.

Consequently, the reaction step leading to adduct formation is regarded as the rate determining and, thus, decisive step for isotopic fractionation. This predicted monodentate electrophilic attack of O_3[2,253] involves one out of at least six carbon atoms present in benzene and its analogs, hence, the nonreactive carbon isotopes will lead to a dilution of the resulting ε_C values. To take this dilution in the average bulk isotopic signature into account the AKIE may be determined according to eq. 5.1.[118,127]

In eq. 5.1, only two variables for all benzene analogs may unequivocally be assigned with numerical values (i.e., *n* and ε_E). For the other two (i.e., *x* and *z*) there are several reasonable possibilities (cf. Table 5.1). In case of benzene all C atoms are chemically identical, making *x* and *z* equal *n*. However, considering toluene (i.e., benzene with only one additional methyl substituent) the assignment of the variables is nontrivial anymore. With regard to the variable *x*, the methyl substituent may be excluded in general since the electrophile O_3 will attack the slightly activated, electron rich aromatic ring.[2] Thus, there are three remaining possibilities which are exemplified here with toluene:

x1. Consideration of all carbon atoms of the aromatic ring (Table 5.1, Type 1)
x2. Consideration of all carbon atoms of the aromatic ring excluding the *ipso*-position (i.e., position C_1 in Figure S5.9) since this one will be subject to steric effects and not favored for adduct formation[253] (Table 5.1, Type 2)
x3. Solely consideration of the *ortho*- and *para*-positions (i.e., positions 2, 6 and 4 in Figure S5.9) which are more favored due to inductive effects (i.e. weak electron donating properties) of the methyl substituent[255] (Table 5.1, Type 3)

The variable *z* specifies the number of equivalent isotopes located in intramolecular competition. The allocation of an unequivocal number may be obvious e.g. in case of transformation reactions limited to the hydrogen isotopes of the methyl group of MTBE[127] but becomes ambiguous in the cases regarded in this study. Here, different aspects could influence the choice of the variable *z* (eq. 5.1). The following options may be considered, again illustrated for toluene as an example:

z1. All considered reactive positions are also equal in intramolecular competition. This is true for all cases of a) in Table 5.1, Type 1-3. In these cases $x = z$, so that these two variables are cancelled out again and n remains the only relevant variable.

z2. All positions which are present twice are considered for the variable z, that is. the two *ortho*- and the two *meta*-positions (Table 5.1, Type 1b), Type 2c)) or the two *ortho*-positions (Table 5.1, Type 3b)).

z3. All carbon isotopes of the aromatic ring are involved in the reaction in principle but due to the directing inductive effect of the methyl substituent to *ortho*- and *para*-positions[255] only the two equal *ortho*-positions may be considered for the variable z (Table 5.1, Type 1d), Type 2e)).

The presented options for the variables x and z open different possible ways of approaching the AKIE calculation of the benzene analogs. All options, if applicable, are illustrated for each considered compound in Table 5.1. Consequently, the question arises which approach of this compilation is chemically meaningful and thus most appropriate. The available literature dealing with isotopic fractionation in abiotic transformation processes of aromatic compounds has not yet dealt with monodentate oxidative reactions in which either $n \neq x$ or $x \neq z$. This means that cases are still missing in which all three variables remain relevant and not two of the implemented variables are cancelled out again.[132,256,257] In the following, several possible approaches will be presented and discussed, which could be used to identify the most suitable approach for calculation of the AKIE.

First of all, it stands out that the option Type 3 is not applicable to all listed compounds in Table 5.1. Moreover, the obtained results for possibility a) or b) do not differ numerically from the respective AKIEs of Type 1 and could not be differentiated on this basis anyway. Hence, the option Type 3 is included for the sake of completeness but will not be considered in the following any further.

Scenario 1: In general, the substituent(s) of the benzene analogs lead(s) to activation for electrophilic attack of the aromatic ring system through inductive effects.[255] Consequently, the reaction rate constants increase with increased number of aromatic substitution (cf. Table S5.1). This increase of reaction rate constants hints to a decrease of the overall required activation energy associated with the entire barrier height between reactant and highest energy transition state.[258] Consequently, a general activation of the aromatic ring system would require consideration of all possibly involved atoms as intramolecular competitors (i.e., $n = z$ and AKIE calculation according to Type 1a) or Type 2a) (Table 5.1)) so that an AKIE range of 1.034 - 1.039 is obtained. This resulting range appears to be very narrow. Furthermore, it would have been expected to observe a trend in the calculated

AKIEs of the homologous series, e.g. a decrease from AKIE of benzene to AKIE of mesitylene. However, in the investigated case there seems to be no dependence between the overall reaction rate constants and the determined ε_C values (cf. Figure 5.1) and the hypothetical AKIEs (Type 1a) or 2a), Table 5.1), respectively. This behavior is also illustrated by plotting the εC values versus the kinetic rate constants of the respective compounds (Figure 5.2).

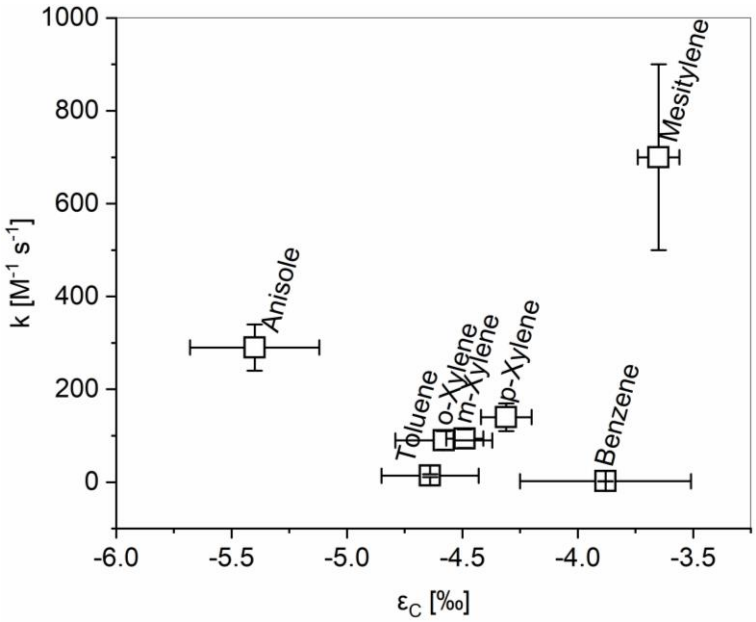

Figure 5.2: Plot of ε_C values (cf. Table S5.24) versus the respective kinetic rate constants of the ozonation of benzene and its methylated and methoxylated analogs (cf. Table S5.1)

Scenario 2: The calculation approach of Scenario 1 did not consider the similarity of the two *ortho*- and *meta*-positions, each. Taking toluene as an example, this could be reflected by consideration of all positions affected by intramolecular competition by the *z*-value (eq. 5.1) without any weighting (i.e., Type 1b) or 2c), Table 5.1). This approach would regard *ortho*- and *meta*-positions as equal points of attack and disregard the directing inductive effects of the methyl substituents of toluene favoring *ortho*- and *para*-positions over *meta*-positions.[255] Consequently, this approach is not entirely conclusive and will be excluded from further considerations, so that Scenario 3 comes into play.

Scenario 3: Based on the well-documented findings of organic chemistry, it is expected to observe a directing inductive effect of the methyl- and methoxy substituents to *ortho*- and *para*-positions[255]. Hence, another possibility is represented by solely including the two *ortho*-positions by the *z*-value for the example of toluene (i.e. Type 1d) or 2e), Table 5.1). This approach deliberately disregards the non-preferred *meta*-position as possible point of attack. From product studies of other reactions initiated by an electrophilic attack at toluene such as

electrophilic bromination or nitration it is known that the meta-products are found with a low percentage of <1 % or 4 %, respectively.[255] Hence, overall product yields of *meta*-products are generally low but, first, will be present within the resulting products so that *meta*-positions cannot be completely excluded and, second, the product yields may not be defined as constant values but may vary depending on the type of electrophile. This discrepancy illustrates that an additional weighting would be required in eq. 5.1 to represent the individual intramolecular competitive effects inherent e.g. in toluene between the two *ortho*- and *meta*-positions. However, since this weighting is highly compound specific (i.e., unique) it is not possible to include a universal complementary term in eq. 5.1.

Scenario 4: Benzene is the only compound under investigation for which only one possibility of AKIE calculation is given (Table 5.1). Wijker et al. have found for oxidation of toluene and nitrobenzene by permanganate that similar oxidation pathways show distinctive AKIEs (i.e., methyl group oxidation versus deoxygenation of the aromatic ring).[132] Following this interpretation, the AKIEs of the benzene analogs should be similar to the AKIE of benzene if the underlying mechanism is similar. Consequently, solely the AKIEs calculated via Type 1b) (Table 5.1) are in accordance to that approach resulting in a narrow range of AKIE = 1.017 - 1.026. However, as described above this approach would regard *ortho*- and *meta*-positions as equal points of attack and disregard the directing inductive effects of the methyl- or methoxy substituents favoring *ortho*- and *para*-positions over *meta*-positions. Consequently, this explanation from the other side of the problem remains not fully conclusive — similarly to the other approaches discussed above.

As mentioned in the introduction, the quantification of primary reaction products (i.e. muconic or phenolic compounds) is not possible using standard experimental approaches due to their significantly faster reaction rate constants with O_3 with regard to benzene and its analogs. Since an experimental approach for solving this problem appears to be impracticable, the applicability of theoretical options undertaken will be evaluated in the following.

5.4.3 Molecular properties from quantum chemistry

In the first step the molecule structures were optimized within water as a polarizable medium. Hereafter, the electrostatic potential was mapped onto the electron density and is illustrated in Figure S5.10. In these graphic representations, it is possible to draw qualitative conclusions of potential sites more and less favorable for an electrophilic attack of e.g. O_3. Overall it becomes obvious that the different sites of the aromatic ring systems of the benzene analogs are not equal in their electrostatic potential. As a consequence,

Figure S5.10 illustrates the necessity of considering a weighting factor for, e.g. *ortho*- and *meta*-positions in toluene or anisole, if AKIEs shall be determined.

In a second step, a condensed Fukui function (f^-_{carbon}, cf. Text S5.9) was employed to identify potential molecule sites preferred for electrophilic attacks[245,259-261]. The results are presented in Table S5.25. Overall, the data may be classified in two divergent groups. The first group (i.e., toluene, *o*-xylene, *p*-xylene and anisole) shows consistent results, whereas the second group (i.e., benzene, *m*-xylene and mesitylene) displays an ambiguous outcome.

Regarding the first group, the *ipso*-positions are generally favored. However, steric hindrance might prevent significant attack rates at those positions. In case of toluene and anisole the most preferable site for an electrophilic attack is the *para*-position at C_4 (cf. Figure S5.9 for carbon numbering) followed by the two *ortho*-positions (C_2 and C_6), whereas the *meta*-positions (C_3 and C_5) exhibit the lowest f^-_{carbon}. Hence, these two cases agree with the expectations known from classical organic chemistry, that is preference for the positions para > ortho > meta.[255] The unsubstituted positions C_2, C_3, C_5 and C_6 of *p*-xylene are equally attractive for an electrophilic attack. In case of *o*-xylene C_4 and C_5 which combine features of a *meta*- and *para*-position show a much higher reactivity for an electrophilic attack than C_3 and C_6 which are combining features of *meta*- and *ortho*-positions. These examples illustrate that a weighting would be required for AKIE calculation and that e.g. *meta*- and *ortho*-positions of toluene or anisole are not equal in intramolecular competition. However, the weighting for the positions which are subject to intramolecular competition appear to be highly specific for the investigated compound set. To that end a generalized weighting factor within eq. 5.1 for a compound group does not seem reasonable.

A restriction of the considerations made above is imparted by the second group (i.e., benzene, *m*-xylene and mesitylene). Here, results of the Fukui function remain ambiguous and probably even misleading. In case of benzene all six carbon positions in the aromatic ring system are expected to be equal. However, f^-_{carbon} values are significantly higher for C_1 and C_4 than for the other four carbon atoms. A similar and ambiguous observation can be made for mesitylene where the three substituted (C_1, C_3 and C_5) and the three unsubstituted positions (C_2, C_4 and C_6), respectively, would be expected to be equally reactive towards electrophilic attacks. Contrary to this expectation, the f^-_{carbon} values differ substantially (cf. Table S5.25). Last but not least, *m*-xylene shows high f^-_{carbon} values at the positions C_4 and C_6 which comprise features of *ortho*- and *para*-positions. Position C_5 shows very low reactivity for an electrophilic attack as it could be expected for a perfect *meta*-position.

However, the f^-_{carbon} value for position C_2 stands out oddly. It would have been expected to find an increased value for reactivity towards an electrophilic attack since this is a true *ortho*-position. Nevertheless, the f^-_{carbon} value for the position C_2 is even lower than for the true *meta*-position C_5. These identified controversial aspects for the Fukui function of the second group (i.e., benzene, *m*-xylene and mesitylene) indicate that the Fukui function despite its prior use for similar questions might not be the required tool to fully answer the open questions of this research.

Consequently, in a third step, the optimized molecule structures were used for investigation of the reaction pathways of benzene and its analogs with O_3. The general goal of this approach was to determine geometries of the transition states and the products besides the reactants in order to subsequently calculate the according kinetic isotope effects (KIEs) with the ISOEFF package[243]. Herewith, the obtained theoretical KIEs could be compared to the several AKIE options listed in Table 5.1 to draw further conclusions and approach a solution of the problem[127]. However, numerous attempts for identification of a transition state for the reaction of a reactant (singlet state) plus O_3 (singlet state) in a monodentate attack yielding an adduct (i.e., ozonide) (singlet state) proved to be futile, except for benzene and *p*-xylene. Unfortunately, these two compounds do contribute little to the key question of identifying a weighting factor for intramolecular competition. Nevertheless, KIEs were determined with ISOEFF[243] for these two compounds (cf. Table S5.26). Both averaged KIEs reflected an *inverse* isotope effect (< 1) as well as the calculated theoretical isotope enrichment factors (ε^*_C) which were positive. Thus, it may be concluded that these quantum chemical models do not yet match with experimental results and require further optimization in the future.

Surprisingly, it was possible to determine transition states for all compounds of interest for the reaction of reactant (singlet state) plus O_3 (triplet state) yielding an adduct (i.e., ozonide) (triplet state) (data not shown). It was not possible to identify any meaningful reason why O_3 should react in a triplet state so that this topic was not explored further and the question whether O_3 may react as triplet at all has to be considered in future research. Adamczyk & Paneth have successfully modelled the reaction of benzene plus O_3 (both in singlet state) not as monodentate but as bidentate attack and obtained an ε_C value of −7.36 ‰.[262] This theoretical value differs significantly from the experimental value determined in the present study ($\varepsilon_{C\,(benzene+O_3)}$ = −3.9 ± 0.4 ‰). This discrepancy between theoretical and experimental values might indicate that O_3 does not initially attack the aromatic ring in a bidentate but in a monodentate attack as it is currently assumed.[2]

The question why it was not possible to find meaningful transition states for all benzene analogs in the reaction with O_3 in a singlet state remains open. A possible reason might be that O_3 does not initially attack one specific carbon atom of the aromatic ring, eventually, to form a σ-adduct as it is currently assumed in literature.[2,253] It might also be possible, that the preliminary π-complex formed in the first place involves all carbons of the aromatic ring system as it has been proposed for $^{\bullet}OH$[263] and other electrophilic aromatic substitutions[264] earlier. In those studies, the π-complex was made accountable for the observed regioselectivity of e.g. the $^{\bullet}OH$ in reactions with methylated benzene analogs[263] despite its close to diffusion controlled kinetic rate constants (cf. Table S5.1). In the presented case of this study, such a π-complex would allow directing inductive effects of the substituent(s) to determine the final position of the σ-adduct (i.e., the ozonide) as well. However, in such a case the formation of the π-complex might also be the rate determining step of the overall reaction. Thus, no specific aromatic carbon bond would primarily be involved in this crucial reaction step so that the observed isotopic fractionation in this study does not originate from chemical bond breakage formation but from π-complex formation.

5.4.4 Significance

This work provides a first systematic evaluation of the utility of CSIA for assessing oxidative processes by a suite of oxidants (i.e., $^{\bullet}OH$ and O_3). Our data show that oxidation with O_3 and $^{\bullet}OH$ of structural moieties in organic contaminants such as benzene and its methylated and methoxylated analogs can lead to significant carbon isotope fractionation. In contrast, the same structural moieties in organic contaminants did not react with ClO_2, thus, also no changes in $^{13}C/^{12}C$ ratios in our probe compounds were observed. These observations suggest that even though several oxidants contribute to contaminant removal in oxidative processes, CSIA may be used selectively to monitor the degradation of target compounds by ozone and to evaluate the suitability of ozonation for specific water treatment applications. The ε_C values derived here provide some guidance for future studies with regard to the magnitude of an anticipated carbon isotope fractionation for comparable oxidation reactions.

A general mechanistic interpretation of electrophilic attack by O_3, however, is particularly challenging. Even for simple molecules such as the compounds studied here, interpretation of inductive substituent effects in terms of reactive positions for initial attack by ozone did not reveal a simple pattern of reactivity for *ortho*-, *meta*-, and *para*-substituted benzene analogs that can be used to rationalize the observed isotope fractionation in terms of kinetic isotope effects. Further work is warranted to understand isotope effects of ozonation reactions with organic contaminants.

Table 5.1: Possible approaches for calculation of AKIEs (cf. eq. 5.1) for oxidation of substituted benzenes with O_3. Type 1: x = all aromatic *C*-atoms; Type 2: x = all aromatic *C*-atoms except for *ipso*-position; Type 3: x = only favored *C*-atoms; Numbers in brackets represent the applied variables in the order of (n/x/z) (cf. eq. 5.1)

		$AKIE_{exp}$	Type 1		Type 2		Type 3	
Benzene		1.024 ± 0.002	(6/6/6)		—		—	
Toluene	a)	1.034 ± 0.002	(7/6/6)		(7/5/5)		(7/3/3)	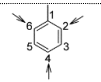
	b)	1.022 ± 0.001	(7/6/4)		—		(7/3/2)	
	c)	1.027 ± 0.001	—		(7/5/4)		—	
	d)	1.011 ± 0.001	(7/6/2)		—		—	
	e)	1.013 ± 0.001	—		(7/5/2)		—	
Anisole	a)	1.039 ± 0.002	(7/6/6)		(7/5/5)		(7/3/3)	
	b)	1.026 ± 0.001	(7/6/4)		—		(7/3/2)	
	c)	1.031 ± 0.002	—		(7/5/4)		—	
	d)	1.013 ± 0.001	(7/6/2)		—		—	
	e)	1.015 ± 0.001	—		(7/5/2)		—	

		$AKIE_{exp}$	Type 1		Type 2		Type 3	
o-Xylene	a)	1.038 ± 0.002	(8/6/6)		(8/4/4)		—	
	b)	1.025 ± 0.001	(8/6/4)		—		—	
	d)	1.012 ± 0.001	(8/6/2)		—		—	
	e)	1.019 ± 0.001	—		(8/4/2)		—	
m-Xylene	a)	1.037 ± 0.001	(8/6/6)	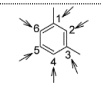	(8/4/4)		(8/3/3)	
	b)	1.025 ± 0.001	(8/6/4)		—		(8/3/2)	
	c)	1.012 ± 0.001	(8/6/2)		—		—	
	d)	1.018 ± 0.001	—		(8/4/2)		—	
p-Xylene	a)	1.036 ± 0.001	(8/6/6)		(8/4/4)		—	
	b)	1.024 ± 0.001	(8/6/4)		—		—	
Mesitylene	a)	1.034 ± 0.001	(9/6/6)		(9/3/3)		—	
	b)	1.017 ± 0.001	(9/6/3)		—		—	

5.5 Supporting information

Text S5.1: Chemicals

All solutions were prepared in ultrapure water (18.1 MΩ·cm, TOC < 10 ppb; ELGA LabWater, Veolia Water Technologies Deutschland GmbH, Celle, Germany).

Following chemicals were used for preparation of the samples: anisole (methoxybenzene; ≥ 99.9 %, Sigma-Aldrich, Steinheim, Germany), benzene (for synthesis, AppliChem, Darmstadt, Germany), carbon dioxide (4.5, Air Liquide, Düsseldorf, Germany), dipotassium hydrogen phosphate (≥ 99 %, p.a., AppliChem), helium (5.0, Air Liquide), hydrogen peroxide (30 %, AppliChem), mesitylene (1,3,5-trimethylbenzene; ≥ 99.8 %, Sigma-Aldrich), methanol (99,99 % HPLC-grade, Fisher Scientific, Loughborough, United Kingdom), *m*-xylene (1,3-dimethylbenzene; ≥ 99 %, Fluka, Steinheim, Germany), nitrogen (5.0, Air Liquide), oxygen (4.8, Air Liquide), *o*-xylene (1,2-dimethylbenzene; ≥ 99 %, Fluka), pH-reference solutions pH 4 (citric acid, sodium hydroxide, sodium chloride) and pH 7 (phosphate mixture) (both Bernd Kraft, Duisburg, Germany), *p*-xylene (1,4-dimethylbenzene; ≥ 99 %, Fluka), sodium chlorite (puriss. p.a. 80 %, Sigma-Aldrich), sodium dihydrogen phosphate (99 %, AppliChem), sodium peroxodisulfate (99 %, Sigma-Aldrich), *tert*-butanol (99.5 %, p.a., AppliChem), toluene (methylbenzene; 99 %, Merck KGaA, Darmstadt, Germany).

Table S5.1: Reaction rate constants of all relevant reactions in oxidation of benzene and its analogs with ozone and OH radicals

Reaction	Second order rate constant k [M^{-1} s^{-1}]	Reference
Benzene + O_3	2.0 ± 0.4	Hoigné and Bader[185]
Benzene + $^{\bullet}OH$	7.8 x 10^9	Buxton et al.[32]
Toluene + O_3	14 ± 3	Hoigné and Bader[185]
Toluene + $^{\bullet}OH$	3.0 x 10^9	Buxton et al.[32]
o-Xylene + O_3	90 ± 20	Hoigné and Bader[185]
o-Xylene + $^{\bullet}OH$	6.7 x 10^9	Buxton et al.[32]
m-Xylene + O_3	94 ± 20	Hoigné and Bader[185]
m-Xylene + $^{\bullet}OH$	7.5 x 10^9	Buxton et al.[32]
p-Xylene + O_3	140 ± 30	Hoigné and Bader[185]
p-Xylene + $^{\bullet}OH$	7.0 x 10^9	Buxton et al.[32]
Mesitylene + O_3	700 ± 200	Hoigné and Bader[185]
Mesitylene + $^{\bullet}OH$	6.4 x 10^9	Buxton et al.[32]
Anisole + O_3	290 ± 50	Hoigné and Bader[185]
Anisole + $^{\bullet}OH$	5.4 x 10^9	Buxton et al.[32]
Phenol + O_3	1.3 x 10^3	Hoigné and Bader[236]
Phenolate + O_3	1.4 x 10^9	Hoigné and Bader[236]
$^{\bullet}OH$ + *tert*-butanol	6 x 10^8	Buxton et al.[32]
$^{\bullet}OH$ + O_3	1.1 ± 0.2 x 10^8	Sehested et al.[183]
$O_3 + HO_2^-$	9.6 ± 2 x 10^6	Sein et al.[24]
$O_3 + H_2O_2$	< 10^{-2}	Staehelin and Hoigné[17]
$O_3 + HO_2^-$ (k_{obs}, pH 9)	1.5 x 10^4	derived from eq. S5.1

$$k_{obs} = k(HO_2^- + O_3) \times 10^{(pH - pKa)} \qquad (S5.1)[24]$$

where: $k(HO_2^- + O_3)$ see Table S5.1, pH = 9, $pK_a(H_2O_2) = 11.8$[265]

Text S5.2: Determination of the minimal necessary scavenger concentrations (adapted from Willach et al.[210]).

The minimal concentrations of the OH radical scavenger *tert*-butanol necessary to scavenge a minimum of 95 % of OH radicals generated were calculated according to Equation S5.2 using the rate constants given in Table S5.1 (exemplarily shown for benzene):

$$c_{\text{tert-butanol(min)}} = \frac{f_{\bullet\text{OH+tert-butanol}} \cdot c_{\text{benzene}} \cdot k_{\bullet\text{OH+}benzene} + f_{\bullet\text{OH+tert-butanol}} \cdot c_{O_3} \cdot k_{\bullet\text{OH+}O_3}}{k_{\bullet\text{OH+tert-butanol}} \cdot \left(1 - f_{\bullet\text{OH+tert-butanol}}\right)} \qquad \text{(S5.2)}$$

Note, since reaction rate constants of the aromatic compounds with ozone are comparably slow a significant amount of ozone will react with the scavenger *tert*-BuOH due to the necessarily high concentrations. These circumstances were acceptable since it was not the aim of this study to determine consumption data of the according reactions in order to achieve oxidation of the aromatic compounds solely by ozone.

Text S5.3: Note for sample composition in Tables S5.2-8

Oxidant and analyte dosage were performed with glass syringes in all cases. The volumes of ozone leading to a suitable degree of transformation of each analyte were determined in pre-experiments. Note that accuracies of added volumes vary due to the accuracies of the syringes applied.

Table S5.2: Volumes used for the preparation of benzene samples treated with ozone in presence of the OH radical scavenger *tert*-butanol. Concentrations of stock solutions were: c (O_3) = 1.2-1.6 mM; c (benzene) = 2.43 mM; c (*tert*-butanol) = 3000 mM; c (phosphate buffer, pH 7) = 100 mM.

V_{O3} [mL]	$V_{\text{stock solution, benzene}}$ [mL]	$V_{\textit{tert}\text{-BuOH}}$ [mL]	$V_{\text{phosphate buffer}}$ [mL]	V_{H2O} [mL]
0	0.100	0.150	0.750	14
1.0	0.100	0.150	0.750	13
3.0	0.100	0.150	0.750	11
5.0	0.100	0.150	0.750	9
7.0	0.100	0.150	0.750	7
9.0	0.100	0.150	0.750	5
11.0	0.100	0.150	0.750	3
13.0	0.100	0.150	0.750	1

Table S5.3: Volumes used for the preparation of toluene samples treated with ozone in presence of the OH radical scavenger *tert*-butanol. Concentrations of stock solutions were: c (O_3) = 1.2-1.6 mM; c (toluene) = 5.15 mM; c (*tert*-butanol) = 3000 mM; c (phosphate buffer, pH 7) = 100 mM.

V_{O3} [mL]	$V_{stock\ solution,\ toluene}$ [mL]	$V_{tert\text{-}BuOH}$ [mL]	$V_{phosphate\ buffer}$ [mL]	V_{H2O} [mL]
0	0.200	0.500	0.750	13.55
1.0	0.200	0.500	0.750	12.55
3.0	0.200	0.500	0.750	10.55
5.0	0.200	0.500	0.750	8.55
7.0	0.200	0.500	0.750	6.55
9.0	0.200	0.500	0.750	4.55
11.0	0.200	0.500	0.750	2.55
13.0	0.200	0.500	0.750	0.55

Table S5.4: Volumes used for the preparation of *o*-xylene samples treated with ozone in presence of the OH radical scavenger *tert*-butanol. Concentrations of stock solutions were: c (O_3) = 1.2-1.6 mM; c (*o*-xylene) = 1.66 mM; c (*tert*-butanol) = 3000 mM; c (phosphate buffer, pH 7) = 100 mM.

V_{O3} [mL]	$V_{stock\ solution,\ o\text{-}xylene}$ [mL]	$V_{tert\text{-}BuOH}$ [mL]	$V_{phosphate\ buffer}$ [mL]	V_{H2O} [mL]
0	1.50	0.300	0.750	12.45
1.0	1.50	0.300	0.750	11.45
2.0	1.50	0.300	0.750	10.45
3.0	1.50	0.300	0.750	9.45
4.0	1.50	0.300	0.750	8.45
5.0	1.50	0.300	0.750	7.45
6.0	1.50	0.300	0.750	6.45
7.0	1.50	0.300	0.750	5.45
8.0	1.50	0.300	0.750	4.45

Table S5.5: Volumes used for the preparation of *m*-xylene samples treated with ozone in presence of the OH radical scavenger *tert*-butanol. Concentrations of stock solutions were: c (O_3) = 1.2-1.6 mM; c (*m*-xylene) = 1.57 mM; c (*tert*-butanol) = 3000 mM; c (phosphate buffer, pH 7) = 100 mM.

V_{O3} [mL]	$V_{stock\ solution,\ m\text{-}xylene}$ [mL]	$V_{tert\text{-}BuOH}$ [mL]	$V_{phosphate\ buffer}$ [mL]	V_{H2O} [mL]
0	0.750	0.300	0.750	13.20
1.0	0.750	0.300	0.750	12.20
2.0	0.750	0.300	0.750	11.20
3.0	0.750	0.300	0.750	10.20
4.0	0.750	0.300	0.750	9.20
5.0	0.750	0.300	0.750	8.20
6.0	0.750	0.300	0.750	7.20
7.0	0.750	0.300	0.750	6.20
8.0	0.750	0.300	0.750	5.20

Table S5.6: Volumes used for the preparation of *p*-xylene samples treated with ozone in presence of the OH radical scavenger *tert*-butanol. Concentrations of stock solutions were: c (O_3) = 1.2-1.6 mM; c (*p*-xylene) = 1.74 mM; c (*tert*-butanol) = 3000 mM; c (phosphate buffer, pH 7) = 100 mM.

V_{O3} [mL]	$V_{stock\ solution,\ p\text{-}xylene}$ [mL]	$V_{tert\text{-}BuOH}$ [mL]	$V_{phosphate\ buffer}$ [mL]	V_{H2O} [mL]
0	1.50	0.250	0.750	12.50
1.0	1.50	0.250	0.750	11.50
2.0	1.50	0.250	0.750	10.50
3.0	1.50	0.250	0.750	9.50
4.0	1.50	0.250	0.750	8.50
5.0	1.50	0.250	0.750	7.50
6.0	1.50	0.250	0.750	6.50
7.0	1.50	0.250	0.750	5.50
8.0	1.50	0.250	0.750	4.50

Table S5.7: Volumes used for the preparation of mesitylene samples treated with ozone in presence of the OH radical scavenger *tert*-butanol. Concentrations of stock solutions were: c (O_3) = 1.2-1.6 mM; c (mesitylene) = 0.455 mM; c (*tert*-butanol) = 3000 mM; c (phosphate buffer, pH 7) = 100 mM.

V_{O3} [mL]	$V_{stock\ solution,\ mesitylene}$ [mL]	$V_{tert\text{-}BuOH}$ [mL]	$V_{phosphate\ buffer}$ [mL]	V_{H2O} [mL]
0	6.00	0.250	0.750	8.00
1.0	6.00	0.250	0.750	7.00
2.0	6.00	0.250	0.750	6.00
3.0	6.00	0.250	0.750	5.00
4.0	6.00	0.250	0.750	4.00
5.0	6.00	0.250	0.750	3.00
6.0	6.00	0.250	0.750	2.00
7.0	6.00	0.250	0.750	1.00
8.0	6.00	0.250	0.750	0.00

Table S5.8: Volumes used for the preparation of anisole samples treated with ozone in presence of the OH radical scavenger *tert*-butanol. Concentrations of stock solutions were: c (O_3) = 1.2-1.6 mM; c (anisole) = 7.41 mM; c (*tert*-butanol) = 3000 mM; c (phosphate buffer, pH 7) = 100 mM.

V_{O3} [mL]	$V_{stock\ solution,\ anisole}$ [mL]	$V_{tert\text{-}BuOH}$ [mL]	$V_{phosphate\ buffer}$ [mL]	V_{H2O} [mL]
0	0.360	0.250	0.750	13.64
1.0	0.360	0.250	0.750	12.64
2.0	0.360	0.250	0.750	11.64
3.0	0.360	0.250	0.750	10.64
4.0	0.360	0.250	0.750	9.64
5.0	0.360	0.250	0.750	8.64
6.0	0.360	0.250	0.750	7.64
7.0	0.360	0.250	0.750	6.64
8.0	0.360	0.250	0.750	5.64

Text S5.4: Determination of the necessary hydrogen peroxide concentrations for the peroxone reactions

The minimal necessary hydrogen peroxide concentration necessary to obtain a fraction of 99.00 % - 99.99 % of hydrogen peroxide reacting with ozone was determined according to Equation S5.3 using the rate constants given in Table S5.1 (exemplarily shown for benzene).

$$c_{H_2O_2} = \frac{f_{O_3+H_2O_2} \cdot k_{O_3+benzene} \cdot c_{benzene}}{k_{O_3+H_2O_2} \cdot \left(1 - f_{O_3+H_2O_2}\right)} \quad \text{(S5.3)}$$

It has to be noted that the hydrogen peroxide concentrations vary depending on the benzene analog to be oxidized. Furthermore, fractions of hydrogen peroxide reacting with ozone could be chosen higher in case of benzene (99.99 %) and toluene (99.90 %) due to the very slow reaction rate constants of the benzene analog itself with ozone (cf. Table S5.1). For all other benzene analogs, fractions were chosen as 99.00 % which can be regarded as completely sufficient for the purpose. The volumes of hydrogen peroxide stock solution used resulting from the calculated hydrogen peroxide concentrations can be found in Table S5.9-15.

Table S5.9: Volumes used for the preparation of benzene samples treated with $OH^{\bullet}$ originating from the peroxone reaction (O_3 + HO_2^-) for $f_{O_3+H_2O_2} = 0.9999$. Concentrations of stock solutions were: c (O_3) = 1.6-1.7 mM; c (benzene) = 2.43 mM; c (H_2O_2) = 10 mM; c (borate buffer, pH 9) = 100 mM.

V_{O3} [mL]	$V_{stock\ solution,\ benzene}$ [mL]	V_{H2O2} [mL]	$V_{borate\ buffer}$ [mL]	V_{H2O} [mL]
0.0	0.620	0.200	0.750	13.43
0.8	0.620	0.200	0.750	12.63
1.2	0.620	0.200	0.750	12.23
1.6	0.620	0.200	0.750	11.83
2.0	0.620	0.200	0.750	11.43
2.4	0.620	0.200	0.750	11.03

Table S5.10: Volumes used for the preparation of toluene samples treated with $OH^{\bullet}$ originating from the peroxone reaction (O_3 + HO_2^-) for $f_{O_3+H_2O_2} = 0.999$. Concentrations of stock solutions were: c (O_3) = 1.6-1.7 mM; c (toluene) = 5.15 mM; c (H_2O_2) = 10 mM; c (borate buffer, pH 9) = 100 mM.

V_{O3} [mL]	$V_{stock\ solution,\ toluene}$ [mL]	V_{H2O2} [mL]	$V_{borate\ buffer}$ [mL]	V_{H2O} [mL]
0.0	0.580	0.285	0.750	13.385
1.0	0.580	0.285	0.750	12.385
2.0	0.580	0.285	0.750	11.385
3.0	0.580	0.285	0.750	10.385
4.0	0.580	0.285	0.750	9.385
5.0	0.580	0.285	0.750	8.385

Table S5.11: Volumes used for the preparation of *o*-xylene samples treated with $OH^{\bullet}$ originating from the peroxone reaction (O_3 + HO_2^-) for $f_{O_3+H_2O_2} = 0.99$. Concentrations of stock solutions were: c (O_3) = 1.6-1.7 mM; c (*o*-xylene) = 1.66 mM; c (H_2O_2) = 10 mM; c (borate buffer, pH 9) = 100 mM.

V_{O3} [mL]	$V_{stock\ solution,\ o\text{-}xylene}$ [mL]	V_{H2O2} [mL]	$V_{borate\ buffer}$ [mL]	V_{H2O} [mL]
0.0	1.90	0.185	0.750	12.165
1.0	1.90	0.185	0.750	11.165
2.0	1.90	0.185	0.750	10.165
3.0	1.90	0.185	0.750	9.165
4.0	1.90	0.185	0.750	8.165
5.0	1.90	0.185	0.750	7.165

Table S5.12: Volumes used for the preparation of *m*-xylene samples treated with $OH^{\bullet}$ originating from the peroxone reaction (O_3 + HO_2^-) for $f_{O_3+H_2O_2} = 0.99$. Concentrations of stock solutions were: c (O_3) = 1.6-1.7 mM; c (*m*-xylene) = 1.57 mM; c (H_2O_2) = 10 mM; c (borate buffer, pH 9) = 100 mM.

V_{O3} [mL]	$V_{stock\ solution,\ m\text{-}xylene}$ [mL]	V_{H2O2} [mL]	$V_{borate\ buffer}$ [mL]	V_{H2O} [mL]
0.0	1.80	0.165	0.750	12.285
1.0	1.80	0.165	0.750	11.285
2.0	1.80	0.165	0.750	10.285
3.0	1.80	0.165	0.750	9.285
4.0	1.80	0.165	0.750	8.285
5.0	1.80	0.165	0.750	7.285

Table S5.13: Volumes used for the preparation of *p*-xylene samples treated with $OH^{\bullet}$ originating from the peroxone reaction ($O_3 + HO_2^-$) for $f_{O_3+H_2O_2} = 0.99$. Concentrations of stock solutions were: c (O_3) = 1.6-1.7 mM; c (*p*-xylene) = 1.74 mM; c (H_2O_2) = 10 mM; c (borate buffer, pH 9) = 100 mM.

V_{O3} [mL]	$V_{stock\ solution,\ p\text{-}xylene}$ [mL]	V_{H2O2} [mL]	$V_{borate\ buffer}$ [mL]	V_{H2O} [mL]
0.0	1.50	0.233	0.750	12.517
1.0	1.50	0.233	0.750	11.517
2.0	1.50	0.233	0.750	10.517
3.0	1.50	0.233	0.750	9.517
4.0	1.50	0.233	0.750	8.517
5.0	1.50	0.233	0.750	7.517

Table S5.14: Volumes used for the preparation of mesitylene samples treated with $OH^{\bullet}$ originating from the peroxone reaction ($O_3 + HO_2^-$) for $f_{O_3+H_2O_2} = 0.99$. Concentrations of stock solutions were: c (O_3) = 1.6-1.7 mM; c (mesitylene) = 0.455 mM; c (H_2O_2) = 10 mM; c (borate buffer, pH 9) = 100 mM.

V_{O3} [mL]	$V_{stock\ solution,\ mesitylene}$ [mL]	V_{H2O2} [mL]	$V_{borate\ buffer}$ [mL]	V_{H2O} [mL]
0.000	2.00	0.410	0.750	11.84
0.240	2.00	0.410	0.750	11.60
0.470	2.00	0.410	0.750	11.37
0.700	2.00	0.410	0.750	11.14
0.950	2.00	0.410	0.750	10.89
1.200	2.00	0.410	0.750	10.64

Table S5.15: Volumes used for the preparation of anisole samples treated with $OH^{\bullet}$ originating from the peroxone reaction ($O_3 + HO_2^-$) for $f_{O_3+H_2O_2} = 0.99$. Concentrations of stock solutions were: c (O_3) = 1.6-1.7 mM; c (anisole) = 7.41 mM; c (H_2O_2) = 10 mM; c (borate buffer, pH 9) = 100 mM.

V_{O3} [mL]	$V_{stock\ solution,\ anisole}$ [mL]	V_{H2O2} [mL]	$V_{borate\ buffer}$ [mL]	V_{H2O} [mL]
0.00	0.510	0.705	0.750	13.035
1.00	0.510	0.705	0.750	12.035
3.00	0.510	0.705	0.750	10.035
5.00	0.510	0.705	0.750	8.035
6.50	0.510	0.705	0.750	6.535
9.00	0.510	0.705	0.750	4.035

Text S5: Generation of the chlorine dioxide stock solution (in reference to Willach et al.[210])

The chlorine dioxide stock solution was prepared in the same manner as described by Willach et al.[210] before. Briefly, 50 mL of a 0.885 M ClO_2 solution were mixed with 50 mL of a 0.164 M $Na_2S_2O_8$ solution. The additional purification steps were performed as described by Gates[1] and illustrated and explained in the Supporting Information of Willach et al.[210]. For spectrophotometrical quantification of the obtained chlorine dioxide stock solution, the absorption of the 1:30-diluted stock solution was determined at 359 nm (ε_{ClO2} = 1200 M^{-1} cm^{-1})[48]. The concentration of the utilized stock solution in this study was 9.63 mM ClO_2.

Text S6: Preparation of samples for oxidation with chlorine dioxide

The preparation and determination of concentrations of the stock solutions of benzene and its analogs were performed in the same way as described in the main manuscript. The initial concentrations were chosen similarly to the ones used for oxidation experiments with ozone (cf. SI Tables S5.2-8). Similarly, the pH was kept constant with a 5 mM phosphate buffer at pH 7. Hypochlorous acid (HOCl) may be formed in reactions of ClO_2 and organic compounds so that it is crucial to use a HOCl scavenger such as glycine. Glycine reacts comparably fast with HOCl ($k_{glycine + HOCl}$ = 1 x 10^5 M^{-1} s^{-1})[266] and significantly slow with ClO_2 ($k_{glycine + ClO2}$ = 1 x 10^{-3} M^{-1} s^{-1})[48]. Glycine concentrations were chosen twice as high as the individual initial analyte concentration (cf. Tables S5.16-21).

Chlorine dioxide and analyte dosage were performed with glass syringes in all cases. Note that accuracies of added volumes vary due to the accuracies of the syringes applied.

Table S5.16: Volumes used for the preparation of benzene samples treated with chlorine dioxide in presence of the HOCl scavenger glycine. Concentrations of stock solutions were: c (ClO_2) = 9.63 mM; c (benzene) = 2.43 mM; c (glycine) = 10 mM; c (phosphate buffer, pH 7) = 100 mM.

V_{ClO2} [mL]	$V_{stock\ solution,\ benzene}$ [mL]	$V_{glycine}$ [mL]	$V_{phosphate\ buffer}$ [mL]	V_{H2O} [mL]
0.000	0.620	0.300	0.750	13.330
0.060	0.620	0.300	0.750	13.270
0.120	0.620	0.300	0.750	13.210
0.170	0.620	0.300	0.750	13.160
0.230	0.620	0.300	0.750	13.100
0.290	0.620	0.300	0.750	13.040
0.340	0.620	0.300	0.750	12.990
0.400	0.620	0.300	0.750	12.930
0.460	0.620	0.300	0.750	12.870

Table S5.17: Volumes used for the preparation of toluene samples treated with chlorine dioxide in presence of the HOCl scavenger glycine. Concentrations of stock solutions were: c (ClO_2) = 9.63 mM; c (toluene) = 5.15 mM; c (glycine) = 10 mM; c (phosphate buffer, pH 7) = 100 mM.

V_{ClO2} [mL]	$V_{stock\ solution,\ toluene}$ [mL]	$V_{glycine}$ [mL]	$V_{phosphate\ buffer}$ [mL]	V_{H2O} [mL]
0.000	0.590	0.600	0.750	13.060
0.030	0.590	0.600	0.750	13.030
0.060	0.590	0.600	0.750	13.000
0.090	0.590	0.600	0.750	12.970
0.120	0.590	0.600	0.750	12.940
0.150	0.590	0.600	0.750	12.910
0.180	0.590	0.600	0.750	12.880
0.210	0.590	0.600	0.750	12.850
0.240	0.590	0.600	0.750	12.820

Table S5.18: Volumes used for the preparation of *o*-xylene samples treated with chlorine dioxide in presence of the HOCl scavenger glycine. Concentrations of stock solutions were: c (ClO_2) = 9.63 mM; c (*o*-xylene) = 1.66 mM; c (glycine) = 10 mM; c (phosphate buffer, pH 7) = 100 mM.

V_{ClO2} [mL]	$V_{stock\ solution,\ o\text{-}xylene}$ [mL]	$V_{glycine}$ [mL]	$V_{phosphate\ buffer}$ [mL]	V_{H2O} [mL]
0.000	1.90	0.630	0.750	11.720
0.025	1.90	0.630	0.750	11.695
0.050	1.90	0.630	0.750	11.670
0.075	1.90	0.630	0.750	11.645
0.100	1.90	0.630	0.750	11.620
0.125	1.90	0.630	0.750	11.595
0.150	1.90	0.630	0.750	11.570
0.175	1.90	0.630	0.750	11.545
0.200	1.90	0.630	0.750	11.520

Table S5.19: Volumes used for the preparation of *m*-xylene samples treated with chlorine dioxide in presence of the HOCl scavenger glycine. Concentrations of stock solutions were: c (ClO_2) = 9.63 mM; c (*m*-xylene) = 1.57 mM; c (glycine) = 10 mM; c (phosphate buffer, pH 7) = 100 mM.

V_{ClO2} [mL]	$V_{stock\ solution,\ m\text{-}xylene}$ [mL]	$V_{glycine}$ [mL]	$V_{phosphate\ buffer}$ [mL]	V_{H2O} [mL]
0.000	1.80	0.540	0.750	11.910
0.020	1.80	0.540	0.750	11.890
0.040	1.80	0.540	0.750	11.870
0.060	1.80	0.540	0.750	11.850
0.080	1.80	0.540	0.750	11.830
0.100	1.80	0.540	0.750	11.810
0.120	1.80	0.540	0.750	11.790
0.140	1.80	0.540	0.750	11.770
0.160	1.80	0.540	0.750	11.750

Table S5.20: Volumes used for the preparation of *p*-xylene samples treated with chlorine dioxide in presence of the HOCl scavenger glycine. Concentrations of stock solutions were: c (ClO_2) = 9.63 mM; c (*p*-xylene) = 1.74 mM; c (glycine) = 10 mM; c (phosphate buffer, pH 7) = 100 mM.

V_{ClO2} [mL]	$V_{stock\ solution,\ p\text{-}xylene}$ [mL]	$V_{glycine}$ [mL]	$V_{phosphate\ buffer}$ [mL]	V_{H2O} [mL]
0.000	1.50	0.510	0.750	12.240
0.100	1.50	0.510	0.750	12.140
0.200	1.50	0.510	0.750	12.040
0.300	1.50	0.510	0.750	11.940
0.400	1.50	0.510	0.750	11.840
0.500	1.50	0.510	0.750	11.740
0.600	1.50	0.510	0.750	11.640
0.700	1.50	0.510	0.750	11.540
0.800	1.50	0.510	0.750	11.440

Table S5.21: Volumes used for the preparation of mesitylene samples treated with chlorine dioxide in presence of the HOCl scavenger glycine. Concentrations of stock solutions were: c (ClO_2) = 9.63 mM; c (mesitylene) = 0.455 mM; c (glycine) = 10 mM; c (phosphate buffer, pH 7) = 100 mM.

V_{ClO2} [mL]	$V_{stock\ solution,\ mesitylene}$ [mL]	$V_{glycine}$ [mL]	$V_{phosphate\ buffer}$ [mL]	V_{H2O} [mL]
0.000	1.80	0.180	0.750	12.270
0.025	1.80	0.180	0.750	12.245
0.050	1.80	0.180	0.750	12.220
0.075	1.80	0.180	0.750	12.195
0.100	1.80	0.180	0.750	12.170
0.125	1.80	0.180	0.750	12.145
0.150	1.80	0.180	0.750	12.120
0.175	1.80	0.180	0.750	12.095
0.200	1.80	0.180	0.750	12.070

Table S5.22: Volumes used for the preparation of anisole samples treated with chlorine dioxide in presence of the HOCl scavenger glycine. Concentrations of stock solutions were: c (ClO_2) = 9.63 mM; c (anisole) = 7.41 mM; c (glycine) = 10 mM; c (phosphate buffer, pH 7) = 100 mM.

V_{ClO2} [mL]	$V_{stock\ solution,\ anisole}$ [mL]	$V_{glycine}$ [mL]	$V_{phosphate\ buffer}$ [mL]	V_{H2O} [mL]
0.000	0.510	0.750	0.750	12.990
0.020	0.510	0.750	0.750	12.970
0.040	0.510	0.750	0.750	12.950
0.060	0.510	0.750	0.750	12.930
0.080	0.510	0.750	0.750	12.910
0.100	0.510	0.750	0.750	12.890
0.120	0.510	0.750	0.750	12.870
0.140	0.510	0.750	0.750	12.850
0.160	0.510	0.750	0.750	12.830

Text S5.7: Quantification of benzene analogs stock solutions with LC-UV/vis

The concentrations of the benzene analogs stock solutions were determined by a HPLC-UV/vis system consisting of LC-20AT, DGU-20A5, CBM-20A, SPD-20A, SIL-20A, CTO-10AS (Shimadzu, Duisburg, Germany). The injection volume was 10 µL for anisole and 50 µL for all other benzene analogs. The analytical column was a Kinetex EVO C18 (100 x 3.0 mm, particle size 2.6 µm) (Phenomenex, Aschaffenburg, Germany) using an isocratic eluent at a flow rate at 0.3 mL min^{-1}. Separation of benzene and toluene were performed with 50:50 methanol:water and for the remaining compounds 40:60 methanol:water was employed. UV-absorption at 260 nm was used for quantification except for the xylenes where 263 nm (*o*-xylene), 264 nm (*m*-xylene) and 267 nm (*p*-xylene) were used. Data processing was performed by LC solutions, version 1.25, SP4 (Shimadzu).

Text S5.8: Isotope-ratio measurements by gas chromatography-isotope-ratio mass spectrometry

Compound-specific stable isotope values of benzene and its analogs were determined by gas chromatography isotope-ratio mass spectrometry (GC-IRMS) using a Trace GC Ultra coupled by the combustion interface Finnigan GC-C/TC III to a Finnigan MAT 253 isotope ratio mass spectrometer (all from Thermo Scientific, Bremen, Germany). The GC system was additionally equipped with a HTX PAL autosampler (CTC Analytics, Zwingen, Switzerland; supplied by Axel Semrau, Sprockhövel, Germany) with an agitator, an Optic 3 injector (ATAS GL-Sciences, Eindhoven, Netherlands; supplied by Axel Semrau). Samples were conditioned in the agitator (mixing time 5 s, pause time 2 s) for 20 min at 70 °C. Hereafter, 500 µL of the headspace were injected with a syringe heated to 73 °C into the injector at 70 °C. Split flow was 20 mL min^{-1} and changed after a transfer time of 60 s to 10 mL min^{-1}. During the transfer time the helium column flow was 2.0 mL min^{-1}. Hereafter, it was switched to 1.6 mL min^{-1} and then lowered within 9 min to 1.3 for anisole, mesitylene and the xylenes and to 1.2 mL min^{-1} for benzene and toluene, respectively. Compounds were separated on a Rxi® 5Sil MS column (60m x 0.25 mm i.d., 0.25 µm film thickness; Restek, Bad Homburg, Germany) using different temperature gradients described below in Table S5.23. After separation, the analytes were oxidized to CO_2 at 940 °C in the combustion interface equipped with Pt, CuO and NiO wires. The wires were reoxidized each time before a new sample set was run. At least every fourth sample run was a reference sample without oxidant addition for normalization. Linearity and precision test were run regularly. The carbon isotope values are given in reference to the international Vienna Pee Dee Belemnite (VPDB) scale.[120] For ion

source stability, at least two to three reference gas pulses were included in each chromatographic run. The peak areas used for the ratio of concentration to initial concentration (c/c_0) originate from the $^{12}CO_2$ peak (*m/z* 44).

Table S5.23: Temperature gradients utilized for gas chromatographic separation of the benzene analogs benzene, toluene, *o*-, *m*-, *p*-xylene, mesitylene and anisole

Compound	Starting Temperature [°C]	Ramp 1 [°C min^{-1}]	Plateau 1 [°C]	Ramp 2 [°C min^{-1}]	Plateau 2 [°C]
Benzene/Toluene	40 (0 min)	20	110 (2 min)	20	180 (1 min)
Anisole	40 (1 min)	20	220		
Others	60 (0.5 min)	15	200		

Text S5.9: Application of the condensed Fukui function

The quantitative reactivity to atomic level was derived by a condensed Fukui function according to Equation S5.4[245,259,261]:

$$f^-_{atom} = q_{atom}(N) - q_{atom}(N-1) \quad \text{(S5.4)}$$

where f^-_{atom} is the condensed Fukui function for electrophilic attack, q_{atom} is the gross Mulliken charge at the respective atom and N is the total number of electrons in the system

The higher f^-_{atom} is the more likely is an electrophilic attack at the respective atom.

Consequently, the maximum value indicates highest reactivity to an electrophilic attack whereas the minimum indicates low reactivity.

The utilized Fukui function calculation program is publicly available under GPL 3.0 License.[244] The software implementation corresponds to the description in Contreras et al..[245]

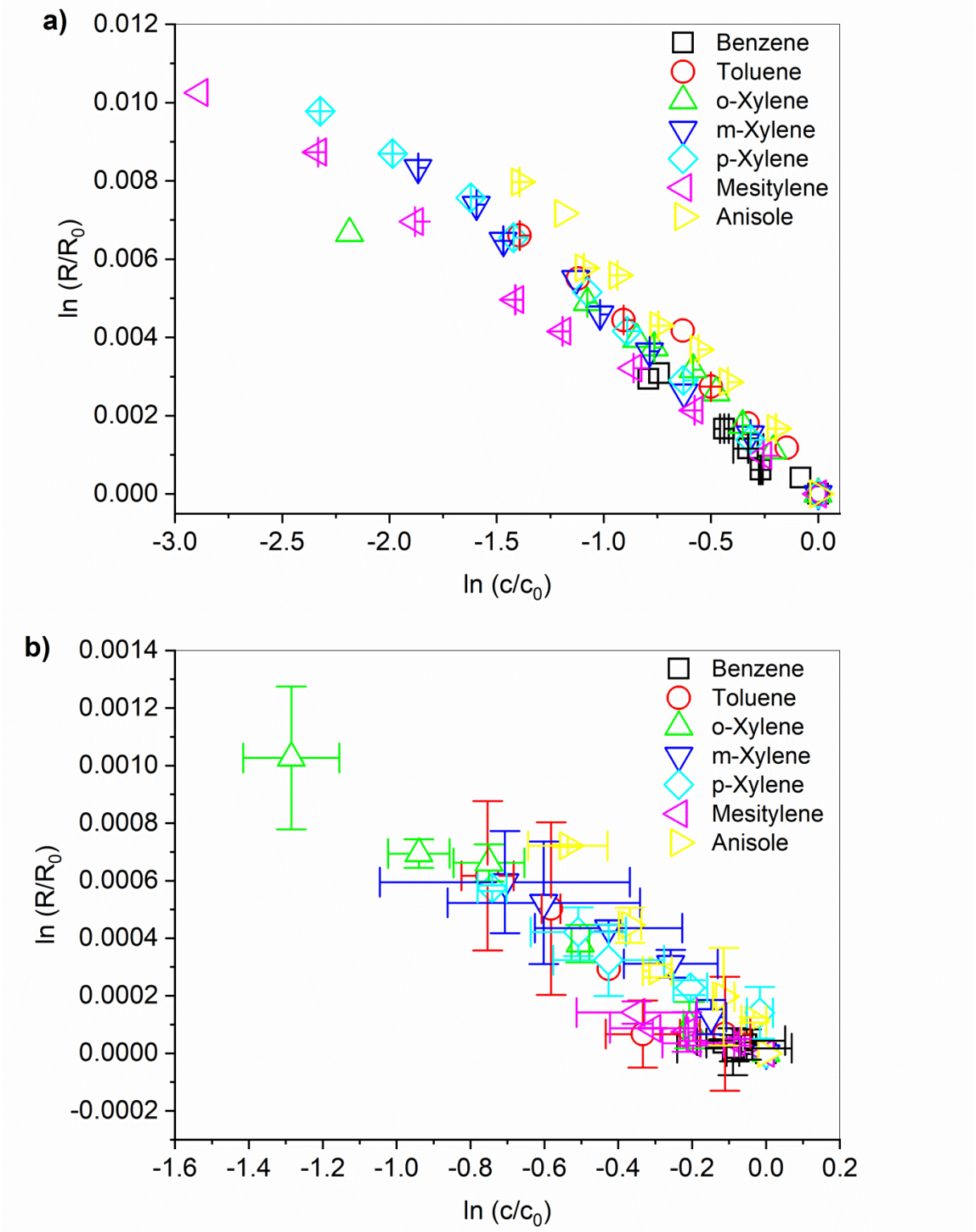

Figure S5.1: Rayleigh-plots of oxidation of benzene and its analogs with a) ozone in presence of an adequate *tert*-BuOH concentration depending on the individual rate constants (cf. sample preparation described in main manuscript and Tables S5.2-8) at pH 7 (5 mM phosphate buffer) as $^{\bullet}$OH scavenger and b) $^{\bullet}$OH generated by the peroxone process (cf. sample preparation described in main manuscript and Tables S5.9-15) at pH 9 (5 mM borate buffer) (symbols in both figures show squares: benzene, circles: toluene, triangle upward: o-xylene, triangle downward: m-xylene, diamond: p-xylene, triangle leftward: mesitylene, triangle rightward: anisole); error bars represent standard deviations of experimental duplicates.

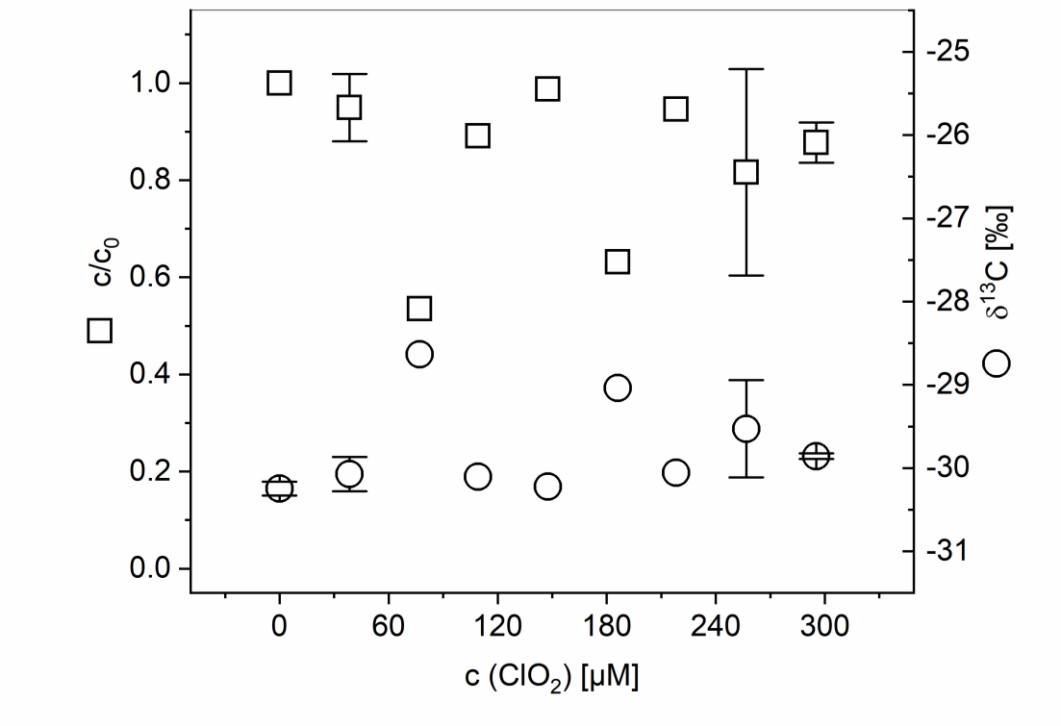

Figure S5.2: Oxidation of benzene (c_0 = 100 µM) with chlorine dioxide in presence of glycine (c = 200 µM) as HOCl scavenger (squares: ratio of benzene concentration after oxidation at given ClO_2 dosage to initial benzene concentration; circles: isotope ratio $^{13}Cl^{12}C$ after respective oxidation). The system was buffered with 5 mM phosphate buffer at pH 7. Error bars represent standard deviations of experimental duplicates.

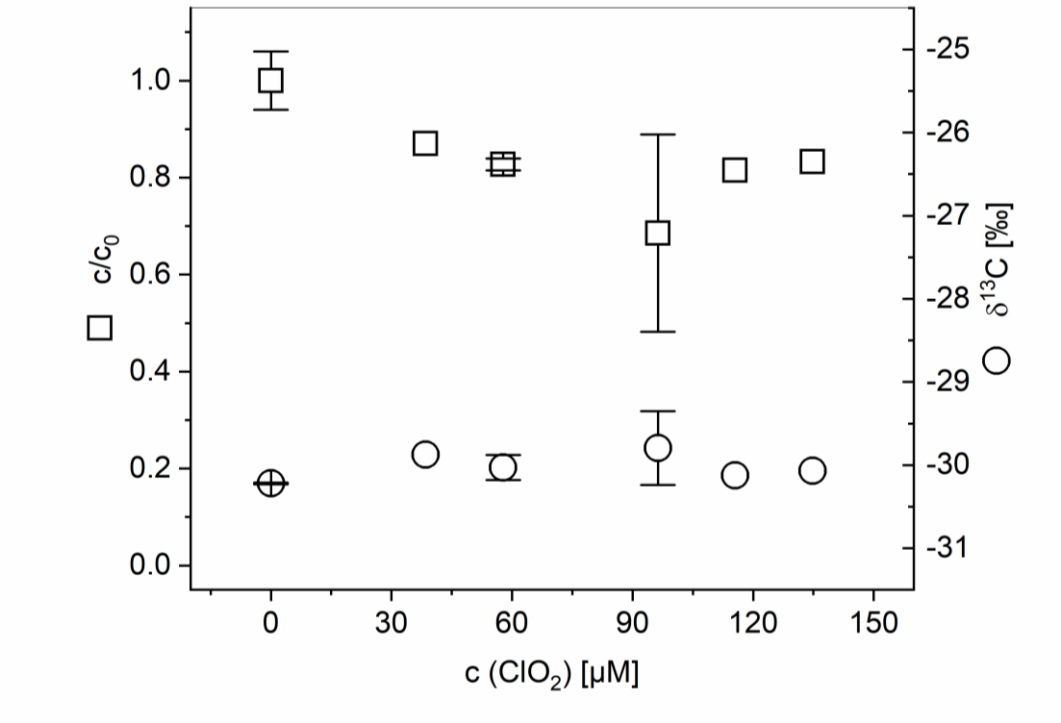

Figure S5.3: Oxidation of toluene (c_0 = 200 µM) with chlorine dioxide in presence of glycine (c = 400 µM) as HOCl scavenger (squares: ratio of toluene concentration after oxidation at given ClO_2 dosage to initial toluene concentration; circles: isotope ratio $^{13}Cl^{12}C$ after respective oxidation). The system was buffered with 5 mM phosphate buffer at pH 7. Error bars represent standard deviations of experimental duplicates.

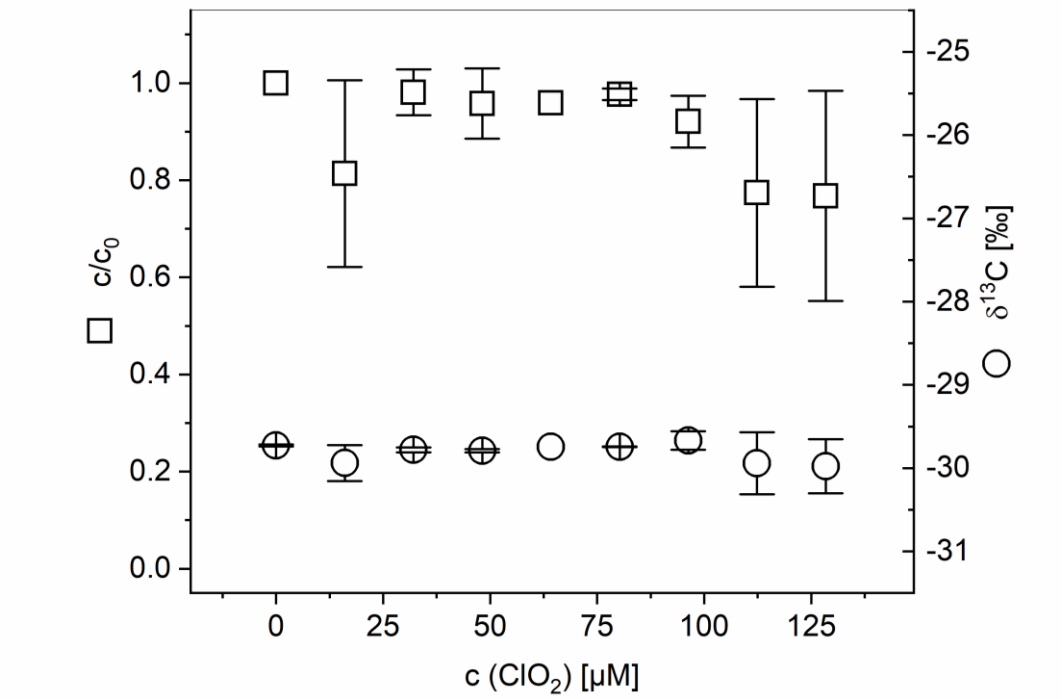

Figure S5.4: Oxidation of *o*-xylene (c_0 = 210 µM) with chlorine dioxide in presence of glycine (c = 420 µM) as HOCl scavenger (squares: ratio of *o*-xylene concentration after oxidation at given ClO_2 dosage to initial *o*-xylene concentration; circles: isotope ratio $^{13}C/^{12}C$ after respective oxidation). The system was buffered with 5 mM phosphate buffer at pH 7. Error bars represent standard deviations of experimental duplicates.

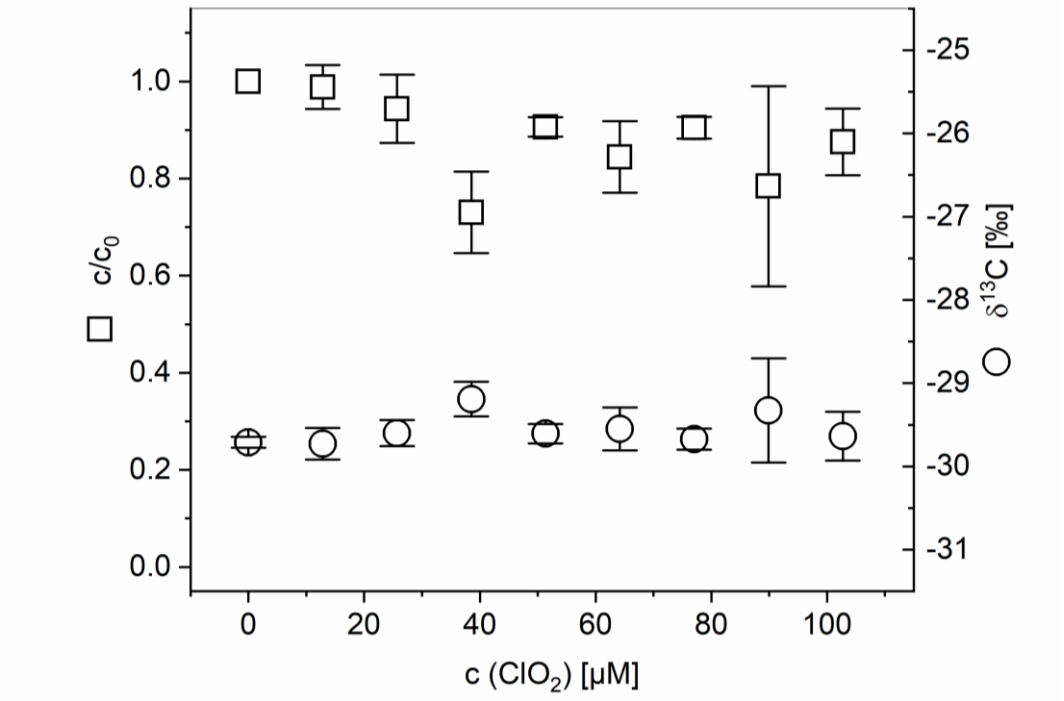

Figure S5.5: Oxidation of *m*-xylene (c_0 = 180 µM) with chlorine dioxide in presence of glycine (c = 360 µM) as HOCl scavenger (squares: ratio of *m*-xylene concentration after oxidation at given ClO_2 dosage to initial *m*-xylene concentration; circles: isotope ratio $^{13}C/^{12}C$ after respective oxidation). The system was buffered with 5 mM phosphate buffer at pH 7. Error bars represent standard deviations of experimental duplicates.

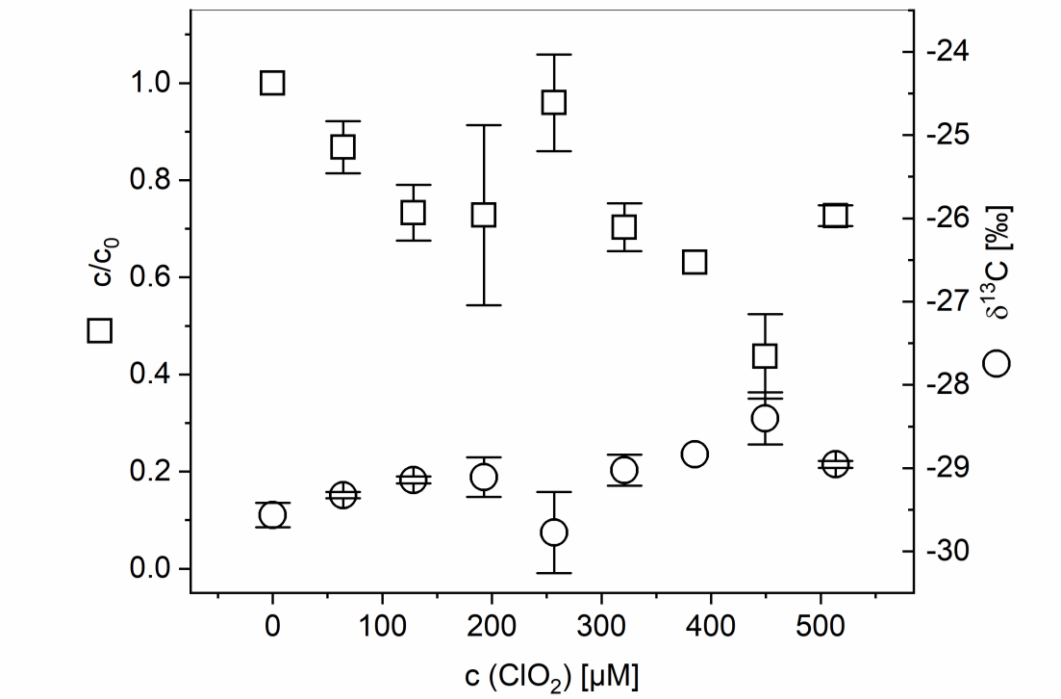

Figure S5.6: Oxidation of *p*-xylene (c_0 = 170 µM) with chlorine dioxide in presence of glycine (c = 340 µM) as HOCl scavenger (squares: ratio of *p*-xylene concentration after oxidation at given ClO_2 dosage to initial *p*-xylene concentration; circles: isotope ratio $^{13}C/^{12}C$ after respective oxidation). The system was buffered with 5 mM phosphate buffer at pH 7. Error bars represent standard deviations of experimental duplicates.

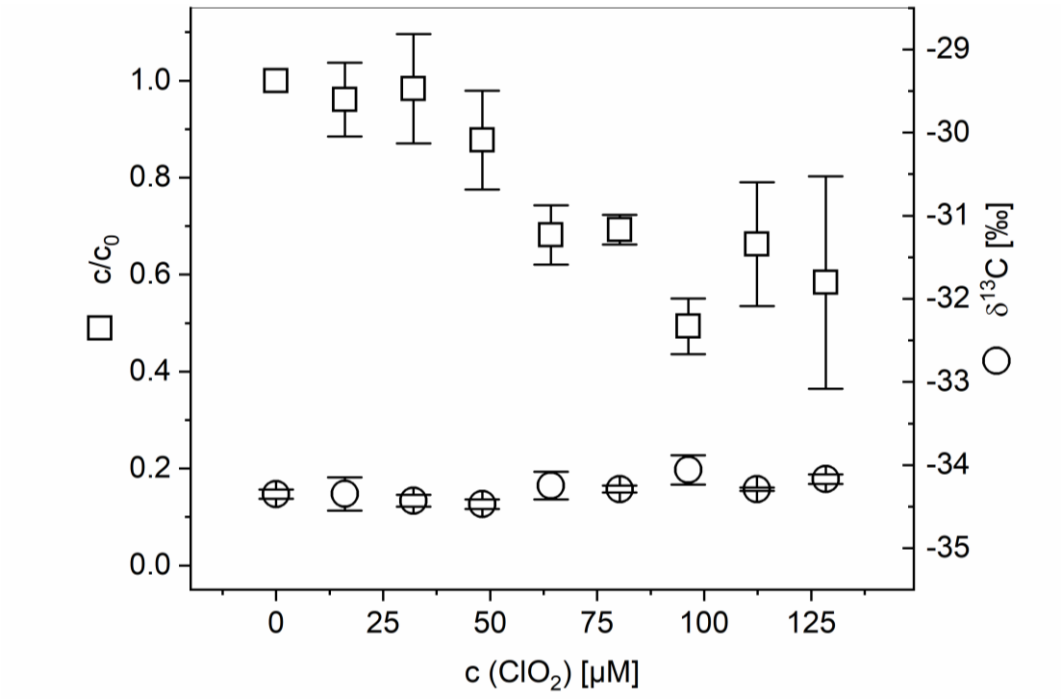

Figure S5.7: Oxidation of mesitylene (c_0 = 60 µM) with chlorine dioxide in presence of glycine (c = 120 µM) as HOCl scavenger (squares: ratio of mesitylene concentration after oxidation at given ClO_2 dosage to initial mesitylene concentration; circles: isotope ratio $^{13}C/^{12}C$ after respective oxidation). The system was buffered with 5 mM phosphate buffer at pH 7. Error bars represent standard deviations of experimental duplicates.

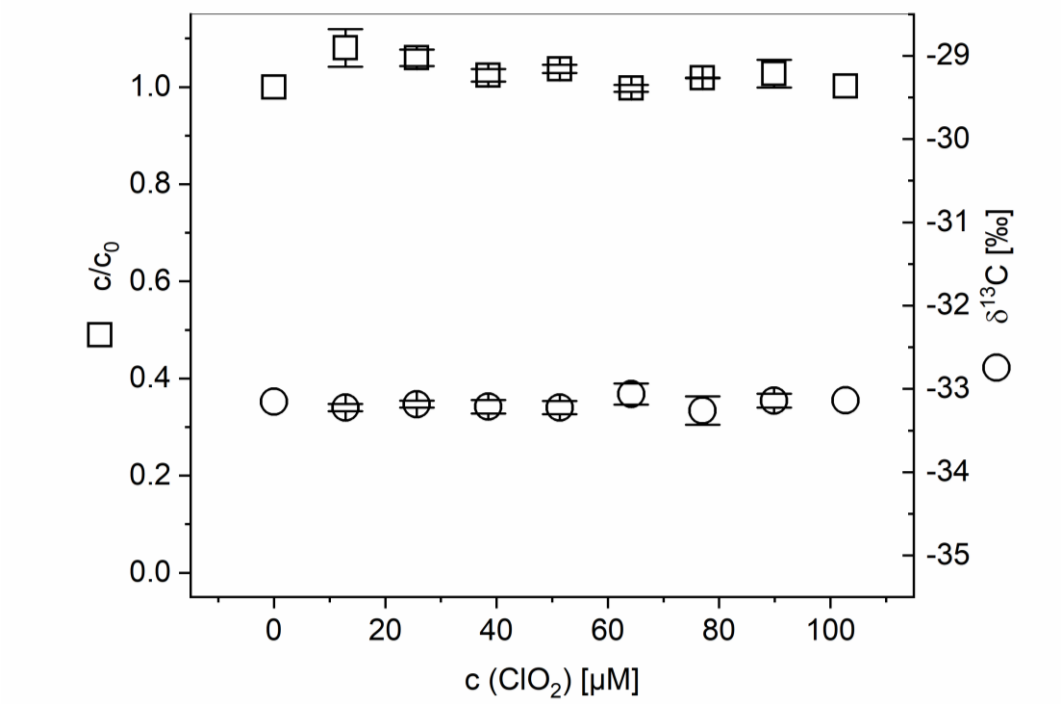

Figure S5.8: Oxidation of anisole (c_0 = 250 µM) with chlorine dioxide in presence of glycine (c = 500 µM) as HOCl scavenger (squares: ratio of anisole concentration after oxidation at given ClO_2 dosage to initial anisole concentration; circles: isotope ratio $^{13}Cl^{12}C$ after respective oxidation). The system was buffered with 5 mM phosphate buffer at pH 7. Error bars represent standard deviations of experimental duplicates.

Table S5.24: Stable isotope enrichment factors (ε_C) for oxidation of benzene and its analogs with either ozone or $^{\bullet}OH$ (generated by the peroxone process); comparison of oxidation of benzene and its analogs by $^{\bullet}OH$ (generated by UV/H_2O_2) published by Zhang et al.[234]

Compound	O_3 [a,b]	$^{\bullet}OH$ [c]	$^{\bullet}OH$ (Zhang et al.) [d]
	ε_C [‰]	ε_C [‰]	ε_C [‰]
Benzene	−3.9 ± 0.4	0.0 ± 0.2	−0.7 ± 0.1
Toluene	−4.6 ± 0.2	−0.9 ± 0.2	−0.36 ± 0.05
o-Xylene	−4.6 ± 0.2	−0.8 ± 0.1	−0.27 ± 0.02
m-Xylene	−4.5 ± 0.1	−0.8 ± 0.1	−0.30 ± 0.06
p-Xylene	−4.3 ± 0.1	−0.7 ± 0.1	−0.31 ± 0.05
Mesitylene	−3.7 ± 0.1	−0.3 ± 0.1	-
Anisole	−5.4 ± 0.3	−1.2 ± 0.1	−0.45 ± 0.04

[a] pH was kept constant for ozone reactions at pH 7 with a phosphate buffer (5 mM)
[b] Intrinsically formed $^{\bullet}OH$ from reaction of ozone and one of the compounds were scavenged by an adequate concentration of *tert*-butanol which was chosen depending of the according reaction rate constants (cf. sample preparation described in main manuscript and Tables S5.2-8)
[c] pH was kept constant for $^{\bullet}OH$ reactions at pH 9 with a borate buffer (5 mM)
[d] values are adapted from Zhang et al. (2016)[234]

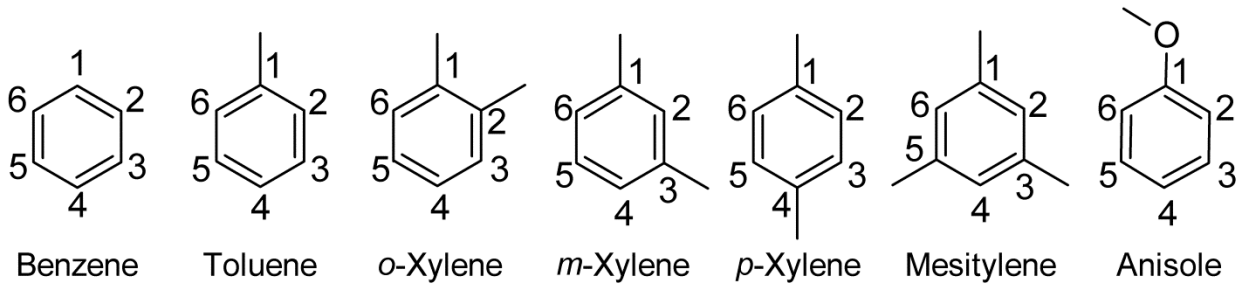

Figure S5.9: Numbering of the aromatic rings of the investigated benzene and its substituted analogs.

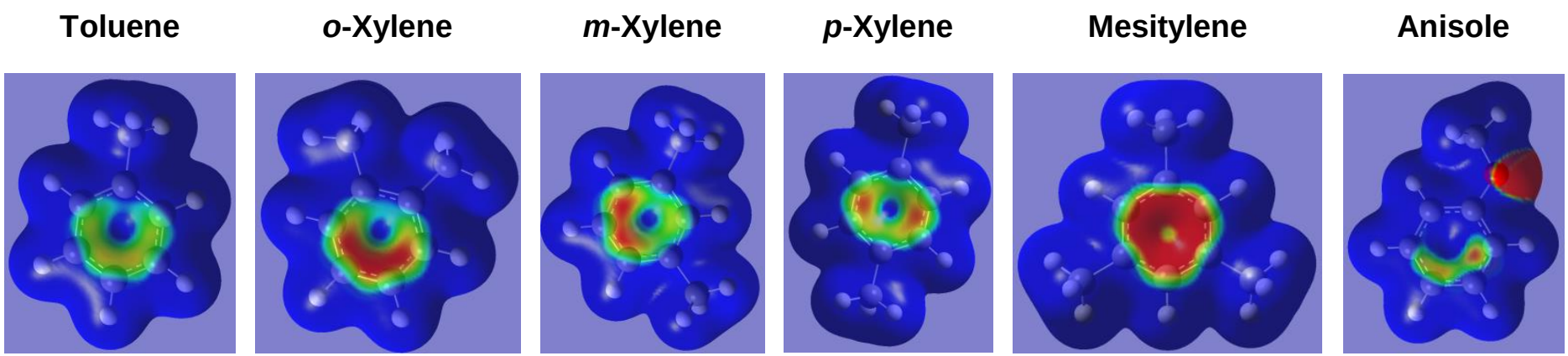

Figure S5.10: Optimized molecule structures of the methylated and methoxylated benzene analogs considered in this study within water as a polarizable medium. The electrostatic potential was mapped onto the electron density of each molecule. The color code was chosen from -3.0×10^{-2} (red) to -2.0×10^{-2} (blue). All molecule parts which appear in dark blue have an electrostatic potential more positive than -2.0×10^{-2}.

Table S5.25: Table of condensed to atom Fukui functions (f^-_{carbon} calculated according to eq. S5.2). Green labelled table fields indicate positions with methyl and methoxy substituents, respectively.

	Position	f^-_{carbon}						
		Benzene	Toluene	*o*-Xylene	*m*-Xylene	*p*-Xylene	Mesitylene	Anisole
Aromatic ring	C_1	0.3252	0.2842	0.2333	0.2068	0.2719	0.2038	0.1707
	C_2	0.0867	0.1034	0.2333	0.0064	0.0845	0.0085	0.1415
	C_3	0.0867	0.0687	0.0101	0.1827	0.0845	0.1872	0.0260
	C_4	0.3252	0.3009	0.2071	0.2622	0.2719	0.2772	0.2503
	C_5	0.0867	0.0687	0.2071	0.0086	0.0845	0.0083	0.0624
	C_6	0.0867	0.1034	0.0101	0.2442	0.0845	0.2281	0.1125
	Sum (aromatic carbon atoms only)	**0.9972**	**0.9293**	**0.9010**	**0.9109**	**0.8818**	**0.9131**	**0.7634**
Substituents	Methyl or Methoxy at C_1		0.0237	0.0158	0.0147	0.0190	0.0162	0.0099
	Methyl at C_2, C_3 or C_4			0.0158	0.0149	0.0190	0.0112	
	Methyl at C_5						0.0006	

Table S5.26: Theoretical evaluation of resulting C-KIEs for oxidation of benzene and *p*-Xylene with O_3. Quantum chemical calculations were conducted as described in the main manuscript. KIE values were derived with the ISOEFF package[243]. The ε^*_C-values (theoretical isotope enrichment factors) were calculated with eq. S5.3. Atom numbering is referring to Figure S5.11.

Position of ^{13}C in aromatic ring	Benzene	*p*-Xylene
	O_3 attack at C_1	O_3 attack at C_2
C_1	1.0299	0.9929
C_2	0.9952	1.0266
C_3	0.9874	0.9959
C_4	0.9790	0.9887
C_5	0.9869	0.9775
C_6	0.9931	0.9846
C_{m1} at C_1	-	0.9987
C_{m2} at C_4	-	0.9998
Average KIE	0.9953	0.9956
ε^*_C (cf. eq. S5.3)	+4.77	+4.43

$$\varepsilon^*_C = \left(\frac{1}{\mathrm{KIE}} - 1\right) \times 1000 \qquad \text{eq. S5.3}$$

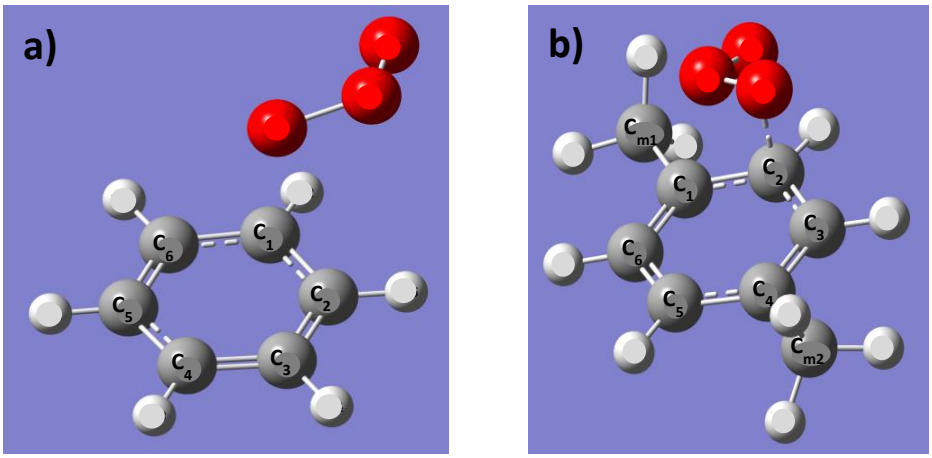

Figure S5.11: Atom numbering for carbon isotopomers for a) benzene and b) *p*-xylene used in Table S5.26.

Chapter 6 -
General conclusion & Outlook

Chapter 6 -
General conclusion & Outlook

In this thesis, the applicability of compound-specific stable isotope analysis (CSIA) for characterization of abiotic oxidative and phototransformation processes as well as elucidation of the underlying reaction mechanisms - also complementary to high-resolution mass spectrometry (HRMS) - was investigated.

Experimental setups in **Chapter 3** and **Chapter 4** have shown that different transformation processes, i.e. ozonation, treatment with chlorine dioxide (ClO_2), photolysis with different irradiation sources such as low pressure Hg lamp or simulated sunlight, cause mostly similar transformation products (TPs) which cannot be differentiated by HRMS alone. In the presented work it was possible to identify distinct isotopic fractionation patterns for the transformation processes listed above. Consequently, CSIA can be a supplementary tool to HRMS in such cases. For this reason, it seems possible that CSIA might be implemented for monitoring tasks in the future. This may be used for example to track the advances of environmental remediation versus plain dilution effects or to differentiate natural attenuation through phototransformation by sunlight from simple dilution of emitters such as waste water treatment plants or diffuse sources from agricultural activities. Maier et al. have performed comparable investigations for Diclofenac so that the suitability for a broader range of micropollutants besides sulfamethoxazole (SMX) appears to be likely[154]. Nevertheless, the broad applicability for various micropollutants still needs to be proven with a larger scope of analytes in combination with the improvement of sensitivity[211]. The recent method developments using solid-phase extraction, preparative HPLC or molecular imprinted polymers are the first steps towards this promising field of application[141,142,147,148].

The elucidation of reaction mechanisms by combining the results obtained from HRMS measurements of TPs with CSIA is an exceedingly challenging task. A shining example is the *N*-nitrosodimethylamine formation during the chloramination of secondary and/or tertiary amines[152,153]. However, an additional value to the HRMS data for the elucidation of reaction mechanisms by CSIA could only be established for the transformation of SMX with the investigated oxidative (**Chapter 3**) but not for the phototransformation processes (**Chapter 4**). The basis which enabled this further understanding of the reaction mechanisms was a systematic experimental set-up which investigated the two environmentally relevant species of SMX, the neutral and the anionic one, respectively, separately from each other (**Chapter 3**). This approach led to distinct results which may be used in future modeling or for creation of a data base containing typical isotope fractionation data of oxidative processes. Experimental data generated in a parallel approach by Birkigt et al., considered pH regimes where both SMX species are present to different extents[172]. Thus, these results may deliver answers for the very exact conditions chosen but do not enable any further generalized insights.

Contrary to this, the systematic experimental approach in **Chapter 4**, implementing the differentiation of the SMX species with distinct UV/vis-irradiation scenarios for the phototransformation of SMX, was not sufficient to enable further insight in the reaction mechanisms to HRMS data by CSIA. However, it was possible to discern several further levers which have to be considered in future studies with CSIA in order to extend the fundamental knowledge of phototransformation reactions. It became obvious that further studies are required which systematically investigate and quantify the individual influence of parameters such as the pH, the concentration, the position of a substituent and the excited states, i.e. singlet and triplet states as it has been performed for chloroanilines[157,158]. Additional information on the kind of excited states could also answer the question if a difference in excited states is responsible for the observed isotopic fractionation in phototransformation with UV-B and UV-A light but not in case of UV-C light. Moreover, further research on pH related phenomena are required to understand if a potential pK_a shift occurs by transition from ground to excited state in case of SMX. Consequently, in case of phototransformation studies a wider pH range using equidistant steps should be investigated as it has been shown for other compounds that acidity constants frequently shift by several orders of magnitude for excited states[267-271].

The work in **Chapter 4** has also illustrated that an in-depth investigation on the discrimination of mass-dependent isotope effects (MDE) and mass-independent isotope effects (MIE) using CSIA is needed to diminish the current uncertainties. An enhanced understanding of MDE and MIE would enable the distinction of, e.g., kinetic and magnetic isotope effects, respectively. Besides phototransformation, which was identified as an interesting field for such investigations inter alia in this work and by Ratti et al.[157,158], oxidative processes employing the free-radical monomer ClO_2[49] would be of relevance as well. Magnetic MIEs usually occur in radical reactions which are energy-cheap[125]. Based on this, CSIA may be a helpful tool in further investigations of the radical character of ClO_2 reactions.

Overall, it became apparent during the work of **Chapters 3** and **Chapter 4** that the current investigations on oxidative processes have considered overly complex probe compounds such as diclofenac[154] or SMX[172,210]. The current approaches usually limit the obtained conclusions to the specific compound under investigation. In order to derive more generalized information on the reactions of pollutants with oxidative agents such as O_3, hydroxyl radicals ($^{\bullet}OH$) or ClO_2, “simpler” probe compounds have to be considered as the initial step in a more holistic approach. The complexity of diclofenac or SMX in this context does not only originate from the molecule size itself but also from the presence of different atoms besides hydrogen or carbon such as oxygen, nitrogen or sulfur. These may strongly

influence the point of attack of the oxidative agent as it was demonstrated for ozonation of anilines or N-heterocyclic aromatic compounds[25,272].

Therefore, it was required to step back in the level of compound complexity in order to enable a basic understanding of stable isotope fractionation in oxidative processes. In **Chapter 5**, benzene and its methylated and methoxylated analogs were used as simple aromatic probe compounds to characterize the reactions of O_3, $^{\bullet}OH$ or ClO_2 and derive the related apparent kinetic isotope effects (AKIE). Here it was shown that pure O_3 and $^{\bullet}OH$ reactions may be distinguished from each other based on the isotope enrichment factors which may be used in environmental monitoring measures or process evaluations in the future.

However, the reaction rate constants of ClO_2 with benzene and its analogs were too slow ($k_{ClO_2+reactant} \leq 10^1$ $M^{-1} s^{-1}$; estimated according to Lee and von Gunten[248]) so that no significant and reasonable degradation of probe compounds could be observed. Hence, it is recommended to conduct such orienting oxidation experiments with ClO_2 with a set of reactants with $k_{ClO_2+reactant} > 10^1$ $M^{-1} s^{-1}$. Possible reactants could be di- and trimethoxylated benzenes or phenols and its analogs in an appropriate pH range which exhibit sufficiently fast reaction rate constants with ClO_2[248]. These additional compound classes were beyond the scope of this study so that these experiments will be part of future investigations.

The calculation of AKIEs for the oxidation of benzene and its analogs with ozone turned out to be nontrivial. Moreover, up to now no precedents which considered monodentate oxidative attacks can be found in the current literature. These would have required considering the influence of the number of atoms in reactive position versus the number of atoms in intramolecular competition as it was necessary in this work. In complementary approaches quantum chemical calculations were performed in order to identify the most likely solution. Unexpectedly, these additional tools did not lead to a clarification but disclosed even more unresolved questions which had also caused discrepancies between experimental and theoretical data in other studies[234,260,273].

In general, theoretical calculations may be a useful tool to obtain additional insights and open new perspectives[132,274]. However, quantum chemical calculations have to be carried out very thoughtfully due to a high number of pitfalls - especially if a treacherous molecule such as ozone shall be investigated[275,276]. This is the reason why quantum chemical calculations require a significant amount of time and often reiterations until one receives the desired information. Additionally, reliable and affordable software for modeling of all included reactants and their reactions is not yet adequate in order to perform appropriate quantum

chemical calculations[274]. The example of **Chapter 5** has illustrated that substantial manpower and experience is required to perform high-level quantum chemical calculations which needs to be considered carefully prior to such a project plan.

Moreover, ozonation of the allegedly simple probe compounds, i.e. benzene and its analogs, and the related reaction pathways proved to be more challenging than expected in the first place. It became obvious that the chemistry of these reactions is not well understood (**Chapter 5**) so that it would be advisable for future studies on oxidative processes to focus on very basic structures as probe compounds before considering more complex molecular structures of pesticides or active ingredients of pharmaceuticals. A current review of available isotopic data for the transformation of benzene and its analogs has demonstrated that the availability of data for abiotic oxidative processes is still poor[229].

Besides further systematic evaluation of isotopic fractionation of oxidative processes using representative and allegedly simple probe compounds containing solely hydrogen and carbon atoms, future studies should also systematically evaluate the influences of other elements such as oxygen or nitrogen in order to complete the picture and create a solid database which comprises basic structures and different (abiotic) oxidative agents. As soon as already developed methods from laboratory tests and applications in liquid chromatography-IRMS (LC-IRMS)[138,277] can be brought to market maturity and become commercially available this might also become possible for polar and non-volatile compounds which cannot be transferred to the gas phase.

Such a database containing data on isotope fractionation for the reactions of various oxidative agents with basic probe compounds could be the starting point to answer one of the key questions raised during the presented work: Are the isotope fractionation data of simple probe compounds transferable to more complex molecule structures, e.g. containing an aromatic moiety as the point of oxidant attack? If the answer to this question is positive, this would open the door widely for CSIA applications in future environmental and process oriented studies.

In conclusion, on many different levels the presented work has shown that the deeper and more detailed one delves into a subject the easier it becomes to find more unresolved questions and problems than to find the answers for the initial ones.

Chapter 7 -

References

Chapter 7 - References

1. Gates, D., The chlorine dioxide handbook. **1998**, American Water Works Association, Denver, CO, USA
2. von Sonntag, C., von Gunten, U., Chemistry of ozone in water and wastewater treatment. **2012**, IWA Publishing, London, UK
3. Knocke, W.R., Van Benschoten, J.E., Kearney, M.J., Soborski, A.W., Reckhow, D.A., Kinetics of manganese and iron oxidation by potassium permanganate and chlorine dioxide. *J Am Water Works Ass,* **1991**, 83 (6), 80-87
4. Wenk, J., Aeschbacher, M., Salhi, E., Canonica, S., von Gunten, U., Sander, M., Chemical oxidation of dissolved organic matter by chlorine dioxide, chlorine, and ozone: effects on its optical and antioxidant properties. *Environ Sci Technol,* **2013**, 47 (19), 11147-56
5. McKenzie, K.S., Sarr, A.B., Mayura, K., Bailey, R.H., Miller, D.R., Rogers, T.D., Norred, W.P., Voss, K.A., Plattner, R.D., Kubena, L.F., Phillips, T.D., Oxidative degradation and detoxification of mycotoxins using a novel source of ozone. *Food Chem Toxicol,* **1997**, 35 (8), 807-820
6. Eliasson, B., Hirth, M., Kogelschatz, U., Ozone synthesis from oxygen in dielectric barrier discharges. *J Phys D Appl Phys,* **1987**, 20 (11), 1421
7. Okazaki, S., Sugimitsu, H., Niwa, H., Kogoma, M., Moriwaki, T., Inomata, T., Ozone formation from the reaction of O2-activated N2 molecules and a new type of ozone generator with fine wire electrode. *Ozone-Sci Eng,* **1988**, 10 (2), 137-151
8. Lawrence, J., Cappelli, F.P., Ozone in drinking water treatment: A review. *Sci Total Environ,* **1977**, 7 (2), 99-108
9. Le Paulouë, J., Langlais, B., State-of-the-art of ozonation in France. *Ozone-Sci Eng,* **1999**, 21 (2), 153-162
10. Böhme, A., Ozone technology of German industrial enterprises. *Ozone-Sci Eng,* **1999**, 21 (2), 163-176
11. von Gunten, U., Ozonation of drinking water: Part I. Oxidation kinetics and product formation. *Water Res,* **2003**, 37 (7), 1443-1467
12. Merényi, G., Lind, J., Naumov, S., von Sonntag, C., The reaction of ozone with the hydroxide ion: mechanistic considerations based on thermokinetic and quantum chemical calculations and the role of HO4− in superoxide dismutation. *Chem-Eur J,* **2010**, 16 (4), 1372-1377
13. Bielski, B.H.J., Cabelli, D.E., Arudi, R.L., Ross, A.B., Reactivity of HO2/O−2 radicals in aqueous solution. *J. Phys. Chem. Ref. Data,* **1985**, 14 (4), 1041-1100
14. Sehested, K., Holcman, J., Hart, E.J., Rate constants and products of the reactions of e-aq, dioxide(1-) (O2-) and proton with ozone in aqueous solutions. *J Phys Chem-Us,* **1983**, 87 (11), 1951-1954
15. Elliot, A.J., McCracken, D.R., Effect of temperature on $O^{\bullet-}$ reactions and equilibria: A pulse radiolysis study. *Radiat Phys Chem,* **1989**, 33 (1), 69-74
16. Merényi, G., Lind, J., Naumov, S., von Sonntag, C., Reaction of ozone with hydrogen peroxide (peroxone process): A revision of current mechanistic concepts based on thermokinetic and quantum-chemical considerations. *Environ Sci Technol,* **2010**, 44 (9), 3505-3507
17. Staehelin, J., Hoigné, J., Decomposition of ozone in water: Rate of initiation by hydroxide ions and hydrogen peroxide. *Environ Sci Technol,* **1982**, 16 (10), 676-681
18. Lee, Y., Gerrity, D., Lee, M., Bogeat, A.E., Salhi, E., Gamage, S., Trenholm, R.A., Wert, E.C., Snyder, S.A., von Gunten, U., Prediction of micropollutant elimination during ozonation of municipal wastewater effluents: use of kinetic and water specific information. *Environ Sci Technol,* **2013**, 47 (11), 5872-81
19. Pocostales, J.P., Sein, M.M., Knolle, W., von Sonntag, C., Schmidt, T.C., Degradation of ozone-refractory organic phosphates in wastewater by ozone and ozone/hydrogen peroxide (peroxone): The role of ozone consumption by dissolved organic matter. *Environ Sci Technol,* **2010**, 44 (21), 8248-8253

20. Norman, R.O.C., Storey, P.M., West, P.R., Electron spin resonance studies. Part XXV. Reactions of the sulphate radical anion with organic compounds. *J Chem Soc B,* **1970**, 1087-1095
21. Nöthe, T., Fahlenkamp, H., von Sonntag, C., Ozonation of wastewater: Rate of ozone consumption and hydroxyl radical yield. *Environ Sci Technol,* **2009**, 43 (15), 5990-5995
22. Mvula, E., von Sonntag, C., Ozonolysis of phenols in aqueous solution. *Org Biomol Chem,* **2003**, 1 (10), 1749-1756
23. Fischbacher, A., von Sonntag, J., von Sonntag, C., Schmidt, T.C., The •OH radical yield in the H2O2 + O3 (peroxone) reaction. *Environ Sci Technol,* **2013**, 47 (17), 9959-9964
24. Sein, M.M., Golloch, A., Schmidt, T.C., Von Sonntag, C., No marked kinetic isotope effect in the peroxone (H2O 2/D2O2 + O3) reaction: Mechanistic consequences. *ChemPhysChem,* **2007**, 8 (14), 2065-2067
25. Tekle-Röttering, A., von Sonntag, C., Reisz, E., Eyser, C.V., Lutze, H.V., Türk, J., Naumov, S., Schmidt, W., Schmidt, T.C., Ozonation of anilines: Kinetics, stoichiometry, product identification and elucidation of pathways. *Water Res,* **2016**, 98 147-59
26. Munoz, F., Mvula, E., Braslavsky, S.E., von Sonntag, C., Singlet dioxygen formation in ozone reactions in aqueous solution. *J Chem Soc Perk T 2,* **2001**, (7), 1109-1116
27. Mark, G., Naumov, S., von Sonntag, C., The reaction of ozone with bisulfide (HS−) in aqueous solution – Mechanistic aspects. *Ozone-Sci Eng,* **2011**, 33 (1), 37-41
28. Neta, P., Huie, R.E., Ross, A.B., Rate constants for reactions of inorganic radicals in aqueous solution. *J. Phys. Chem. Ref. Data,* **1988**, 17 (3), 1027-1284
29. von Sonntag, C., The basics of oxidants in water treatment. Part A: OH radical reactions. *Wa Sci Technol,* **2007**, 55 (12), 19-23
30. Söylemez, T., von Sonntag, C., Hydroxyl radical-induced oligomerization of ethylene in deoxygenated aqueous solution. *J Chem Soc Perk T 2,* **1980**, (2), 391-394
31. Veltwisch, D., Janata, E., Asmus, K.-D., Primary processes in the reaction of OH.-radicals with sulphoxides. *J Chem Soc Perk T 2,* **1980**, (1), 146-153
32. Buxton, G.V., Greenstock, C.L., Helman, W.P., Ross, A.B., Critical review of rate constants for reactions of hydrated electrons, hydrogen atoms and hydroxyl radicals (·OH/·O−) in aqueous solution. *J. Phys. Chem. Ref. Data,* **1988**, 17 (2), 513-886
33. Christensen, H.C., Sehested, K., Hart, E.J., Formation of benzyl radicals by pulse radiolysis of toluene in aqueous solutions. *J Phys Chem,* **1973**, 77 (8), 983-987
34. Fischbacher, A., Löppenberg, K., von Sonntag, C., Schmidt, T.C., A new reaction pathway for bromite to bromate in the ozonation of bromide. *Environ Sci Technol,* **2015**, 49 (19), 11714-11720
35. Liu, Y., Jiang, J., Ma, J., Yang, Y., Luo, C., Huangfu, X., Guo, Z., Role of the propagation reactions on the hydroxyl radical formation in ozonation and peroxone (ozone/hydrogen peroxide) processes. *Water Res,* **2015**, 68 750-758
36. von Gunten, U., Ozonation of drinking water: Part II. Disinfection and by-product formation in presence of bromide, iodide or chlorine. *Water Res,* **2003**, 37 (7), 1469-1487
37. USEPA, Alternative disinfectants and oxidants guidance manual. EPA 815-R-99-014, US Environmental Protection Agency - Office of Water, **1999**
38. Theruvathu, J.A., Flyunt, R., Aravindakumar, C.T., von Sonntag, C., Rate constants of ozone reactions with DNA, its constituents and related compounds. *J Chem Soc Perk T 2,* **2001**, (3), 269-274
39. Aieta, E.M., Berg, J.D., A review of chlorine dioxide in drinking-water treatment. *J Am Water Works Ass,* **1986**, 78 (6), 62-72
40. Wajon, J.E., Rosenblatt, D.H., Burrows, E.P., Oxidation of phenol and hydroquinone by chlorine dioxide. *Environ Sci Technol,* **1982**, 16 (7), 396-402
41. UBA, Bekanntmachung der Liste der Aufbereitungsstoffe und Desinfektionsverfahren gemäß § 11 der Trinkwasserverordnung – 18. Änderung – **2015**, Umweltbundesamt (Bartel, H.)

42. USEPA, National primary drinking water regulations. EPA 816-F-09-004, US Environmental Protection Agency - Office of ground water and drinking water, **2009**
43. Uhlmann, H., Verfahren zur Herstellung einer wässrigen stabilen Chlordioxidlösung. **2012**, PCT/EP2011/006510 //
44. Lee, G.F., Morris, J.C., Kinetics of chlorination of phenol - chlorophenolic tastes and odors. *Air Water Pollut,* **1962**, 6 419-431
45. Rav-Acha, C.H., The reactions of chlorine dioxide with aquatic organic materials and their health effects. *Water Res,* **1984**, 18 (11), 1329-1341
46. Wallwork, J.F., Bentley, M., Symonds, D.C., Identification of phenols in the river test and their treatment with chlorine dioxide. *Water Treat Exam,* **1969**, 18 (pt 3), 203-219
47. Terhalle, J., Kaiser, P., Jütte, M., Buss, J., Yasar, S., Marks, R., Uhlmann, H., Schmidt, T.C., Lutze, H.V., Chlorine dioxide—pollutant transformation and formation of hypochlorous acid as a secondary oxidant. *Environ Sci Technol,* **2018**, 52 (17), 9964-9971
48. Hoigné, J., Bader, H., Kinetics of reactions of chlorine dioxide (OClO) in water-I. Rate constants for inorganic and organic compounds. *Water Res,* **1994**, 28 (1), 45-55
49. Gates, D., Ziglio, G., Ozekin, K., State of the science of chlorine dioxide in drinking water. **2009**, Water Research Foundation and Fondazione AMGA, Denver, CO, USA
50. Tratnyek, P.G., Hoigné, J., Kinetics of reactions of chlorine dioxide (OCIO) in water—II. Quantitative structure-activity relationships for phenolic compounds. *Water Res,* **1994**, 28 (1), 57-66
51. Lee, Y., von Gunten, U., Oxidative transformation of micropollutants during municipal wastewater treatment: comparison of kinetic aspects of selective (chlorine, chlorine dioxide, ferrate VI, and ozone) and non-selective oxidants (hydroxyl radical). *Water Res,* **2010**, 44 (2), 555-66
52. Rosenblatt, D.H., Hull, L.A., De Luca, D.C., Davis, G.T., Weglein, R.C., Williams, H.K.R., Oxidations of amines. II. Substituent effects in chlorine dioxide oxidations. *J Am Chem Soc,* **1967**, 89 (5), 1158-163
53. Hull, L.A., Davis, G.T., Rosenblatt, D.H., Williams, H.K.R., Weglein, R.C., Oxidations of amines. III. Duality of mechanism in the reaction of amines with chlorine dioxide. *J Am Chem Soc,* **1967**, 89 (5), 1163-170
54. Ison, A., Odeh, I.N., Margerum, D.W., Kinetics and mechanisms of chlorine dioxide and chlorite oxidations of cysteine and glutathione. *Inorg Chem,* **2006**, 45 (21), 8768-8775
55. Rav-Acha, C.H., Blits, R., The different reaction mechanisms by which chlorine and chlorine dioxide react with polycyclic aromatic hydrocarbons (PAH) in water. *Water Res,* **1985**, 19 (10), 1273-1281
56. Deborde, M., von Gunten, U., Reactions of chlorine with inorganic and organic compounds during water treatment—Kinetics and mechanisms: A critical review. *Water Res,* **2008**, 42 (1), 13-51
57. Morris, J.C., The acid ionization constant of HOCl from 5 to 35°. *J Phys Chem-Us,* **1966**, 70 (12), 3798-3805
58. Rav-Acha, C.H., Blits, R., Choshen, E., Serri, A., Limoni, B., The action of chlorine dioxide on aquatic organic materials during the disinfection of drinking water. *J Environ Sci Heal A,* **1983**, 18 (5), 651-671
59. USEPA, Treatment techniques for controlling trihalomethanes in drinking water. EPA/600/2-81/156, US Environmental Protection Agency - Drinking water research division, Cincinnati, OH, USA, **1981**
60. USEPA, Ultraviolet disinfection guidance manual for the final long term 2 enhanced surface water treatment rule. EPA 815-R-06-007, US Environmental Protection Agency - Office of Water Washington, DC, USA, **2006**
61. Sharpless, C.M., Linden, K.G., UV photolysis of nitrate: Effects of natural organic matter and dissolved inorganic carbon and implications for UV water disinfection. *Environ Sci Technol,* **2001**, 35 (14), 2949-2955
62. Bolton, J.R., Cotton, C.A., The ultraviolet disinfection handbook. **2008**, American Water Works Association, Denver, CO, USA

63. Betancourt, W.Q., Rose, J.B., Drinking water treatment processes for removal of Cryptosporidium and Giardia. *Vet Parasitol,* **2004**, 126 (1), 219-234
64. Onidas, D., Markovitsi, D., Marguet, S., Sharonov, A., Gustavsson, T., Fluorescence properties of DNA nucleosides and nucleotides: A refined steady-state and femtosecond investigation. *J Phys Chem B,* **2002**, 106 (43), 11367-11374
65. Zimmer, J.L., Slawson, R.M., Potential repair of Escherichia coli DNA following exposure to UV radiation from both medium- and low-pressure UV sources used in drinking water treatment. *Appl Environ Microb,* **2002**, 68 (7), 3293-3299
66. Oguma, K., Katayama, H., Ohgaki, S., Photoreactivation of Escherichia coli after low- or medium-pressure UV disinfection determined by an endonuclease sensitive site assay. *Appl Environ Microb,* **2002**, 68 (12), 6029
67. Sakai, H., Oguma, K., Katayama, H., Ohgaki, S., Effects of low- or medium-pressure ultraviolet lamp irradiation on Microcystis aeruginosa and Anabaena variabilis. *Water Res,* **2007**, 41 (1), 11-18
68. Leifer, A., The kinetics of environmental aquatic photochemistry - Theory and practice. **1988**, American Chemical Society, York, PA, USA
69. Wöhrle, D., Tausch, M.W., Stohrer, W.-D., Photochemie: Konzepte, Methoden, Experimente. **1998**, Wiley-VCH, Weinheim
70. Canonica, S., Meunier, L., von Gunten, U., Phototransformation of selected pharmaceuticals during UV treatment of drinking water. *Water Res,* **2008**, 42 (1–2), 121-128
71. Katsoyiannis, I.A., Canonica, S., von Gunten, U., Efficiency and energy requirements for the transformation of organic micropollutants by ozone, O3/H2O2 and UV/H2O2. *Water Res,* **2011**, 45 (13), 3811-3822
72. Kuhn, H.J., Braslavsky, S.E., Schmidt, R., Chemical actinometry (IUPAC technical report). *Pure Appl. Chem.,* **2004**, 76 (12), 2105-2146
73. von Sonntag, C., Schuchmann, H.-P., UV disinfection of drinking water and by-product formation - some basic considerations. *J Water Supply Res T,* **1992**, 41 (2), 67-74
74. Janssen, E.M.L., Marron, E., McNeill, K., Aquatic photochemical kinetics of benzotriazole and structurally related compounds. *Environmental Sci Proc Imp,* **2015**, 17 (5), 939-946
75. Dulin, D., Mill, T., Development and evaluation of sunlight actinometers. *Environ Sci Technol,* **1982**, 16 (11), 815-820
76. Jekel, M., Dott, W., Bergmann, A., Dünnbier, U., Gnirss, R., Haist-Gulde, B., Hamscher, G., Letzel, M., Licha, T., Lyko, S., Miehe, U., Sacher, F., Scheurer, M., Schmidt, C.K., Reemtsma, T., Ruhl, A.S., Selection of organic process and source indicator substances for the anthropogenically influenced water cycle. *Chemosphere,* **2015**, 125 155-67
77. Pal, A., Gin, K.Y.-H., Lin, A.Y.-C., Reinhard, M., Impacts of emerging organic contaminants on freshwater resources: Review of recent occurrences, sources, fate and effects. *Sci Total Environ,* **2010**, 408 (24), 6062-6069
78. Burrows, H.D., Canle L, M., Santaballa, J.A., Steenken, S., Reaction pathways and mechanisms of photodegradation of pesticides. *J Photoch Photobio B,* **2002**, 67 (2), 71-108
79. Katagi, T., Direct photolysis mechanism of pesticides in water. *J Pestic Sci,* **2018**, 43 (2), 57-72
80. Remucal, C.K., The role of indirect photochemical degradation in the environmental fate of pesticides: A review. *Environmental Sci Proc Imp,* **2014**, 16 (4), 628-653
81. Waldemer, R.H., Tratnyek, P.G., Kinetics of contaminant degradation by permanganate. *Environ Sci Technol,* **2006**, 40 (3), 1055-1061
82. Wols, B.A., Hofman-Caris, C.H.M., Review of photochemical reaction constants of organic micropollutants required for UV advanced oxidation processes in water. *Water Res,* **2012**, 46 (9), 2815-2827

83. Hijnen, W.A.M., Beerendonk, E.F., Medema, G.J., Inactivation credit of UV radiation for viruses, bacteria and protozoan (oo)cysts in water: A review. *Water Res,* **2006**, 40 (1), 3-22
84. Wacławek, S., Lutze, H.V., Grübel, K., Padil, V.V.T., Černík, M., Dionysiou, D.D., Chemistry of persulfates in water and wastewater treatment: A review. *Chem Eng J,* **2017**, 330 44-62
85. Liang, L., Singer, P.C., Factors influencing the formation and relative distribution of haloacetic acids and trihalomethanes in drinking water. *Environ Sci Technol,* **2003**, 37 (13), 2920-2928
86. Villanueva, C.M., Cantor, K.P., Grimalt, J.O., Malats, N., Silverman, D., Tardon, A., Garcia-Closas, R., Serra, C., Carrato, A., Castaño-Vinyals, G., Marcos, R., Rothman, N., Real, F.X., Dosemeci, M., Kogevinas, M., Bladder cancer and exposure to water disinfection by-products through ingestion, bathing, showering, and swimming in pools. *Am J Epidemiol,* **2007**, 165 (2), 148-156
87. Richardson, S.D., Postigo, C., Drinking water disinfection by-products. **2012**, In: Emerging organic contaminants and human health, 93-137, Barceló, D., Springer Berlin Heidelberg, Berlin, Heidelberg
88. WHO, Guidelines for drinking-water quality, fourth edition. **2011**, World Health Organization
89. TrinkwV, Verordnung über die Qualität von Wasser für den menschlichen Gebrauch (Trinkwasserverordnung –TrinkwV 2001). **2016**, Teil I, Nr. 12, 459-491, Bundesgesetzblatt, Bonn
90. CWB (California Water Boards), NDMA and other nitrosamines - Drinking water issues. **2018**, 06/09/2018, https://www.waterboards.ca.gov/drinking_water/certlic/drinkingwater/NDMA.html
91. Yang, Y., Lu, X., Jiang, J., Ma, J., Liu, G., Cao, Y., Liu, W., Li, J., Pang, S., Kong, X., Luo, C., Degradation of sulfamethoxazole by UV, UV/H2O2 and UV/persulfate (PDS): Formation of oxidation products and effect of bicarbonate. *Water Res,* **2017**, 118 196-207
92. Glaze, W.H., Reaction products of ozone: a review. *Environ Health Persp,* **1986**, 69 151-157
93. von Gunten, U., Oxidation processes in water treatment: Are we on track? *Environ Sci Technol,* **2018**, 52 (9), 5062-5075
94. Dodd, M.C., Kohler, H.P.E., von Gunten, U., Oxidation of antibacterial compounds by ozone and hydroxyl radical: Elimination of biological activity during aqueous ozonation processes. *Environ Sci Technol,* **2009**, 43 (7), 2498-504
95. Lange, F., Cornelissen, S., Kubac, D., Sein, M.M., von Sonntag, J., Hannich, C.B., Golloch, A., Heipieper, H.J., Möder, M., von Sonntag, C., Degradation of macrolide antibiotics by ozone: A mechanistic case study with clarithromycin. *Chemosphere,* **2006**, 65 (1), 17-23
96. Huber, M.M., Ternes, T.A., von Gunten, U., Removal of estrogenic activity and formation of oxidation products during ozonation of 17α-ethinylestradiol. *Environ Sci Technol,* **2004**, 38 (19), 5177-5186
97. Fiss, E.M., Rule, K.L., Vikesland, P.J., Formation of chloroform and other chlorinated byproducts by chlorination of triclosan-containing antibacterial products. *Environ Sci Technol,* **2007**, 41 (7), 2387-2394
98. Rule, K.L., Ebbett, V.R., Vikesland, P.J., Formation of chloroform and chlorinated organics by free-chlorine-mediated oxidation of triclosan. *Environ Sci Technol,* **2005**, 39 (9), 3176-3185
99. Schmidt, C.K., Brauch, H.-J., N,N-dimethylsulfamide as precursor for n-nitrosodimethylamine (NDMA) formation upon ozonation and its fate during drinking water treatment. *Environ Sci Technol,* **2008**, 42 (17), 6340-6346
100. Schlüsener, M.P., Kunkel, U., Ternes, T.A., Quaternary triphenylphosphonium compounds: A new class of environmental pollutants. *Environ Sci Technol,* **2015**, 49 (24), 14282-14291

101. Schymanski, E.L., Singer, H.P., Slobodnik, J., Ipolyi, I.M., Oswald, P., Krauss, M., Schulze, T., Haglund, P., Letzel, T., Grosse, S., Thomaidis, N.S., Bletsou, A., Zwiener, C., Ibáñez, M., Portolés, T., de Boer, R., Reid, M.J., Onghena, M., Kunkel, U., Schulz, W., Guillon, A., Noyon, N., Leroy, G., Bados, P., Bogialli, S., Stipaničev, D., Rostkowski, P., Hollender, J., Non-target screening with high-resolution mass spectrometry: Critical review using a collaborative trial on water analysis. *Anal Bioanal Chem,* **2015**, 407 (21), 6237-6255
102. Li, Z., Kaserzon, S.L., Plassmann, M.M., Sobek, A., Gómez Ramos, M.J., Radke, M., A strategic screening approach to identify transformation products of organic micropollutants formed in natural waters. *Environmental Sci Proc Imp,* **2017**, 19 (4), 488-498
103. Petrovic, M., Barceló, D., LC-MS for identifying photodegradation products of pharmaceuticals in the environment. *TrAC Trend Anal Chem,* **2007**, 26 (6), 486-493
104. Funke, J., Prasse, C., Ternes, T.A., Identification of transformation products of antiviral drugs formed during biological wastewater treatment and their occurrence in the urban water cycle. *Water Res,* **2016**, 98 75-83
105. Prasse, C., Ternes, T.A., Application of orbitrap mass spectrometry for the identification of transformation products of trace organic contaminants formed in the environment. **2016**, In: Applications of time-of-flight and orbitrap mass spectrometry in environmental, food, doping and forensic analysis, 71, 263-282, Pérez, S., Eichhorn, P., Barceló, D., Elsevier, Heidelberg
106. Schmidt, T.C., Recent trends in water analysis triggering future monitoring of organic micropollutants. *Anal Bioanal Chem,* **2018**, 410 (17), 3933-3941
107. Richardson, S.D., Kimura, S.Y., Water analysis: Emerging contaminants and current issues. *Anal Chem,* **2016**, 88 (1), 546-582
108. Krauss, M., Singer, H., Hollender, J., LC–high resolution MS in environmental analysis: from target screening to the identification of unknowns. *Anal Bioanal Chem,* **2010**, 397 (3), 943-951
109. Simon, C., Roth, V.-N., Dittmar, T., Gleixner, G., Molecular signals of heterogeneous terrestrial environments identified in dissolved organic matter: A comparative analysis of orbitrap and ion cyclotron resonance mass spectrometers. *Front Earth Sci,* **2018**, 6 (138),
110. Fjeldsted, J.C., Advances in time-of-flight mass spectrometry. **2016**, In: Applications of time-of-flight and orbitrap mass spectrometry in environmental, food, doping and forensic analysis, 71, 19-49, Pérez, S., Eichhorn, P., Barceló, D., Elsevier, Heidelberg
111. Martins, C.P.B., Bromirski, M., Prieto Conaway, M.C., Makarov, A.A., Orbitrap mass spectrometry: Evolution and applicability. **2016**, In: Applications of time-of-flight and orbitrap mass spectrometry in environmental, food, doping and forensic analysis, 71, 3-18, Pérez, S., Eichhorn, P., Barceló, D., Elsevier, Heidelberg
112. Hollender, J., Schymanski, E.L., Singer, H.P., Ferguson, P.L., Nontarget screening with high resolution mass spectrometry in the environment: Ready to go? *Environ Sci Technol,* **2017**, 51 (20), 11505-11512
113. Ghaste, M., Mistrik, R., Shulaev, V., Applications of fourier transform ion cyclotron resonance (FT-ICR) and orbitrap based high resolution mass spectrometry in metabolomics and lipidomics. *Int. J. Mol. Sci.,* **2016**, 17 (6), 816
114. García-Galán, M.J., Silvia Díaz-Cruz, M., Barceló, D., Identification and determination of metabolites and degradation products of sulfonamide antibiotics. *TrAC Trend Anal Chem,* **2008**, 27 (11), 1008-1022
115. Deeb, A.A., Stephan, S., Schmitz, O.J., Schmidt, T.C., Suspect screening of micropollutants and their transformation products in advanced wastewater treatment. *Sci Total Environ,* **2017**, 601-602 1247-1253
116. Gao, S., Zhao, Z., Xu, Y., Tian, J., Qi, H., Lin, W., Cui, F., Oxidation of sulfamethoxazole (SMX) by chlorine, ozone and permanganate—A comparative study. *J Hazard Mater,* **2014**, 274 258-69

117. Hofstetter, T.B., Bolotin, J., Pati, S.G., Skarpeli-Liati, M., Spahr, S., Wijker, R.S., Isotope effects as new proxies for organic pollutant transformation. *Chimia,* **2014**, 68 (11), 788-792
118. Elsner, M., Stable isotope fractionation to investigate natural transformation mechanisms of organic contaminants: principles, prospects and limitations. *J Environ Monit,* **2010**, 12 (11), 2005-31
119. Schmidt, T.C., Jochmann, M.A., Origin and fate of organic compounds in water: characterization by compound-specific stable isotope analysis. *Annu Rev Anal Chem (Palo Alto Calif),* **2012**, 5 133-55
120. Jochmann, M.A., Schmidt, T.C., Compound-specific stable isotope analysis. **2012**, The Royal Society of Chemistry, Cambridge, UK
121. Werner, R.A., Brand, W.A., Referencing strategies and techniques in stable isotope ratio analysis. *Rapid Commun Mass Spectrom,* **2001**, 15 (7), 501-19
122. CIAAW (Commission on isotopic abundances and atomic weights), Isotopic reference materials. **2015**, 14/10/2018, http://www.ciaaw.org/reference-materials.htm
123. JRC (European Commission, Joint Research Centre Geel, Belgium), Certified reference materials. **2016**, 14/10/2018, https://ec.europa.eu/jrc/en/reference-materials
124. Paul, D., Skrzypek, G., Forizs, I., Normalization of measured stable isotopic compositions to isotope reference scales--A review. *Rapid Commun Mass Spectrom,* **2007**, 21 (18), 3006-14
125. Buchachenko, A.L., Mass-independent isotope effects. *J Phys Chem B,* **2013**, 117 (8), 2231-2238
126. Wolfsberg, M., van Hook, W.A., Paneth, P., Rebelo, L.P.N., Isotope effects : in the chemical, geological, and bio sciences. **2010**, Springer, Heidelberg
127. Elsner, M., Zwank, L., Hunkeler, D., Schwarzenbach, R.P., A new concept linking observable stable isotope fractionation to transformation pathways of organic pollutants. *Environ Sci Technol,* **2005**, 39 (18), 6896-916
128. Buchachenko, A.L., Magnetic isotope effect: Nuclear spin control of chemical reactions. *J Phys Chem A,* **2001**, 105 (44), 9995-10011
129. Meckenstock, R.U., Morasch, B., Griebler, C., Richnow, H.H., Stable isotope fractionation analysis as a tool to monitor biodegradation in contaminated acquifers. *J Contam Hydrol,* **2004**, 75 (3), 215-255
130. Hofstetter, T.B., Berg, M., Assessing transformation processes of organic contaminants by compound-specific stable isotope analysis. *TrAC Trend Anal Chem,* **2011**, 30 (4), 618-627
131. Hartenbach, A.E., Hofstetter, T.B., Aeschbacher, M., Sander, M., Kim, D., Strathmann, T.J., Arnold, W.A., Cramer, C.J., Schwarzenbach, R.P., Variability of nitrogen isotope fractionation during the reduction of nitroaromatic compounds with dissolved reductants. *Environ Sci Technol,* **2008**, 42 (22), 8352-8359
132. Wijker, R.S., Adamczyk, P., Bolotin, J., Paneth, P., Hofstetter, T.B., Isotopic analysis of oxidative pollutant degradation pathways exhibiting large H isotope fractionation. *Environ Sci Technol,* **2013**, 47 (23), 13459-68
133. Brenna, J.T., Corso, T.N., Tobias, H.J., Caimi, R.J., High-precision continuous-flow isotope ratio mass spectrometry. *Mass Spectrom Rev,* **1997**, 16 (5), 227-258
134. Douthitt, C.B., Hyphenation of gas chromatographic techniques with isotope ratio mass spectrometry: Present and future. *Analusis,* **1999**, 27 (3), 197-199
135. Elsner, M., Jochmann, M.A., Hofstetter, T.B., Hunkeler, D., Bernstein, A., Schmidt, T.C., Schimmelmann, A., Current challenges in compound-specific stable isotope analysis of environmental organic contaminants. *Anal Bioanal Chem,* **2012**, 403 (9), 2471-2491
136. Reinnicke, S., Bernstein, A., Elsner, M., Small and reproducible isotope effects during methylation with trimethylsulfonium hydroxide (TMSH): a convenient derivatization method for isotope analysis of negatively charged molecules. *Anal Chem,* **2010**, 82 (5), 2013-9

137. Wiese, S., Teutenberg, T., Schmidt, T.C., General strategy for performing temperature programming in high performance liquid chromatography: Prediction of linear temperature gradients. *Anal Chem,* **2011**, 83 (6), 2227-2233
138. Federherr, E., Willach, S., Roos, N., Lange, L., Molt, K., Schmidt, T.C., A novel high-temperature combustion interface for compound-specific stable isotope analysis of carbon and nitrogen via high-performance liquid chromatography/isotope ratio mass spectrometry. *Rapid Commun Mass Sp,* **2016**, 30 (7), 944-952
139. Brand, W.A., Mass spectrometer hardware for analyzing stable isotope-ratios; in: *Handbook of stable isotope analysis*. **2004**, de Groot, P.A., Elsevier, Amsterdam
140. Coplen, T., Böhlke, J., De Bièvre, P., Ding, T., Holden, N.E., Hopple, J.A., Krouse, H.R., Lamberty, A., Peiser, H.S., Revesz, K., Rieder, S.E., Rosman, K.J.R., Roth, E., Taylor, P.D.P., Vocke Jr., R.D., Xiao, Y.K., Isotope-abundance variations of selected elements (IUPAC technical report). *Pure Appl. Chem.,* **2002**, 74 (10), 1987-2017
141. Melsbach, A., Ponsin, V., Torrentó, C., Lihl, C., Hofstetter, T.B., Hunkeler, D., Elsner, M., 13C- and 15N-isotope analysis of desphenylchloridazon by liquid chromatography–isotope-ratio mass spectrometry and derivatization gas chromatography–isotope-ratio mass spectrometry. *Anal Chem,* **2019**, 91 (5), 3412-3420
142. Torrentó, C., Bakkour, R., Glauser, G., Melsbach, A., Ponsin, V., Hofstetter, T.B., Elsner, M., Hunkeler, D., Solid-phase extraction method for stable isotope analysis of pesticides from large volume environmental water samples. *Analyst,* **2019**, 144 (9), 2898-2908
143. Jochmann, M.A., Blessing, M., Haderlein, S.B., Schmidt, T.C., A new approach to determine method detection limits for compound-specific isotope analysis of volatile organic compounds. *Rapid Commun Mass Spectrom,* **2006**, 20 (24), 3639-48
144. Kujawinski, D.M., Stephan, M., Jochmann, M.A., Krajenke, K., Haas, J., Schmidt, T.C., Stable carbon and hydrogen isotope analysis of methyl tert-butyl ether and tert-amyl methyl ether by purge and trap-gas chromatography-isotope ratio mass spectrometry: method evaluation and application. *J Environ Monit,* **2010**, 12 (1), 347-54
145. Berg, M., Bolotin, J., Hofstetter, T.B., Compound-specific nitrogen and carbon isotope analysis of nitroaromatic compounds in aqueous samples using solid-phase microextraction coupled to GC/IRMS. *Anal Chem,* **2007**, 79 (6), 2386-2393
146. Zwank, L., Berg, M., Schmidt, T.C., Haderlein, S.B., Compound-specific carbon isotope analysis of volatile organic compounds in the low-microgram per liter range. *Anal Chem,* **2003**, 75 (20), 5575-83
147. Schreglmann, K., Hoeche, M., Steinbeiss, S., Reinnicke, S., Elsner, M., Carbon and nitrogen isotope analysis of atrazine and desethylatrazine at sub-microgram per liter concentrations in groundwater. *Anal Bioanal Chem,* **2013**, 405 (9), 2857-2867
148. Bakkour, R., Bolotin, J., Sellergren, B., Hofstetter, T.B., Molecularly imprinted polymers for compound-specific isotope analysis of polar organic micropollutants in aquatic environments. *Anal Chem,* **2018**, 90 (12), 7292-7301
149. Hofstetter, T.B., Schwarzenbach, R.P., Bernasconi, S.M., Assessing transformation processes of organic compounds using stable isotope fractionation. *Environ Sci Technol,* **2008**, 42 (21), 7737-7743
150. Bouchard, D., Hunkeler, D., Gaganis, P., Aravena, R., Höhener, P., Broholm, M.M., Kjeldsen, P., Carbon isotope fractionation during diffusion and biodegradation of petroleum hydrocarbons in the unsaturated zone: Field experiment at Værløse airbase, Denmark, and modeling. *Environ Sci Technol,* **2008**, 42 (2), 596-601
151. Penning, H., Sørensen, S.R., Meyer, A.H., Aamand, J., Elsner, M., C, N, and H isotope fractionation of the herbicide isoproturon reflects different microbial transformation pathways. *Environ Sci Technol,* **2010**, 44 (7), 2372-2378
152. Spahr, S., Cirpka, O.A., von Gunten, U., Hofstetter, T.B., Formation of N-nitrosodimethylamine during chloramination of secondary and tertiary amines: Role of molecular oxygen and radical intermediates. *Environ Sci Technol,* **2017**, 51 (1), 280-290

153. Spahr, S., von Gunten, U., Hofstetter, T.B., Carbon, hydrogen, and nitrogen isotope fractionation trends in N-nitrosodimethylamine reflect the formation pathway during chloramination of tertiary amines. *Environ Sci Technol,* **2017**, 51 (22), 13170-13179
154. Maier, M.P., Prasse, C., Pati, S.G., Nitsche, S., Li, Z., Radke, M., Meyer, A., Hofstetter, T.B., Ternes, T.A., Elsner, M., Exploring trends of C and N Isotope fractionation to trace transformation reactions of diclofenac in natural and engineered systems. *Environ Sci Technol,* **2016**, 50 (20), 10933-10942
155. Hartenbach, A.E., Hofstetter, T.B., Tentscher, P.R., Canonica, S., Berg, M., Schwarzenbach, R.P., Carbon, hydrogen, and nitrogen isotope fractionation during light-induced transformations of atrazine. *Environ Sci Technol,* **2008**, 42 (21), 7751-6
156. Skarpeli-Liati, M., Jiskra, M., Turgeon, A., Garr, A.N., Arnold, W.A., Cramer, C.J., Schwarzenbach, R.P., Hofstetter, T.B., Using nitrogen isotope fractionation to assess the oxidation of substituted anilines by manganese oxide. *Environ Sci Technol,* **2011**, 45 (13), 5596-604
157. Ratti, M., Canonica, S., McNeill, K., Erickson, P.R., Bolotin, J., Hofstetter, T.B., Isotope fractionation associated with the direct photolysis of 4-chloroaniline. *Environ Sci Technol,* **2015**, 49 (7), 4263-4273
158. Ratti, M., Canonica, S., McNeill, K., Bolotin, J., Hofstetter, T.B., Isotope fractionation associated with the photochemical dechlorination of chloroanilines. *Environ Sci Technol,* **2015**, 49 (16), 9797-9806
159. Kümmerer, K., Antibiotics in the aquatic environment - A review - Part I. *Chemosphere,* **2009**, 75 (4), 417-34
160. Shimizu, A., Takada, H., Koike, T., Takeshita, A., Saha, M., Rinawati, Nakada, N., Murata, A., Suzuki, T., Suzuki, S., Chiem, N.H., Tuyen, B.C., Viet, P.H., Siringan, M.A., Kwan, C., Zakaria, M.P., Reungsang, A., Ubiquitous occurrence of sulfonamides in tropical Asian waters. *Sci Total Environ,* **2013**, 452-453 108-15
161. Bu, Q., Wang, B., Huang, J., Deng, S., Yu, G., Pharmaceuticals and personal care products in the aquatic environment in China: A review. *J Hazard Mater,* **2013**, 262 189-211
162. Carballa, M., Omil, F., Lema, J.M., Llompart, M., García-Jares, C., Rodríguez, I., Gómez, M., Ternes, T., Behavior of pharmaceuticals, cosmetics and hormones in a sewage treatment plant. *Water Res,* **2004**, 38 (12), 2918-2926
163. Knopp, G., Prasse, C., Ternes, T.A., Cornel, P., Elimination of micropollutants and transformation products from a wastewater treatment plant effluent through pilot scale ozonation followed by various activated carbon and biological filters. *Water Res,* **2016**, 100 580-92
164. Verlicchi, P., Al Aukidy, M., Zambello, E., Occurrence of pharmaceutical compounds in urban wastewater: removal, mass load and environmental risk after a secondary treatment - A review. *Sci Total Environ,* **2012**, 429 123-55
165. Dodd, M.C., Buffle, M.O., Von Gunten, U., Oxidation of antibacterial molecules by aqueous ozone: moiety-specific reaction kinetics and application to ozone-based wastewater treatment. *Environ Sci Technol,* **2006**, 40 (6), 1969-77
166. Huber, M.M., Korhonen, S., Ternes, T.A., von Gunten, U., Oxidation of pharmaceuticals during water treatment with chlorine dioxide. *Water Res,* **2005**, 39 (15), 3607-17
167. Boreen, A.L., Arnold, W.A., McNeill, K., Photochemical fate of sulfa drugs in the aquatic environment: Sulfa drugs containing five-membered heterocyclic groups. *Environ Sci Technol,* **2004**, 38 (14), 3933-3940
168. Yu, H., Ge, P., Chen, J., Xie, H., Luo, Y., The degradation mechanism of sulfamethoxazole under ozonation: a DFT study. *Environmental Sci Proc Imp,* **2017**, 19 (3), 379-387
169. Abellán, M.N., Gebhardt, W., Schröder, H.F., Detection and identification of degradation products of sulfamethoxazole by means of LC/MS and - MSn after ozone treatment. *Water Sci. Technol.,* **2008**, 58 1803-1812

170. Gomez-Ramos Mdel, M., Mezcua, M., Aguera, A., Fernandez-Alba, A.R., Gonzalo, S., Rodriguez, A., Rosal, R., Chemical and toxicological evolution of the antibiotic sulfamethoxazole under ozone treatment in water solution. *J Hazard Mater,* **2011**, 192 (1), 18-25
171. Kujawinski, D.M., Zhang, L., Schmidt, T.C., Jochmann, M.A., When other separation techniques fail: compound-specific carbon isotope ratio analysis of sulfonamide containing pharmaceuticals by high-temperature-liquid chromatography-isotope ratio mass spectrometry. *Anal Chem,* **2012**, 84 (18), 7656-63
172. Birkigt, J., Gilevska, T., Ricken, B., Richnow, H.H., Vione, D., Corvini, P.F., Nijenhuis, I., Cichocka, D., Carbon stable isotope fractionation of sulfamethoxazole during biodegradation by Microbacterium sp. strain BR1 and upon direct photolysis. *Environ Sci Technol,* **2015**, 49 (10), 6029-36
173. Rudy, B.C., Senkowski, B.Z., Sulfamethoxazole. **1973**, In: Analytical Profiles of Drug Substances, 2, 467-486, Florey, K., Academic Press,
174. Flyunt, R., Makogon, O., Schuchmann, M.N., Asmus, K.-D., von Sonntag, C., OH-Radical-induced oxidation of methanesulfinic acid. The reactions of the methanesulfonyl radical in the absence and presence of dioxygen. *J Chem Soc Perk T 2,* **2001**, (5), 787-792
175. Sein, M.M., Zedda, M., Tuerk, J., Schmidt, T.C., Golloch, A., Von Sonntag, C., Oxidation of diclofenac with ozone in aqueous solution. *Environ Sci Technol,* **2008**, 42 (17), 6656-62
176. Rav-Acha, C., Choshen, E., Aqueous reactions of chlorine dioxide with hydrocarbons. *Environ Sci Technol,* **1987**, 21 (11), 1069-74
177. Aguilar, C.A.H., Narayanan, J., Singh, N., Thangarasu, P., Kinetics and mechanism for the oxidation of anilines by ClO2: a combined experimental and computational study. *J Phys Org Chem,* **2014**, 27 (5), 440-449
178. Jia, Z., Margerum, D.W., Francisco, J.S., General-acid-catalyzed reactions of hypochlorous acid and acetyl hypochlorite with chlorite ion. *Inorg Chem,* **2000**, 39 (12), 2614-20
179. Sherwood Lollar, B., Hirschorn, S.K., Chartrand, M.M., Lacrampe-Couloume, G., An approach for assessing total instrumental uncertainty in compound-specific carbon isotope analysis: implications for environmental remediation studies. *Anal Chem,* **2007**, 79 (9), 3469-75
180. Guo, W.Q., Yin, R.L., Zhou, X.J., Du, J.S., Cao, H.O., Yang, S.S., Ren, N.Q., Sulfamethoxazole degradation by ultrasound/ozone oxidation process in water: kinetics, mechanisms, and pathways. *Ultrason Sonochem,* **2015**, 22 182-7
181. Martín de Vidales, M.J., Robles-Molina, J., Domínguez-Romero, J.C., Cañizares, P., Sáez, C., Molina-Díaz, A., Rodrigo, M.A., Removal of sulfamethoxazole from waters and wastewaters by conductive-diamond electrochemical oxidation. *J Chem Technol Biot,* **2012**, 87 (10), 1441-1449
182. Huber, M.M., Göbel, A., Joss, A., Hermann, N., Löffler, D., McArdell, C.S., Ried, A., Siegrist, H., Ternes, T.A., von Gunten, U., Oxidation of pharmaceuticals during ozonation of municipal wastewater effluents: A pilot study. *Environ Sci Technol,* **2005**, 39 (11), 4290-9
183. Sehested, K., Holcman, J., Bjergbakke, E., Hart, E.J., A pulse radiolytic study of the reaction OH + O3 in aqueous medium. *J Phys Chem-Us,* **1984**, 88 (18), 4144-4147
184. Hoigné, J., Bader, H., Haag, W.R., Staehelin, J., Rate constants of reactions of ozone with organic and inorganic compounds in water-III. Inorganic compounds and radicals. *Water Res,* **1985**, 19 (8), 993-1004
185. Hoigné, J., Bader, H., Rate constants of reactions of ozone with organic and inorganic compounds in water-I. Non-dissociating organic compounds. *Water Res,* **1983**, 17 (2), 173-183
186. Pryor, W.A., Giamalva, D.H., Church, D.F., Kinetics of ozonation .2. Amino-acids and model compounds in water and comparisons to rates in nonpolar-solvents. *J Am Chem Soc,* **1984**, 106 (23), 7094-7100

187. Laszlo, B., Alfassi, Z.B., Neta, P., Huie, R.E., Kinetics and mechanism of the reaction of •NH2 with O2 in aqueous solutions. *J Phys Chem A,* **1998**, 102 (44), 8498-8504
188. Wu, J.J., Muruganandham, M., Chen, S.H., Degradation of DMSO by ozone-based advanced oxidation processes. *J Hazard Mater,* **2007**, 149 (1), 218-25
189. 32645:2008-11, D., Chemical analysis - Decision limit, detection limit and determination limit under repeatability conditions - Terms, methods, evaluation. **2008**, Beuth-Verlag, Berlin
190. von Sonntag, C., Schuchmann, H.-P., Peroxyl radicals in aqueous solution. **1997**, In: Peroxyl Radicals, 173-234, Alfassi, Z.B., Wiley, Chichester
191. Loos, R., Gawlik, B.M., Locoro, G., Rimaviciute, E., Contini, S., Bidoglio, G., EU-wide survey of polar organic persistent pollutants in European river waters. *Environ Pollut,* **2009**, 157 (2), 561-568
192. Hughes, D.T.D., Russell, N.J., The use of trimethoprim-sulfamethoxazole in the treatment of chest infections. *Rev Infect Dis,* **1982**, 4 (2), 528-532
193. Lode, H., Co-trimoxazole from the therapeutic viewpoint. *Infection,* **1987**, 15 (5), S222-S226
194. Lai, H.T., Wang, T.S., Chou, C.C., Implication of light sources and microbial activities on degradation of sulfonamides in water and sediment from a marine shrimp pond. *Bioresour Technol,* **2011**, 102 (8), 5017-23
195. Luo, Y., Guo, W., Ngo, H.H., Nghiem, L.D., Hai, F.I., Zhang, J., Liang, S., Wang, X.C., A review on the occurrence of micropollutants in the aquatic environment and their fate and removal during wastewater treatment. *Sci Total Environ,* **2014**, 473-474 619-41
196. Kasprzyk-Hordern, B., Dinsdale, R.M., Guwy, A.J., The occurrence of pharmaceuticals, personal care products, endocrine disruptors and illicit drugs in surface water in South Wales, UK. *Water Res,* **2008**, 42 (13), 3498-518
197. Andreozzi, R., Raffaele, M., Nicklas, P., Pharmaceuticals in STP effluents and their solar photodegradation in aquatic environment. *Chemosphere,* **2003**, 50 (10), 1319-1330
198. Kümmerer, K., Antibiotics in the aquatic environment – A review – Part II. *Chemosphere,* **2009**, 75 (4), 435-441
199. Guo, X., Pang, W., Dou, C., Yin, D., Sulfamethoxazole and COD increase abundance of sulfonamide resistance genes and change bacterial community structures within sequencing batch reactors. *Chemosphere,* **2017**, 175 21-27
200. Larcher, S., Yargeau, V., Biodegradation of sulfamethoxazole: current knowledge and perspectives. *Appl Microbiol Biotechnol,* **2012**, 96 (2), 309-18
201. Bahnmüller, S., von Gunten, U., Canonica, S., Sunlight-induced transformation of sulfadiazine and sulfamethoxazole in surface waters and wastewater effluents. *Water Res,* **2014**, 57 183-92
202. Chen, H., Zhang, M., Effects of advanced treatment systems on the removal of antibiotic resistance genes in wastewater treatment plants from Hangzhou, China. *Environ Sci Technol,* **2013**, 47 (15), 8157-8163
203. Lindenauer, K.G., Darby, J.L., Ultraviolet disinfection of wastewater: Effect of dose on subsequent photoreactivation. *Water Res,* **1994**, 28 (4), 805-817
204. Conkle, J.L., White, J.R., Metcalfe, C.D., Reduction of pharmaceutically active compounds by a lagoon wetland wastewater treatment system in Southeast Louisiana. *Chemosphere,* **2008**, 73 (11), 1741-1748
205. Kang, S.J., Allbaugh, T.A., Reynhout, J.W., Erickson, T.L., Olmstead, K.P., Thomas, L., Thomas, P., Selection of an ultaviolet disinfection system for a municipal wastewater treatment plant. *Water Sci. Technol.,* **2004**, 50 163-169
206. Bonvin, F., Omlin, J., Rutler, R., Schweizer, W.B., Alaimo, P.J., Strathmann, T.J., McNeill, K., Kohn, T., Direct photolysis of human metabolites of the antibiotic sulfamethoxazole: evidence for abiotic back-transformation. *Environ Sci Technol,* **2013**, 47 (13), 6746-55

207. Lekkerkerker-Teunissen, K., Benotti, M.J., Snyder, S.A., van Dijk, H.C., Transformation of atrazine, carbamazepine, diclofenac and sulfamethoxazole by low and medium pressure UV and UV/H2O2 treatment. *Sep Purif Technol,* **2012**, 96 33-43
208. Trovo, A.G., Nogueira, R.F., Aguera, A., Sirtori, C., Fernandez-Alba, A.R., Photodegradation of sulfamethoxazole in various aqueous media: persistence, toxicity and photoproducts assessment. *Chemosphere,* **2009**, 77 (10), 1292-8
209. Lam, M.W., Mabury, S.A., Photodegradation of the pharmaceuticals atorvastatin, carbamazepine, levofloxacin, and sulfamethoxazole in natural waters. *Aquat Sci,* **2005**, 67 (2), 177-188
210. Willach, S., Lutze, H.V., Eckey, K., Löppenberg, K., Lüling, M., Terhalle, J., Wolbert, J.-B., Jochmann, M.A., Karst, U., Schmidt, T.C., Degradation of sulfamethoxazole using ozone and chlorine dioxide - Compound-specific stable isotope analysis, transformation product analysis and mechanistic aspects. *Water Res,* **2017**, 122 280-289
211. Elsner, M., Imfeld, G., Compound-specific isotope analysis (CSIA) of micropollutants in the environment - current developments and future challenges. *Curr Opin Biotechnol,* **2016**, 41 60-72
212. Wegelin, M., Canonica, S., Mechsner, K., Fleischmann, T., Pesaro, F., Metzler, A., Solar water disinfection: Scope of the process and analysis of radiation experiments. *J Water Supply Res T,* **1994**, 43 (4), 154-169
213. Lutze, H.V., Kerlin, N., Schmidt, T.C., Sulfate radical-based water treatment in presence of chloride: Formation of chlorate, inter-conversion of sulfate radicals into hydroxyl radicals and influence of bicarbonate. *Water Res,* **2015**, 72 349-360
214. Zhou, W., Moore, D.E., Photochemical decomposition of sulfamethoxazole. *Int J Pharm,* **1994**, 110 (1), 55-63
215. Gmurek, M., Horn, H., Majewsky, M., Phototransformation of sulfamethoxazole under simulated sunlight: Transformation products and their antibacterial activity toward Vibrio fischeri. *Sci Total Environ,* **2015**, 538 58-63
216. Su, T., Deng, H., Benskin, J.P., Radke, M., Biodegradation of sulfamethoxazole photo-transformation products in a water/sediment test. *Chemosphere,* **2016**, 148 518-525
217. Perisa, M., Babic, S., Skoric, I., Fromel, T., Knepper, T.P., Photodegradation of sulfonamides and their N (4)-acetylated metabolites in water by simulated sunlight irradiation: kinetics and identification of photoproducts. *Environ Sci Pollut Res Int,* **2013**, 20 (12), 8934-46
218. Poirier-Larabie, S., Segura, P.A., Gagnon, C., Degradation of the pharmaceuticals diclofenac and sulfamethoxazole and their transformation products under controlled environmental conditions. *Sci Total Environ,* **2016**, 557 257-267
219. Trovó, A.G., Nogueira, R.F.P., Agüera, A., Fernandez-Alba, A.R., Sirtori, C., Malato, S., Degradation of sulfamethoxazole in water by solar photo-Fenton. Chemical and toxicological evaluation. *Water Res,* **2009**, 43 (16), 3922-3931
220. Boreen, A.L., Arnold, W.A., McNeill, K., Triplet-sensitized photodegradation of sulfa drugs containing six-membered heterocyclic groups: Identification of an SO2 extrusion photoproduct. *Environ Sci Technol,* **2005**, 39 (10), 3630-3638
221. Elsner, M., McKelvie, J., Lacrampe Couloume, G., Sherwood Lollar, B., Insight into methyl tert-butyl ether (MTBE) stable isotope fractionation from abiotic reference experiments. *Environ Sci Technol,* **2007**, 41 (16), 5693-5700
222. Skarpeli-Liati, M., Turgeon, A., Garr, A.N., Arnold, W.A., Cramer, C.J., Hofstetter, T.B., pH-dependent equilibrium isotope fractionation associated with the compound specific nitrogen and carbon isotope analysis of substituted anilines by SPME-GC/IRMS. *Anal Chem,* **2011**, 83 (5), 1641-1648
223. Skarpeli-Liati, M., Jiskra, M., Turgeon, A., Garr, A.N., Arnold, W.A., Cramer, C.J., Schwarzenbach, R.P., Hofstetter, T.B., Using Nitrogen Isotope Fractionation to Assess the Oxidation of Substituted Anilines by Manganese Oxide. *Environ Sci Technol,* **2011**, 45 (13), 5596-5604
224. Buchachenko, A.L., MIE versus CIE: Comparative analysis of magnetic and classical isotope effects. *Chem Rev,* **1995**, 95 (7), 2507-2528

225. Montalti, M., Credi, A., Prodi, L., Gandolfi, M.T., Handbook of photochemistry. **2006**, CRC Press Taylor & Francis Group, Boca Raton, FL, USA
226. Ellison, S.L.R., Barwick, V.J., Farrant, T.J.D., Practical statistics for the analytical scientist. **2009**, Royal Society of Chemistry, Cambridge
227. Kneubühl, F.K., Sigrist, M.W., Laser. **2008**, Vieweg+Teubner, Wiesbaden
228. Schwarzenbach, R.P., Gschwend, P.M., Imboden, D.M., Environmental organic chemistry. **2003**, John Wiley & Sons, Inc., Hoboken, NJ, USA
229. Solano, F.M., Marchesi, M., Thomson, N.R., Bouchard, D., Aravena, R., Carbon and hydrogen isotope fractionation of benzene, toluene, and o-xylene during chemical oxidation by persulfate. *Ground Water Monit R,* **2018**, 38 (4), 62-72
230. Liu, H., Bruton, T.A., Doyle, F.M., Sedlak, D.L., In situ chemical oxidation of contaminated groundwater by persulfate: Decomposition by Fe(III)- and Mn(IV)-containing oxides and aquifer materials. *Environ Sci Technol,* **2014**, 48 (17), 10330-10336
231. Fedrizzi, F., Ramos, D.T., Lazzarin, H.S.C., Fernandes, M., Larose, C., Vogel, T.M., Corseuil, H.X., A Modified Approach for in Situ Chemical Oxidation Coupled to Biodegradation Enhances Light Nonaqueous Phase Liquid Source-Zone Remediation. *Environ Sci Technol,* **2017**, 51 (1), 463-472
232. Gottschalk, C., Libra, J.A., Saupe, A., Ozonation of Water and Waste Water - A Practical Guide to Understanding Ozone and its Application. **2000**, Wiley-VCH, Weinheim, Germany
233. Aelion, C.M., Höhener, P., Hunkeler, D., Aravena, R., Environmental isotopes in biodegradation and bioremediation. **2010**, CRC Press Taylor & Francis Group, Boca Raton, FL, USA
234. Zhang, N., Geronimo, I., Paneth, P., Schindelka, J., Schaefer, T., Herrmann, H., Vogt, C., Richnow, H.H., Analyzing sites of OH radical attack (ring vs. side chain) in oxidation of substituted benzenes via dual stable isotope analysis (δ(13)C and δ(2)H). *Sci Total Environ,* **2016**, 542 (Pt A), 484-94
235. Spahr, S., Bolotin, J., Schleucher, J., Ehlers, I., von Gunten, U., Hofstetter, T.B., Compound-specific carbon, nitrogen, and hydrogen isotope analysis of N-nitrosodimethylamine in aqueous solutions. *Anal Chem,* **2015**, 87 (5), 2916-2924
236. Hoigné, J., Bader, H., Rate constants of reactions of ozone with organic and inorganic compounds in water—II: Dissociating organic compounds. *Water Res,* **1983**, 17 (2), 185-194
237. Foresman, J.B., Frisch, A., Exploring chemistry with electronic structure methods. **2015**, Gaussian Inc., Wallingford, CT, USA
238. Frisch, M.J., Trucks, G.W., Schlegel, H.B., Scuseria, G.E., Robb, M.A., Cheeseman, J.R., Scalmani, G., Barone, V., Petersson, G.A., Nakatsuji, H., Li, X., Caricato, M., Marenich, A.V., Bloino, J., Janesko, B.G., Gomperts, R., Mennucci, B., Hratchian, H.P., Ortiz, J.V., Izmaylov, A.F., Sonnenberg, J.L., Williams, Ding, F., Lipparini, F., Egidi, F., Goings, J., Peng, B., Petrone, A., Henderson, T., Ranasinghe, D., Zakrzewski, V.G., Gao, J., Rega, N., Zheng, G., Liang, W., Hada, M., Ehara, M., Toyota, K., Fukuda, R., Hasegawa, J., Ishida, M., Nakajima, T., Honda, Y., Kitao, O., Nakai, H., Vreven, T., Throssell, K., Montgomery Jr., J.A., Peralta, J.E., Ogliaro, F., Bearpark, M.J., Heyd, J.J., Brothers, E.N., Kudin, K.N., Staroverov, V.N., Keith, T.A., Kobayashi, R., Normand, J., Raghavachari, K., Rendell, A.P., Burant, J.C., Iyengar, S.S., Tomasi, J., Cossi, M., Millam, J.M., Klene, M., Adamo, C., Cammi, R., Ochterski, J.W., Martin, R.L., Morokuma, K., Farkas, O., Foresman, J.B., Fox, D.J., Gaussian 16 Rev. C.01. Wallingford, CT, **2016**
239. Schlegel, H.B., Exploring potential energy surfaces for chemical reactions: An overview of some practical methods. *J Comput Chem,* **2003**, 24 (12), 1514-1527
240. Schlegel, H.B., Moeller-Plesset perturbation theory with spin projection. *J Phys Chem-Us,* **1988**, 92 (11), 3075-3078
241. Schlegel, H.B., Potential energy curves using unrestricted Moeller–Plesset perturbation theory with spin annihilation. *J Chem Phys,* **1986**, 84 (8), 4530-4534

242. Scalmani, G., Frisch, M.J., Continuous surface charge polarizable continuum models of solvation. I. General formalism. *J Chem Phys,* **2010**, 132 (11), 114110
243. Anisimov, V., Paneth, P., ISOEFF98. A program for studies of isotope effects using Hessian modifications. *J Math Chem,* **1999**, 26 (1), 75-86
244. Steglenko, D.V., Fukui-function-calculation. https://github.com/dmsteglenko/Fukui-function-calculation, **2017**
245. Contreras, R.R., Fuentealba, P., Galván, M., Pérez, P., A direct evaluation of regional Fukui functions in molecules. *Chem Phys Lett,* **1999**, 304 (5), 405-413
246. Becke, A.D., Density-functional thermochemistry. III. The role of exact exchange. *J Chem Phys,* **1993**, 98 (7), 5648-5652
247. Perdew, J.P., Schmidt, K., Jacob's ladder of density functional approximations for the exchange-correlation energy. *AIP Conf Proc,* **2001**, 577 (1), 1-20
248. Lee, Y., von Gunten, U., Quantitative structure–activity relationships (QSARs) for the transformation of organic micropollutants during oxidative water treatment. *Water Res,* **2012**, 46 (19), 6177-6195
249. Ahad, J.M.E., Slater, G.F., Carbon isotope effects associated with Fenton-like degradation of toluene: Potential for differentiation of abiotic and biotic degradation. *Sci Total Environ,* **2008**, 401 (1), 194-198
250. Elovitz, M.S., von Gunten, U., Hydroxyl radical/ozone ratios during ozonation processes. I. The Rct concept. *Ozone-Sci Eng,* **1999**, 21 (3), 239-260
251. Kaiser, H.-P., Köster, O., Gresch, M., Périsset, P.M.J., Jäggi, P., Salhi, E., von Gunten, U., Process control for ozonation systems: A novel real-time approach. *Ozone-Sci Eng,* **2013**, 35 (3), 168-185
252. Elovitz, M.S., von Gunten, U., Kaiser, H.-P., Hydroxyl radical/ozone ratios during ozonation processes. II. The effect of temperature, pH, alkalinity, and DOM properties. *Ozone-Sci Eng,* **2000**, 22 (2), 123-150
253. Naumov, S., von Sonntag, C., Quantum chemical studies on the formation of ozone adducts to aromatic compounds in aqueous solution. *Ozone-Sci Eng,* **2010**, 32 (1), 61-65
254. Mvula, E., Naumov, S., von Sonntag, C., Ozonolysis of lignin models in aqueous solution: Anisole, 1,2-dimethoxybenzene, 1,4-dimethoxybenzene, and 1,3,5-trimethoxybenzene. *Environ Sci Technol,* **2009**, 43 (16), 6275-6282
255. Vollhardt, K.P., Schore, N.E., Organische Chemie; Chapter 16, pp. 787-830. **2011**, Wiley-VCH, Weinheim, Germany
256. Pati, S.G., Shin, K., Skarpeli-Liati, M., Bolotin, J., Eustis, S.N., Spain, J.C., Hofstetter, T.B., Carbon and nitrogen isotope effects associated with the dioxygenation of aniline and diphenylamine. *Environ Sci Technol,* **2012**, 46 (21), 11844-11853
257. Skarpeli-Liati, M., Pati, S.G., Bolotin, J., Eustis, S.N., Hofstetter, T.B., Carbon, hydrogen, and nitrogen isotope fractionation associated with oxidative transformation of substituted aromatic N-alkyl amines. *Environ Sci Technol,* **2012**, 46 (13), 7189-98
258. Anslyn, E.V., Dougherty, D.A., Modern physical organic chemistry. **2006**, University Science Books, Sausalito, CA, USA
259. Parr, R.G., Yang, W., Density functional approach to the frontier-electron theory of chemical reactivity. *J Am Chem Soc,* **1984**, 106 (14), 4049-4050
260. Bao, Y., Deng, S., Jiang, X., Qu, Y., He, Y., Liu, L., Chai, Q., Mumtaz, M., Huang, J., Cagnetta, G., Yu, G., Degradation of PFOA substitute: GenX (HFPO–DA ammonium salt): Oxidation with UV/persulfate or reduction with UV/sulfite? *Environ Sci Technol,* **2018**, 52 (20), 11728-11734
261. Ayers, P.W., Levy, M., Perspective on "Density functional approach to the frontier-electron theory of chemical reactivity". *Theor Chem Acc,* **2000**, 103 (3), 353-360
262. Adamczyk, P., Paneth, P., Theoretical evaluation of isotopic fractionation factors in oxidation reactions of benzene, phenol and chlorophenols. *J Mol Model,* **2011**, 17 (9), 2285-2296

263. Kenley, R.A., Davenport, J.E., Hendry, D.G., Gas-phase hydroxyl radical reactions. Products and pathways for the reaction of hydroxyl with aromatic hydrocarbons. *J Phys Chem-Us,* **1981**, 85 (19), 2740-2746
264. Olah, G.A., Aromatic substitution. XXVIII. Mechanism of electrophilic aromatic substitutions. *Accounts Chem Res,* **1971**, 4 (7), 240-248
265. Elliot, A.J., McCracken, D.R., Effect of temperature on $O^{\cdot-}$ reactions and equilibria. A pulse radiolysis study. *Radiat Phys Chem,* **1989**, 33 (1), 69-74
266. Pattison, D.I., Davies, M.J., Absolute Rate Constants for the Reaction of Hypochlorous Acid with Protein Side Chains and Peptide Bonds. *Chem Res Toxicol,* **2001**, 14 (10), 1453-1464
267. Duarte, L.G.T.A., Germino, J.C., Braga, C.d.Á., Barboza, C.A., Atvars, T.D.Z., Santos, F.d.S., Rodembusch, F.S., Photoacidity as a tool to rationalize excited state intramolecular proton transfer reactivity in flavonols. *Photoch Photobio Sci,* **2018**, 17 (2), 231-238
268. Bartok, W., Lucchesi, P.J., Snider, N.S., Protolytic dissociation of electronically excited organic acids. *J Am Chem Soc,* **1962**, 84 (10), 1842-1844
269. Tajima, S., Shiobara, S., Shizuka, H., Tobita, S., Excited-state proton-dissociation of N-alkylated anilinium ions in aqueous solution studied by picosecond fluorescence measurements. *Phys Chem Chem Phys,* **2002**, 4 (14), 3376-3382
270. Lazar, A.I., Rohacova, J., Nau, W.M., Comparison of complexation-induced pKa shifts in the ground and excited states of dyes as well as different macrocyclic hosts and their manifestation in host-retarded excited-dye deprotonation. *J Phys Chem B,* **2017**, 121 (50), 11390-11398
271. Jin, X., Xu, H., Qiu, S., Jia, M., Wang, F., Zhang, A., Jiang, X., Direct photolysis of oxytetracycline: Influence of initial concentration, pH and temperature. *J Photoch Photobio A,* **2017**, 332 224-231
272. Tekle-Röttering, A., Reisz, E., Jewell, K.S., Lutze, H.V., Ternes, T.A., Schmidt, W., Schmidt, T.C., Ozonation of pyridine and other N-heterocyclic aromatic compounds: Kinetics, stoichiometry, identification of products and elucidation of pathways. *Water Res,* **2016**, 102 582-593
273. Chen, S., Blaney, L., Chen, P., Deng, S., Hopanna, M., Bao, Y., Yu, G., Ozonation of the 5-fluorouracil anticancer drug and its prodrug capecitabine: Reaction kinetics, oxidation mechanisms, and residual toxicity. *Front Env Sci Eng,* **2019**, 13 (4), 59
274. Tentscher, P.R., Lee, M., von Gunten, U., Micropollutant oxidation studied by quantum chemical computations: Methodology and applications to thermodynamics, kinetics, and reaction mechanisms. *Accounts Chem Res,* **2019**, 52 (3), 605-614
275. Wheeler, S.E., Ess, D.H., Houk, K.N., Thinking out of the black box: Accurate barrier heights of 1,3-dipolar cycloadditions of ozone with acetylene and ethylene. *J Phys Chem A,* **2008**, 112 (8), 1798-1807
276. Zhao, Y., Tishchenko, O., Gour, J.R., Li, W., Lutz, J.J., Piecuch, P., Truhlar, D.G., Thermochemical kinetics for multireference systems: Addition reactions of ozone. *J Phys Chem A,* **2009**, 113 (19), 5786-5799
277. Köster, D., Jochmann, M.A., Lutze, H.V., Schmidt, T.C., Monitoring of the total carbon and nitrogen balance during the mineralization of nitrogen containing compounds by heat activated persulfate. *Chem Eng J,* **2019**, 367 160-168

Chapter 8 -
Supplements

8.1 List of figures

8.2 List of schemes

8.3 List of tables

8.4 List of abbreviations

AKIE	apparent kinetic isotope effect
AOP	advanced oxidation process
BSIA	bulk stable isotope ratio analysis
CIAAW	Commission on isotopic abundances and atomic weights
CSIA	compound-specific stable isotope analysis
DBE	double bond equivalent
DBP	disinfection byproducts
DMSO	dimethyl sulfoxide
DAD	diode array detector
DNA	deoxyribonucleic acid
DOM	dissolved organic matter
CF	cut-off filter
cf.	confer
Cl^-	chloride
$Cl_{2(g)}$	gaseous chlorine
ClO_2	chlorine dioxide
ClO_2^-	chlorite
ClO_3^-	chlorate
$E^{avg}_{\lambda=254nm}$	average fluence rate
EA	elemental analyzer
e.g.	example given
FT-ICR	Fourier transform ion cyclotron resonance mass analyzers
GC	gas chromatography
HAA	haloacetic acid
HCl	hydrochloric acid
H_2O_2	hydrogen peroxone
HOCl	hypochlorous acid
HP	high pressure
HPLC-ESI(-)-ToF-MS	high performance liquid chromatograph-electrospray ionization in negative mode-time-of-flight mass spectrometer
HRMS	high-resolution mass spectrometry
HT-LC	high-temperature-liquid chromatography
$HO_2^\bullet$	perhydroxyl radical

$HO_3^\bullet$	hydrotrioxyl radical
IAEA	International atomic energy agency
i.e.	id est
IC	ion chromatography
IRMS	isotope ratio mass spectrometer
JRC	Joint Research Centre of the European Union in Geel, Belgium
$k_{E_p^0}$	photon fluence-based rate constant
$k_{E_p^0}^{app}$	apparent photon fluence-based rate constant
k_p^{app}	apparent pseudo-first-order rate constants for phototransformation
$^{light}k$	reaction rate constants of the compound containing the light isotope
$^{heavy}k$	reaction rate constants of the compound containing the heavy isotope
KIE	kinetic isotope effect
LC	liquid chromatography
LOQ	limit of quantification
LP	low pressure
LTQ Orbitrap	linear ion trap/orbitrap
MDE	mass-dependent isotope effect
MIE	mass-independent isotope effect
MP	medium pressure
MSIS	methanesulfinic acid
MSUS	methanesulfonic acid
MTBE	methyl *tert*-butyl ether
$NaClO_2$	sodium chlorite
$Na_2S_2O_8$	sodium peroxodisulfate
Nd:YAG-laser	neodymium-doped yttrium aluminum garnet (Nd:$Y_3Al_5O_{12}$) laser
NDMA	*N*-nitrosodimethylamine
NOM	natural organic matter
$^\bullet OH$	hydroxyl radicals
OH^-	hydroxide ions
O_2	oxygen
$^1O_2$	singlet oxygen
$^3O_2$	triplet oxygen
$O_2^{\bullet-}$	superoxide anion
O_3	ozone
$O_3^{\bullet-}$	ozonide radical anion

PAR	peak area ratios
PCM	polarizable continuum model
pK_a	acid dissociation constant
PNA/pyr	*p*-nitroanisole-pyridine
PNAP/pyr	*p*-nitroacetophenon-pyridine
qToF	quadrupole time of flight mass spectrometer
$R_{0,c}$	ratio of $^{heavy}E / ^{light}E$ compound *c* at time *0*
R_c	ratio of the heavy to light isotope E of the compound c
R_{ref}	ratio of the heavy to light isotope E the reference ref
$R_{t,c}$	ratio of $^{heavy}E / ^{light}E$ compound *c* at time *t*
SCRF	self-consistent reaction field
SI	supporting information
SIA	stable isotope analysis
SMX	sulfamethoxazole
SMX^-	anionic sulfamethoxazole
SMX^+	cationic sulfamethoxazole
SMX-OH	hydroxylated sulfamethoxazole
SMX-NO	TP266 (TP after photolysis of SMX, cf. chapter 4.4.2)
tert-BuOH	*tertiary* butanol
THM	trihalomethane
TOX	total organic halides
TP	transformation product
t_R	retention time
UV	ultraviolet
VPDB	Vienna Pee Dee Belemnite
δ-scale	delta scale
$\delta^{heavy}E_{c,ref}$	δ-value of a compound c related to the reference ref
ε_E^{bulk}	isotopic fractionation of all isotopes of element E
ε_λ	molar absorption coefficient
λ	wavelength
Φ_λ	quantum yield

8.5 List of publications

8.5.1 Publications in peer-reviewed journals

Koch, C., Dundua, A., Aragon-Gomez, J., Nachev, M., Stephan, S., Willach, S., Ulbricht, M., Schmitz, O.J., Schmidt, T.C., Sures, B., Degradation of polymeric brominated flame retardants: Development of an analytical approach using PolyFR and UV irradiati*on*. *Environmental Science and Technology*, **2016**, 50 (23), 12912-12920

Willach, S., Brauch, H.-J., Lange, F.T., Contribution of selected perfluoroalkyl and polyfluoroalkyl substances to the adsorbable organically bound fluorine in German rivers and in a highly contaminated groundwater. *Chemosphere*, **2016**, 145, 342-350

Federherr, E., Willach, S., Roos, N., Lange, L., Molt, K., Schmidt, T.C., A novel high-temperature combustion interface for compound-specific stable isotope analysis of carbon and nitrogen via high-performance liquid chromatography/isotope ratio mass spectrometry. *Rapid Communications in Mass Spectrometry*, **2016**, 30 (7), 944-952

Willach, S., Lutze, H.V., Eckey, K., Löppenberg, K., Lüling, M., Terhalle, J., Wolbert, J.-B., Jochmann, M.A., Karst, U., Schmidt, T.C., Degradation of sulfamethoxazole using ozone and chlorine dioxide - Compound-specific stable isotope analysis, transformation product analysis and mechanistic aspects. *Water Research*, **2017**, 122, 280-289

Willach, S., Lutze, H. V., Eckey, K., Löppenberg, K., Lüling, M., Wolbert, J.-B., Kujawinski, D. M., Jochmann, M. A., Karst, U., Schmidt, T. C., Direct photolysis of sulfamethoxazole using various irradiation sources and wavelength ranges - Insights from degradation product analysis and compound-specific stable isotope analysis. *Environmental Science and Technology*, **2018**, 52 (3), 1225-1233

Tekle-Röttering, A., Lim, S., Reisz, E., Lutze, H. V., Abdighahroudi, M. S., Willach, S., Schmidt, W., Tentscher, P. R., Rentsch, D., McArdell, C. S., Schmidt, T. C., von Gunten, U., Reactions of pyrrole, imidazole, and pyrazole with ozone: kinetics and mechanisms. *Environmental Science: Water Research & Technology*, **2020**, DOI: https://doi.org/10.1039/C9EW01078E

Willach, S., Lutze, H. V., Somnitz, H., Terhalle, J., Stojanovic, N., Lüling, M., Jochmann, M. A., Hofstetter, T. B., Schmidt, T. C., Carbon isotope fractionation of substituted benzene analogs during oxidation with ozone or hydroxyl radicals: How should experimental data be interpreted? *Environmental Science and Technology*, **2020**, submitted

8.5.2 Oral presentations

Willach, S., Brauch, H.J., Lange, F. T., *Optimisation and application of an analytical method for the determination of AOF in the water cycle*. 29th September – 2nd October 2013, 6th Late Summer Workshop Maurach, Maurach, Germany

Willach, S., Brauch, H.J., Lange, F. T., *Optimisation and application of an analytical method for the determination of AOF in the water cycle*. 24th July 2014, participation on the project „Network for cooperation of academic institution and private sector in the field of environmentally friendly water and soil treatment" of the OP VK (Operation Programme Education for Competitiveness), reg. no. CZ.1.07/2.4.00/31.0189, internal grant no. 17090, Technical University of Liberec, Liberec, Czech Republic

Willach, S., Lutze, H. V., Eckey, K., Lüling, M., Terhalle, J.,. Wolbert, J.-B, Jochmann, M.A., Karst, U., Schmidt, T.C., *Oxidation of sulfamethoxazole by ozone and chlorine dioxide - New perspectives gained by compound-specific stable isotope analysis*. 22nd – 25th May 2017, Donaueschingen, Germany

8.5.3 Poster presentations

Willach, S., Lutze, H. V., Kerpen, K., Schmidt, T. C., *New setup for the wet oxidation of organic model compounds by irradiation with laser light for coupling of HPLC and compound-specific stable isotope analysis*. 26th – 28th May 2014, Wasser, Haltern am See, Germany

Willach, S., Löppenberg, K., Lutze, H. V., Wolbert, J. B., Jochmann, M. A., Schmidt, T. C., *Direct photolysis of sulfamethoxazole at different irradiation conditions and the resulting carbon stable isotope fractionation*. 28th – 30th September 2015, Jahrestagung der Arbeitsgemeinschaft Stabile Isotope e. V., Heidelberg, Germany

Willach, S., Löppenberg, K., Lutze, H. V., Wolbert, J. B., Jochmann, M. A., Schmidt, T. C., *Carbon isotope fractionation in direct photolysis of sulfamethoxazole at different irradiation conditions*. 2nd – 4th May 2016, Wasser, Bamberg, Germany

Willach, S., Löppenberg, K., Yasar, S., Lutze, H. V., Wolbert, J. B., Jochmann, M. A., Schmidt, T. C., Carbon stable isotope fractionation in the oxidation of sulfamethoxazole by ozone and chlorine dioxide. 11th – 14th September, 1st Int. Conference on Sustainable Water Processing, Sitges - Barcelona, Spain

Eckey, K., Willach, S., Lutze, H. V., Schmidt, T. C., Karst, U., *LC/MS analysis of the chlorine dioxide based oxidation of sulfamethoxazole*. 3rd – 6th of April 2017, Anakon, Tübingen, Germany

Eckey, K., Willach, S., Lutze, H. V., Schmidt, T. C., Karst, U., *Untersuchung der Abbauprodukte von Sulfamethoxazol in Wasser nach Behandlung mit Chlordioxid*. 22nd – 24th of May 2017, Wasser, Donaueschingen, Germany

Eckey, K., Willach, S., Lutze, H. V., Schmidt, T. C., Karst, U., *Degradation products of sulfamethoxazole after treatment with chlorine dioxide*. 18th – 22nd June 2017, HPLC, Prague, Czech Republic

Willach, S., Löppenberg, K., Yasar, S., Lutze, H. V., Wolbert, J. B., Jochmann, M. A., Schmidt, T. C., *Carbon stable isotope fractionation in the oxidation of sulfamethoxazole by ozone and chlorine dioxide*. 07th – 12th of July 2019, Isotopes 2019, Raitenhaslach, Germany

8.6 Declaration of scientific contributions

This thesis includes work that has been conducted and published together with co-authors. The single contributions are declared in the following:

Chapter 3:

> Willach, S., Lutze, H.V., Eckey, K., Löppenberg, K., Lüling, M., Terhalle, J., Wolbert, J.-B., Jochmann, M.A., Karst, U., Schmidt, T.C., Degradation of sulfamethoxazole using ozone and chlorine dioxide - Compound-specific stable isotope analysis, transformation product analysis and mechanistic aspects. *Water Research*, **2017**, 122, 280-289

Declaration of own contributions: Planning and evaluation of the oxidation experiments were done by SW. Experiments were conducted by SW and KL with support of ML and JT. HPLC-IRMS measurements were performed by SW with support of JBW. HRMS measurements were conducted by KE at the University of Muenster. The manuscript draft was written and corrected by SW. Revisions of the manuscript were done before submission by HVL, KE, MAJ, UK and TCS.

Chapter 4:

> Willach, S., Lutze, H. V., Eckey, K., Löppenberg, K., Lüling, M., Wolbert, J.-B., Kujawinski, D. M., Jochmann, M. A., Karst, U., Schmidt, T. C., Direct photolysis of sulfamethoxazole using various irradiation sources and wavelength ranges - Insights from degradation product analysis and compound-specific stable isotope analysis. *Environmental Science and Technology*, **2018**, 52 (3), 1225-1233

Declaration of own contributions: The phototransformation experiments were designed and evaluated by SW. The experiments were performed by KL and ML with support of SW. HPLC-IRMS measurements were run by SW with support of JBW. KE conducted the HRMS measurements at the University of Muenster. The manuscript draft was written and corrected by SW. Revisions of the manuscript were done before submission by HVL, KE, DMK, MAJ, UK and TCS.

Chapter 5:

Willach, S., Lutze, H. V., Somnitz, H., Terhalle, J., Stojanovic, N., Lüling, M., Jochmann, M. A., Hofstetter, T. B., Schmidt, T. C., Carbon isotope fractionation of substituted benzene analogs during oxidation with ozone or hydroxyl radicals: How should experimental data be interpreted? *Environmental Science and Technology*, **2020**, submitted

Declaration of own contributions: The oxidation experiments were designed and evaluated by SW. The experiments were performed by SW with support of JT and ML. The GC-IRMS measurements were conducted by SW with support of NS. Quantum chemical calculations were performed by HS. The manuscript draft was written and corrected by SW. Revisions of the manuscript were done before submission by HVL, HS, JT, NS, MAJ, TBH and TCS.

8.7 Curriculum Vitae

Der Lebenslauf ist in der Online-Version aus Gründen des Datenschutzes nicht enthalten.

8.8 Erklärung

Hiermit versichere ich, dass ich die vorliegende Arbeit mit dem Titel:

“Oxidative processes - Insights in reaction mechanisms gained by high resolution and isotope ratio mass spectrometry”

selbständig verfasst habe, zur Abfassung der Dissertation nur die angegebenen Hilfsmittel benutzt wurden und ich alle wörtlich oder inhaltlich übernommenen Stellen als solche gekennzeichnet habe. Ich habe nie ein anderes Promotionsverfahren begonnen und bin daher in keinem vorausgegangenen Promotionsverfahren endgültig gescheitert. Die vorliegende Dissertation wurde nur in diesem Promotionsverfahren eingereicht.

Essen, im Februar 2020

_____

Sarah Willach